UNIVERSITY OF CALIFORNIA

Los Angeles

Self-Adaptive Control of Integrated Ultrafiltration and Reverse Osmosis Desalination Systems

A dissertation submitted in partial satisfaction

of the requirements for the degree Doctor of Philosophy

in Chemical Engineering

by

Larry Gao

2017

ABSTRACT OF THE DISSERTATION

Self-Adaptive Control of Integrated Ultrafiltration and Reverse Osmosis Desalination Systems

by

Larry Gao

Doctor of Philosophy in Engineering

University of California, Los Angeles 2017

Professor Yoram Cohen, Co-Chair

Professor Panagiotis D. Christofides, Co-Chair

Water shortages in many areas of the world have increased the need for fresh water production through water desalination in applications such as the production of potable water, use in agricultural irrigation, and wastewater reuse. In this regard, reverse osmosis (RO) membrane desalination of both seawater and inland brackish water has emerged as the leading technology for water desalination, with a growing number of large-scale desalination plants in the planning and/or construction stages.

Currently, the design of a water desalination plant is typically tailored to the specific water source in terms of meeting productivity targets and pre-treatment requirements. The standard operating procedure is to determine one optimal operating state for an RO system (e.g., overall water recovery, membrane cleaning frequency) and maintain this specific operating point for the duration of operation. However, these methods do not adequately account for the variability in feed water salinity and fouling propensity, and may result in suboptimal operation with respect to excessive energy consumption, poor RO feed pre-treatment, and degradation of RO membrane performance. Therefore, it is crucial to develop effective process control approaches which can

mitigate membrane fouling and reduce RO energy consumption in order to improve the robustness of the RO desalination process.

In order to reduce membrane fouling, several concepts which involve improvements to RO plant pre-filtration capability (e.g., the addition of a separate, modular ultrafiltration membrane process, the use of a transient high-flux "pulse" backwash) were developed. The concept of direct integration of ultrafiltration (UF) and RO was introduced, whereby the UF filtrate is fed directly to the RO and the RO concentrate is used for UF backwash. Additionally, a control system was designed for the UF pre-treatment unit whereby membrane fouling was reduced through optimization of backwash through a combination of varying the backwash frequency and varying the coagulant dose. This approach was shown to significantly reduce membrane fouling and significantly increased operation duration before chemical cleaning was required (~900% longer).

In order to reduce energy consumption of RO desalination, energy-optimal control systems featuring a novel two-layered controller architecture were developed and implemented using fundamental models of specific energy consumption (SEC) of single-stage and two-stage RO systems. The implemented control algorithms utilized extensive sensor measurements from the pilot plants (i.e., flow rate, pressure, conductivity, etc.) to determine the optimal operating set-points for the RO systems (e.g., system feed flow rate, system feed pressure, and overall system water recovery). Accordingly, the control system shifted the RO system operation to the operating conditions that resulted in the lowest energy consumption for a given feed salinity and for a given target product water productivity while accounting for system constraints.

The control and design concepts developed in this dissertation were tested on two water purification systems, constructed by a team at UCLA. The two pilot plants were the Smart Integrated Membrane System – Seawater (SIMS-SW) and the Smart Integrated Membrane

System – Brackish Water (SIMS-BW). Field tests of the control systems were conducted and the results successfully demonstrated the ability for the control systems presented in this dissertation to reduce membrane fouling and RO energy consumption.

The dissertation of Larry Gao is approved.

Tsu-Chin Tsao

Jim Davis

Yoram Cohen, Committee Co-Chair

Panagiotis D. Christofides, Committee Co-Chair

University of California, Los Angeles

2017

Table of Contents

List of Figures

List of Tables

Acknowledgements

I would like to thank my family for their love and support. Without Mom, Dad, and Carl, I would not be in the position I am today. I would like to thank my parents for having the courage to immigrate to a foreign land and for having the patience to raise two sons. I would like to thank Carl for being together with me every step of my life, and for the unconditional help that he always gives me.

I would also like to show my gratitude for my Ph. D. faculty advisors, Dr. Panagiotis D. Christofides and Dr. Yoram Cohen, for their patience and time spent in helping me during my years at UCLA. Their experience, knowledge, and advice were all instrumental in helping me be productive and motivated in a research environment.

I would also like to thank my colleagues that worked closely with me on many of our collaborative projects, including Alex Bartman, Han Gu, Anditya Rahardianto, John Thompson, Tae Lee, Richard Zhu, Xavier Pascual Caro, and Sirikarn Surawanvijit. I especially want to thank Andi for his tireless efforts to keep everyone on schedule and for the great compassion he showed me even during the most difficult times. I would also like to thank my good friend and mentor Alex Bartman; his presence was invaluable for me to hit the ground running, and I have no doubt in my mind that if it weren't for him, I would not have accomplished as much as I have.

I am also grateful to have shared the same office space with the Wolf Pac, including Michael Nayhouse, Matt Ellis, Sang-Il Kwon, Liangfeng Lao, Grant Crose, and Anh Tran. I will miss our legendary ventures for free food, the hoarding of coupons, and tearing through IM softball and dodgeball together.

During my time in LA I had the great fortune to meet people who I consider friends for life. I would like to thank Diana Chien, Alex Jury, Allison Yorita, Calvin Pham, Jennifer Takasumi, and Po-Hen Lin. Our Spades sessions where we were OOOOH-ing at each other all night long

were some of the funniest moments in my life. I'd like to especially thank Diana and Alex for hosting me under their roof for 3 years, and allowing me to be a part of their wonderful, growing family. I'm so glad that I was able to bond with you guys over Disney, football, and ramen. My life would be pretty empty if I weren't able to gloat to Alex about two fantasy football championships.

I would also like to thank all the people who I met at UC Berkeley. I'd like to thank Matthew Traylor, for kick starting my academic career. I'd like to thank my Chem E crew, Jack Wang, Cindy Xu, Ariel Tsui, Alvin Mao, Anita Kalathil, Kyle Caldwell, Matt Richards, and Qiang Liu for being just the right mix of hilarious and crazy. Those fun late night study sessions at the library were anything but fun. I'd like to thank all the members of the Spruce House, including Gautam Wilkins, Frank Liu, Guy Zehavi, Danny Mondo, Justin Peng, Alex Jacobson, and Chad Bunting. I will always tell people the two years we spent together were probably the best times in my life. Our Warcraft 3 High Perching shenanigans were ultimate trolling that won't be matched for generations of RTSs. I would also like to thank my high school friends, Robert Yu, Seaver Mai, Darwin Fu, and Kevin Huang, for tolerating me and putting in the effort to keep in touch with me. I also want to thank Mark Andre and Jennifer Brazil for being two fantastic individuals and always being there for me, no matter what.

Finally, I'd like to thank the UCLA CBE administrative staff, especially John Berger and Sara Reubelt, for their immense assistance.

I would like to end this section by noting that 27 years ago my father, who had such high confidence in me despite me being just an infant, predicted in his Ph. D. dissertation that I would eventually go on to earn a Ph. D. degree just like he did. Therefore, in honor of his prediction, I would like to hope that someday, my child will also eventually go on to earn a Ph. D. degree.

VITA

2010	Bachelor of Science, Chemical Engineering
	University of California, Berkeley
2010-2017	Graduate Student Researcher, Teaching Assistant
	Department of Chemical and Biomolecular Engineering
	University of California, Los Angeles

Publications and Presentations

Publications

1. L. Gao, A. Rahardianto, H. Gu, P.D. Christofides, Y. Cohen, “Energy-Optimal Control of RO Desalination,” Ind Eng Chem Res, (2013)

2. L.X. Gao, A. Rahardianto, H. Gu, P.D. Christofides, Y. Cohen, “Novel design and operational control of integrated ultrafiltration — Reverse osmosis system with RO concentrate backwash,” Desalination, (2016)

3. L.X. Gao, H. Gu, A. Rahardianto, P.D. Christofides, Y. Cohen, “Self-Adaptive Cycle-to-Cycle Control of In-line Coagulant Dosing in Ultrafiltration for Pre-Treatment of Reverse Osmosis Feed Water,” Desalination, (2016)

Presentations

1. L.X. Gao, A. Rahardianto, H. Gu, P.D. Christofides, Y. Cohen, "Real-Time Operation and Control of an Integrated Ultrafiltration-Reverse Osmosis Membrane Desalination System," North American Membrane Society Annual Meeting, 2012, New Orleans, LA

2. L.X. Gao, A. Rahardianto, H. Gu, P.D. Christofides, Y. Cohen, "Real-Time Operation and Control of an Integrated Ultrafiltration-Reverse Osmosis Membrane Desalination System,"American Institute of Chemical Engineers Annual Meeting, 2012, Pittsburgh, PA

3. L.X. Gao, A. Rahardianto, H. Gu, P.D. Christofides, Y. Cohen, "Integrated UF/RO System for Shipboard Desalination,"American Water Works Association Annual Meeting, 2012, San Diego, CA

4. L.X. Gao, A. Rahardianto, H. Gu, P.D. Christofides, Y. Cohen, "Energy-Optimal Control of an Integrated UF-RO Seawater Desalination Plant,"American Institute of Chemical Engineers Annual Meeting, 2013, San Francisco, CA

5. L.X. Gao, A. Rahardianto, H. Gu, P.D. Christofides, Y. Cohen, "Energy-Optimal Control of an Integrated UF-RO Seawater Desalination Plant," North American Membrane Society Annual Meeting, 2014, Houston, TX

6. L.X. Gao, A. Rahardianto, H. Gu, P.D. Christofides, Y. Cohen, "Direct Integration of RO Desalination and UF Pre-Treatment with Self-Adaptive RO Concentrate Backwash,"American Institute of Chemical Engineers Annual Meeting, 2014, Atlanta, GA

7. L.X. Gao, A. Rahardianto, H. Gu, P.D. Christofides, Y. Cohen, "Integrated Ultrafiltration-Reverse Osmosis System with RO Concentrate Backwash," North American Membrane Society Annual Meeting, 2015, Boston, MA

8. L.X. Gao, H. Gu, A. Rahardianto, P.D. Christofides, Y. Cohen, "Self-Adaptive UF Filtration with Optimal Coagulant Dosing,"American Institute of Chemical Engineers Annual Meeting, 2015, Salt Lake City, UT

9. L.X. Gao, A. Rahardianto, H. Gu, P.D. Christofides, Y. Cohen, "Optimized Ultrafiltration Backwash with Real-Time Control of Coagulant Dosing," North American Membrane Society Annual Meeting, 2016, Seattle, WA

Chapter 1 Introduction and Objectives

1.1 Reverse Osmosis Desalination

Freshwater shortages are now prevalent in many areas of the world due to overutilization and contamination of water resources, drought conditions attributed to climate change, and increased demand due to population growth. A vast majority (97.5%) of the water available on the planet is saline, while only 0.8% of water available is considered to be fresh water, with the rest (1.7%) located in ice caps [1]. Saline water (seawater, inland brackish water, and water reuse) could be converted into a significant sustainable water resource if potable water can be extracted at a reasonable cost [2, 3]. Reverse osmosis (RO) desalination has emerged as one of the leading methods for water desalination and water reuse due to its ability to remove ~99% of dissolved solids from saline water to product water of potable quality [1-4].

1.1.1 Reverse Osmosis Feed Pre-Treatment

Despite widespread use of RO technology, membrane fouling remains a critical impediment, causing reduced membrane permeability and increasing maintenance costs due to requirements of cleaning and replacements of damaged membranes [2, 3, 5-8]. In order to avoid RO membrane fouling, RO feed water pre-treatment units are typically used in order to improve the quality of the RO feed water and extend the life of the RO membranes [8, 9]. It is important to note that when using a pre-treatment unit, the burden of alleviating the adverse impact of membrane fouling (e.g., higher required applied pressure for a given water production level), is assumed by the pre-treatment unit [8, 9]. However, it is advantageous to allow fouling to occur in the pre-treatment unit as opposed to on the RO membranes since accumulated fouling on the pre-treatment unit can be in principle be reduced by a periodic backwashing procedure (i.e.,

reversing the flow direction, **Figure 1.1**) [9-12] and routine chemical cleaning-in-place (CIP) [13-15]. Existing RO pre-treatment technologies include the use of media filters (e.g., sand filters, cartridge filters) or the use of a multi-membrane approach where microfiltration (MF)/ultrafiltration (UF) membranes are used upstream of the RO membranes to filter out bigger suspended solids [8, 9]. Frequently, these filtration steps are paired with a coagulation process designed to improve filtration efficiency by promoting the formation of flocs (i.e., aggregation of fine particles and colloidal matter) [16-22].

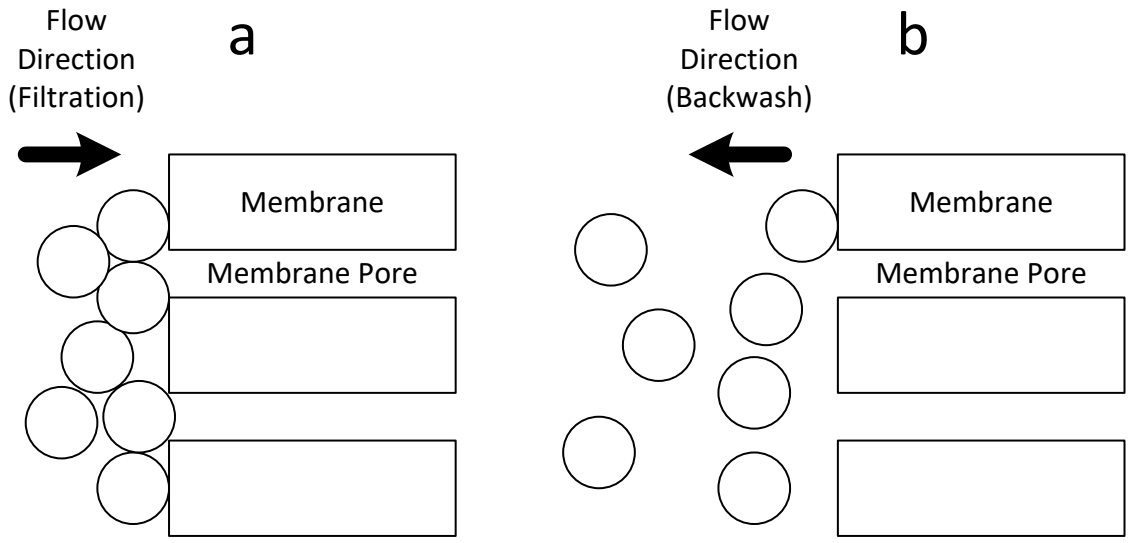

Figure 1.1. Illustration of a) fouling on a membrane surface during filtration and b) the removal of the foulant through a backwash procedure

Specifically, UF membrane filtration has proven to be effective for providing high quality filtrate water compared to its alternates (i.e., in a study by Chua et al. [9], the silt density index, or SDI, of pre-treated feed water was measured to be 6.1-6.5 SDI for media filters, 2.5-3.0 SDI for an MF system, and 0.9-1.2 for an UF system). RO desalination systems with UF membrane pre-treatment has been used for applications in a wide variety of applications, such as for medium- and large-scale municipal and industrial plants, small-scale water treatment applications for remote communities, emergency response, and shipboard deployments [9, 12, 14,

23-27]. Currently, most RO systems are typically tailored to the specific water source in terms of meeting productivity targets and pre-treatment requirements. Pre-treatment system parameters such as the backwash frequency or coagulant dosage are set at a fixed value determined through the combination of laboratory testing (e.g., jar testing to determine the optimal coagulant dose) [16, 21, 28, 29] and preliminary pilot-plant runs [17, 19, 30]. However, in reality, UF feed water quality and fouling propensity vary significantly with time in the short term, as well as seasonally (e.g., algae blooms), and can cause suboptimal operation (e.g., ineffective UF backwash can lead to more frequent chemical cleanings, while overdosing the coagulant may lead to RO membrane damage downstream) [6, 12, 29, 31-33]. For example, the adverse effect of a severe "red tide" algae bloom incident in the Gulf of Oman in 2008-2009 on RO systems has been well-documented [6, 33]: the increase in concentration of biofouling particulates produced by the algae population overwhelmed pre-treatment units designed to operate under much cleaner feed water conditions and caused the shut-down of several plants [6, 33].

1.1.2 Reverse Osmosis Energy Consumption

A major component in the effort to make the RO process more economically feasible is the reduction of its electrical energy cost. For example, electrical energy consumed in providing RO feed inflow at the required pressure represent 32-44% of the total cost of seawater desalination (**Figure 1.2**) [34-37]. RO desalination has improved over the years with reduction in energy consumption primarily due to the development of membranes of increased permeability [38-41], the introduction of energy recovery devices (ERDs) [42, 43], more efficient high pressure pumps [44] and optimization of membrane module hydrodynamics [45-52]. It is noted that ERDs have enabled efficient recovery (e.g., up to ~95%) of unutilized pressure energy from the RO concentrate and have proven particularly effective for large-scale seawater RO plants [53-55].

Recently, in the area of energy optimization, it has been shown that the specific energy consumption, or SEC (energy cost per volume of permeate water produced), is a useful metric to quantify reverse osmosis water desalination system energy usage [56-58]. Within the SEC framework, the issues of unit cost optimization with respect to water recovery, energy recovery, system efficiency, feed/permeate flow rate, membrane module topology [56-58], and optimization of the transmembrane pressure subject to feed salinity fluctuations [59] have been studied. However, experimental verification of the theoretically computed energy optimal operating points was not carried out in the aforementioned works [56-59]. An energy optimization non-linear control algorithm (without the inclusion of an ERD) that builds on the above SEC modeling framework was also demonstrated with a small laboratory spiral-wound RO system [60]. It was shown, in limited proof-of-concept laboratory tests, that energy optimal control for spiral-wound RO operation, subject to a simple step change in feed salinity was feasible through simultaneous control of feed pressure and feed flow rate [60]. However, the proposed control algorithm did not account for potential temporal changes in RO membrane permeability (e.g., due to membrane fouling or aging) and cannot be used on an RO system equipped with an ERD of a two-stage RO system (i.e., since the control approach does not take into account the presence of an ERD or an intermediate booster pump for the second RO stage).

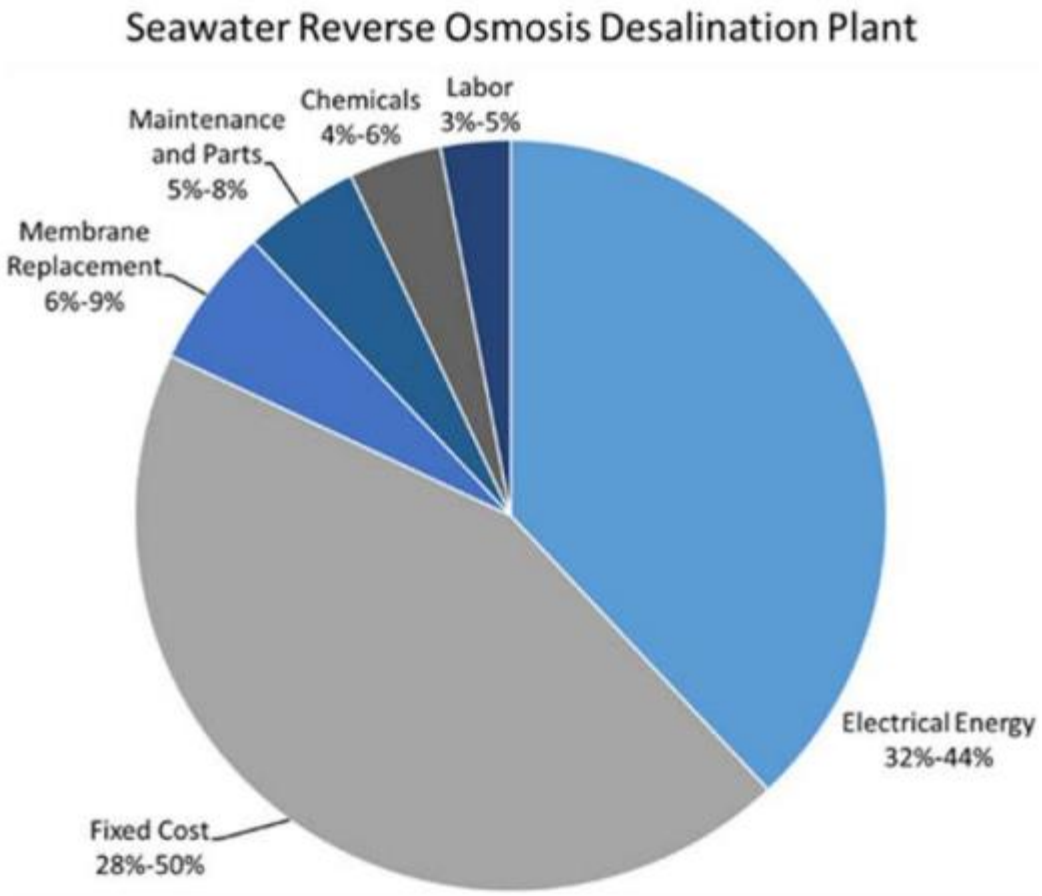

Figure 1.2. Operational costs for a typical seawater RO desalination plant

1.2 Dissertation Objectives

The major goals of this dissertation were to develop and demonstrate real-time control systems which a) lengthens the operating duration of an UF filtration unit by reducing the cumulative increase of UF fouling in order to reduce the frequency of required chemical cleaning, and b) operates the system in an energy-optimal operating state and is capable of driving the system to a new operating state if changes in the feed water salinity or membrane permeability occurs. The above goals are rooted in the hypothesis that ***reductions in operational costs of***

existing RO systems can be achieved through the implementation of smart, self-adaptive control strategies. The specific objectives are listed below.

1. Investigate the advantages of direct integration of UF and RO, whereby the UF membranes are backwashed using RO concentrate.
    - Develop a control system which enables a directly integrated UF-RO system to backwash its UF pre-treatment unit while still providing a constant feed flow rate and pressure to its RO desalination skid.
    - Develop a variable backwash frequency strategy (i.e., which is enabled by the direct integration of UF and RO) in order to reduce cumulative build-up of UF fouling.
2. Develop a real-time coagulant controller to reduce cumulative build-up of UF membrane fouling while reducing coagulant usage.
    - Develop a metric which measures in real-time how changes in coagulant dose impact the efficiency with which the UF backwash removes the UF fouling layer.
3. Develop an energy-optimal control system which can achieve and maintain RO system operation at energy-optimal conditions.
    - Develop a specific energy consumption framework which can determine the energy-optimal operating water recovery for an RO system operating under constant permeate flow rate conditions.
    - Interface the above specific energy consumption framework with a control system which can actuate the calculated energy-optimal operating water recovery onto a single-stage RO system (e.g., calculate and control the flow rates and pressures required for RO modules to operate at a specified recovery).

- Expand upon this approach to develop an energy-optimal controller for a two-stage system which is capable of determining the energy-optimal permeate production split between the two stages.

1.3 Dissertation Structure

The previously stated objectives were achieved through a combination of theoretical analysis and detailed field studies performed using two pilot-scale RO desalination systems. The two pilot-scale RO desalination systems (i.e., one of seawater desalination and another for brackish water desalination) were developed and constructed by a team of graduate students at UCLA. These systems served to verify the various improvements to the RO process realized by the various control systems presented in this dissertation. The two pilot-scale systems are described in **Chapter 2**.

In **Chapter 3**, a new operational approach is presented for a novel integrated RO-UF system in which the UF filtrate is fed directly to the RO feed and the RO concentrate is used to backwash the UF. This direct integration eliminated the need for intermediate UF filtrate tank and backwash pump, enhanced operational flexibility, and enabled implementation of self-adaptive backwashing strategies. Ensuring continuous UF filtrate production of RO feed even during periods of UF backwash was achieved through a combination of system design and control. Concepts such as UF backwash enhanced by short periods of high-flux backwash (pulse backwash) and self-adaptive backwash triggering based on UF fouling behavior was also explored and proven to improve UF backwash effectiveness.

Chapter 4 describes the use of a self-adaptive coagulant dosing strategy to further improve UF backwash. The approach, based on real-time tracking of the resistance-dose (RD) factor, was developed as a metric to quantify the impact of coagulant dose on UF backwash effectiveness

(i.e., with respect to removal of the UF foulant layer). It was shown that self-adaptive coagulant dosing approach is effective in reducing coagulant use while maintaining robust UF operation even during periods of both mild and severe water quality degradation.

In **Chapter 5**, a general energy-optimal RO control algorithm for a single-stage RO is presented which only requires a target permeate production set-point. The control system considers constraints imposed by the required permeate production, system operability (e.g., operational limitation of system components), high pressure feed pump and ERD efficiencies, membrane permeability (i.e., which may change over the course of the system operation), and temporal variability of feed salinity. The proposed controller was evaluated in a series of field experiments demonstrating a capability for maintaining energy optimal operation despite temporally variable feed salinity.

Chapter 6 expands upon the work done presented in **Chapter 5** and presents an energy-optimal RO control algorithm for a two-stage RO system. The energy-optimal controller regulated the permeate production split between the two stages as well as the overall water recovery to minimize energy consumption. The pump efficiencies of the first-stage and second-stage pumps were also considered to vary with flow rate and pump outlet pressures. The proposed controller was evaluated in a series of brackish water field experiments and demonstrated the ability to reduce energy consumption of a two-stage RO system through the optimization of its overall water recovery and permeate production split between the two stages.

Chapter 2 Background and Literature Review

2.1 Reverse Osmosis

Reverse osmosis (RO) is the process by which pressure is applied to a feed solution across a semipermeable membrane that allows water passage, but largely rejects solute passage resulting in a solute lean stream (permeate or product) and a solute rich stream (retentate or concentrate) [61]. An RO membrane can be characterized by its permeability, L_P, and its salt rejection, R. Membrane permeability is a measure of how easily water passes through the membrane and is proportional to the inverse of the membrane's resistance to water passage. Salt rejection is a measure of the degree to which dissolved ions are rejected from passing through the membrane. The transport of the solvent through a RO membrane can be described using a solution-diffusion model as expressed below [62]:

$$J_P = L_P(\overline{\Delta P_m} - \sigma\overline{\Delta\pi}) \qquad \textbf{2.1}$$

where J_P is the permeate flux, L_p is the membrane hydraulic permeability, $\overline{\Delta P_m}$ is the average pressure difference between the feed and permeate side of the membrane (transmembrane pressure), σ is the reflection coefficient which represents the selectivity of water passage relative to salt passage, and $\overline{\Delta\pi}$ is the average osmotic pressure difference across the membrane. The osmotic pressure of saline water increases with solute concentration and for dilute solutions can be calculated through the following equation [63]:

$$\pi = iC_sRT \qquad \textbf{2.2}$$

where π is the osmotic pressure (atm), i is the van't Hoff factor for a given solute, C_S is the solute concentration (mol/L), R is the ideal gas constant (0.08206 $L{\cdot}atm{\cdot}mol^{-1}{\cdot}K^{-1}$), and T is temperature (K). As indicate by **Eq. 2.1**, for separation to occur (i.e., non-zero permeate flux) the

applied transmembrane pressure must be greater than the osmotic pressure on the feed side of the membrane.

RO desalination is typically carried out in a cross-flow configuration in which the saline feed water enters the membrane channel and flows tangentially across the membrane surface under high pressure. The feed stream exits the membrane channel as a concentrate stream. In plate-and frame type modules, the membrane is supported by a rigid, porous layer as shown in **Figure 2.1**. When treating large volumes of feed water, spiral-wound membrane modules (**Figure 2.2**) are often used because they provide a large membrane surface area to volume ratio and most state of-the-art RO membranes are manufactured in this arrangement [1-4]. A spiral-wound module consists of alternating layers of RO membrane sheets and mesh spacer sheets wrapped around a central channel, all encased within a plastic shell. The spacers facilitate the channels (i.e. space) through which feed and permeate water can flow. Most large scale RO desalination plants use a multistage arrangement of spiral-wound modules connected in series with each stage containing modules in parallel as needed based on the expected flows. As the permeate is separated from the feed the volume of the concentrate stream decreases, often necessitating fewer modules in parallel in the second stage (and subsequent stages if present) as illustrated in **Figure 2.3**. However, as most natural feed waters contain suspended particles, pre-treatment is required prior to desalting to remove particulates and debris that could damage or plug the RO membranes.

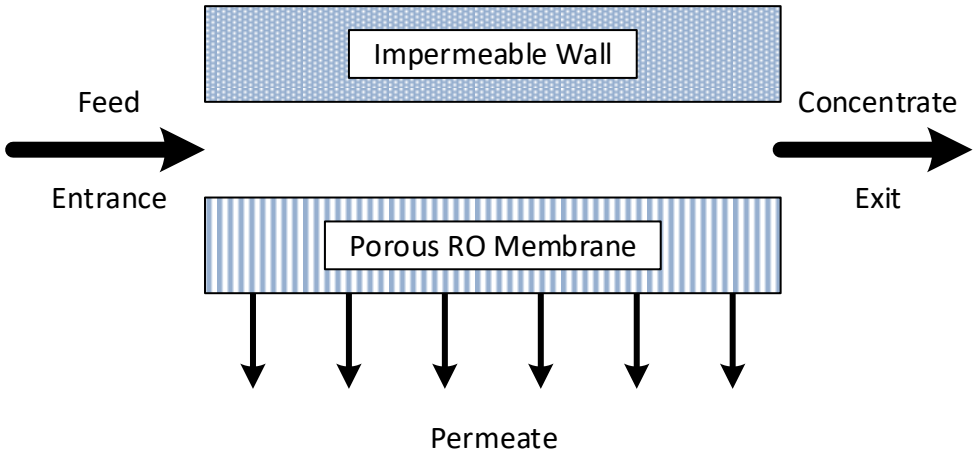

Figure 2.1. Schematic of cross-flow RO in a rectangular channel

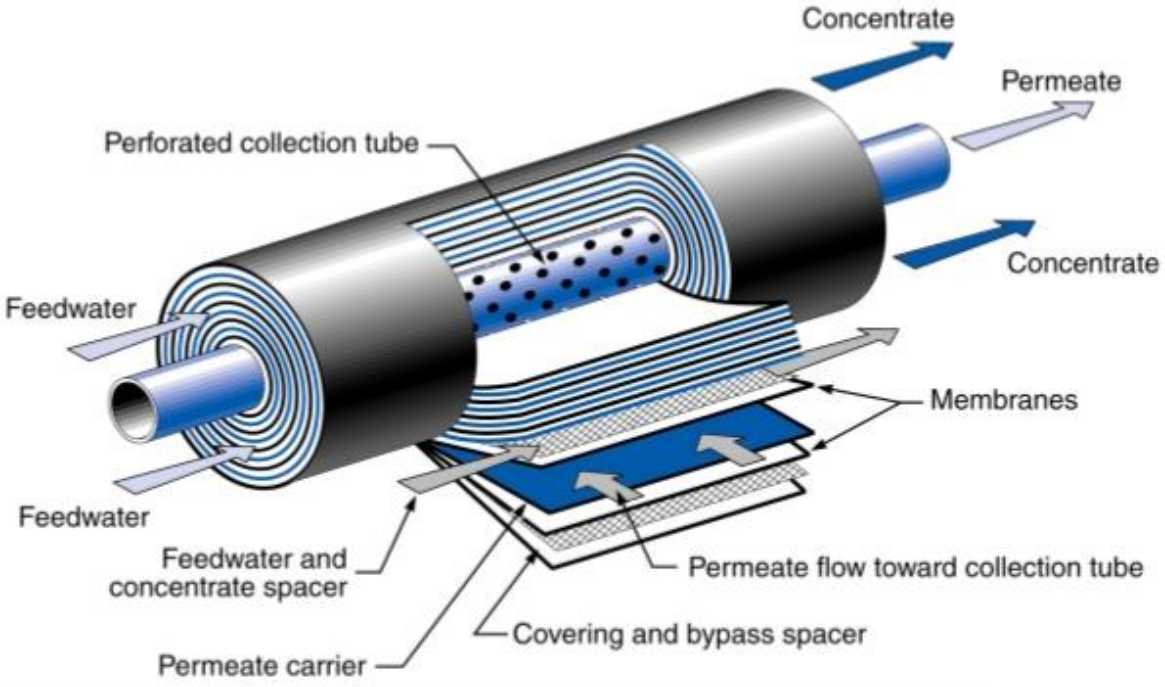

Figure 2.2. Cut-away of a spiral-wound RO membrane module [64]

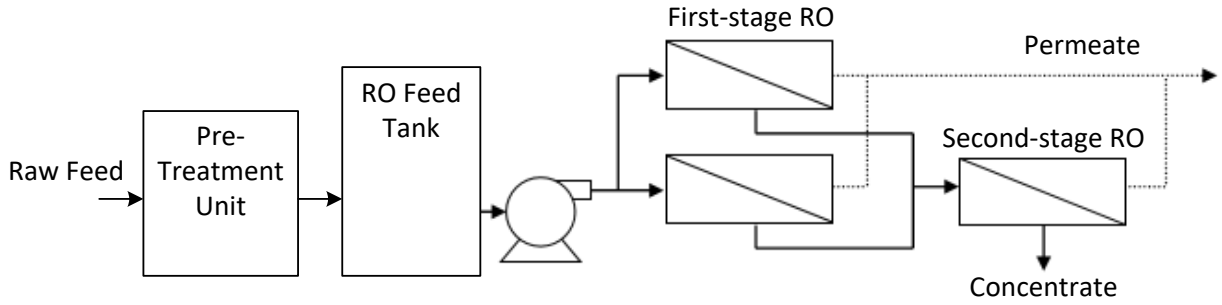

Figure 2.3. Schematic of a typical two-stage RO desalination process with an RO feed pre-treatment unit.

2.2 Background on Integration of UF and RO

The use of UF membrane filtration for RO feed pre-treatment has proven to be popular since UF membranes consistently produce high-quality RO feed water and can be backwashed to recover its permeability (**Section 1.1.1**). Integration of UF with RO is practiced in a variety of industrial and municipal applications [9, 12, 14, 25-27]. However, conventional UF-RO systems typically utilize UF filtrate for periodic UF backwash, necessitating the use of intermediate tanks to store UF backwash water (during periods in between backwash cycles) and for assuring continuous delivery of UF filtered RO feed **(Figure 2.3)** [9, 12, 14, 25, 26, 65-67]. A dedicated UF backwash pump is typically needed to drive UF backwash, while a separate low-pressure RO booster pump may be needed to re-pressurize UF filtrate to prevent cavitation in downstream the high-pressure RO feed pump. In addition to added maintenance and cleaning requirements [12, 30, 68, 69], intermediate UF filtrate tanks and the associated pumps present a system design challenge when space is limited or portability is important. More importantly, operational flexibility of UF backwashing using UF filtrate may be constrained by the UF filtrate tank capacity, coupled with the need to maintain continuous RO feed flow. As consequence, a fixed

UF backwash strategy (whereby backwash frequency, duration, and intensity are fixed) is often practiced in conventional UF operations. Such passive strategy may not be optimal for robust UF-RO plant operation as UF feed water quality and fouling propensity can vary significantly with time in the short term, as well as seasonally [6, 12, 32].

When UF filtrate is utilized for UF backwash, implementation of a variable UF backwash strategy (i.e., backwash frequency, duration, and intensity to adapt to changing feed water quality) may necessitate concurrent variation or reduction of UF productivity (e.g. for subsequent RO treatment) in order to achieve the required backwash effectiveness while still meeting the constraint imposed by UF filtrate tank capacity [32]. Frequent changes in RO feed flow is undesirable as it necessitates RO process controllers to make frequent, significant operational adjustments (in order to maintain constant RO productivity), which may lead to chronic, excessive fluctuations of RO feed pressures that can potentially induce telescoping damage to RO membrane elements [70, 71].

Instead of using UF filtrate, RO concentrate or permeate can be utilized for UF backwash [72-77]. Studies have indicated that demineralized water can enhance UF backwash effectiveness by reducing charge screening effects and thus natural organic matter (NOM) affinity to negatively-charge UF membrane surfaces [72, 73]. Pilot plant studies have also shown that backwash using RO permeate is more effective than with UF filtrate [74]. Utilization of RO permeate for backwash, however, does require the use of permeate storage and additional backwash pump, with the disadvantage of loss of RO productivity. The alternative technology of direct use of RO concentrate for UF backwash, as disclosed by UCLA [75], is particularly beneficial since it enables UF operation at 100% UF recovery (i.e. no loss of UF permeate). A later pilot study confirmed that UF backwash using RO concentrate (collected in a backwash tank and delivered via a backwash pump) can be as effective as using UF filtrate [76]. In this

regard, it is interesting to note that periodic hyperosmotic stress has been suggested to slow the maturation process of marine bacterial biofilm growing on filtration membranes, induced by cell mortality [77]. Although previous work has suggested the potential benefits of UF backwash with RO concentrate [75-77], direct UF-RO integration has not yet been evaluated to demonstrate its advantage of flexible backwashing strategy without loss of UF or RO productivity.

2.3 Background on Coagulation of RO Feed Pre-Treatment

The use of coagulation in combination with membrane pre-treatment has been shown by a body of work to improve RO feed water quality and reduce membrane fouling [16-22]. It is generally accepted that coagulant dosing promotes the formation of flocs (i.e., aggregation of fine particles and colloidal matter) which improves both UF and MF membrane filtration and hydraulic cleaning [17, 22, 78]. Also, membrane pore plugging and irreversible fouling have been reported to decrease with increasing coagulant dose up to an optimal maximum limit [28] beyond which there is little added benefit. However, excessive coagulant dosing increases process cost and the potential for coagulant passage across the membrane to the permeate stream. Accordingly, the common approach to UF operation is to search for the optimal coagulant dose via the combination of jar testing (i.e., introduced nearly 100 years ago) [16, 21, 28, 29] and preliminary pilot-plant runs [17, 19]. However, in reality, the source water quality and thus UF fouling propensity may vary significantly with time in the short term, as well as seasonally [6, 12, 29, 31, 32]. Incidents have been reported where worsening feed water quality caused irreversible fouling in pre-treatment units equipped with in-line coagulation which has led to shut-downs of RO desalination plants [6, 33]. Coagulant underdosing is an issue as well if feed water quality improves, since excessive passage of coagulants through the pre-treatment unit may cause

damage to RO membranes downstream [79]. Therefore, the optimal coagulant dose can change as feed water quality changes; thus, operating at a fixed coagulant dose can lead to suboptimal UF operation. Clearly, under conditions of variable feed water quality, determination of the optimal coagulant dose(s), which is dependent on source water quality, is infeasible by off-line methods (e.g., jar testing). Hence, real-time adjustment of coagulant dose is needed where variable source water quality is encountered.

Real-time adjustment of coagulant dose through feed-forward control was introduced in [80] for particulate matter removal from river water via sedimentation aided by coagulation. The approach relied on formulating an empirical relation, based on historical data of sedimentation under coagulant treatment, that correlates the suitable coagulant dose with feed water turbidity, conductivity, and temperature [80]. The above approach was successfully implemented for the one specific feed water source for which the correlation was determined, but the control approach was found to be deficient at two other sites. More recently, a feed-back control approach was reported for coagulant dose adjustment, also for a coagulant-sedimentation process, whereby the residual aluminum concentration in the mixing tank served as the metric for assessing coagulation efficiency [81, 82]. Deployment of the approach was successful for reducing source water of turbidity from 0.5 - 100 NTU to below 1 NTU.

The application of real-time adjustment of coagulant dose for in-line coagulation in dead-end UF filtration systems was first reported in [83]. The approach involved the formulation of an empirical correlation of the trajectory of initial UF filtration cycle resistance (i.e., UF filtration resistance immediately post UF backwash, termed hereinafter UF “PB” resistance) with respect to the filtered volume based on a series of short-term pilot tests. The deviation of the measured UF PB resistance from the value calculated from the empirical UF PB resistance-filtered volume (PBR/FV) trajectory correlation was used as input to a proportional-integral controller to adjust

the coagulant dose. The controller function was set to adjust the coagulant dose so as to drive the UF system operation toward the selected PBR/FV trajectory. The above approach should be useful when water quality is essentially time-invariant. As noted in [83], however, the selection of an optimal UF PBR/FV trajectory was arbitrary and the authors did not demonstrate that it is feasible to arrive at an optimal trajectory. The above limitation of the approach is understandable given that a specific PBR/FV trajectory could not be used to establish optimal operation for situations in which water source quality (i.e., in terms of its fouling potential) is temporally variable.

Determination of an optimal coagulant dose in real-time for the wide range of water quality conditions that may occur in various locations is a daunting task. Therefore, it would be beneficial to develop and deploy a coagulation controller, capable of adjusting the coagulant dose, without the need for establishing specific pre-determined empirical relationships of coagulant dose with multiple measurements of water quality and/or UF resistance metrics.

2.4 Background on Energy-Optimal Control of Single-Stage RO

Traditionally, RO process control has focused on regulating the permeate productivity and the permeate quality. RO plant control via classical control algorithms (i.e., proportional-integral (PI) control) has been deployed to control system pressure in order to meet permeate production set-points [84]. Multi-loop control of both permeate flow rate and quality have also been proposed [85]. In addition to classical control, several non-linear model-based control strategies have been developed to improve RO process control under conditions of varying feed water quality and correct various faults that may occur during operation [86, 87]. Model-predictive control (MPC) and Lyapunov-based control have also been designed and evaluated through computer simulations [87-91].

More recently, an RO control strategy that considers minimization of energy consumption through the optimization of the specific energy consumption, or SEC (energy cost per volume of permeate water produced) has been explored and demonstrated in a small laboratory RO system [60]. RO SEC optimization was investigated and the impact of various parameters such as water recovery, energy recovery and pumping efficiencies, feed and permeate flow rate constraints, membrane module topology [56-58], and feed pressure subject to feed salinity fluctuations [59] was investigated theoretically. Through these studies, Zhu et al. concluded that the global minimum for both single-stage and two-stage RO occurs at the limit imposed by the thermodynamic cross-flow restriction (i.e., defined as when the RO feed pressure is equivalent to the osmotic pressure difference at the RO membrane exit region to ensure permeate productivity along the entire RO membrane module) [58]. The aforementioned study presented a control strategy that attempted to minimize energy consumption through an energy optimization non-linear control algorithm (without the inclusion of an ERD) that builds on the above SEC modeling framework, which was also demonstrated with a small laboratory spiral-wound RO system [60]. Energy-optimal control for spiral-wound RO operation was shown, in limited proof-of-concept laboratory tests, where the RO system was operated as close to the thermodynamic restriction as physical system constraints allowed [60]. However, the proposed control algorithm did not account for potential temporal changes in RO membrane permeability (e.g., due to membrane fouling or aging) and cannot be used on an RO system equipped with an ERD of a two-stage RO system (i.e., since the control approach does not take into account the presence of an ERD or an intermediate booster pump for the second RO stage).

2.5 Background on Energy-Optimal Control of Two-Stage RO

The use of multiple membrane stages to achieve high product water recovery has become desirable in brackish water applications in order to minimize concentrate management [58, 92-94]. In addition to the advantages of high recovery operation, the use of a multi-stage RO process configuration with intermediate booster pumps between membrane stages has also been shown to be more energy-efficient than single-stage RO (i.e., potential energy savings due to multi-stage RO configuration can range from 15% - 40%) [58, 94]. This energy reduction is a significant advantage with respect to reducing RO operational costs since energy is a significant portion of the total cost of water desalination (i.e., exceeding in most cases 50% of the total cost of desalination).

Another approach which has been used to reduce RO energy consumption is through the optimization of RO operational parameters with respect to RO energy consumption. RO operation is typically confronted with temporal variability of feed water salinity [3, 34, 59, 95-98] (e.g., in one example, the total dissolved solids, or TDS, content at one location in the central San Joaquin Valley deviated up to 52% from its annual average due to seasonal rainfalls [3]), which may shift RO systems to suboptimal operating states during operation [3, 34, 59, 95].

With respect to RO energy optimization, several previous studies have used the theoretical framework of specific energy consumption (SEC) at the thermodynamic restriction to arrive at a strategy for reducing RO energy consumption by determining the energy-optimal operating states (e.g., energy-optimal overall water recovery). Zhu et al. [56-58] explored the global minimum SEC of RO desalination and concluded that the global minimum for both single-stage and two-stage RO occurs at the limit imposed by the thermodynamic cross-flow restriction (i.e., defined as when the RO feed pressure is equivalent to the osmotic pressure difference at the RO

membrane exit region to ensure permeate productivity along the entire RO membrane module). There are also studies by Li et al. [37, 38] which evaluated whether or not an existing RO plant is operating under energy-optimal conditions by inputting data gathered from an off-line system analysis of a single-stage RO system (i.e., Chino Desalter 1, a brackish water system located in Chino, California, which operates with four parallel membrane trains with a dedicated feed pump for each train) into a SEC model for the plant. In this study, a simplified mathematical model derived from first principles was proposed and utilized to calculate the SEC as a function of various system parameters such as membrane permeability and feed salinity. Values of the membrane permeability and the feed salinity were obtained from the 280 m^3/h Chino Desalter 1 operated over three days. The proposed mathematical model also incorporated feed pump efficiency as a variable (i.e., pump efficiency ranged between 0.747 – 0.785 and varied with respect to flow rate and pump head). The results of the post-process analysis indicated that the energy consumption could have been reduced by 10% upon increasing the recovery from 80% to 90% [99, 100]. The study also demonstrated the importance of accounting for variable pump efficiencies. Analysis based on an assumed constant pump efficiency predicted an operating SEC ~5% higher relative to the more realistic condition of variable pump efficiencies. However, post-process analysis as in the above study did not take into account the possibility of feed water salinity variations and potential changes in the membrane permeability (i.e., due to suboptimal feed pre-treatment) during operation. Moreover, the previous study did not propose a control system for handling temporal changes in feed water quality and membrane permeability.

Real-time energy process control with a SEC optimization algorithm was previously successfully demonstrated on a laboratory-scale single-stage RO system [60]. An optimization problem was formulated and solved to determine the feed flow rate and concentrate valve position which resulted in the minimum SEC for a prescribed permeate productivity (i.e., flow

rate). More recently, a two-level control system which involved the integration of an upper-level supervisory control system (i.e., which calculated the energy-optimal Y) with a lower-level control system (i.e., which drove the RO system to the operating state dictated as energy-optimal by the supervisory controller) was investigated [101]. This two-level control architecture allowed for modularity of the supervisory controller since its outputs of flow rate and pressure set-points are independent of the specific RO system control scheme; this latter responsibility is delegated to a lower-level controller, which can be customized for specific RO systems. The two-level control system was implemented in a pilot-scale single-stage RO system with successful demonstration of real-time optimization of SEC despite feed salinity fluctuations [101].

While previous studies focused on energy minimization of a single-stage RO process, implementing these approaches for a two-stage RO process is difficult since how the permeate production load, which is split between the two stages, can vary and impact the SEC. Typically, the permeate production load is distributed between individual stages at a split which ensures the same permeate flux across all the stages (i.e., to ensure sufficient crossflow velocity for both stages) [54, 70, 102, 103]. Lee et al. [103] ran field tests with a two-stage pilot-scale RO system (i.e., capable of processing up to 27 gal/min of feed water) at Buena Vista Water Storage District in Buttonwillow, California. Field tests lasted for approximately one and a half months and the feed water salinity varied from 3,500 to 8,400 mg/L. Lee et al. concluded that, with respect to energy, the use of lower rejection (i.e., higher permeability) membranes led to lower required operating feed pressures (i.e., with measured rejections of 96.3, 96.8, 97.3 and 97.8 % corresponding to RO feed pressures of 127.2, 131.1, 151.4 and 165.4 psi, respectively). Bartels et al. [54, 102] also proposed a two-stage RO configuration where different types of membranes are used for the two stages. These authors also concluded that using a lower rejection, higher permeability membrane in the second stage (i.e., 99.83% TD rejection in the first stage, 99.8%

total dissolved solids rejection in the second stage) resulted in a lower energy operation at the cost of permeate quality (i.e., when operation with lower rejection membranes were compared to operation with both stages with the higher rejection membranes, pressure was reduced from 819 psi to 758 psi but permeate TDS increased from 181 mg/L to 341 mg/L). It is noted that the above studies focused on optimizing the two-stage RO by equalizing flux between the two stages as facilitated by swapping out membranes. At present, however, there are no approaches which can be implemented on an already existing two-stage RO desalination system whereby real-time optimization of energy consumption can be attained within the system's physical constraints (i.e., imposed by its equipment which cannot be readily changed).

Chapter 3 Experimental Systems

3.1 Smart Integrated Membrane System for Seawater Desalination (SIMS-SD)

A pilot-scale RO desalination plant with a dedicated pre-filtration, integrated with the RO desalination unit, which was designed and constructed at UCLA, served as a testing platform for the various novel control approaches presented in this dissertation. The integration of the UF and RO was achieved by connecting the two whereby the UF filtrate is fed to the RO feed and the RO concentrate was used for UF backwash (**Figure 3.1**) [104]. This Smart Integrated Membrane System- Seawater Desalination (SIMS-SD) was capable of a permeate production capacity of 45.4 m^3/day (12,000 gallons/day). The UF pre-treatment system consisted of three hollow-fiber (inside-out) UF modules (Dizzer 5000+, Inge, Greifenberg, Germany) each containing 50 m^2 UF membrane elements. Each element was housed in a module that enabled inlet for feed or backwash outlet at either the module bottom or top. An array of actuators allowed for independent operation of each UF membrane module in either filtration or backwash mode. A self-cleaning 200 µm screen filter (TAF-500, Amiad, Mooresville, NC) was installed upstream of the UF unit. A centrifugal low-pressure UF pump (XT100 SS, 5 hp, Price Pump, Sonoma, USA) with VFD control (VLT AQUA Drive FC 202, 4.0 kW, Danfoss, Nordborg, Denmark) served for both UF feed and directing the UF filtrate to the RO feed pump. In-line coagulant dosing into the UF feed line was achieved using a dosing pump (DDA, Grundfos, Downders Grove, IL). Ferric Chloride ($FeCl_3$; Gallade Chemical, Santa Ana, CA) was selected for coagulation given its widespread use for filtration pre-treatment [105]. UF backwash was achieved with the RO concentrate delivered directly from the RO unit also making use of two hydraulic accumulators (Sentry C111ND, 370 cm^3 accumulator volume, Blacoh Fluid Control, Riverside, CA, USA).

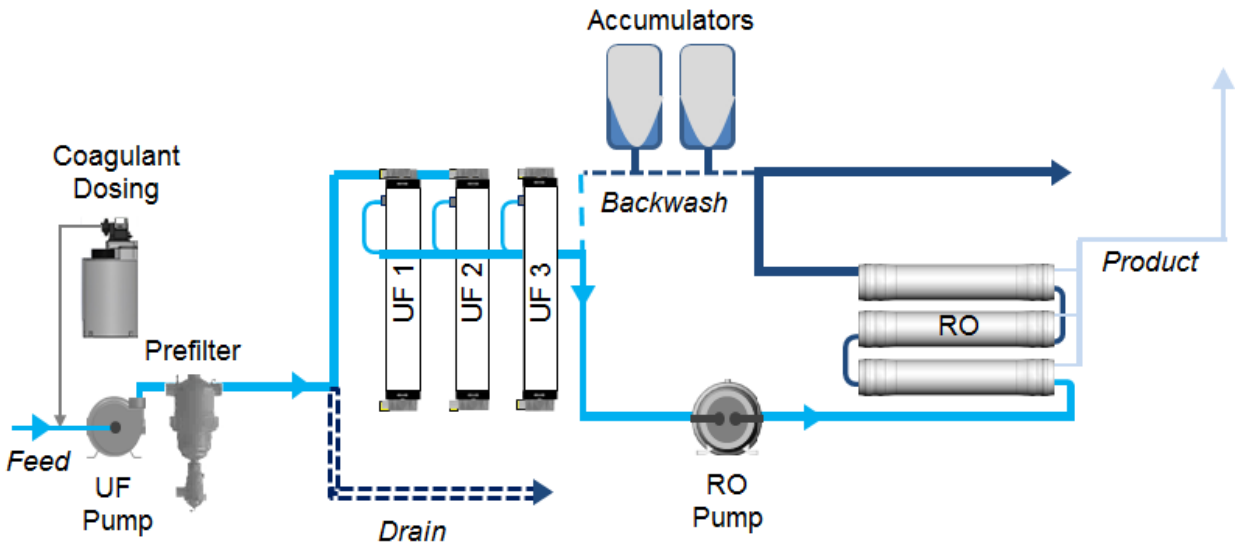

Figure 3.1. Process diagram of integrated UF-RO pilot plant. RO concentrate is used as the UF backwash water source.

The RO feed pump was a high-pressure axial piston positive displacement pump (APP 10.2, Danfoss, Nordborg, Denmark) with a premium efficiency motor (CEM4103T, 25 hp, TEFC, Baldor, Fort Smith, AR) and Variable Frequency Drive (VFD) control (VLT AQUA Drive FC 202, 22 kW, Danfoss, Nordborg, Denmark). A minimum manufacturer recommended pump inlet pressure of 137.9 kPa was specified in order to avoid cavitation. In addition, the RO feed pump is equipped with a sensor which cuts off power to the pump if the pump inlet pressure decreases below 50 kPa in order to prevent pump damage. The RO pump efficiency was 91.5% as determined in the present study and had a manufacturer-specified operational range of outlet flow and pressure of 66-170 L/min and 2-8 MPa, respectively. The above specified minimum pump feed flow rate and pressure were required in order to ensure adequate pump self-lubrication.

The UF filtrate was fed to the high pressure RO pump which then delivered the RO feed to three spiral-wound elements in series (Dow FILMTEC SW30HRLE-400, Dow, Edina, MN, USA). Each element was 8 inch diameter and 40 inch long housed in a fiberglass pressure vessel

(8" End Ported, Protec Arisawa PRO-8-1000-EP-1, Vista, CA) with a manufacturer-specified maximum operating pressure of 6.89 MPa (1000 psi). The manufacturer's reported RO element salt rejection was 99.65 % (at 32,000 ppm NaCl, 800 psi or 5.5 MPa) with a maximum water recovery per element of 15% enabling up to 38.6% total recovery with the three elements in series. An actuated needle valve (Mark 708LMO, Richard Industries, Cincinnati, OH), installed at the RO concentrate exit, along with the pump VFD, enabled control of both the feed pressure and flow rates.

The system was equipped with a network of various sensors (conductivity, pH, temperature, turbidity, and chlorophyll B), flow meters and pressure transducers interfaced with an embedded controller (cRIO-9022, National Instruments, Austin, TX USA) and data acquisition system.

The pilot plant was deployed at the NAVFAC Seawater Desalination Test Facility in the Naval Base Ventura County (Port Hueneme, CA, USA). Raw seawater feed was pumped from an open-sea intake through a strainer to the pilot plant. Feed salinity (33,440-36,800 mg/L total dissolved solids) and pH (7.5-8.2) varied within a relatively narrow range; however, variations of the feed total suspended solids (0.1-5.2 ppm), turbidity (0.4-14 NTU), and temperature (11.2-19.7 ^{o}C) were significant. The feed pretreatment system (200 μm screen filter and UF) provided water of turbidity $\lesssim$ 0.1 NTU which was sufficiently below the recommended maximum limit for RO desalting.

3.2 Smart Integrated Membrane System for Brackish Water Desalination (SIMS-BWD)

The SIMS-BWS is an integrated brackish water ultrafiltration (UF) – RO plant capable of two-stage brackish water RO operation and having permeate production capacity of up to 40,000 gallons/day. Raw feed water was drawn from a feed tank and pumped through the pre-treatment unit by a centrifugal low-pressure pump (CRNE5-6 A-P-G-E HQQE 2 HP, Grundfos,

Bjerringbro, Denmark). The raw feed water is first pre-treated by a 300 micron filter (2" Brushaway Filter, Amiad, Mooresville, NC). Water is then fed into the UF unit, which consisted of two multi-channel hollow-fiber (inside-out) UF elements (60 m^2 each; Dizzer XL 0.9 MB 60 W, Inge, Greifenberg, Germany). The UF filtrate is collected and stored in an intermediate tank.

The RO system consists of two RO membrane trains, a high-pressure feed pump, and an intermediate booster pump between the two membrane trains. The first-stage feed pump is a high pressure centrifugal pump (CRNE3-23 HS-P-GI-E-HQQE 10 HP, Grundfos, Bjerringbro, Denmark) designed for up to 600 psi output. A booster pump (CRN5-4 A-P-G-E-HQQE 1.5 HP, Grundfos, Bjerringbro, Denmark) pumps the UF filtrate into the first-stage feed pump inlet in order to provide sufficient inlet pressure for the high pressure pump. The intermediate booster pump (i.e., second-stage pump) is also a high pressure centrifugal pump (CRNE 1-23 HS HS-P-GI-E-HQQE 6.2 HP, Grundfos, Bjerringbro, Denmark). Both high-pressured pumps are equipped with variable frequency drives (VFDs) for control. The first RO stage consists of 14 4' brackish water RO membranes (TM710D, Toray, Poway, CA, USA), while the second RO stage consists of 7 4' seawater RO membranes (TM810V, Toray, Poway, CA, USA).

The RO system was equipped with a network of various sensors (conductivity, pH, temperature, and turbidity), flow meters, and pressure transducers interfaced with an embedded controller (cRIO-9022, National Instruments, Austin, TX USA) and data acquisition system. The process diagram of a two-stage RO desalination system and its primary process variables used for system control are illustrated in **Fig. 7.1**.

Chapter 4 Novel Design and Operational Control of Integrated Ultrafiltration – Reverse Osmosis System with RO Concentrate Backwash

4.1 Overview

In this chapter, a novel operational approach is presented for the operation of a reverse osmosis (RO) desalination system directly integrated with an ultrafiltration (UF) pre-treatment unit. The integration involved direct RO feed from the UF filtrate and UF backwash using the RO concentrate. This alignment reduces overall plant footprint, while the use of RO concentrate for UF backwash allows 100% UF recovery and implementation of flexible backwash strategies. The system design utilized a control scheme, whereby RO productivity can be prescribed independently of the UF system which self-adjusts to provide the RO system with its required feed flow rate at the specified RO pump inlet pressure. UF backwash, which was achieved via direct RO concentrate flow from the RO system, provided a continuous flow for sequential UF backwash which was additionally integrated with pulse backwash using a hydraulic accumulator. Seawater desalination field studies with the SIMS-SD (**Section 3.1**) successfully demonstrated the advantage of RO concentrate UF backwash that was triggered based on a membrane resistance threshold. The above self-adaptive UF backwash strategy significantly extended the projected UF operation period (by a factor of nine) to the threshold of required chemical cleaning.

4.2 Direct UF-RO Integration

Direct UF-RO system integration, in contrast with conventional UF-RO systems (**Figure 4.1**), involves feeding UF filtrate directly to the RO high pressure feed pump and RO concentrate directly for UF backwash (**Figure 4.2**). The need for a UF backwash pump is eliminated since

the RO concentrate is pressurized but throttled to a level that is suitable for UF backwash. It is noted that for an RO system with an energy recovery device (ERD), energy recovery would be set to a level that provides sufficient residual RO concentrate pressure for backwash. Direct UF-RO integration provides continuous RO concentrate flow (derived from UF operation at 100% recovery) and thus reduces the constraint on UF backwash period and frequency, thereby allowing for more flexible self-adaptive UF backwash strategies.

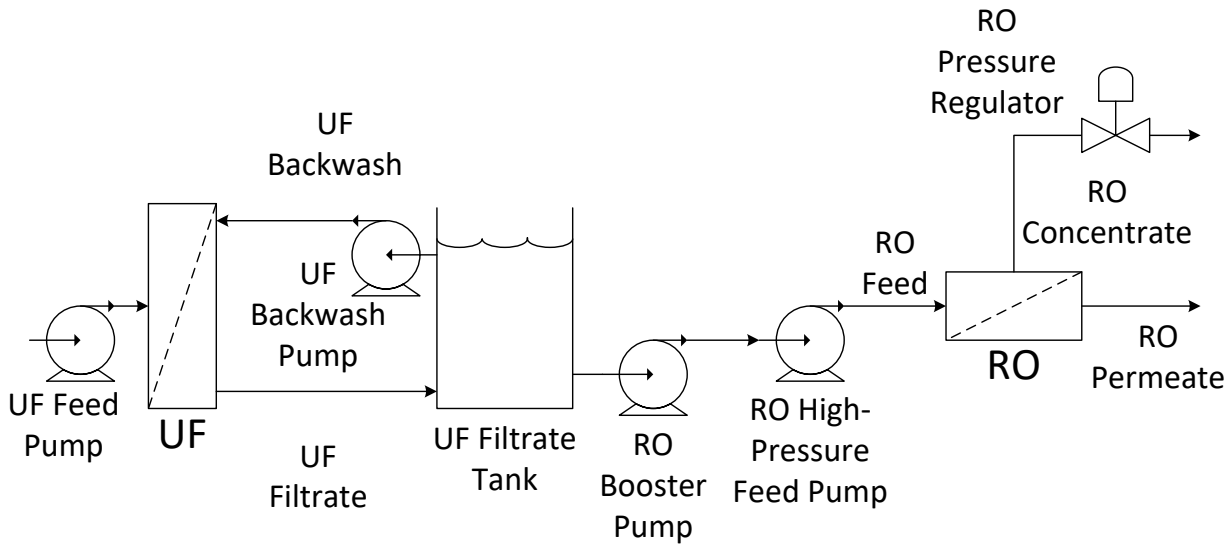

Figure 4.1. Process diagram of a conventional integrated UF-RO system design that utilizes an intermediate UF filtrate storage tank for UF backwash water, UF backwash pump, and RO booster pump.

UF membranes require periodic backwash during which the membrane modules being backwashed are not producing UF filtrate. Moreover, since the systems are dynamically coupled, unsteady-state UF operation will impact RO operation. Changes to the UF filtrate flow rate, which is equal to the RO feed flow rate, would require the RO system to adjust its operating parameters (e.g. RO feed pressure, recovery). Typically, it is preferred to operate RO systems at a set freshwater productivity target [84] and avoid frequent (or unnecessary) RO feed pressure changes that can result in telescoping of RO elements [70, 71]. Thus, for the operation of an

integrated UF-RO system, it is desirable to minimize fluctuations of RO operation (e.g., during UF filtration/backwash transitions).

It is generally accepted that effective UF backwash requires backwash flux that is approximately two to three times the UF filtrate flux for current UF elements [9, 106]. For a directly integrated UF-RO system (**Figure 4.2**), the UF filtrate flux (J_{UF}) is determined by the total UF filtrate flow rate (Q_{UF}), the total number of UF membrane modules in filtration mode (i.e., not being backwashed), and the active UF membrane area per module (A_m):

$$J_{UF} = \frac{Q_{UF}}{n \cdot A_m} \quad \textbf{4.1}$$

The steady-state UF backwash flux depends on the available RO concentrate flow rate, which is governed by the RO feed flow rate (equivalent to Q_{UF}), the RO water recovery (Y_{RO}), and the number of UF membrane modules in backwash (k)*:*

$$J_{BW,SS} = \frac{(1 - Y_{RO}) \cdot Q_{UF}}{k \cdot A_m} \quad \textbf{4.2}$$

The ratio of the steady-state UF backwash flux to the filtration flux can then be expressed as follows:

$$\frac{J_{BW,SS}}{J_{UF}} = (1 - Y_{RO}) \cdot \frac{n}{k} \quad \textbf{4.3}$$

For certain applications (e.g. high recovery operations), UF backwash with the RO concentrate stream cannot be achieved at or above the recommended $J_{BW,SS}/J_{UF}$ ratio of 2-3 (e.g. for a system with Y_{RO} = 60%, n = 3, and k = 1, $J_{BW,SS}/J_{UF}$ ratio is 1.2). Therefore, in order to maintain effective UF backwash during integrated UF-RO operation, it is critical to introduce a method of increasing the backwash flux (**Section 4.2.1.2**).

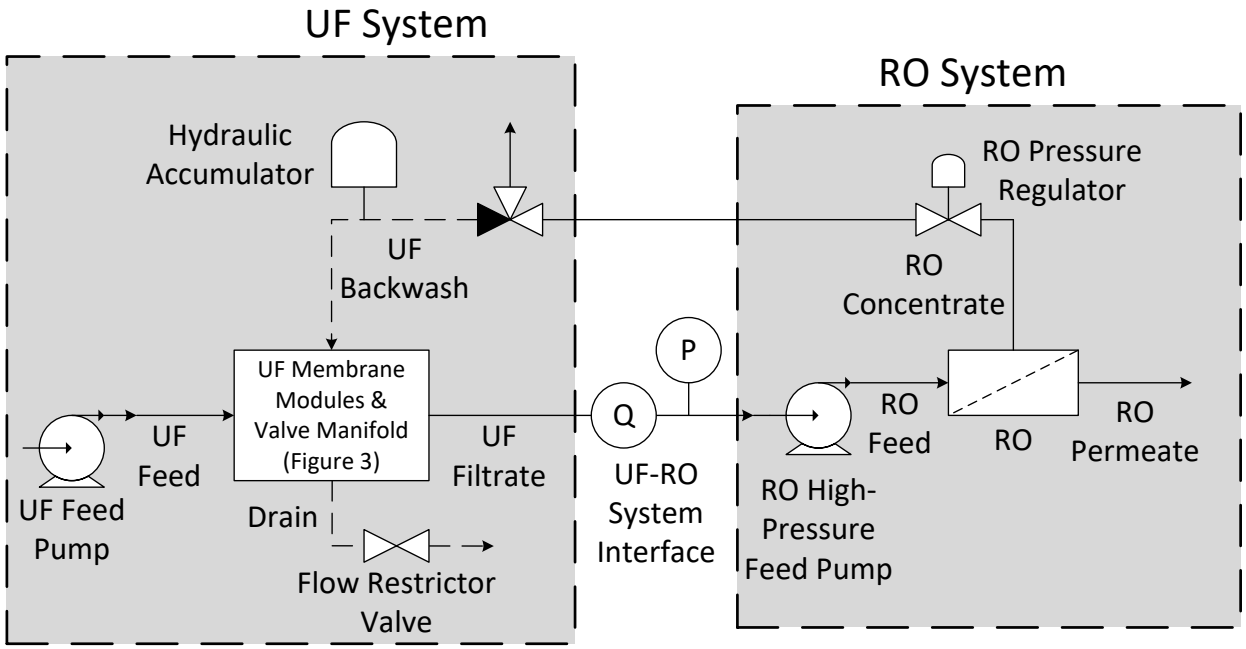

Figure 4.2. Process Diagram of a directly integrated UF-RO system. Flow rate (Q) and pressure (P) at the UF-RO system interface are maintained by the control system.

4.2.1 UF Backwash

4.2.1.1 UF System Valve Configuration

In order to maintain a constant RO feed flow rate during UF membrane backwash, the UF system requires membrane modules whose operation can be independently configured. In such a system (**Figure 4.3**), feed filtration can take place through all the UF modules simultaneously or through only some of the modules. At all times at least one or more of the UF units are in operation, at the required flux, in order to provide the RO system with its required feed flow rate. When backwash is initiated for specific UF modules, their operational mode is transitioned from filtration to backwash while the filtration flux for the remaining modules is increased to accommodate the required RO feed. The above transitions can be done in any order and for any

number of UF membrane modules as long as a reasonable number of UF membrane module remains in filtration mode to provide the needed RO feed.

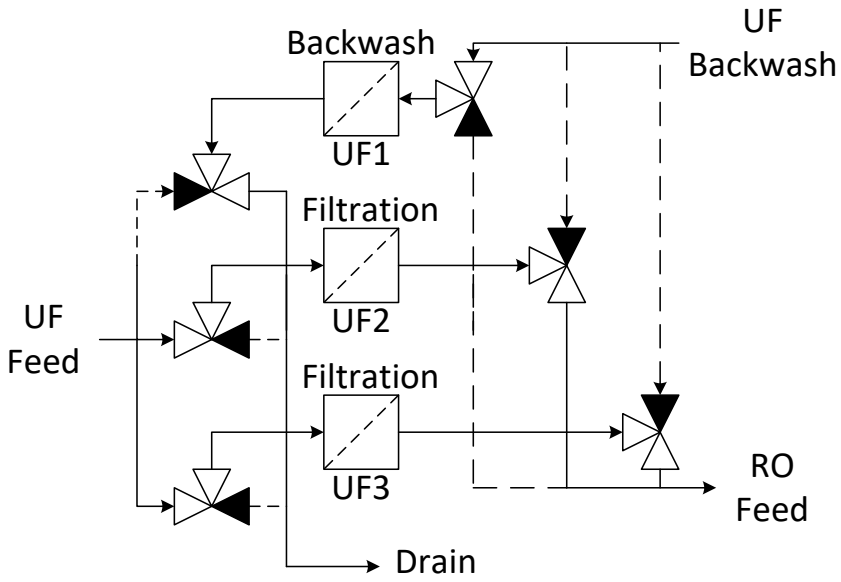

Figure 4.3. Process diagram of three independently configurable UF membrane modules. Note: Any single module (UF1, UF2, or UF3) can be backwashed while the others remain in filtration mode.

4.2.1.2 Pulse Backwash

A pulse of a high RO concentrate backwash flux, for enhancing the effectiveness of UF backwash, can be achieved using a hydraulic accumulator on the RO concentrate backwash line (**Figure 4.4**). During backwash operation, RO concentrate is partially diverted (by restricting backwash flow) to charge the accumulator. The accumulated RO concentrate is subsequently discharged into the backwash line to provide a short burst of high flow rate RO concentrate backwash. In the above approach, the total backwash flow rate, Q_{BW}, is the sum of the RO concentrate, Q_C, and accumulator discharge/charge, Q_A, flow rates:

$$Q_{BW} = Q_A + Q_A \qquad \textbf{4.4}$$

For RO operation at constant productivity and recovery *Qc* is time invariant while Q_A is an accumulator discharge flow rate that rises to a maximum to achieve a significant (short-term) increase of the overall UF backwash flow rate. The discharge flow rate from hydraulic accumulator is governed by the pressure decreases in the accumulator bladder where the gas undergoes essentially adiabatic expansion during the discharge period [107-109]. Therefore, one should expect a discharge flow rate that increases to a maximum and then decreases as the pressure in the accumulator decreases. Rapid filling of the accumulator with the RO concentrate and subsequent discharge are achieved via a fast-acting flow restrictor valve downstream of the UF backwash line. When engaged, the flow restrictor valve increases the RO backwash line pressure, thereby forcing concentrate to flow into the accumulator (i.e. value of Q_A is negative) and thus reducing Q_{BW} (i.e., the continuous portion of the backwash flow stream). Immediately after the accumulator is filled (indicated when the pressure P_A is at steady state; **Figure 4.4**), the flow restrictor valve is disengaged, causing a rapid pressure decrease and correspondingly discharge of the accumulated RO concentrate (i.e., typically charging takes ~30s, while discharging only lasts ~5s). Throughout the backwash pulse (i.e., accumulator filling/discharge cycle) the RO feed pressure is maintained via a feedback controller on the RO pressure regulator valve as described previously [110].

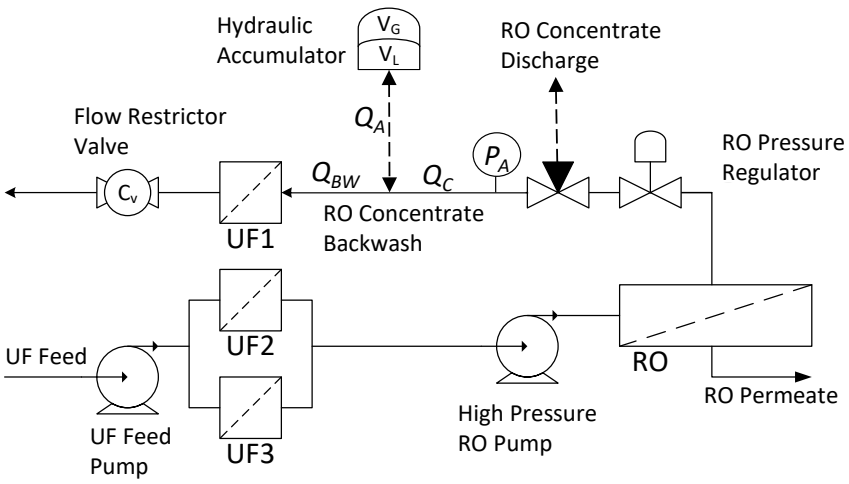

Figure 4.4. Process schematic for RO concentrate UF pulse backwash operation. A pulse of high concentrate flow rate (for UF backwash) is generated by a two-step sequential approach: a) engagement of flow restrictor valve to enable charging (i.e., filling) of the accumulator with RO concentrate, b) open flow restrictor valve to discharge RO concentrate from the accumulator. P_A: RO concentrate pressure (throttled); Q_C: RO concentrate flow rate; Q_{BW}: UF backwash flow rate; Q_A: flow out of the accumulator; V_G, V_L: gas and liquid volumes in the accumulator, respectively.

4.2.1.3 UF Self-Adaptive Backwash Triggering

UF backwash that is triggered by a set level of UF transmembrane pressure (TMP) has been shown to be more effective than fixed backwash frequency [32]. However, implementation of such a strategy in conventional UF-RO with an intermediate UF filtrate storage tank (**Figure 4.1**) has to consider: (a) the level of acceptable backwash effectiveness versus the reduction in UF productivity (i.e., due to utilization of UF filtrate), (b) balancing the flows of the UF feed, RO feed, and UF backwash streams, and (c) constraints on flux and its duration that are imposed by the finite water volume stored in the UF filtrate storage tank, thereby limiting the water volume available for UF backwash. In contrast, direct UF-RO integration with utilization of RO concentrate for UF backwash (without intermediate storage tanks) enables implementation of adaptive backwash with less strict constraints on backwash frequency and duration.

Reliance on variable backwashing strategy in which backwash is triggered when the UF membrane TMP exceeds a critical level is impractical for an integrated UF-RO. The reason for

the above is readily apparent when considering the relationship between UF filtrate flux (J_{UF}) and UF membrane TMP (ΔP_m) can be expressed using Darcy's law [111, 112]:

$$J_{UF} = \frac{Q_{UF}}{n \cdot A_m} = \frac{\Delta P_m}{\mu \cdot R_T} \quad , \quad R_T = \frac{n \cdot A_m \cdot \Delta P_m}{\mu \cdot Q_{UF}} \qquad \textbf{4.5}$$

where R_T is the total UF resistance (i.e., membrane and foulant layer) and μ is the water viscosity. As the membrane filtration flux changes (when membranes are taken off line for backwash, i.e., n in **Eq. 4.5** is reduced), the TMP must be increased to accommodate the needed RO feed flow. Therefore, the impact of fouling is not properly reflected by the TMP change. Therefore, for an integrated UF-RO system, the UF resistance, R_T, is a better metric for triggering backwash since it is an intrinsic function of the membrane and fouling resistances.

4.2.2 Control of the UF System

The UF system serves to pretreat the RO feed and thus the objective of its control system is to ensure that the UF filtrate flow rate required by the RO system is provided at the needed RO pump inlet pressure. A control scheme for regulating the above two control variables (UF filtrate flow rate and pressure) is illustrated in **Figure 4.5.** The RO control system regulates the RO feed flow rate subject to operational targets (e.g. productivity, recovery), thus dictating the flow rate through the entire system. The UF control system regulates the pressure at the UF-RO interface. This architecture allows the UF and RO control systems to be decoupled (**Figure 4.5**) despite the fact that the UF and RO system dynamics are coupled. For example, if the RO system mandates a RO feed flow rate adjustment (e.g. operator changes permeate productivity set-point), the flow rate through the entire system will change to match that value. Changes to the UF filtrate flow rate will affect operating pressures such as the UF TMP (**Eq. 4.5**), the difference between UF feed and UF filtrate pressures. Since the UF control system's set-point is at the RO pump inlet

pressure, the UF controller will change the UF feed pressure such that, irrespective of the UF TMP, the UF outlet pressure (i.e., RO pump inlet pressure), remains at the established set-point and the UF feed flow rate continues to provide the required RO feed flow rate. Similarly, if any of the UF modules undergo backwash operation, the RO system will continue to draw the same flow rate through the UF system. However, during backwash (i.e. membrane modules are taken offline) less UF membrane area is available for filtration; therefore, a greater pressure drop is required to increase the UF filtrate flux and maintain constant UF filtrate flow rate. Here also, the UF control system will respond by increasing the UF feed pressure so that despite the increase in pressure drop across the UF system, the RO pump inlet pressure will remain the same. Simultaneously, such control action also ensures that the UF filtrate flow rate remains unaltered despite the reduction in available membrane area (i.e., the filtration flux increases for membranes remaining in filtration mode). In both examples, when either the UF or RO is undergoing an operational change, the UF and RO control systems do not need to exchange processed sensor data. This architecture allows for a greatly simplified and modular UF-RO integration that requires only physical connections of the two systems.

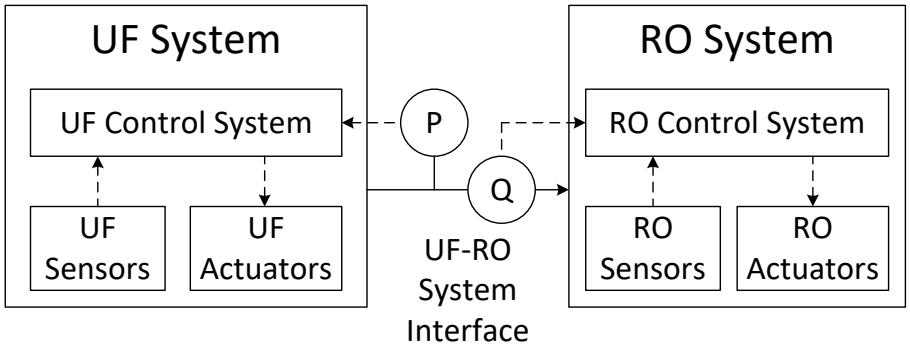

Figure 4.5. Illustration of a modular control architecture for an integrated UF-RO system, where the monitored flow rate (Q) and pressure (P) at the UF-RO interface are inputs to the decoupled UF and RO controllers, respectively.

4.3 Experimental

4.3.1 Control of RO Pump Inlet Pressure

A transition from UF operational mode (*n* membrane modules configured for filtration) to backwash mode (*n-k* membrane modules configured for filtration, where *k* is the number of UF modules undergoing backwash and where *n>k*) results in RO pump inlet pressure decrease (**Section 4.2.2**). This pressure decline could fall below the manufacturer recommended limit and can result in cavitation. In order to avoid such a pressure decline, a proportional-integral (PI) feedback controller was implemented for the UF pump VFD. The RO pump inlet pressure was set as the controlled variable for the feedback controller as per the PI control relation:

$$VFD_{SP}^{UF} = K_p\big(P_{SP} - P(t)\big) + \frac{K_p}{\tau_i}\int_0^t \big(P_{SP} - P(\tau)\big)d\tau \qquad \textbf{4.6}$$

in which VFD_{SP}^{UF} is the control action applied to the UF VFD in rpm, P_{SP} is the pressure set-point for the RO pump inlet pressure, K_p is the proportional gain, and τ_i is the integral time constant. The Ziegler-Nichols method was used and the PI control parameters were determined to be K_p = 0.798 $\frac{Valve\,\%}{KPa}$ and $\frac{K_p}{\tau_i}$ = 0.1 s.

4.3.2 UF Self-Adaptive Backwash

Self-adaptive backwash triggering using overall UF membrane resistance (i.e. average resistance of 3 membrane modules), R_T, was implemented in the pilot UF-RO plant (**Section 4.2.1.3**). In self-adaptive mode, filtration for any given cycle is allowed to proceed until the incremental total resistance increase for a given cycle, ΔR_T, reaches a set threshold ε (i.e. maximum allowable UF resistance increase). Backwash was triggered when

$$\Delta R_T = R_T\left(t_{0,i} + \Delta t\right) - R_T\left(t_{0,i}\right) > \varepsilon \qquad \textbf{4.7}$$

where $R_T(t_{0,I} + \Delta t)$ is the UF membrane resistance at time Δt after the beginning of a filtration cycle, and $R_T(t_{0,i})$ (i.e. $R_{T,i}$ for short) is the UF membrane resistance at the beginning of a filtration cycle. $R_T(t_{0,i})$ at $i = 1$ (i.e. first filtration cycle) is defined as R_m, the resistance of the clean membrane. UF backwash effectiveness can be ascertained by the degree of cumulative increase in overall resistance with progressive filtration/backwash cycles. Residual fouling, which cannot be removed by simple backwash (i.e. often termed irreversible fouling), typically occurs for desalination of most water sources (e.g., due to the strong adsorption of organic matter present in seawater including extracellular polymeric substances [113] and possibly pore-plugging [114]). When the overall resistance increases to the extent that the upper operating pressure limit for the UF membranes is reached, chemical cleaning in place (CIP) is typically required. Clearly, more effective backwash will lead to less residual fouling after each backwash and thus will retard the rate of increase of overall membrane fouling with progressive filtration/backwash cycles. In this regard, the goal of effective self-adaptive backwash strategy is to lower the rate of increase of $R_{T,i}/R_m$ and increase the operational period before CIP is required. More effective backwash will be indicated by a lower slope of $R_{T,i}/R_m$ versus time curve. In the current study, preliminary experiments were carried out, with UF backwash triggering at various resistance thresholds, revealing that ε=1.36·10^{11} m^{-1} was adequate for the present UF system as it enabled operation with at the lowest rate of normalized UF resistance ($R_{T,i}/R_m$) increase.

In the present implementation of self-adaptive backwash, upon backwash triggering each of the three membrane modules are taken offline and backwashed in a sequential order. Accordingly, at any given time during the backwash period, two modules are always in filtration mode. Upon backwash triggering the first membrane module is put into backwash mode; once backwash is concluded the module is transitioned back to filtration operation. The above process

is then applied sequentially to the second and then third module. Once all three modules have been backwashed, a new filtration period begins and all three membrane modules remain in filtration mode until the next backwash period is triggered; a complete filtration and backwash sequence is considered a filtration cycle.

4.3.3 Field Study

The directly integrated UF-RO pilot plant was deployed at the NAVFAC Seawater Desalination Test Facility in the Naval Base Ventura County (Port Hueneme, CA, USA). Raw seawater feed was pumped from an open-sea intake through strainer to the UF-RO pilot plant. The feed salinity (33,440-36,800 mg/L total dissolved solids) and pH (7.5-8.2) varied within a relatively narrow range; however, variations of the feed total suspended solids (0.1-5.2 ppm), turbidity (0.4-14 NTU), and temperature (11.2-19.7 ^{o}C) were significant. The feed pretreatment system (200 μm screen filter and UF) provided water of turbidity $\lesssim$ 0.1 NTU which was well below the recommended maximum limit for RO desalting [115]. Field tests included demonstration of the UF-RO control system, particularly the decoupled nature of the UF and RO control systems and its ability to maintain adequate RO pump inlet pressure during various UF transitions. Subsequently, the effectiveness of UF pulse backwash using RO concentrate delivered from the RO system to the UF unit was evaluated. Self-adaptive backwash that includes the above strategy was also implemented and its effectiveness was compared with the use of self-adaptive freshwater (i.e., RO permeate) backwash.

4.4 Results & Discussion

4.4.1 Performance of the Integrated UF-RO System Control Strategy

The performance of the integrated UF-RO system control strategy, based on the control system architecture described in **Figure 4.5** and **Section 4.2.2**, was assessed from the observed dynamic system responses to various UF and RO controllers' set-point changes. First, the pilot plant was operated without control action to demonstrate why dynamic pressure control of the UF-RO interface is essential for the operation of an integrated UF-RO system. Operational parameters were set at an RO feed flow rate of 75.7 L/min and RO pump inlet pressure of 137.9 kPa. The UF feed pump VFD was operated at a constant RPM without control action. When the UF system was transitioned from filtration to backwash, the number of UF membrane modules in filtration decreases from 3 to 2 and an increase in UF TMP was expected due to the decrease of membrane area available for filtration. Without control action, the UF feed pressure remained constant; thus when UF TMP was increased, the UF outlet pressure, or the RO pump inlet pressure, decreased (**Figure 4.6a**). For this specific experiment, when the transition from filtration to backwash occurs, the pressure decreased rapidly within 2 seconds from 137.9 kPa to 43.43 kPa, which caused a pump shut down (i.e. shut down threshold of below 50 kPa) (**Section 3.1**) as evidenced by the RO pump RPM going to zero (**Figure 4.6b**).

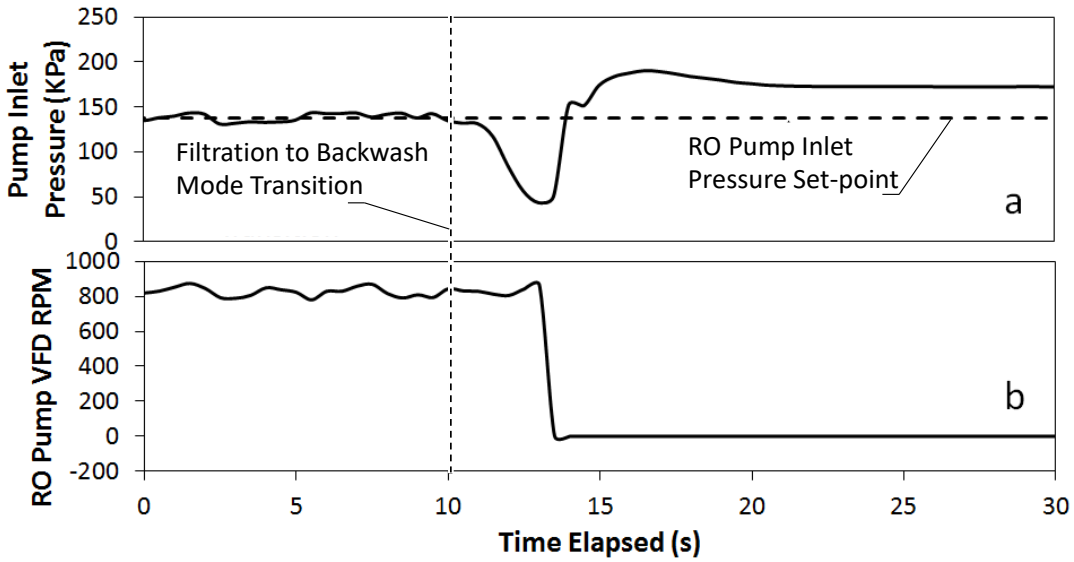

Figure 4.6. Illustration of time profiles of (a) RO pump inlet pressure and (b) RO pump VFD RPM during a transition from filtration (three modules filtering) to backwash mode (two modules filtering) without any control action. UF inlet flow rate was set to 75.7 L/min.

The above illustration of the integrated UF-RO operation indicate that control of the UF-RO interface pressure (i.e. RO pump inlet pressure) is critical and accordingly the proposed control scheme as described in **Sections 4.2.2 and 4.3.1** was implemented and tested. Illustration of the control system performance is shown in **Figure 4.7**, where the RO feed flow rate set-point was changed from 90.7 L/min to 77.29 L/min (change induced by the RO controller) for a set RO operation at 35% recovery and RO pump inlet pressure, or UF filtrate pressure set-point of 137.9 kPa. The RO recovery was maintained through control of RO feed flow rate and RO feed pressure as described in an earlier study [110]. As expected, the RO inlet pressure increased somewhat (by up to ~5 kPa, for ~20 sec) due to the decreased system flow rate leading to a decrease in UF TMP. However, the UF feedback controller effectively adjusted (via reduction of the UF feed pump motor speed) the pressure to the set-point RO pump inlet pressure constant.

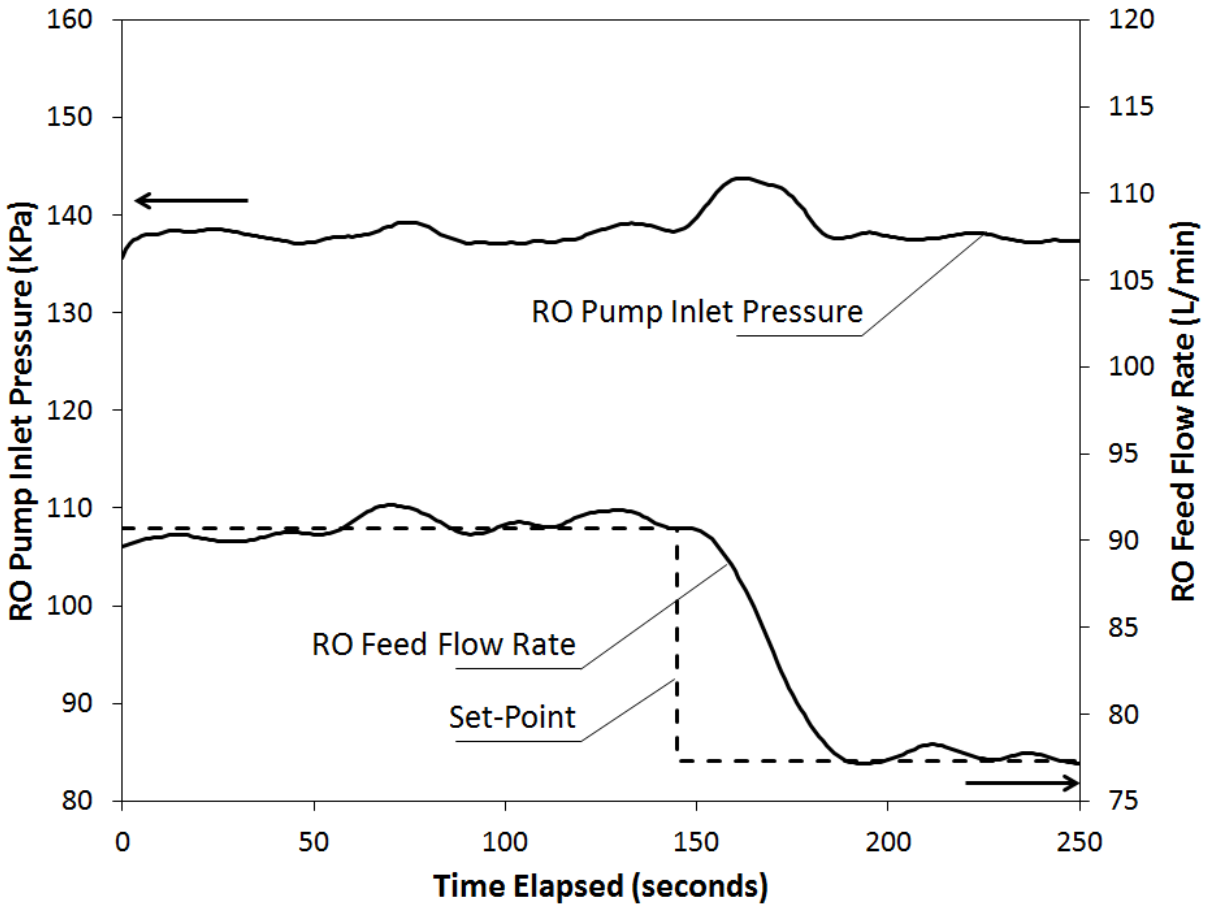

Figure 4.7. Effect of RO feed flow rate set point change on the time profiles of the RO pump inlet pressure and RO feed flow rate. UF inlet flow rate was changed from 90.7 L/min to 77.29 L/min.

In a subsequent experiment, the ability of the UF controller to handle filtration/backwash UF transitions that affect the RO pump inlet pressure was demonstrated. In this test self-adaptive backwash triggering was implemented based on the UF membrane resistance as described in **Section 4.3.2**. The operation of the RO unit was at a set feed flow rate of 75.7 L/min and permeate recovery of 35%. The RO pump inlet pressure set-point of 137.9 kPa was maintained by the UF controller. During filtration mode, the flow rate through each membrane module was 25.2 L/min (flux of 10.1 L/m^{2}h), while during backwash (with two membranes modules in filtration mode), the flow rate through each module was 37.9 L/min (flux 15.1 L/m^{2}h). A sharp rise in the TMP is apparent upon transition from filtration to backwash (**Figure 4.8b**). In contrast,

the progressive increase in UF membrane resistance was a clear indication of progressive fouling. Moreover, this metric is not altered by the flux change imposed when other membranes are being placed in backwash mode. In addition, as shown in **Figure 4.8c**, the RO pump inlet pressure was effectively maintained at its set-point despite the repeated filtration/backwash transitions.

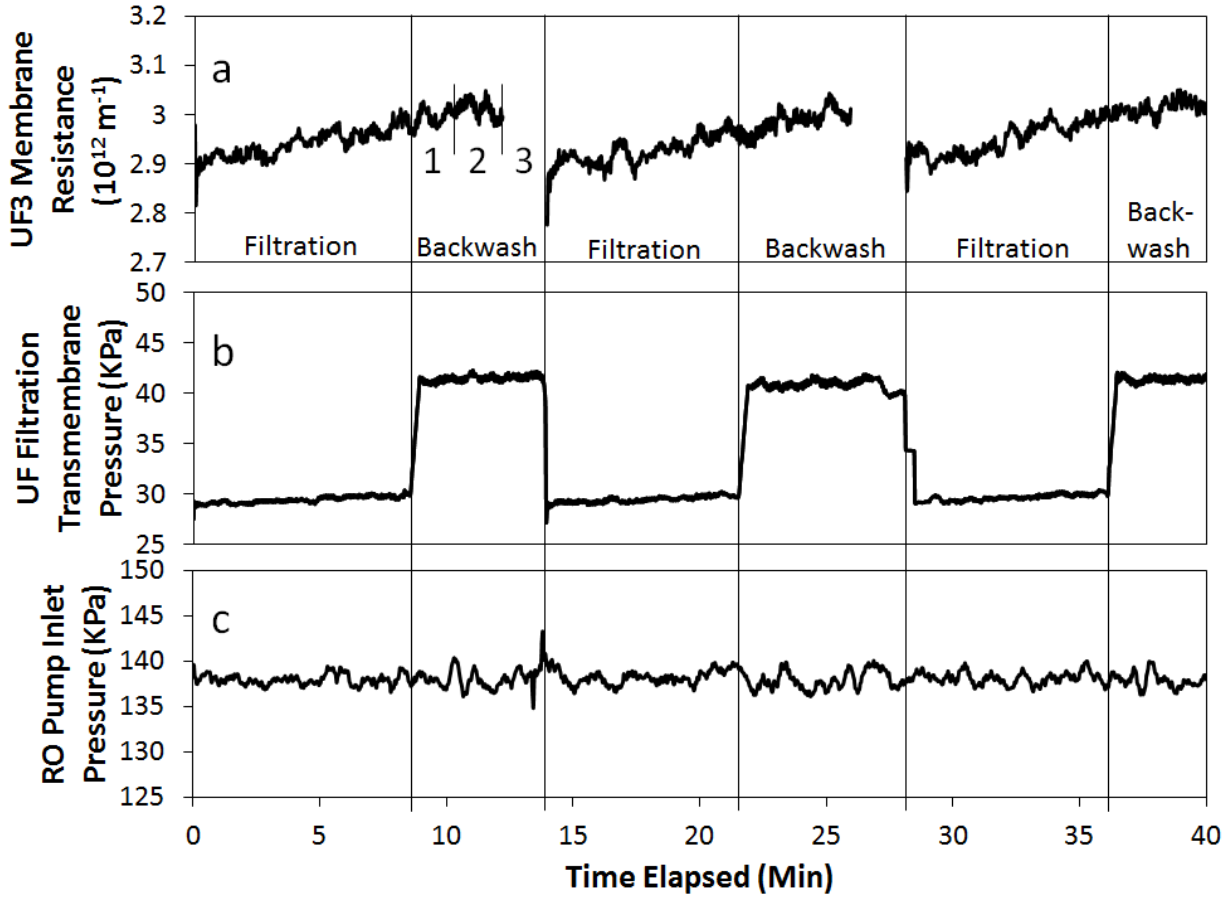

Figure 4.8. (a) UF3 module resistance, (b) UF transmembrane pressure, and (c) RO pump inlet pressure (at a set point of 137.9 kPa) during three consecutive filtration-backwash cycles. During each UF backwash period, only two membrane modules are filtering at any given time as the modules are backwashed sequentially one at a time (indicated by the numbers 1, 2, and 3 in a), resulting in temporary elevation of overall UF filtrate flux and thus UF trans-membrane pressure (in b). It is noted that the gap in (a) is due to the fact that UF 3 filtration resistance is not measured when UF 3 is being backwashed. Disturbances resulting from UF backwash operations are overcome by the control actions of the UF controller maintaining a stable RO pump inlet pressure. (RO operation at 35% recovery for feed flow rate of 4.54 m^3/h; UF filtration flux: 10.1 L/m^2h and 15.1 L/m^2h during filtration (3 modules) and backwash (2 modules) modes, respectively).

4.4.2 UF Pulse Backwash using RO Concentrate

An evaluation of the suitability of pulse backwash for enhancing the UF backwash flux was undertaken with the seawater desalination system operating at 30% recovery for RO feed flow rate of 167.5 L/min, For the above operation, UF filtrate flux during filtration with all three modules was 67.0 L/m^{2}h. The maximum attainable backwash flux, via direct use of RO concentrate flow from the RO system was 140.6 L/m^{2}h (**Eq. 4.2**), which was significantly below the manufacturer recommended UF backwash flux of 230 L/m^{2}h [106]. Backwash flux enhancement can be achieved with a hydraulic accumulator as illustrated in **Figure 4.9**. As the accumulator is charged (typically over a period of ~40 s) the continuous concentrate backwash flux (**Section 4.2.1.2**; **Figure 4.9**) decreases initially, but then was restored as the accumulator was fully charged. Upon discharging accumulator, the attained pulse backwash flux was above the manufacturer recommended value, increasing up to a maximum value (287.6 L/m^{2}h) being a factor of 4.3 above the filtration flux.

Although the high backwash flux was achieved for a short period it was effective for achieving effective UF backwash that restored membrane permeability and prevented progressive irreversible fouling. A demonstration of the benefit of using the pulsed backwash is shown in **Figure 4.10** for operation over a period of about 8 days. Two separate tests (with and without pulse UF backwash) were conducted with the RO unit operating at the same condition as in the previous experiment. For UF backwash operation without a pulse the backwash period was set to 3 minutes. UF backwash with a pulse was carried out with 2 pulses (each lasting ~40 s) followed 2 minutes of direct RO concentrate backwash. In both cases the UF unit was operated in a self-adaptive mode for backwash triggering (**Section 4.2.1.3**). Comparison of the normalized UF resistance ($R_{T,i}/R_m$) with and without pulse backwash (**Figure 4.10**) clearly indicates

progressive fouling for the latter operation due to ineffective backwash. In contrast, after an initial stabilization period (within ~ 48 h), the normalized UF membrane resistance did not appreciably change remaining at a value of 1.15 ± 0.05. It is noted that by the end of the test period the normalized UF membrane resistance for operation without pulse backwash was about 26% higher than operation employing with pulse backwash. The above test demonstrates that, even with self-adaptive operation, pulse backwash is essential for effective UF backwash.

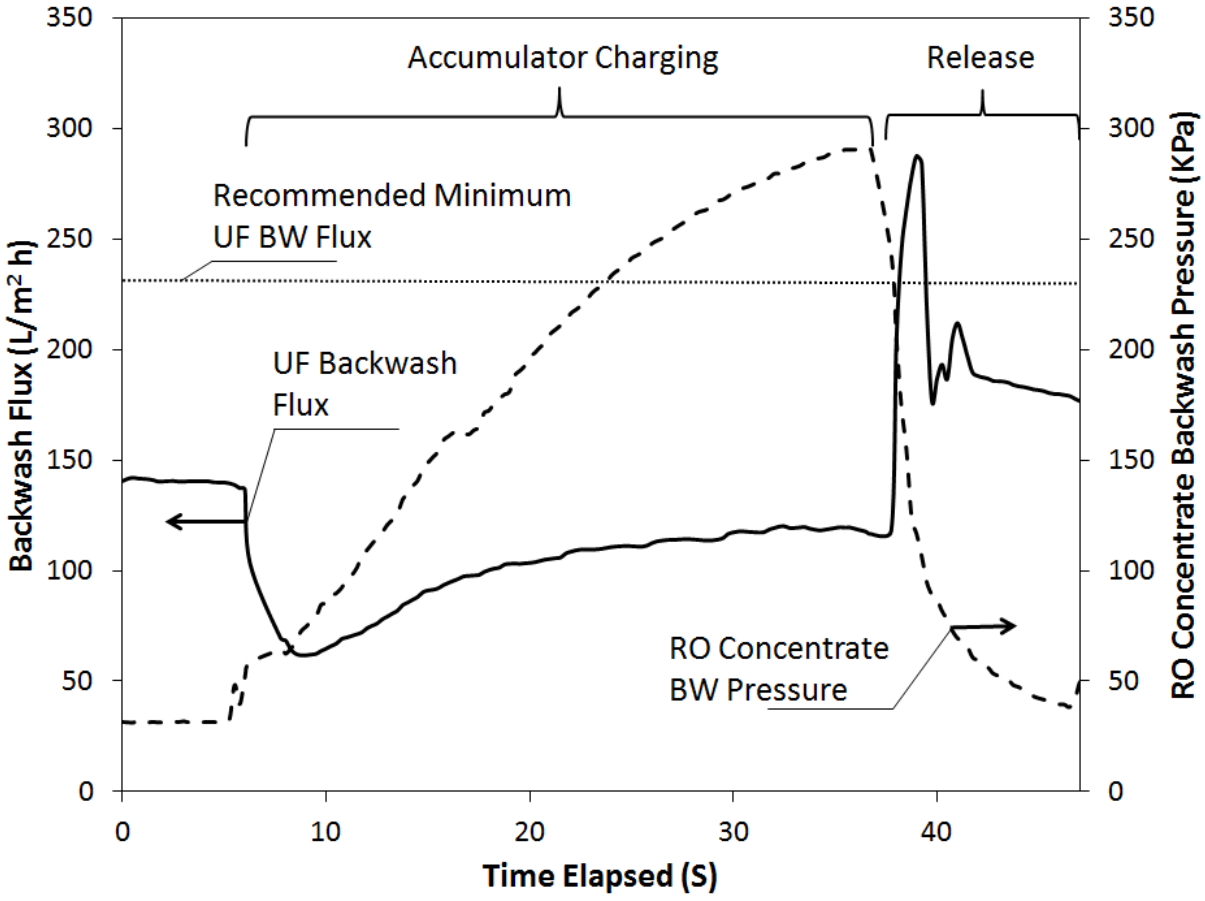

Figure 4.9. UF backwash (BW) flux for a single UF module and pressure during a pulse backwash operation using RO concentrate. Accumulator charging via flow restriction (Fig. 4) and discharge actuated by opening of the restrictor valve enables generation of a rapid pulse of high flow rate (~239.7 L/min equivalent to backwash flux of 287.6 L/m^{2}h) of RO concentrate for UF backwash, resulting in total backwash flux a factor of 4.3 times above the recommended minimum. It is noted that the backwash flux and pressure during the first 5s are for direct backwash with the RO concentrate, at a RO concentrate flow rate of 117.3 L/min or backwash flux of 140.6 L/m^{2}h.

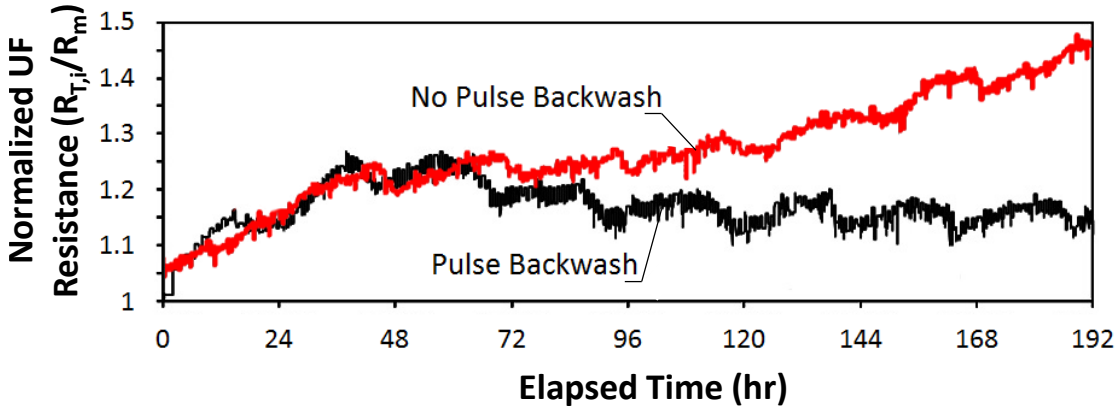

Figure 4.10. Comparison of the effect of RO concentrate backwash with and without pulse generation on the evolution of UF resistance (normalized with respect to the initial value). Operation of integrated UF-RO plant for seawater desalination (UF feed flow rate: 4.54 m^3/h; RO recovery: 35%).

4.4.3 Effectiveness of Self-Adaptive Backwash Strategy

The effectiveness of self-adaptive UF backwash (**Section 4.2.1.3)** with pulse backwash was evaluated in three comparative field test: (i) RO concentrate UF backwash at a fixed frequency of backwash triggering every 18 min (constant backwash), (ii) RO concentrate UF backwash with self-adaptive backwash triggering (self-adaptive backwash), and (iii) freshwater (i.e., RO permeate) UF backwash for a duration of 30s at a flux equal to the maximum attainable pulse backwash flux (287.6 L/m^2h), also with self-adaptive backwash triggering (freshwater backwash). In tests (i) and (ii) UF backwash consisted of two pulses (~ 40 s each) followed by 2 minutes of direct RO concentrate backwash. For experiment (i), a backwash triggering frequency of 18 minutes was selected to match the average backwash frequency for experiment (ii) with self-adaptive backwash. It is noted that test (i) was terminated earlier than the other two tests in order to protect the UF membranes given the significantly higher fouling rate in test (i). In test (iii), a backwash duration of 30s was chosen based on preliminary runs since this was the shortest

duration that resulted in the lowest rate of UF resistance increase. For the above tests the UF feed flow rate was 75.7 L/min and the RO operation was at 35% recovery.

Results for the above three tests (**Figure 4.11**) showed that UF membrane resistance increased, essentially linearly, with time. It is noted that the UF membrane modules have a maximum (manufacturer-specified) operating ΔP_m limit of 20 psi [106], which, when only two modules are filtering (flux of 45.42 L/m^{2}h) the maximum allowable normalized UF resistance is 3.1. For UF operation with self-adaptive RO concentrate pulse backwash, the UF system would be expected to operate for approximately 3,433 hours (~143 days, or ~4.8 months) before reaching the above operational limit. Operation at a fixed UF backwash frequency with RO concentrate was estimated to enable operation of up to 381 hours before reaching the above operational limit. For self-adaptive UF operation with freshwater backwash, UF operation up to 4,919 hours (~ 205 days, or ~6.8 months) would have been possible. Considering that chemical cleaning would be necessary once the operational pressure limit (or maximum allowable resistance) have been reached, the projected operating duration (before chemical cleaning was required) is 901% longer with self-adaptive RO concentrate pulse backwash than with constant (fixed frequency) backwash. The projected operating duration was 143% higher with self-adaptive freshwater backwash over the self-adaptive RO concentrate backwash. However, it is important to recognize that freshwater backwash effectively lowered the overall water recovery of the UF-RO system to 24.5% (i.e. compared to 35% when using RO concentrate for backwash) and thus increased the overall energy consumption per volume of produced permeate by about 40%.

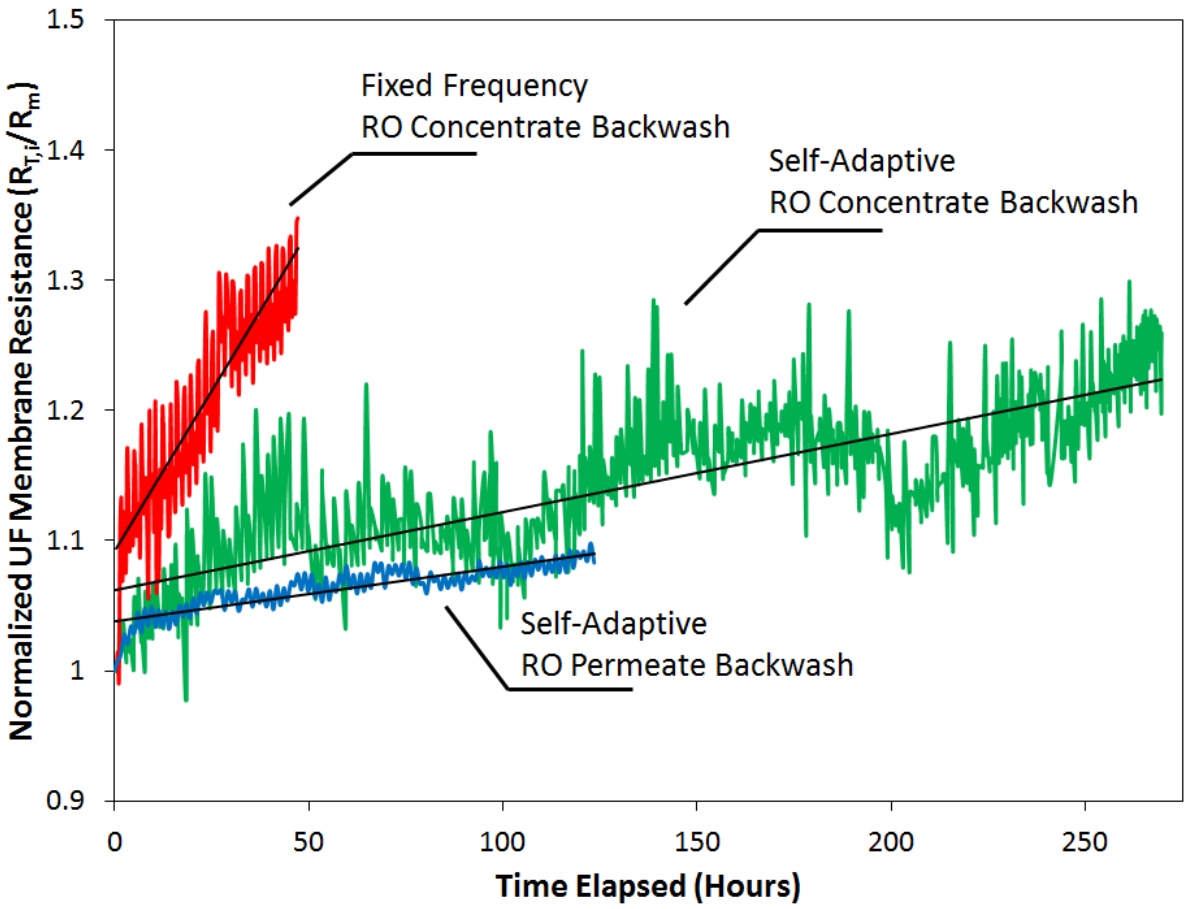

Figure 4.11. Comparison of the effects of three different UF backwash strategies on the progression of UF resistance (normalized with respect to the initial value) in seawater desalination operation for the integrated-UF-RO system (UF feed flow rate: 4.54 m3/h; RO recovery: 35%).

4.5 Summary

A novel RO desalination system was developed that directly integrates UF pretreatment of RO feed whereby UF backwash is accomplished using the RO concentrate. This direct integration reduces the overall system footprint through elimination of intermediate storage tanks and UF backwash pump which also reduces associated maintenance costs, while allowing for flexible and effective UF backwash strategies. Given the unique decoupling of the RO and UF systems control, RO productivity can be set independently of the UF system which is able to

autonomously adjust and provide the RO system with the required RO feed and at the set inlet RO pump pressure. Self-adaptive backwash in the present system was implemented by integrating direct diversion of RO concentrate from the RO system for continuous and sequential backwash with pulse backwash using a hydraulic accumulator. It is noted that while self-adaptive backwash with RO permeate was somewhat more effective than with RO concentrate, this approach resulted in reduced permeate production (~35%). Seawater desalination field studies demonstrated that triggering of UF backwash with RO concentrate, based on a membrane resistance threshold, was superior to fixed frequency backwash extending the projected UF operation from about 16 to 143 days before requiring CIP. Further enhancement of UF filtration and backwash effectiveness by integrating coagulation with the present self-adaptive UF backwash.

Chapter 5 Self-Adaptive Cycle-to-Cycle Control of In-line Coagulant Dosing in Ultrafiltration for Pre-Treatment of Reverse Osmosis Feed Water

5.1 Overview

This chapter presents a real-time self-adaptive approach to in-line UF coagulant dosing and its field demonstration in an integrated UF-RO seawater desalination system (SIMS-SD, **Section 3.1**). The coagulant controller, which tracks the UF resistance during filtration and backwash, adjusts coagulant dose to the UF feed with the objective of reducing the incremental cycle-to-cycle UF post-backwash (PB) resistance change (i.e., Δ_n). Real-time tracking the above UF resistance metrics, as well as the rate of change of Δ_n with coagulant dose, enabled the controller to quantify the progression of both irreversible fouling and UF backwash effectiveness. The above information was then utilized by the controller to make the appropriate coagulant dose adjustment. Field tests of the proposed self-adaptive coagulant dosing approach demonstrated measurable coagulant dose reduction while maintaining robust UF operation even during periods of both mild and severe water quality degradation.

5.2 Self-Adaptive Cycle-to-Cycle Coagulant Dose Controller

5.2.1 UF and backwash performance metrics

UF operation consists of successive filtration cycles, defined as the duration of a filtration period and of the subsequent UF backwash period. During a filtration period, filtered matter (e.g., particles, colloids, and bacteria) in the feed water is retained on the UF membrane surface or within its pores, forming a foulant layer which gradually increases in thickness. The impact of

the foulant layer is typically quantified by UF resistance to fluid permeation through the UF module:

$$R_T = \frac{\Delta P_m}{\mu \cdot J_{UF}} \qquad \textbf{5.1}$$

where R_T is the total UF resistance (i.e., membrane and foulant layer), ΔP_m is the UF transmembrane pressure, μ is the water viscosity, and J_{UF} is the UF filtrate flux. The resistance as determined in **Eq. 5.1** was normalized to 20^{o}C following the recommended correction factor [106] for the specific UF modules used in the present study (i.e., $R_{T=20^{o}C} = R_T \exp\left[0.019(T-20)\right]$).

As filtration proceeds, coagulant is added to the feed stream at a constant dose rate (e.g., ppm) and the overall UF membrane resistance increases. UF backwash is triggered once the resistance reaches a critical level or after a prescribed time period. Upon the completion of a given UF module backwash, the module is reverted back to filtration mode. Illustrations of UF membrane resistance during UF operation are shown schematically in **Figure 5.1**. The change in UF PB resistance for cycle *n* (i.e., also equivalent to the initial UF resistance for cycle *n+1*) relative to the previous cycle (*n-1*) is expressed as $\Delta_n = R_n - R_{n-1}$.

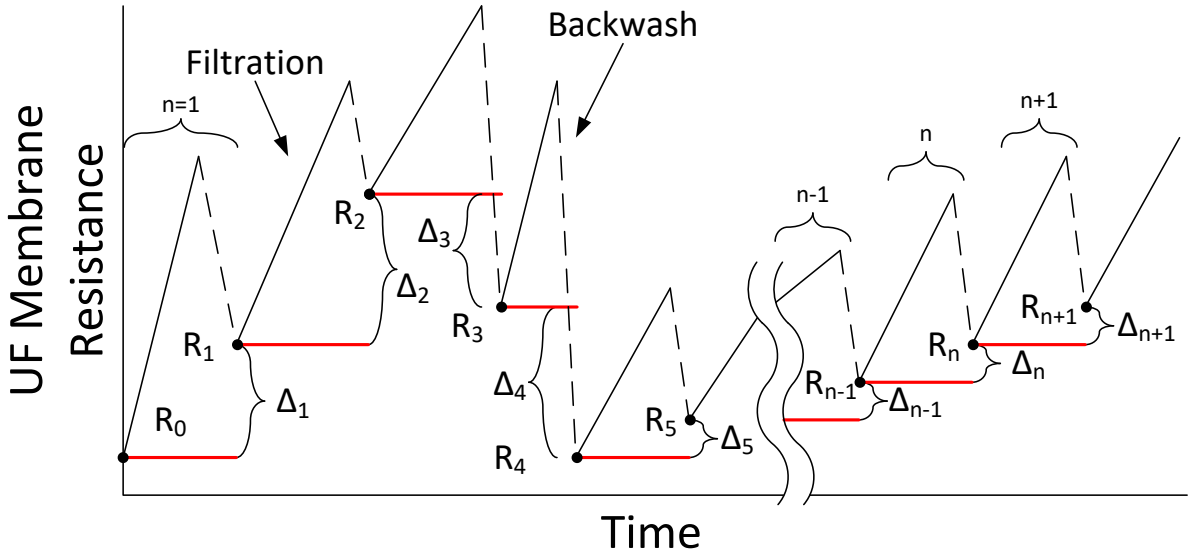

Figure 5.1. An illustration of UF membrane resistance-time profiles for multiple filtration/backwash cycles. R_n is the UF post-backwash (PB) resistance for filtration cycle *n* (i.e., also same as the initial UF resistance for cycle *n+1*). A given cycle *n* begins with UF resistance of R_{n-1} and ends after backwash with UF resistance of R_n. The cycle-to-cycle change in UF post-backwash (PB) resistance for cycle *n* relative to the previous cycle (*n-1*) is defined as $\Delta_n = R_n - R_{n-1}$. Cycles *n* = 1-2 are examples of the build-up of unbackwashed UF resistance, which resulted in positive values of Δ_n. Cycles 3-4 illustrate situations where previously unbackwashed resistance is removed, resulting in negative Δ_n values.

The cycle-to-cycle change in UF PB resistance as quantified by Δ_n governs the rate of UF PB resistance trajectory during UF operation. An illustration of the implication of Δ_n tracking is provided in **Figure 5.1** for a hypothetical series of UF cycles. A decrease in Δ_n, signifies improved backwash effectiveness and/or reduction in the cycle-to-cycle buildup of membrane fouling resistance, while an increase in Δ_n indicates reduced backwash effectiveness and greater rate of foulant buildup on the membrane. Values of Δ_n can be positive (e.g., the typical case as illustrated for Δ_n, for cycles *n*=1-3 and *n-1* through *n+1* in **Figure 5.1**) or negative (e.g., Δ_4 and Δ_5 in **Figure 5.1**) indicating increased fouling (i.e., buildup of unbackwashed resistance) or effective backwash that result in removal of previously unbackwashed foulant buildup, respectively. When the overall system UF operation is such that $\Delta_n > 0$ is the dominant behavior then the unbackwashed UF resistance will gradually increase. The slower UF resistance increase

is apparent for cycles *n-1* through *n+1* (i.e., lower Δ_n) compared to operation during cycles 1-3. UF operation with such gradual resistance increase will typically be allowed to continue until chemical cleaning will be required (i.e., when the prescribed resistance or transmembrane pressure threshold for the UF operation limit is reached) in order to restore the membrane to its original clean state. Given the above, the overall coagulant control strategy is to reduce Δ_n in order to reduce the rate of increase of unbackwashed (i.e., or irreversible) UF fouling and reduce the frequency of chemical cleaning.

5.2.2 Coagulant dose adjustment strategy and control logic

Based on previous UF studies [17, 22, 28, 78], which demonstrated that increasing coagulant dose improves backwash effectiveness, it can be argued that Δ_n is expected to decrease with increasing coagulant dose (i.e., UF backwash effectiveness improves and UF fouling is reduced as coagulant dose increases) up to a critical threshold above which Δ_n is not appreciably affected. The latter regime is where coagulant dose is at a high level where it no longer impacts UF backwash effectiveness. Accordingly, two distinct regions are expected with respect to the dependence of Δ_n on coagulant dose: a) a region where an increase in coagulant dose leads to decreased Δ_n hereinafter is termed the "underdosed region," and b) a region in which the coagulant dose is at or above a certain critical threshold (i.e., no further improvement in Δ_n with increased dose) designated as "overdosed region." The quantitative functional behavior of the above trends (i.e., an example is shown in **Section 5.4.1**) is expected to be specific for the UF system configuration and capacity and for the given source water quality. Accordingly, in the present approach, the objective is to adjust the coagulant dose such that there is proper reduction or increased coagulant dose in the underdosed region. Moreover, system drift to the overdosed region is detected and where the appropriate control action is to reduce the coagulant dose.

In order to determine the required coagulant dose adjustment, the present control approach is to monitor Δ_n for each filtration/backwash cycle as impacted by the coagulant dose. This information is then utilized to establish the appropriate coagulant dose change as per the logic flow chart of **Figure 5.2** (additional specific details of the algorithm are provided in flow chart in the **Section 5.6**). As described previously (**Section 5.2.1**), the condition of $\Delta_n > 0$ signifies an incremental buildup of unbackwashed foulant that adds to the accumulated foulant layer. When the above condition is encountered for the current cycle (*n*) and the previous one (*n-1*) (i.e., $\Delta_n > 0$ and $\Delta_{n-1} > 0$), the control system first determines the difference in cycle-to-cycle change in UF PB resistance (i.e., Δ_n relative to Δ_{n-1}) with respect to the coagulant dose quantified as $\delta = \frac{\Delta_n - \Delta_{n-1}}{u_n - u_{n-1}}$, where u_n and u_{n-1} are the coagulant doses that impact cycles *n* and *n-1*, respectively. The parameter δ, which is a measure of the slope of Δ_n vs u_n and termed hereinafter the resistance-dose (RD) factor, is essentially a first order sensitivity of Δ_n with respect to u_n. If $\delta = 0$ this indicates that a cycle-to-cycle change coagulant dose did not produce a measurable difference in the cycle-to-cycle change in UF PB resistance (i.e., $\Delta_n - \Delta_{n-1} = 0$). Therefore, the controller concludes that the system is in the overdose region (with respect to coagulant dose) and thus the coagulant dose is decreased. If, however, it is determined that $\delta < 0$ and where $\Delta_n - \Delta_{n-1} > 0$ (i.e., backwash effectiveness is declining due to the decrease in coagulant dose and/or increased in feed water fouling potential) then UF operation is determined to be in the underdosed region (since $u_n < u_{n-1}$) with respect to the coagulant dose (see **Figure 5.2**). The controller action is then to increase the coagulant dose in order to improve backwash effectiveness. For the same conditions of $\delta < 0$ if $\Delta_n - \Delta_{n-1} < 0$ (i.e., cycle-to-cycle decrease in the incremental buildup of unbackwashed resistance) given the increasing coagulant dose (i.e., $u_n > u_{n-1}$), the control action is continue increasing the coagulant dose so as to further improve backwash effectiveness. The

condition of $\delta > 0$ can also arise when: (a) $\Delta_n - \Delta_{n-1} < 0$ (e.g., due to improvement in backwash effectiveness and/or improved feed water quality) while the coagulant dose is decreased (i.e. $u_n < u_{n-1}$). Thus, the appropriate control action is to further reduce the coagulant dose; and (b) Coagulant dose is increasing $u_n > u_{n-1}$ but the incremental buildup of unbackwashed UF is rising, (i.e., $\Delta_n - \Delta_{n-1} > 0$) which suggests that the coagulant dose is too low and thus the control decision is to increase the coagulant dose.

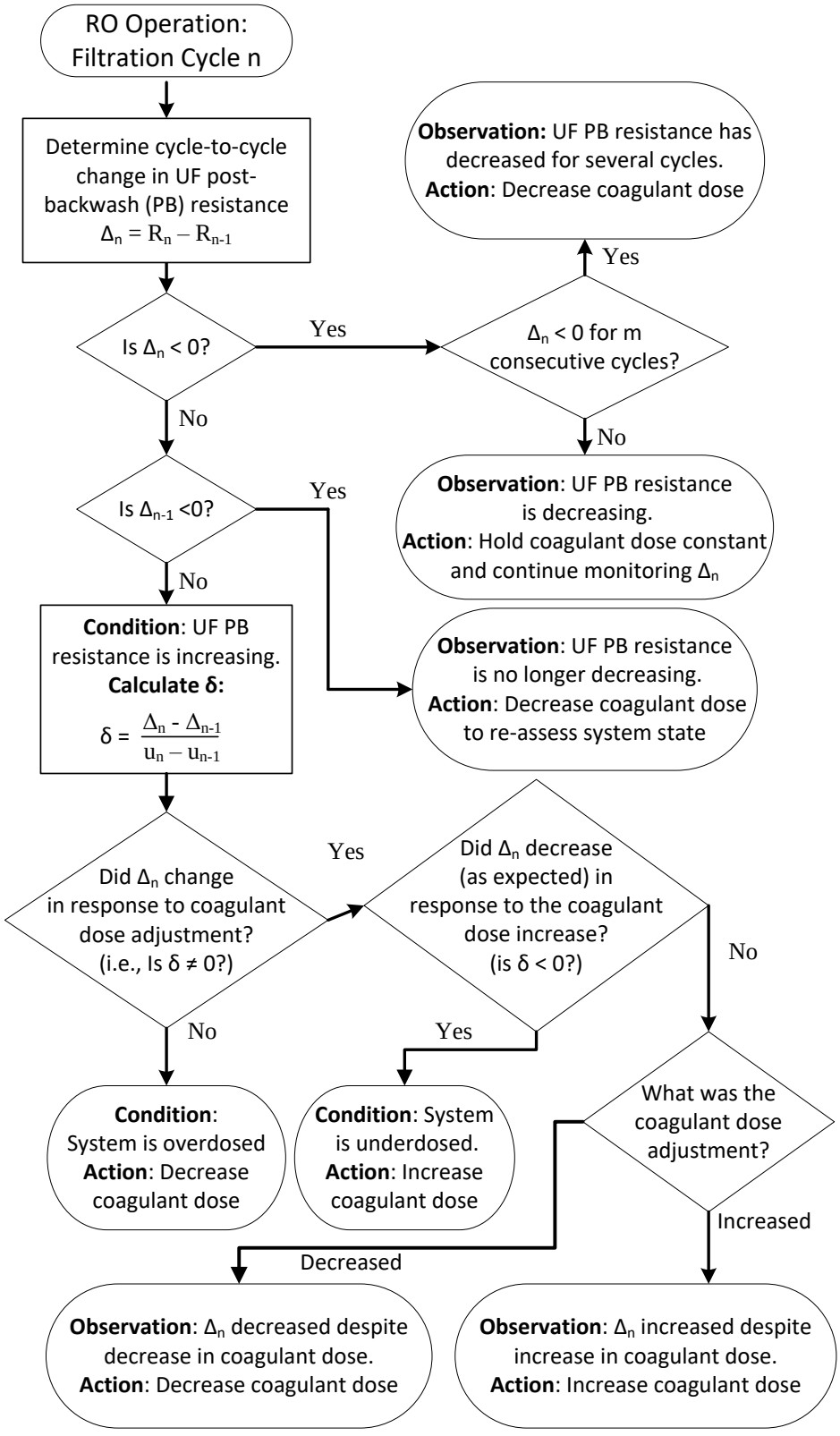

Figure 5.2. A flow diagram of the self-adaptive coagulant control logic. Upon completion of a given filtration cycle *n*, the cycle-to-cycle change in UF resistance (Δ_n) is determined to establish the appropriate control action.

It is generally expected that the accumulated unbackwashed fouling will increase over the period of UF operation (i.e., $\Delta_n > 0$). However, it is also possible for the UF PB resistance to decrease (i.e., $\Delta_n < 0$) under certain conditions (i.e., when previously unbackwashed foulant is removed). The logical control action is to keep the coagulant dose unchanged. Here we note that, in principle, one can employ a conservative control action by decreasing the coagulant dose once the trend of $\Delta_n < 0$ persists for a prescribed number (m) of cycles. It is noted that in the situation where $\Delta_n > 0$ and where the previous performance was such that $\Delta_{n-1} < 0$, a control action to change the coagulant dose must be undertaken to avoid a situation where δ cannot be calculated (i.e., since potentially $u_n = u_{n-1}$); a conservative control action is to reduce (rather than increase) the coagulant dose so as to avoid inadvertent overdosing.

5.2.3 Coagulant dose controller

The control strategy as described in **Section 5.2.1** was implemented as a coagulant dose controller shown schematically in **Figure 5.3**. In this control scheme, the coagulant dose change that may be required for a new cycle ($n+1$) is determined based on information regarding the impact of the dose change on UF PB resistance as quantified by Δ_n, u_n and δ. It is noted that in a practical setting, inevitable process variability and sensor noise must be considered with respect to establishing the coition for δ being above, below or at zero. Accordingly, in the present coagulant controller implementation a threshold ε is introduced such that when $\delta < -\varepsilon$, $-\varepsilon < \delta < -\varepsilon$ or $\delta > \varepsilon$ the RD factor (**Section 5.2.2**) is considered negative, vanishingly small (i.e. ~ 0) or positive, respectively.

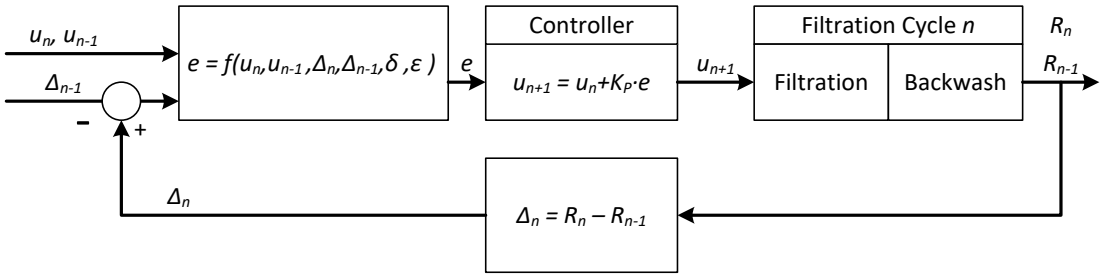

Figure 5.3. Illustration of the control system for a self-adaptive coagulant dose controller. The detailed controller implementation can be seen in **Figure 5.10**.

The control algorithm is specified as per the following relation:

$$u_{n+1} = u_n + K_P \cdot e(u_n, u_{n-1}, \Delta_n, \Delta_{n-1}, \delta, \varepsilon) \qquad \textbf{5.2}$$

in which K_P is the proportional gain (i.e., $K_P > 0$) and the function e takes on the values of +1, -1 or 0 corresponding to the control action of coagulant dose increase, decrease or no-action based on the categories described in **Section 5.2.1**,

$$e(u_n, u_{n-1}, \Delta_n, \Delta_{n-1}, \delta, \varepsilon) = \begin{cases} 1. & 0, & \text{if} & \Delta_n < 0 \\ 2. & -1, & \text{else if} & \Delta_n \geq 0 \;\&\; \Delta_{n-1} < 0 \\ 3. & +1, & \text{else if} & \delta < -\varepsilon \\ 4. & -1, & \text{else if} & -\varepsilon \leq \delta \leq \varepsilon \\ 5. & \text{sgn}(u_n - u_{n-1}), & \text{else if} & \delta > \varepsilon \end{cases} \qquad \textbf{5.3}$$

in which conditions 1 and 2 are for cases when the condition of $\Delta_n < 0$ or Δ_{n-1}, while conditions 3-5 apply when $\Delta_n > 0$ (**Section 5.2.1**, **Figure 5.1**). The proportional gain, K_P, which is the incremental dose change set by the controller, can be tuned with initial UF field performance data with respect to coagulant dose (**Section 5.4.1**). It is critical for the proportional gain to provide sufficient incremental coagulant dose increase that will materialize in observed change in UF backwash performance. A reasonable value for K_p can be established based on series of short-term UF filtration/backwash tests at different coagulant dose as detailed in **Section 5.4.1**. If needed, K_P can be refined throughout the course of UF operation based on the history of

variation of UF backwash effectiveness with coagulant dose, along with sensor input regarding feed water quality (i.e., turbidity, fluorescence).

5.3 Field studies and demonstration of coagulant dose control strategy

For the duration of this study, the UF system was operated in a self-adaptive mode whereby backwash was triggered based on a maximum allowable resistance of $1.36 \cdot 10^{11}$ m^{-1} as described in a previous study [104] with a typical filtration cycle being about 16-22 minutes. It is noted that the UF modules were operated in dead-end filtration mode and given that UF backwash was with the RO concentrate, UF recovery was maintained at 100%. The UF filtration resistance was recorded at a frequency of 1 Hz. The UF PB resistance for a given cycle *n* (i.e., the initial UF resistance for cycle *n+1*) was taken as the average of the first 60 data points post-backwash. UF backwash was accomplished sequentially such that when one membrane module was being backwashed, the other two remained in filtration mode, but with increased operational flux in order to ensure that the RO system was provided with uninterrupted feed flow at the prescribed level [104]. Filtration with the UF modules (positioned in the vertical configuration) was also alternated between top filtration (i.e., UF module fed from top) and bottom filtration (i.e., UF module fed from bottom). The UF PB resistance used by the controller was then averaged over eighteen complete filtration/backwash cycles (i.e., consisting of three sets of sequential filtration/backwash for the three UF modules).

Pilot plant experiments were first carried out (**Section 5.4.1**) with the objective of arriving at a preliminary quantification of the impact of coagulant dose (0-4.9 mg/L Fe^{3+}) on the cycle-to-cycle change in UF PB resistance (Δ_n) (**Section 5.2.1**). The pilot plant was operated at feed flow rate of 75.7 L/min with the UF filtration flux being 15.1 L/m^2h and with self-adaptive backwash triggering along with pulse backwash as described in [104]. These short-term (i.e., each of 5-6

hours duration) tests were conducted in order to establish the existence of the coagulant underdosed and overdosed regions and the control action thresholds for establishing whether a change in Δ_n can be considered to be significant (**Section 5.2.2**). Subsequently, a series of field tests were conducted with UF operation at two different constant coagulant doses (1.9 and 4.1 mg/L Fe^{3+}). These were followed by a series of field demonstrations (i.e., duration of 70 - 140 hours) of the effectiveness of UF operation with real time coagulant dose control.

5.4 Results & Discussion

5.4.1 Coagulant dose regimes and coagulant controller tuning

The impact of coagulant dose on the change in UF PB resistance (Δ_n) was evaluated in a series of short-term experiments (**Figure 5.4**) revealing, consistent with previous coagulation studies [28], the existence of: (a) an underdosed (i.e., low coagulant dose) region, where Δ_n decreases linearly with respect to coagulant dose, and (b) an overdosed (i.e., high coagulant dose) region where Δ_n is invariant with respect to coagulant dose. The short-term experiments were carried out at a UF system operated at a flux of 15.1 L/m^2h and RO system seawater desalting at recovery of 30%. The system was operated for 18 filtration cycles for each coagulant dose value. A fixed frequency backwash strategy where a backwash was triggered every 20 minutes was used. UF backwash consisted of two pulses (~ 40 s each) followed by 2 minutes of direct RO concentrate backwash.

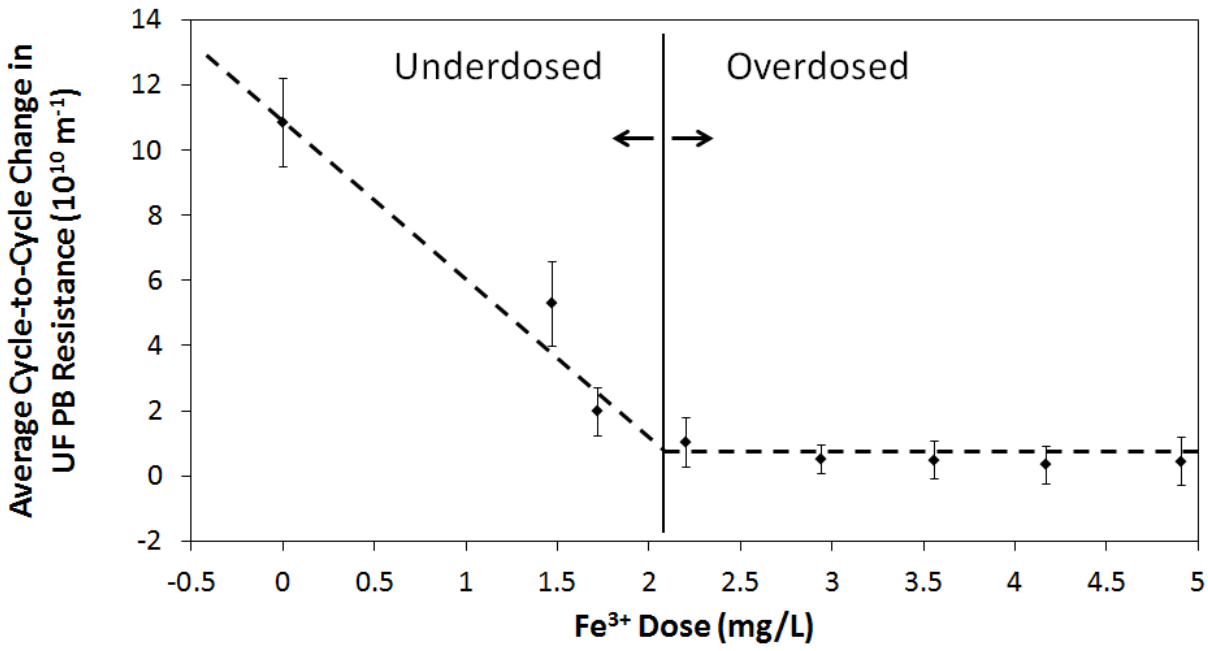

Figure 5.4. The averaged cycle-to-cycle change in UF PB resistance (Δ_n) with respect to coagulant ($FeCl_3$) dose. At low coagulant dose, Δ_n decreases with increasing coagulant dose. Above a critical dose of about 2.1 mg/L Fe^{3+}, Δ_n is insensitive to further increase in coagulant dose. The UF system operated at a flux of 15.1 L/m^{2}h and RO system seawater desalting at recovery of 30%. The system was operated for 18 filtration cycles for each coagulant dose value.

Based on the filtration runs at different coagulant doses, the value of Δ_n at a given dose (obtained from multiple runs) was determined within a standard deviation of $\sigma = 1.128 \cdot 10^{-10}$ m^{-1}. A change in Δ_n equivalent to σ in the underdosed region (**Figure 5.4**) would be expected to be due to a coagulant dose change of 0.241 ppm Fe^{3+} (**Figure 5.4**). Therefore, the controller proportional gain, K_P, was set to the above value. A significant change in backwash effectiveness is considered to have occurred if the change in Δ_n relative to Δ_{n-1} is such that $|\Delta_n - \Delta_{n-1}| > \sigma$ and where this change occurs due an incremental dose change of K_p. Accordingly, the RD factor threshold (**Eqs. 5.2** and **5.3**) is set to $\varepsilon = \sigma / K_P$. In principle, one can establish a strategy of refining K_p as feed water quality varies and long-term performance data are accumulated (i.e., gain scheduling). It is stressed that such an approach, however, will not change the essence of the controller but can serve to increase or decrease the rate at which the coagulant dose adjustment

responds to changes in UF backwash effectiveness. In the current study, a K_p that is sufficiently low, but adequate for producing a measurable change in Δ_n (i.e., when in the underdosed region), was selected for a conservative UF coagulant dose adjustment in order to avoiding unintended overshoot of coagulant dose.

5.4.2 Impact of coagulant dose on continuous UF/RO operation

The impact of a coagulant dose on UF performance was initially evaluated over a 10 day field operation for which water turbidity and chlorophyll varied as shown in **Table 5.1**. The pilot plant was operated at UF average module filtration flux of 15.1 L/m^{2}h (overall UF feed flow rate of 76 L/min), with the RO unit operating rate at recovery of 30%. Self-adaptive backwash triggering was implemented as described previously (**Section 4.2.1.3**). Each UF backwash consisted of two pulses (~ 40 s each) followed by 2 minutes of direct RO concentrate backwash.

During the first 90 hours, at constant coagulant dose of 1.9 mg/L Fe^{3+} to the UF feed, noticeable UF and RO performance deterioration was encountered (**Figure 5.5**). UF membrane resistance increased by 38% relative to the beginning of operation, while RO membrane permeability decreased by 8%. At t=90 h the coagulant dose was increased to 4.1 mg/L Fe^{3+} (i.e., a dose level utilized in a previous long-term desalination study at the same location [104]) and a dramatic performance improvement was observed for both the UF and RO units. Backwash effectiveness improved as indicated by UF resistance decreasing, within 20 hrs, to a level of only 12% above the initial value; the above UF performance improvement is attributed to removal of some of the previously unbackwashed UF foulants. UF performance at the higher coagulant dose remained relatively stable for the remainder ~ 8 days of the field test illustrating the well accepted knowledgebase that proper coagulant dose is critical to ensuring robust UF and in turn RO operations. It is emphasized that at the above high (constant) coagulant dose, and with

variability of field water source quality and absent coagulant dose control, UF operation was likely (and unnecessary) in the overdosed region (**Figure 5.4**) over portions of the test period.

Table 5.1. Source water turbidity and chlorophyll *a* during the test period

Water Quality	Average	Standard deviation	Range
Turbidity (NTU)	2.98	± 2.44	0.29 - 83.26
Chlorophyll *a* (RFU)	74.6	± 15	9.7 - 269.1

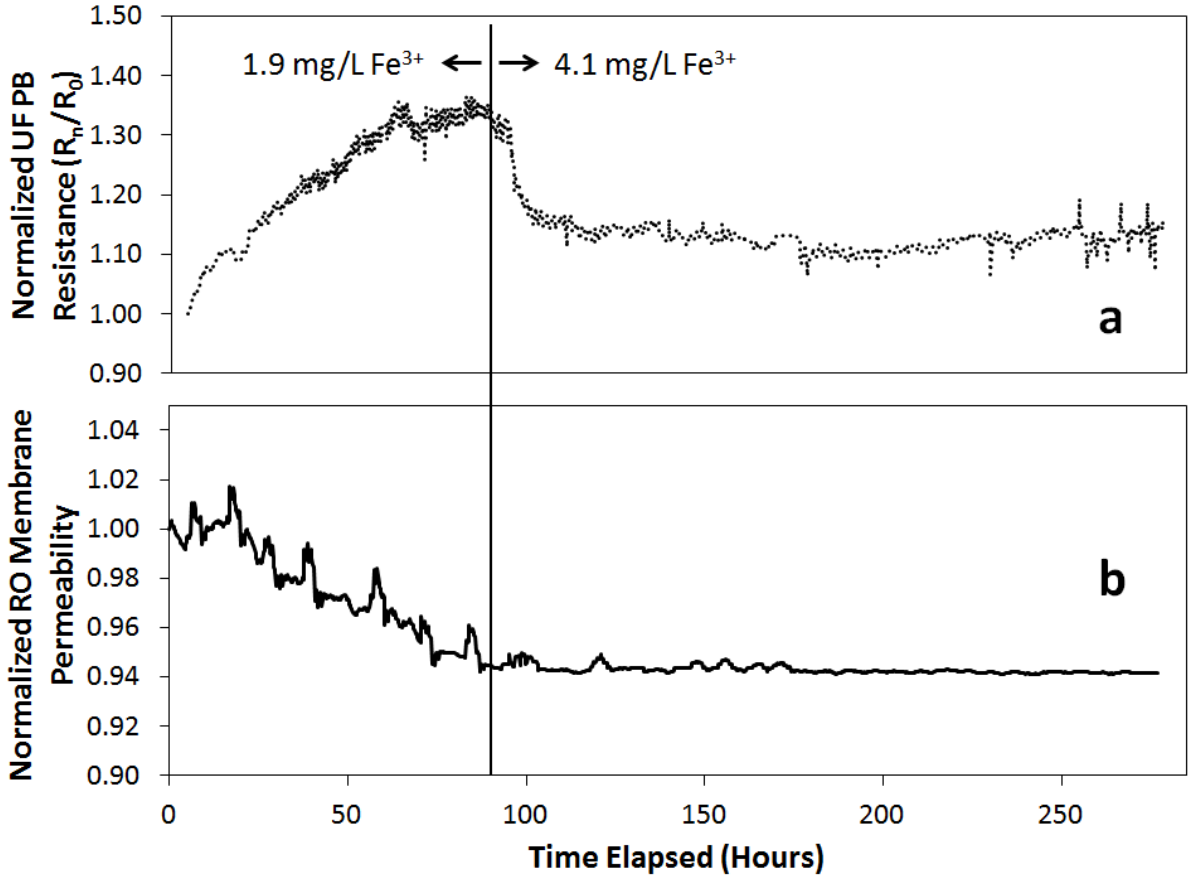

Figure 5.5. (a) Normalized UF PB resistance with respect to initial UF resistance (R_0), and (b) normalized RO membrane permeability (i.e., normalized with respect to initial RO membrane permeability) during two operational periods: (i) UF filtration with coagulant dose of 1.9 mg/L Fe^{3+} demonstrating increased UF resistance and decline in RO membrane permeability, and (ii) At hour 90, the coagulant dose was increased to 4.1 mg/L Fe^{3+} leading to improved UF performance (i.e., reduction in UF resistance) and stable RO membrane permeability.

5.4.3 Effectiveness of self-adaptive coagulant dosing strategy

In order to demonstrate the self-adaptive coagulant dosing strategy via the coagulant dose controller (**Section 5.2**), four consecutive field tests of 70 - 140 hours duration were carried out (**Table 5.2**) with the UF system operating at a flux of 15.1 L/m^{2}h and RO system seawater desalting at recovery of 30%. Self-adaptive backwash triggering was implemented as described previously (**Section 4.2.1.3**). Each UF backwash consisted of two pulses (~ 40 s each) followed by 2 minutes of direct RO concentrate backwash. The initial coagulant dose for three self-adaptive coagulation runs (2-4, **Table 5.2**) was in the range of 2.9 - 4.4 mg/L Fe^{3+} and these tests were compared to UF operation at constant coagulant dose of 4.1 mg/L Fe^{3+}. The range of water quality in terms of chlorophyll *a* and turbidity during each of the four runs is provided in **Table 5.2** with the detailed time-series given in **Section 5.6** (**Figure 5.8, Figure 5.13**, **Figure 5.14**, and **Figure 5.15**).

Table 5.2. Field tests of UF operation at constant coagulant dose and self-adaptive coagulant dosing strategy.

Test	Coagulant Dosing Strategy	Coagulant Dose, mg/L Fe^{3+}	Field Test Duration (hours)	Water Quality		Coagulant consumption rate relative to Run #1[(b)]
				Turbidity (NTU)	Chlorophyll *a* (RFU)	
1	Constant dose	4.1	70	1.05 ± 0.3	151.7 ± 45.3	1
2	Self-adaptive	2.2 – 4.4 (4.1[(a)])	140	1.53 ± 0.4	102.9 ± 39.2	0.83
3	Self-adaptive	2.5 – 3.6 (2.9[(a)])	123	1.08 ± 0.4	139.1 ± 48.4	0.71
4	Self-adaptive	1.7 – 5.1 (4.4[(a)])	124	0.42 ± 0.2	73.3 ± 26.1	0.88

(a) Initial coagulant dose for self-adaptive operation. The coagulant dose is subsequently adjusted as per the determination of the coagulant-dose controller. (b) The rate of coagulant consumption in Test #1 was 311.6 mg/min. Note: Values expressed in the water quality columns are the averages given along with the standard deviations of sensor readings.

UF operation at constant coagulant dose (Run 1) resulted in increased UF PB resistance that was measurably above that for the self-adaptive coagulant dosing (**Figure 5.6**). For example, after 60 hours of operation the UF PB resistance increase for constant coagulant dose operation was ~13% above the initial UF resistance (i.e., constant dose operation at 4.1 mg/L Fe^{3+}) compared to ~7% increase for self-adaptive dosing also at initial dose of 4.1 mg/L Fe^{3+}. While the above improvement may seem small, it is important to note that the ranges of coagulant dose for the self-adaptive Runs 2-4 were 2.2 - 4.4, 2.5 - 3.6, and 1.7 - 5.1 mg/L Fe^{3+}, respectively and resulted in significant reduction in coagulant consumption rate (i.e., by about 12% - 29%, shown in **Table 5.2**). The coagulant dose was adjusted by the controller as water quality varied over the course of the different field tests (**Figure 5.8, Figure 5.13, Figure 5.14,** and **Figure 5.15**) which in turn impacted the rate of UF fouling and backwash effectiveness. UF operation with self-adaptive coagulant dosing led to superior UF performance, relative to constant coagulant dosing (i.e., expected operation duration before required CIP increased by ~57%), and reduced coagulant consumption relative to constant dose operation.

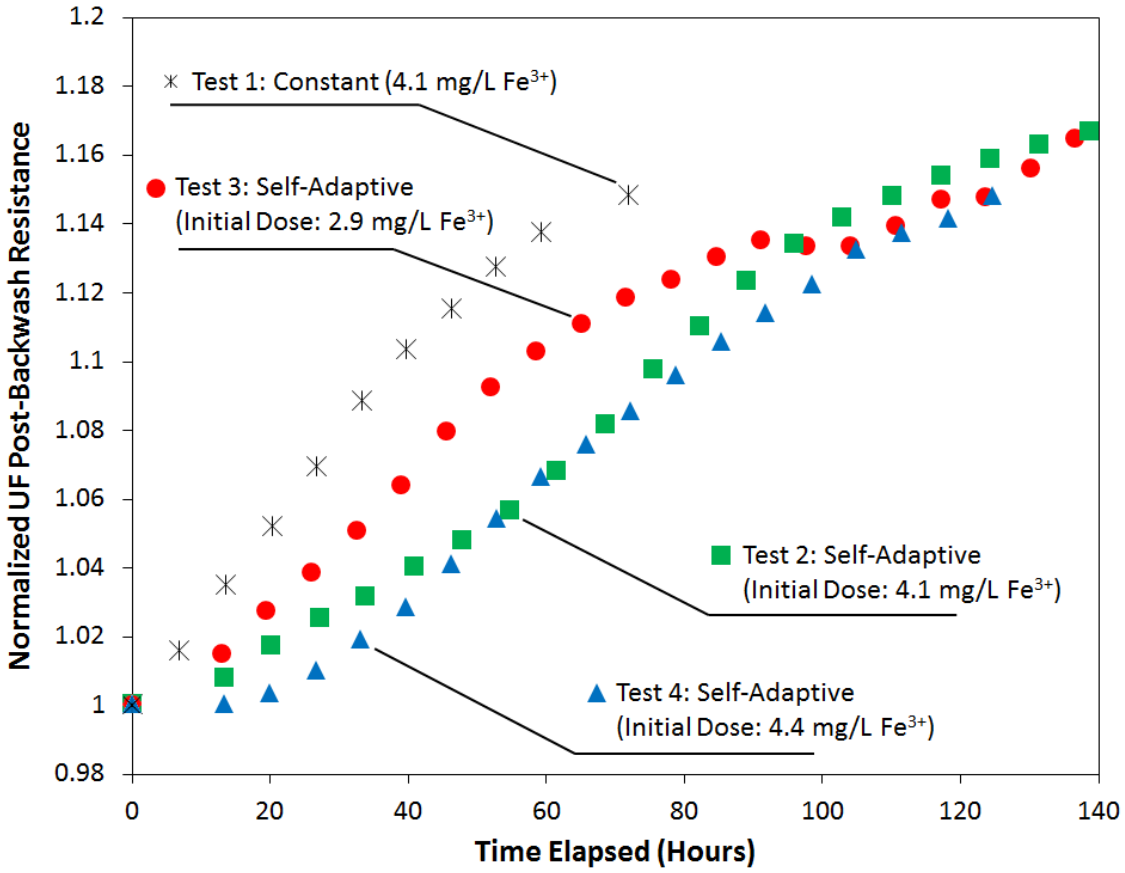

Figure 5.6. Progression of UF post-backwash resistance (equivalent to initial UF cycle resistance) comparing self-adaptive (at different initial coagulant dose) and constant coagulant dosing strategies. Post-backwash UF resistance is normalized with respect to the initial run value.

The coagulant controller action is illustrated in **Figure 5.7** for Run #2 (**Table 5.2**) showing incrementally increasing UF PB resistance for the first 55 hours (Segment (i) in **Figure 5.7**). For segment (i) the coagulant dose was incrementally decreased as condition $|\delta| \leq \varepsilon$ was met (**Section 5.2.2, Eq. 5.3, Condition 4**). Although chlorophyll *a* was relatively high (**Figure 5.8**) during the above period, there was no appreciable change in Δ_n and it is clear that the progressive reduction in coagulant dose did not adversely impact UF performance. In the subsequent operational period (ii) (i.e., t=55 - 85 hrs) the cycle-to-cycle change in UF PB resistance increased despite the fact that the source water turbidity and chlorophyll *a* readings did not seem to change with time (**Figure 5.8**) and resulted in a faster rate of increase of UF PB resistance. In

period (ii), the conditions $\delta < -\varepsilon$ and $\delta > \varepsilon$ (where $u_n > u_{n-1}$) were encountered and thus the coagulant controller action (**Eq. 5.3, Conditions 3 and 5**) was to incrementally increase the coagulant dose; this action ultimately (i.e., toward the end of period (ii)) led to a decline in the rate of cycle-to-cycle change in UF PB resistance (**Figure 5.7b**) which continued essentially throughout period (iii). In period (iii) the conditions $|\delta| \leq \varepsilon$ and $\delta > \varepsilon$ (where $u_n < u_{n-1}$) were met and thus the coagulant dose was decreased (**Eq. 5.3, Conditions 4 and 5**). Details of the control action for Runs #3 and #4, provided in **Figure 5.11** and **Figure 5.12** (**Section 5.6**), also demonstrated that the coagulant controller action was to reduce or elevate the coagulant dose in response to the progression of UF backwash effectiveness. The trend in water quality was complex (**Figure 5.8**, **Figure 5.13**, **Figure 5.14**, and **Figure 5.15**) and while a clear correlation with the coagulant controller actions could not be ascertained, the controller clearly enabled stable UF performance. Overall, the series of field tests demonstrated that relying on the cycle-to-cycle change in UF PB resistance (Δ_n) and the RD factor (δ) as a metric of UF backwash effectiveness is an alternative to using traditional feed water quality sensors (i.e., turbidity, chlorophyll *a* measurements) which proved to be a reliable metric for establishing real-time adjustment of coagulant dose and for reducing coagulant use.

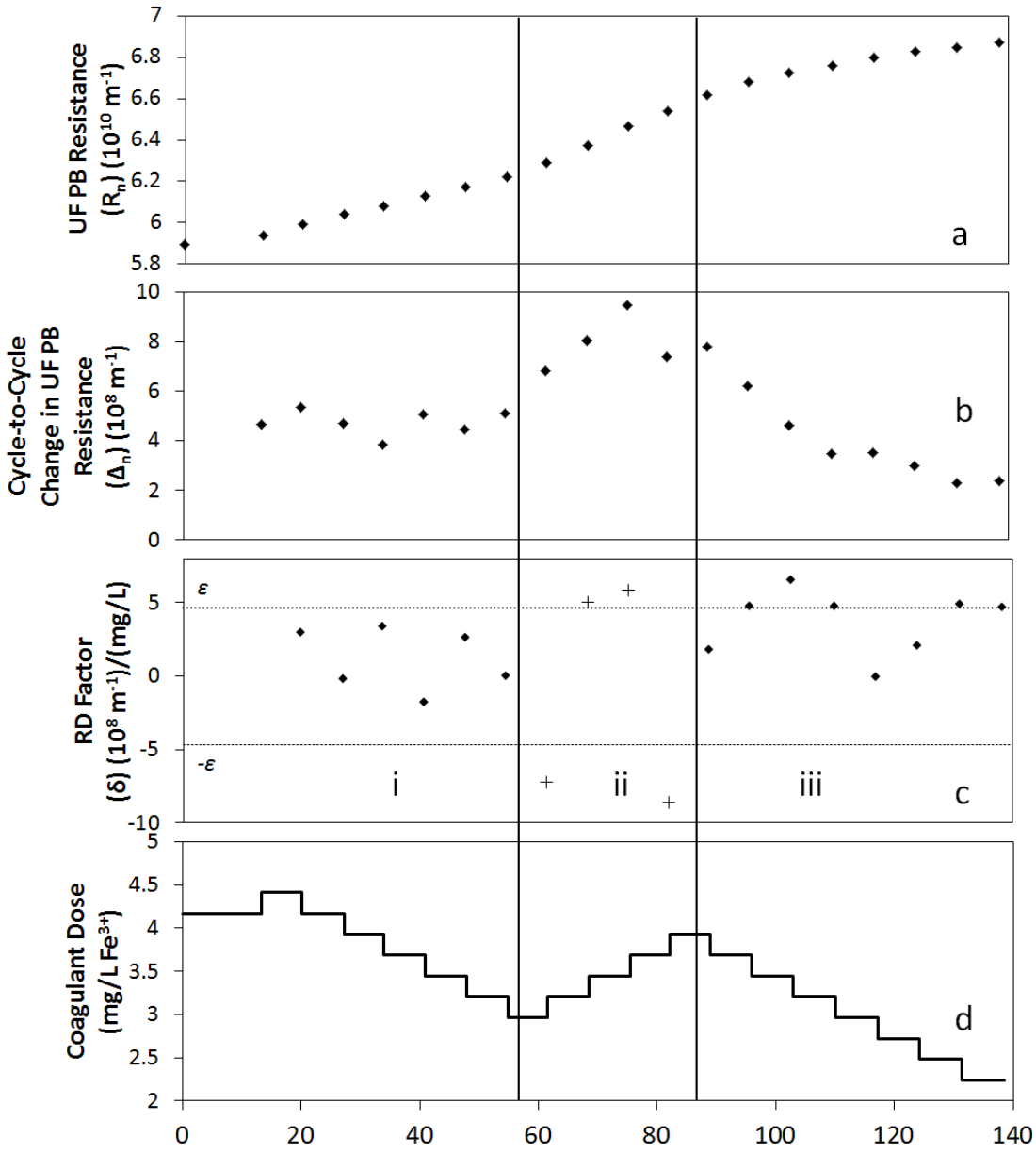

Figure 5.7. UF performance and coagulant impact for Run 2 (**Table 5.2**) demonstrating the time-profiles for (a) UF PB resistance (R_n), (b) cycle-to-cycle change in PB UF resistance (Δ_n), (c) Resistance Dose (RD) factor (δ) and (d) coagulant dose, in mg/L of Fe^{3+}. The controller gradually decreased the coagulant dose in period (i) since the unbackwashed UF resistance did not significantly change over the test duration. In period (ii) the coagulant dose was increased in response to the rise of the change initial UF cycle resistance. Toward the end of period (ii) and through period (iii) backwash effectiveness increased (i.e., unbackwashed UF resistance buildup decreased) and correspondingly the controller decreased the coagulant dose.

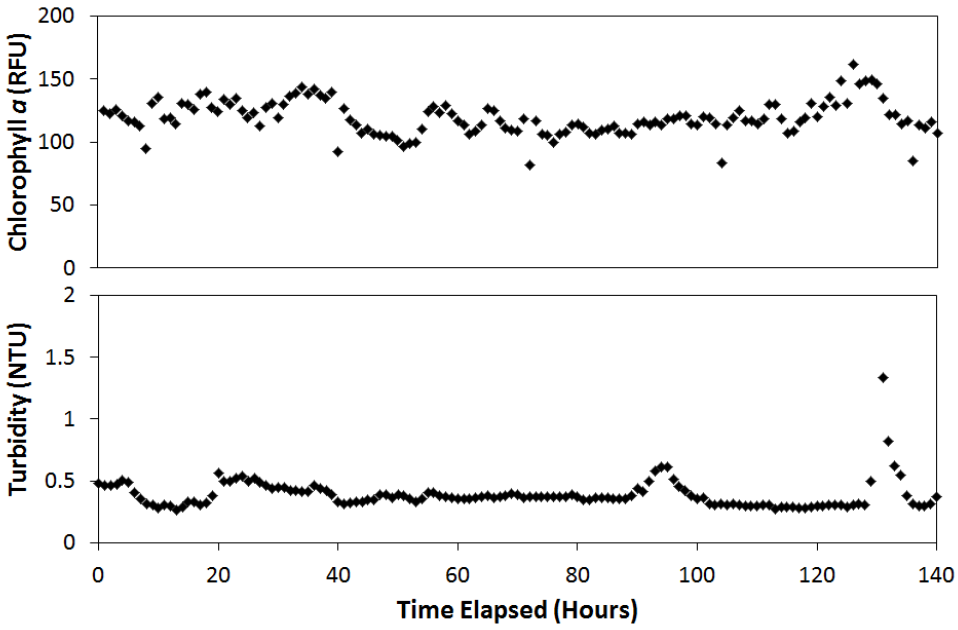

Figure 5.8. UF feed water quality during UF Run #2 of self-adaptive coagulant dosing.

5.4.4 Performance of coagulant dosing controller during a storm event

During the field study, a looming storm event provided a unique opportunity for a stress test of the UF coagulant dose controller. The integrated UF-RO system was operated for a period of ~7 days at the same conditions (e.g., UF feed flow rate, RO recovery, and backwash parameters) as in the previous test (**Section 5.4.3**). For a period of ~55 hours, prior to the storm event, the plant operated with UF coagulant dosing of 3.7 mg/L Fe^{3+}. The UF performance was such that the cycle-to-cycle change in UF PB resistance was reasonably maintained. The storm event led to a significant increase in water source turbidity (~1500%) and chlorophyll *a* (~220%) relative to the pre-storm conditions. Deterioration of feed water quality led to increased UF PB resistance (**Figure 5.9b**), as well as increased Δ_n (**Figure 5.9c**). At ~15 hours past the storm onset (i.e., t = 70 hours), the coagulant controller was activated and reacted to the increase in Δ_n by increasing the coagulant dose for three consecutive filtration cycles (**Figure 5.9d**). This action improved UF

performance, despite the ongoing storm event, resulting in decreased cycle-to-cycle change in PB UF resistance. As the UF backwash efficiency improved and the storm subsided, previously unbackwashed UF resistance was removed through UF backwash, leading to the condition $\Delta_n < 0$. The above condition of $\Delta_n < 0$ persisted for the remaining period after t = 105 hours, (**Eq. 5.3, Condition 1**) and thus the coagulant dose was maintained at ~3.9 mg/L Fe^{3+}. The above field test demonstrated that: a) change in Δ_n is indeed a relevant and strong indicator of the impact of varying feed water quality, b) UF performance is sensitive to the coagulant dose, and c) self-adaptive coagulant dosing enabled robust UF performance even under conditions of deteriorating feed water quality.

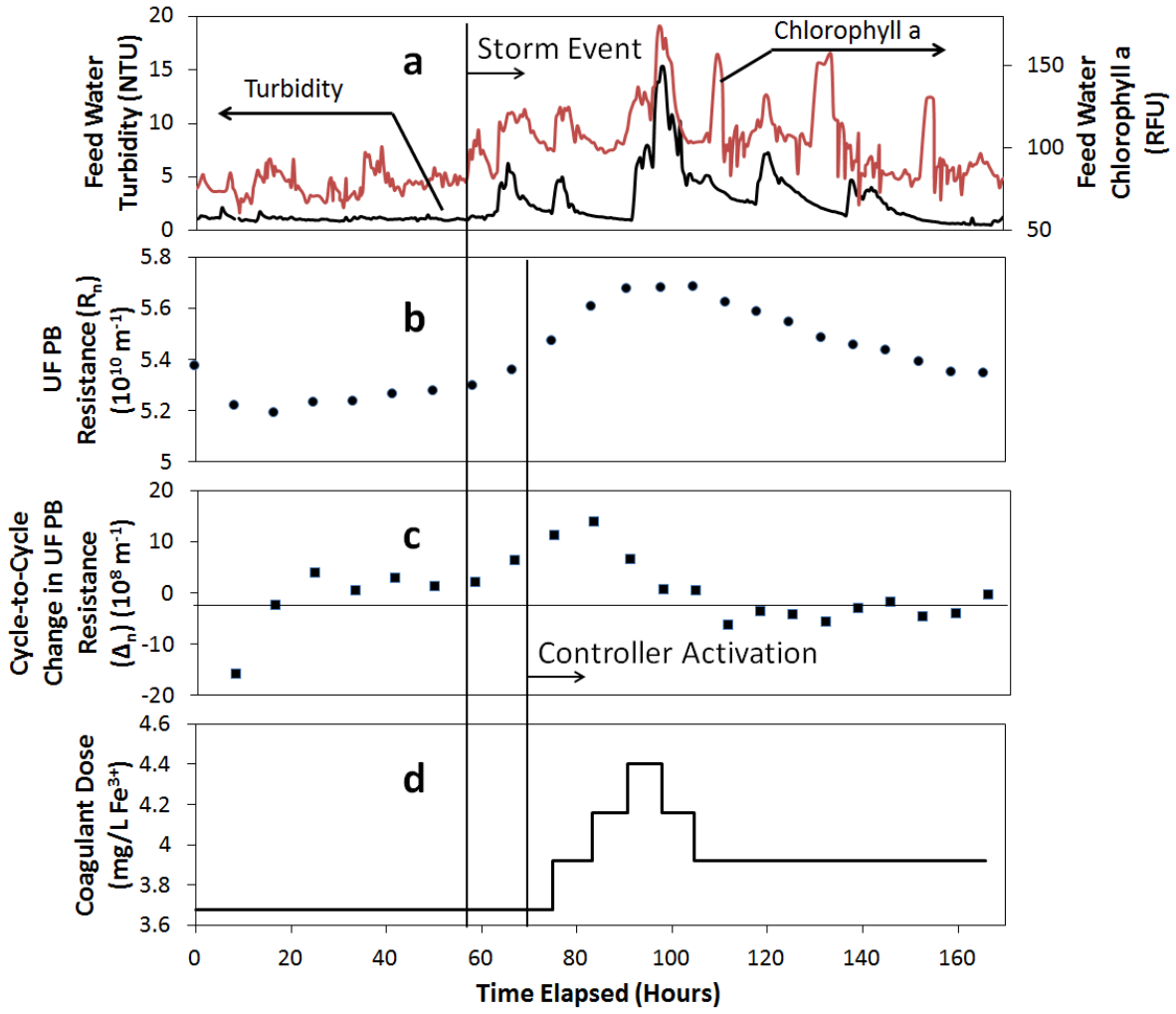

Figure 5.9. UF Coagulant dose controller performance for UF operation during a storm event: (a) Feed water turbidity and chlorophyll *a*, (b) UF PB resistance (R_n), (b) cycle-to-cycle change in PB UF resistance (Δ_n), and (d) coagulant dose before and past storm event. UF system was operated at a constant coagulant dose of 3.7 mg/L Fe^{3+} for ~55 hours prior to the storm event with the coagulant dose controller activated at t = 70 hours.

5.5 Summary

A novel approach for self-adaptive control of in-line UF coagulant dosing was developed and field demonstrated for integrated UF-RO seawater desalination. A coagulant dose controller was developed whereby UF filtration resistance is tracked in real-time, in addition to evaluating the change in post-backwash (PB) UF resistance in response to coagulant dose adjustments. The objective of the coagulant controller was to adjust the inline coagulant dose to the UF feed so as

to reduce the incremental cycle-to-cycle PB resistance change (i.e., Δ_n). Tracking both Δ_n and the rate of change with respect to coagulant dose (labeled as "Resistance–Dose" or RD Factor) enabled the coagulant controller to quantify UF backwash effectiveness and accordingly establish the appropriate coagulant adjustment. The coagulant controller was successfully demonstrated in a UF-RO seawater desalination pilot plant with field tests ranging up to eight days over a period of 1 year. Field testing demonstrated that the proposed approach to self-adaptive coagulant dosing, in addition to self-adaptive backwash triggering, can be effective in: (a) reducing coagulant use while ensuring effective UF operation during periods of varying water quality, and (b) potentially reducing the required frequency of CIP. While the present coagulant controller was demonstrated for seawater UF-RO desalination, it is envisioned that the approach can be adapted to inland water UF treatment to provide both stable UF operation and significant savings in coagulant use.

5.6 Supplementary Materials

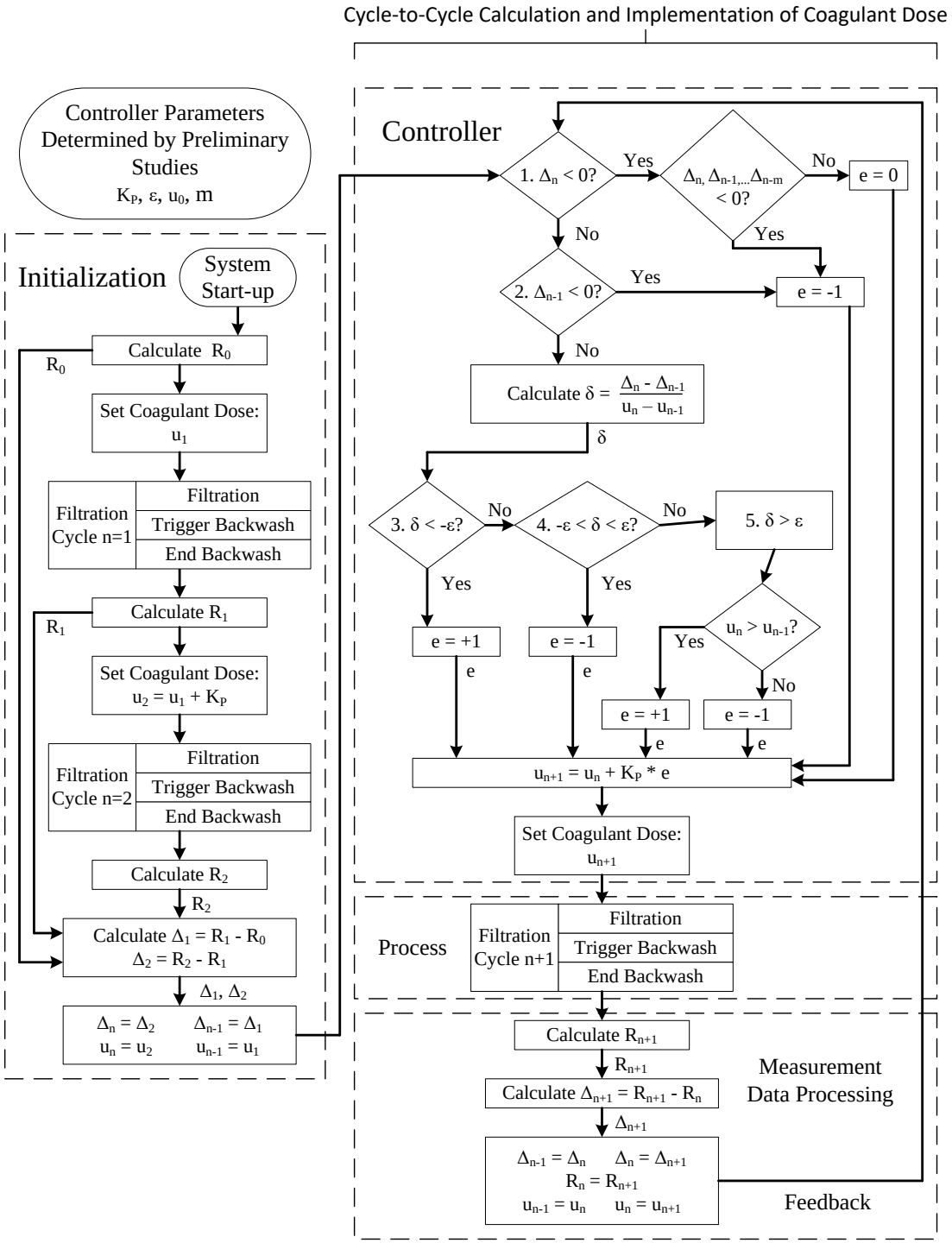

Figure 5.10. Overall coagulant controller implementation. Note: At system start-up, the UF plant is operated for two filtration cycles at two sequential coagulant doses (u_0 and u_1) in order to attain initial two cycle values of Δ_n and its rate of change with respect to coagulant dose (i.e., δ). The parameters K_P, ε, m, and u_0 are established via initial filtration/backwash tests (**Section 5.4.1)**.

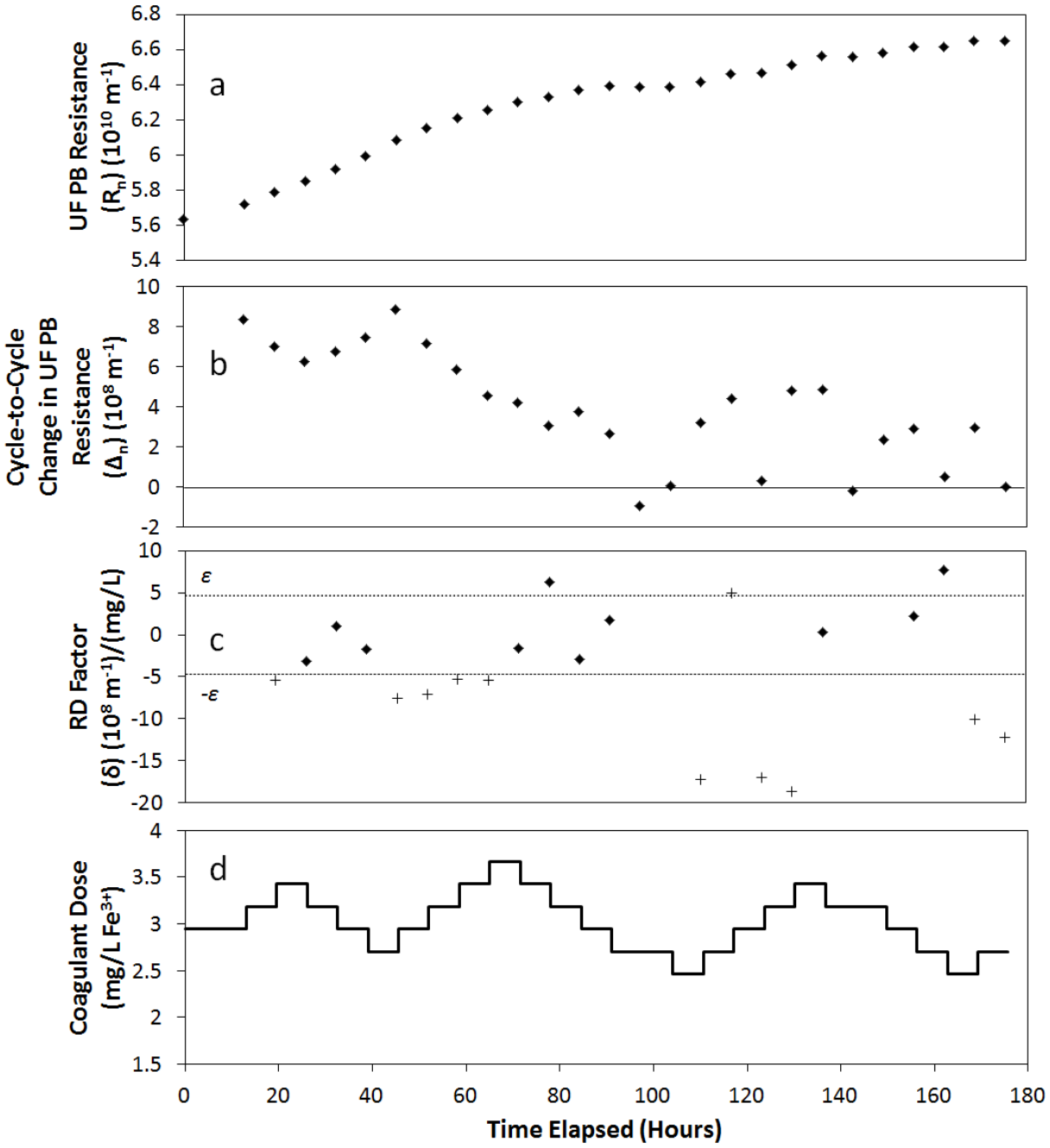

Figure 5.11. UF performance and coagulant impact for Run #3 (Table 2) demonstrating the time-profiles for: (a) UF PB resistance (R_n), (b) cycle-to-cycle change in PB UF resistance (Δ_n), (c) Resistance Dose (RD) factor (δ), and (d) coagulant dose (mg/L Fe^{3+}). Experimental conditions are shown in **Section 5.4.3**.

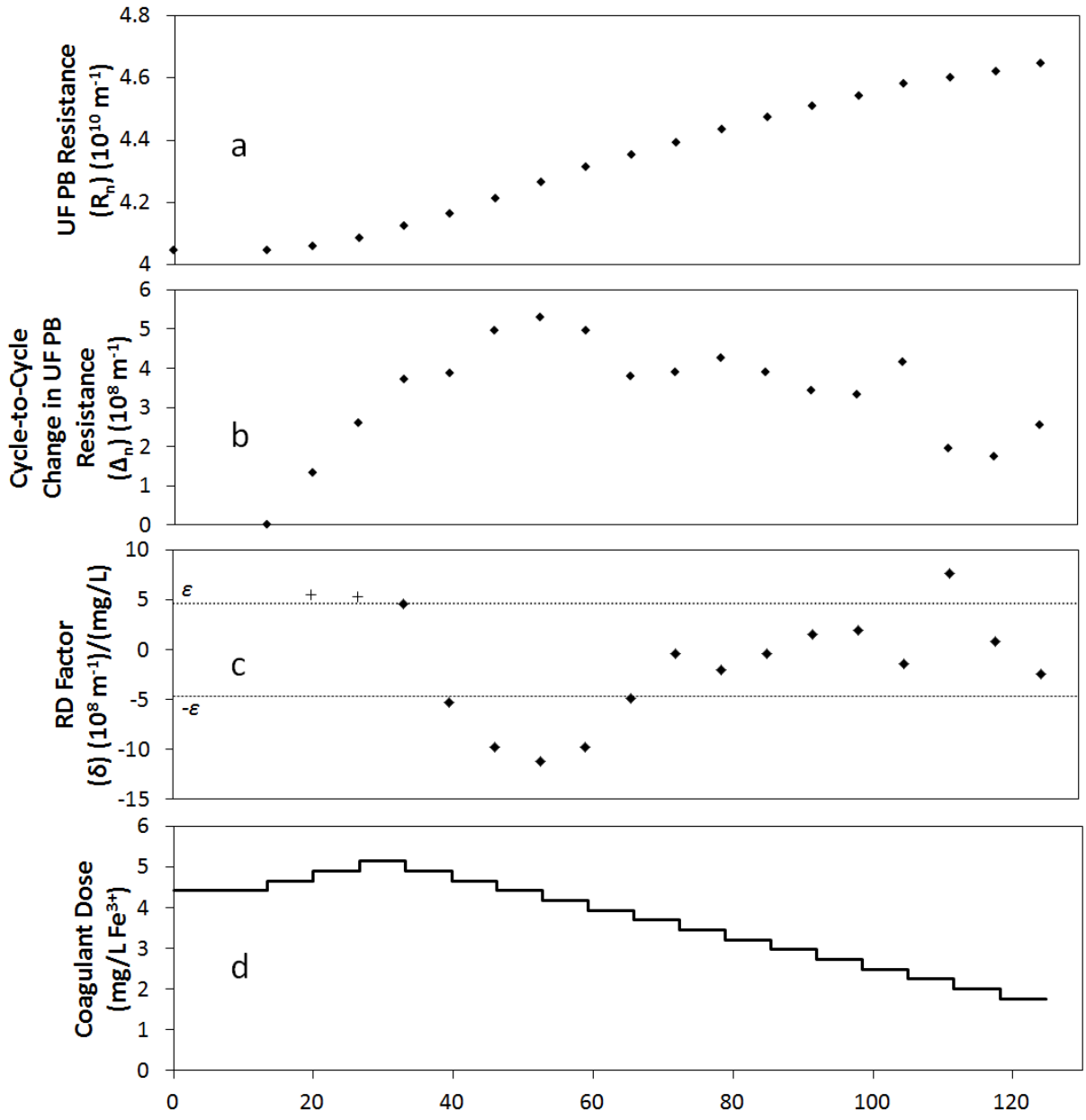

Figure 5.12. UF performance and coagulant impact for Run #4 (Table 2) demonstrating the time-profiles for: (a) UF PB resistance (R_n), (b) cycle-to-cycle change in PB UF resistance (Δ_n), (c) Resistance Dose (RD) factor (δ), and (d) coagulant dose (mg/L Fe^{3+}). Experimental conditions are shown in **Section 5.4.3**.

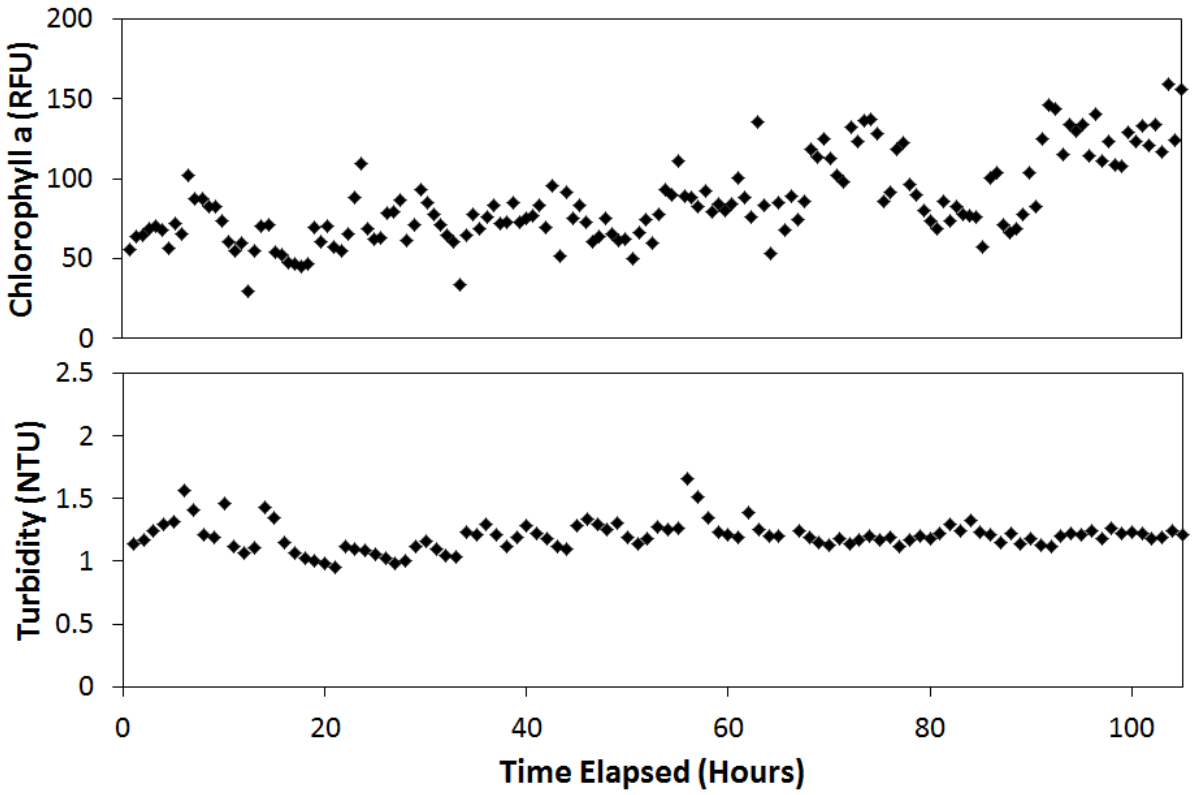

Figure 5.13. UF feed water quality data during Run #1 in which UF operation was at constant coagulant dosing (coagulant dose: 4.1 mg/L Fe^{3+}).

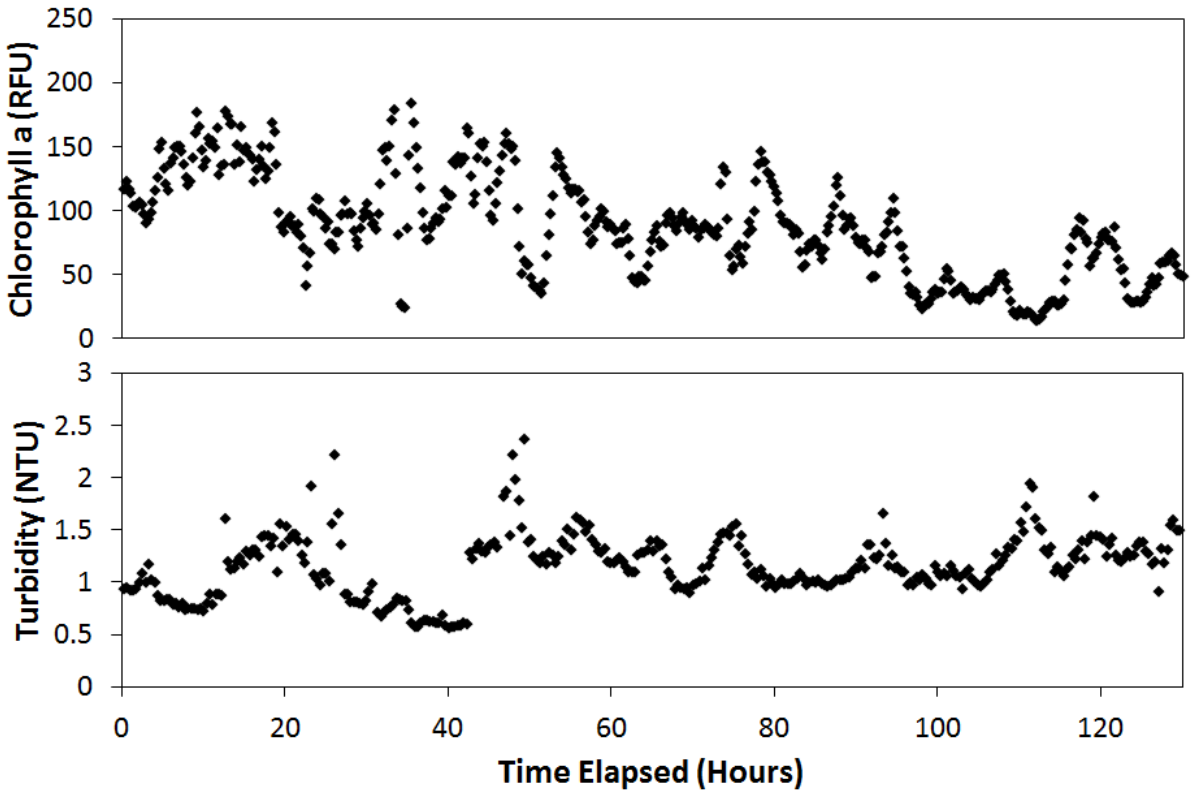

Figure 5.14. UF feed water quality data during Run #3 of UF operation with self-adaptive coagulant dosing (initial coagulant dose: 2.9 mg/L as Fe^{3+}).

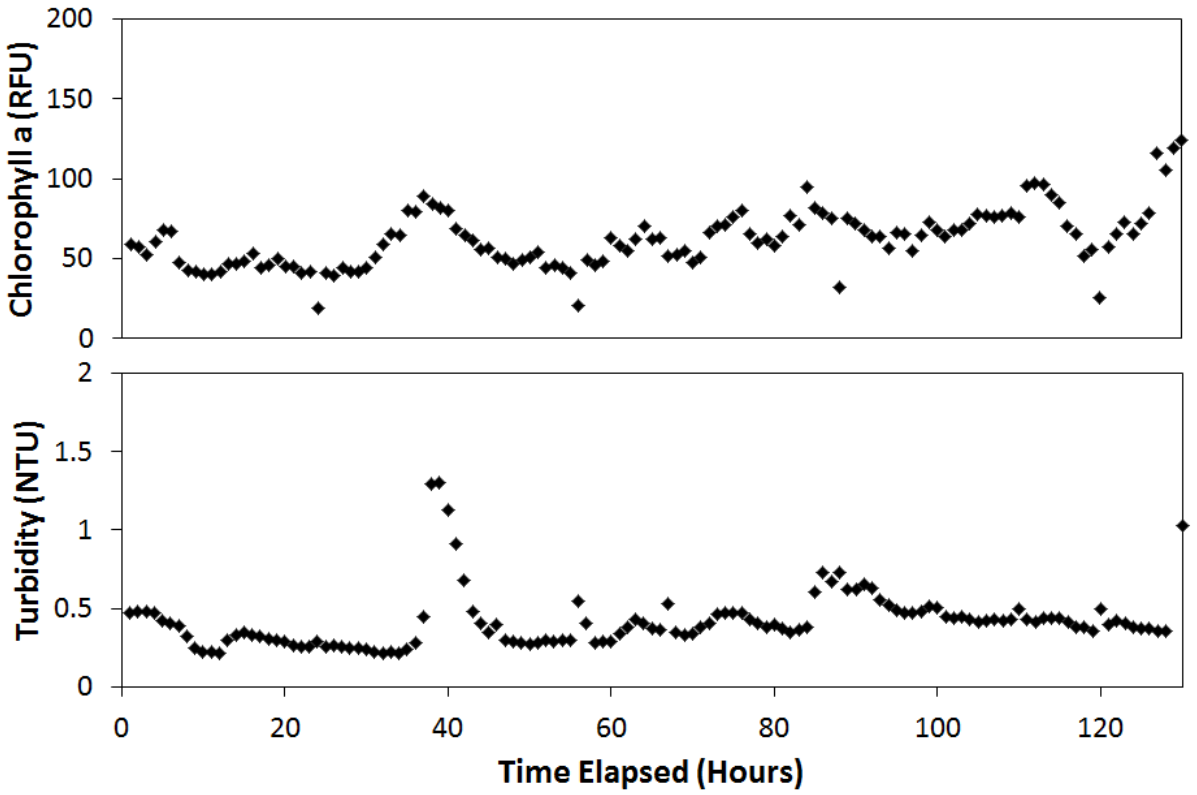

Figure 5.15. UF feed water quality data during Run #4 for UF operation with self-adaptive coagulant dosing (initial coagulant dose: 4.4 mg/L as Fe^{3+}).

Chapter 6 Energy-Optimal Control of Single-Stage RO Desalination

6.1 Overview

This chapter describes the development and validation of a novel model-based control for the operation of a spiral-wound RO membrane desalination system with a focus on energy optimal operation. The control scheme utilized an operational model for spiral-wound RO desalting (i.e., based on a solution-diffusion model which describes transport of water as a solvent through a semi-permeable membrane) with a supervisory controller providing real-time updates of membrane permeability and the appropriate feed pressure set points for maintaining the target permeate productivity at the lowest feasible specific energy consumption. The RO system feed pressure and flow rates were controlled by a lower-level RO controller through adjustment of the RO high pressure feed pump VFD and RO concentrate valve. Seawater desalination tests with the SIMS-SD plant (**Section 3.1**) demonstrated effective self-adaptive energy optimal operation capable of handling feed salinity fluctuations and constraints imposed by the system physical limitations (i.e., minimum and maximum feasible operational pressures and flow rates) and the thermodynamic restriction for cross flow RO operation.

6.2 Control System Architecture

The SIMS-SD plant (**Section 3.1**) was operated via a control system (**Figure 6.2**) that consisted of a supervisory controller and lower-level RO controllers. The supervisory controller (**Figure 6.3**) collects and processes sensor data and performs necessary calculations to establish the operational set points and trajectories and to communicate those to the lower level RO controllers. During desalting operation, data from system sensors (e.g., flow, pressure) are acquired and passed to the supervisory controller for online calculation of membrane

permeability. The supervisory controller then uses an energy-optimization algorithm to determine the optimal product water recovery and the corresponding RO feed flow rate set-point for a desired preset RO permeate flow rate. Subsequently, the supervisory RO controller calculates the required RO feed pressure via the RO process model to achieve the desired permeate flow rate set-point. The computed parameters are then communicated to the lower-level RO controller, which controls the RO pump VFD and concentrate valve to attain their specified set-points. The above process is repeated dynamically at a prescribed rate (typically every ~10-20 s) at a frequency which is set at the supervisory controller level.

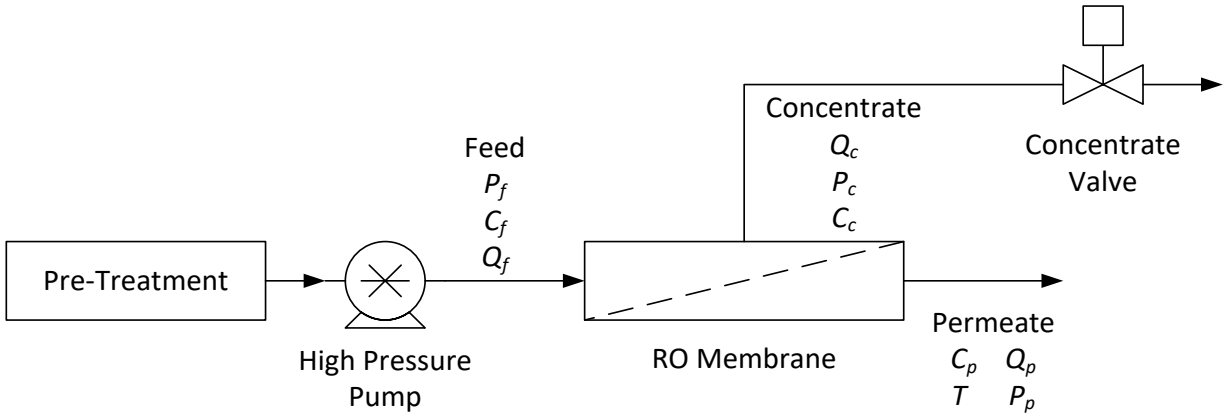

Figure 6.1. Schematic of the RO desalination process depicting the various monitored process variables.

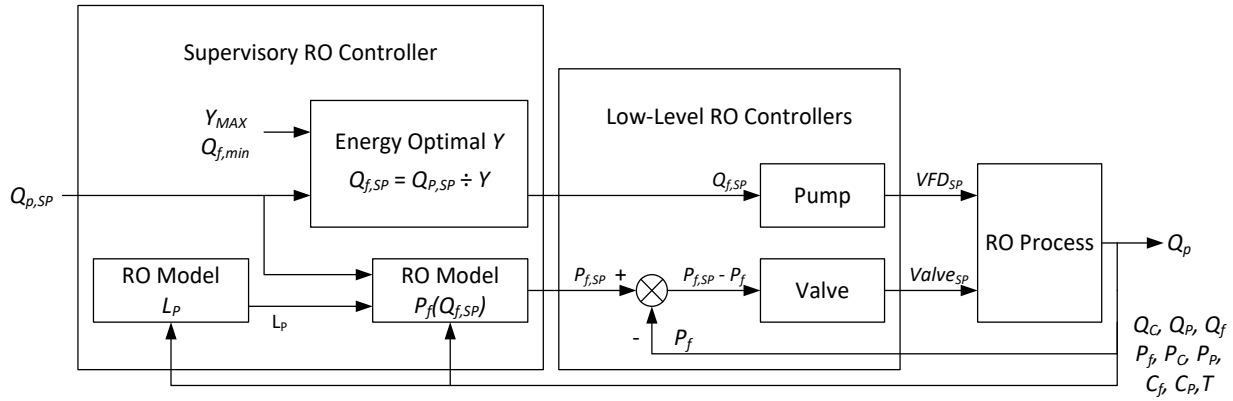

Figure 6.2. Schematic diagram of the RO system control architecture. The overall control system is separated into a supervisory RO controller and a lower-level RO controller. (Note: Definitions of the monitored process variables are provided in Section 3.1, subscript *sp* denotes a control set-point for the specific variable, L_p is the membrane permeability, Y is the operational water recovery, and VFD_{sp} and $Valve_{sp}$ refer to the set-point settings for these system components).

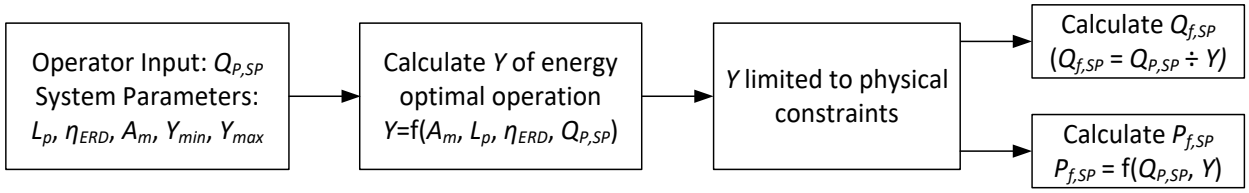

Figure 6.3. A flow chart of the RO supervisory controller used to calculate $Q_{f,sp}$ and $P_{f,sp}$.

6.2.1 Energy Optimal Operation

Optimal control of RO desalination requires a framework for predicting energy consumption with considerations of system physical constraints (e.g., with respect to permeate productivity, feed flow rate and system pressure) as well as limitations imposed by the thermodynamic restriction in cross flow operation[58]. In the present work, a generalized framework was adopted for modeling the specific energy consumption (SEC) for RO desalting, defined as the energy expended for producing a unit volume of permeate. A simplified approach for determining the SEC-optimal operating water recovery without the use of a minimization algorithm and when this approach is valid will is also discussed. The optimal SEC (for a given

recovery) for a system that can operate up to the limit imposed by the thermodynamic restriction can be expressed as [58]:

$$SEC_{norm} = \left[\frac{1-\eta_{ERD}(1-Y)}{Y(1-Y)}\right]\left(\frac{R}{\eta_{pump}}\right) \qquad \textbf{6.1}$$

where η_{pump} and η_{ERD} are the pump and ERD efficiencies, respectively, R is the membrane salt rejection, Y is the permeate recovery (i.e., $Y=Q_p/Q_f$), and the normalized SEC_{norm} is defined as $SEC_{norm} = SEC/\pi_o$, where π_o is the RO feed osmotic pressure. When the given RO system is constrained with respect to its permeate production flow rate (Q_p), the SEC is given by [58]:

$$SEC_{norm} = \left[\frac{Q_{p,norm}}{Y} - \frac{\ln(1-Y)}{Y^2}\right][1-\eta_{ERD}(1-Y)]\left(\frac{R}{\eta_{pump}}\right) \qquad \textbf{6.2}$$

where $Q_{p,norm}$ is the normalized permeate flow rate defined as $Q_{p,norm} = Q_p / (A_m L_p \pi_o)$, in which A_m and L_p are the membrane surface area and permeability, respectively. It is noted that for a constrained feed flow rate operation the first term on the right hand side of **Eq. 6.2** is replaced by Q_f [58]. It is also noted that **Eq. 6.1** and **Eq. 6.2** provide a lower SEC limit with respect to axial pressure drop along the RO element retentate channel and average concentration polarization level by assuming that the effects of both of these factors on SEC are negligible. (i.e., It is noted that these assumptions are not realistic, but are made in this analysis in order to allow formulate the rationale for a simplified approach of determining the SEC-optimal water recovery without the need for a minimization algorithm). The relationship between the operational recovery, Y_{min}, at the global minimum energy consumption for a constrained permeate flow rate $Q_{p,\mathrm{norm}}$, can be obtained by setting ($\partial(SEC_{norm}) / \partial Y$) = 0 and solving to obtain the following explicit relationship for $Q_{p,norm}$:

$$Q_{p,norm} = \frac{\ln(1-Y_{min})[2(1-\eta_{ERD}) + Y_{min}\cdot\eta_{ERD}]}{Y_{min}(1-\eta_{ERD})} + \frac{1-\eta_{ERD}(1-Y_{min})}{(1-Y_{min})(1-\eta_{ERD})} \qquad \textbf{6.3}$$

Eq. 6.3 is both twice continuously differentiable with respect to Y_{min} and for any given $Q_{p,norm}$ has a single, isolated root for Y_{min} for values of Y_{min} in the domain of $Y = (0,1)$. Therefore, for any given $Q_{p,norm}$ a corresponding Y_{min} can be calculated using Newton's or secant method. However, it is noted that RO operation, for a given recovery, below the SEC_{norm} as set by **Eq. 6.1** is thermodynamically infeasible [58]. For these cases, the RO system must operate at recovery Y_{tl} where the constant $Q_{p,norm}$ curve intersects the curve representing operation up to the thermodynamic limit (**Figure 6.4**). As an example, the functional dependencies of SEC_{norm} on recovery for different values of η_{ERD} for operation up to the thermodynamic limit and for cases of constrained permeate flow rate are illustrated in **Figure 6.4** for the case of $\eta_{pump} = 1$, $R = 1$, and $Q_{p,norm} = 1$.

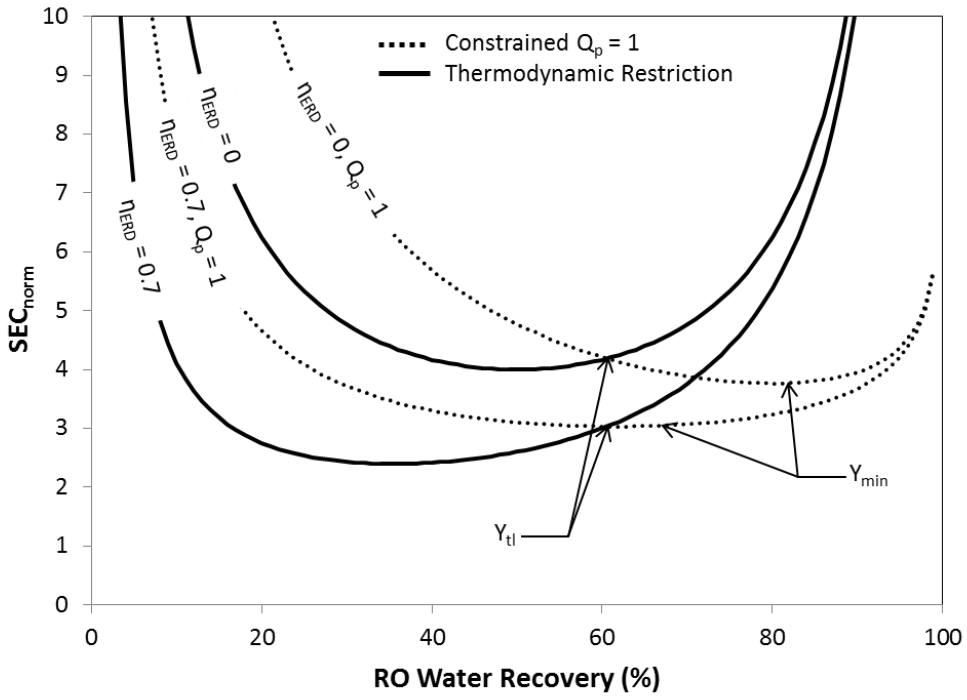

Figure 6.4. A plot of SEC_{norm} with respect to fractional water recovery Y, for η_{ERD} values of 0 and 0.7 and $Q_{p,norm}$ of 1. The Figure also indicates: (a) Y_{tl}, the recovery at which the constrained $Q_{p,norm}$ curve intersects the curve representing operation up to the thermodynamic limit, and (b) Y_{min}, the recovery at the globally minimum SEC_{norm} for the case of constrained Q_p. **Eq. 6.1** was used to plot the thermodynamic restriction, while **Eq. 6.2** was used to plot the constrained Q_P curve.

In order to simplify the control algorithm, it is convenient to first identify if Y_{min} would be located above or below the curve representing operation up to the thermodynamic limit (e.g., solid curves in **Figure 6.4**). The above can be achieved by noting that Y_{tl}, or the point at which the constant $Q_{p,norm}$ curve intersects with the curve representing operation up to the thermodynamic limit, can be determined by equating **Eq. 6.1** and **Eq. 6.2**, resulting in:

$$Q_{p,norm} = \frac{1}{(1 - Y_{tl})} + \frac{\ln(1 - Y_{tl})}{Y_{tl}} \qquad \textbf{6.4}$$

The right hand side of **Eq. 6.4** is a strictly increasing function of Y_{tl} over the domain Y = (0,1) with a unique value of Y_{tl} for each $Q_{p,norm}$. It is also noted that as $Y \rightarrow 0$, SEC_{norm} for operation with constrained Q_p (**Eq. 6.2**) is greater than SEC_{norm} for operation up to the thermodynamic limit (**Eq. 6.1**), i.e.,

$$\left[\frac{Q_{p,norm}}{Y} - \frac{\ln(1 - Y)}{Y^2}\right][1 - \eta_{ERD}(1 - Y)] > \frac{1 - \eta_{ERD}(1 - Y)}{Y(1 - Y)} \qquad \textbf{6.5}$$

The above inequality can be proven by multiplying it by Y and setting $1\text{-}Y \approx 1$ for the case of $Y \rightarrow 0$ which imply that $Q_{p,norm} > 0$. Thus, the inequality holds as $Y \rightarrow 0$ for all valid values of $Q_{p,norm}$ which are by definition greater than zero. Since **Eq. 6.1** and **Eq. 6.2** have one unique intersection, inequality **Eq. 6.5** holds true for all values of Y from 0 up to Y_{tl}. This implies that in the region of Y = (0, Y_{tl}], the globally minimum SEC for a constrained Q_p operation exists above the SEC for operation up to the thermodynamic limit. However, for the region of Y = [Y_{tl},1), the globally minimum SEC for a constrained Q_p process exists below the SEC for RO desalting operation up to the thermodynamic limit and hence is infeasible. Therefore, the above analysis concludes that if $Y_{min} < Y_{tl}$, then Y_{min} will be the SEC-optimal operating recovery and a minimization algorithm will be required in order to determine the SEC-optimal operating recovery. However, if $Y_{min} > Y_{tl}$, then Y_{tl} will be the global SEC-optimal operating recovery, whereby operation at a constrained Q_P above the thermodynamic restriction results a situation where increasing the water recovery

results in reduced SEC over the entire possible range of $Y = (0, Y_{tl}]$ (i.e., since by definition, the derivative of SEC as a function of Y in the region $Y = (0, Y_{min})$ must be negative). Therefore, it can be concluded that, if $Y_{min} > Y_{tl}$ and the system is operating under the constraints of a constant permeate flow rate, then the maximum possible operating recovery is also the SEC-optimal operating recovery.

6.2.2 Physical System Constraints

RO desalination plants are not typically designed to operate up to the limit imposed by the thermodynamic restriction. RO plant operation may be constrained by production targets, finite membrane area, and finite membrane permeability, all of which may force operation away from the limit imposed by the thermodynamic restriction. Moreover, physical constraints imposed by system components (i.e., pumps, pressure vessels) can limit the range of RO plant operability (e.g., in terms of the attainable ranges of feed pressure, feed flow rate and permeate recovery). As a result, the optimal RO plant operation as derived in **Section 6.2.1**, for a given permeate flow rate, will lead to SEC that is higher relative to the optimal minimum expressed by **Eq. 6.1**. Therefore, optimal operation of the RO system must consider constraints that affect water recovery (Y), product flow rate (Q_p), and feed flow rate (Q_f). The implications of the above, with respect to the SEC, are illustrated in the SEC curves shown in **Figure 6.5** for the RO system used in the present study (**Section 3.1**). The SEC curves were generated by first determining the permeate flow rate that can be achieved by the present RO system at the maximum and minimum feed pressures and feed flow rates and subsequently calculating the SEC as per **Eq. 6.2**. It is noted that the SEC_{norm} for any of the constrained conditions is above the SEC_{norm} for operation up to the thermodynamic limit. At the minimum system pressure, the SEC_{norm} approaches operation up to the thermodynamic limit, however, such operation is infeasible for the present system due

to the minimum Q_f constraint for the physical system. More importantly, the feasible operational domain for the RO system (indicated in the shaded gray area) is bounded by the maximum and minimum feed flow rate, maximum feed pressure, and maximum recovery constraints. Between the possible operating $Q_{p,norm}$ of 0.035 ~ 0.88 (1.9 L/min ~ 47.3 L/min), Y_{min} is calculated to be 72% ~ 79%; both values exist above the manufacturer stated Y_{max} of 38.6% (**Section 3.1**). Hence within this operating region, while the permeate flow rate is constrained, increased recovery would lead to lower SEC_{norm}. Therefore, energy optimal operation for constrained permeate flow rate dictates operation at the highest achievable recovery, subject to the constraints imposed by the system. It is noted that for several experiments, more conservative system constraints were implemented instead of values specified by the manufacturer. The specific values used for the constraints are shown with their respective experiments in **Section 0**. All physical system constraints for the RO plant used in this study are illustrated in **Figure 6.5**.

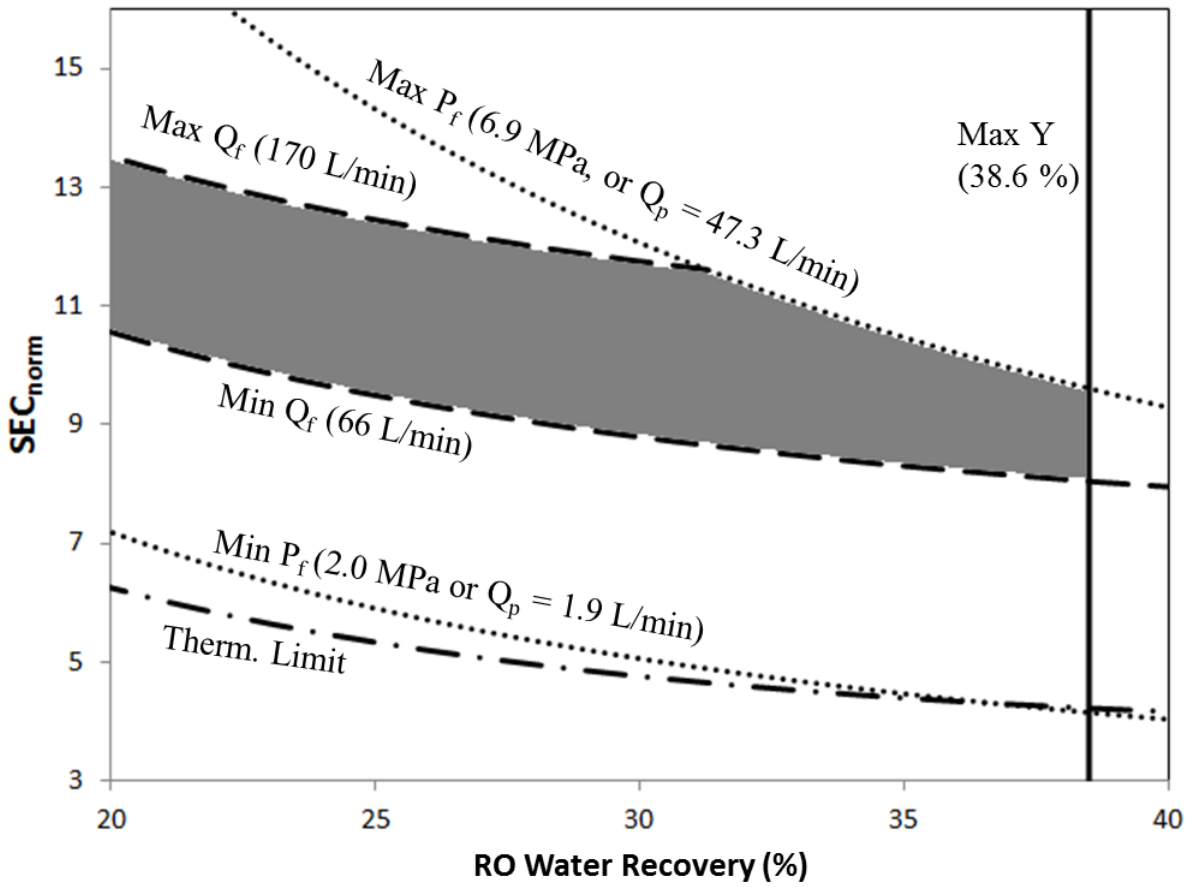

Figure 6.5. Normalized SEC with respect to RO recovery, with physical plant constraints plotted. Solid lines represent the maximum Y constraint, dashed lines represent the Q_f constraint, the dotted lines represent the Q_p constraint which is governed by the P_f constraint, and the dash dotted line represents the thermodynamic limit. The operating region of the experimental RO system is shaded. **Eq. 6.1** was used to plot the thermodynamic restriction, while **Eq. 6.2** was used to plot the constrained Q_P (Min and max P_f) and constrained Q_f (min and max Q_f) curves. How **Eq. 6.2** was used to create a constrained Q_f curve was explained in **Section 6.2.1**.

6.2.3 RO Feed Pressure Set-Point

In order to operate the RO system at the desired level of permeate productivity but minimize energy consumption, the RO system should be an operated at a specified water recovery determined to be energy-optimal. Accordingly, one of the functions of the supervisory controller is to calculate the RO feed pressure required to achieve the permeate production set-point at the specified water recovery making use of the classical permeate flux expression [62]:

$$Q_p = A_m L_p(\overline{\Delta P_m} - \overline{\Delta\pi}) \quad \textbf{6.6}$$

where A_m is the active membrane area, L_p is the membrane hydraulic permeability, $\overline{\Delta P_m}$ is the average transmembrane pressure, and $\overline{\Delta\pi}$ is the average osmotic pressure difference across the membrane. Assuming a linear pressure profile along the retentate channel of the RO elements [95], the average transmembrane pressure can be expressed as:

$$\overline{\Delta P_m} = \frac{P_f + P_c}{2} - \overline{P_p} \quad \textbf{6.7}$$

where $\overline{P_p}$ is the average permeate-side pressure, P_f is the RO feed pressure, and P_c is the RO concentrate pressure at the RO module exit. The first term on the right hand side of **Eq. 6.7** represents the average feed-side pressure. The average feed osmotic pressure can be approximated as the log-mean average along the membrane [70], and the average feed-side osmotic pressure difference is given as follows [116]:

$$\overline{\Delta\pi} = \pi_0 \frac{ln(1-Y)}{Y} \cdot \overline{CP} - \pi_0 \cdot (1-R) \quad \textbf{6.8}$$

in which π_0 is the feed osmotic pressure, $\overline{CP}$ is the average concentration polarization modulus in each RO membrane element (i.e., $\overline{CP} = C_m/C_b$, where C_b and C_m are the average salt concentrations in the bulk and at the membrane surface, respectively), and R is the observed salt rejection. The first term on the right hand side of **Eq. 6.8** is the feed side osmotic pressure, while the second term on the right-hand side of **Eq. 6.8** is the permeate side osmotic pressure. The observed salt rejection R is defined as:

$$R = 1 - \frac{C_p}{C_f} \quad \textbf{6.9}$$

where C_p and C_f are permeate and feed concentrations, respectively. The feed osmotic pressure for the Dow FILMTEC 8-in elements used in the SIMS-SD can be estimated by [116]:

$$\pi_0 = \emptyset \cdot C_f \cdot (273.15 + T) \quad \textbf{6.10}$$

in which feed concentration (C_f), the osmotic pressure coefficient ($\emptyset$), and temperature (T) are used for a temperature correction factor. The average concentration polarization applicable to the Dow FILMTEC 8-in elements used in the SIMS-SD (**Section 3.1**) was estimated as [116]:

$$\overline{CP} = exp\left(0.7 \cdot \left[1 - (1 - Y)^{1/n}\right]\right) \quad \textbf{6.11}$$

in which n is the number of RO membrane elements in series (n=3 for the present system).

Combining **Eqs. 6.6 - 6.8** results in the following equation for the permeate flow rate:

$$Q_p = A_m L_p \left[\frac{P_f + P_c}{2} - P_p - \pi_0 \frac{ln(1 - Y)}{Y} \cdot \overline{CP} + \pi_0 \cdot (1 - R)\right] \quad \textbf{6.12}$$

from which the membrane permeability, L_p, can be initially determined as the system ramps up its operation given measured values of Q_p and P_f . Subsequently, the permeate production set-point and the calculated permeability are used to calculate the required RO feed pressure P_f. The membrane permeability is calculated and updated dynamically as needed in the calculation of the required feed pressure.

6.2.4 Lower-Level RO Controller

The supervisory RO controller provides the lower-level RO controller (**Figure 6.2**) with the necessary feed pressure and flow rate set-points. The lower-level controller consists of a linear model for the RO pump VFD and a PI controller for the concentrate valve. The lower-level controllers do not enforce decoupling of the two control loops in the closed-loop system, i.e., a change in the RO pump VFD setting may affect the RO feed pressure regulated by the RO concentrate valve feedback controller. In this regard, it is stressed that the required feed pressure set-point for optimal operation is determined via a process model derived from a solution-diffusion model (**Eq. 6.12**). However, at the same time it is important to constrain the VFD ramp

speed in order to partially decouple the dynamics of the two control loops and allow the valve controller to provide responsive pressure control even when confronted with changing RO feed flow rate. While the determination of these time constants of the two control loops (**Eq. 6.13** and **Eq. 6.14**) can be done a priori on the basis of a process model, in the present work, step tests were used to determine these time constants and subsequently determine the present system's 5 rpm/s VFD ramp speed constraint. It is noted that multivariable control design could be used to provide an integrated approach to control action calculation for both inputs. However, given the significantly different time constants of the two control loops when the VFD ramp speed is constrained, such an approach is not expected to substantially improve the achievable closed-loop performance. At the same time, coupling of the controllers would considerably increase the burden of controller maintenance and decrease the robustness of the overall control architecture.

For the present RO pump/VFD combination (**Section 3.1**), the linear relationship between the pump RPM (VFD_{SP}^{RO}) and feed low rate ($Q_f^{desired}$) was determined experimentally as:

$$VFD_{SP}^{RO} = \left(11.38 \frac{RPM}{L/min}\right) Q_f^{desired} - 29.009\ RPM \qquad \textbf{6.13}$$

The Q_f set-point is calculated using the energy optimal Y determined in **Section 6.2.1, 6.2.2** and the Q_p set-point as specified by the desired permeate productivity. Given this Q_f set-point as provided by the supervisory controller, **Eq. 6.13** was then used to determine the required RO VFD setting.

Adjustment of the applied feed pressure is most sensitive to the RO concentrate valve position ($Valve_{SP}$) which was controlled by a PI controller of the following form:

$$Valve_{SP} = K_p^1 \left(P_{RO\,feed}^{SP} - P_{RO\,feed}(t)\right) + \frac{K_p^1}{\tau_i^1} \int_0^t \left(P_{RO\,feed}^{SP} - P_{RO\,feed}(\tau)\right) d\tau \qquad \textbf{6.14}$$

in which $Valve_{SP}$ is the control action applied to the RO valve, $P_{RO\,feed}^{SP}$ is the pressure set-point for the RO feed pressure, K_p^1 is the proportional gain, and τ_i^1 is the integral time constant. The Ziegler-Nichols method was used to tune the PI controller parameters to values of K_p^1 = -0.0725 $\frac{Valve\,\%}{MPa}$, and $\frac{K_p^1}{\tau_i^1}$ = 0.001 s.

Due to feed pressure fluctuations caused by the pump (e.g., ±70KPa in amplitude, or 8% of the feed pressure), tighter control of the pressure cannot be achieved once the set-point tracking error (i.e., absolute difference between the pressure and its set-point) becomes very small (as defined by an upper bound on the error which was set at 70 KPa). Therefore, the use of the PI controller when the tracking error becomes smaller than the upper error bound is counterproductive and would increase sensitivity of the closed-loop system to disturbances due to pump operation. Therefore, in the present control scheme, the PI controller was intermittently deactivated when the difference between the set-point and the pressure was below the upper bound pressure error threshold such that:

$$\text{If } |\,\mathrm{P}_{\mathrm{RO\,feed}}^{\mathrm{SP}} - \mathrm{P}_{\mathrm{RO\,feed}}(\mathrm{t})| > 70\ KPa,\ \ then\ \mathrm{K}_{\mathrm{p}}^{1} = -0.0725\,\frac{\text{Valve \%}}{MPa}\ ,\ \frac{K_p^1}{\tau_i^1} = 0.001\ \text{s}$$

$$\text{If } |\,\mathrm{P}_{\mathrm{RO\,feed}}^{\mathrm{SP}} - \mathrm{P}_{\mathrm{RO\,feed}}(\mathrm{t})| < 70\ KPa,\ \ then\ \mathrm{K}_{\mathrm{p}}^{1} = 0\,\frac{\text{Valve \%}}{\text{MPa}}\ ,\ \frac{K_p^1}{\tau_i^1} = 0\ \text{s}$$

6.3 Field study

The RO desalination pilot was deployed at Port Hueneme (Oxnard, CA, USA) with raw seawater feed pumped from an open-sea intake through a screen filter to the feed pretreatment subsystem. The range of feed water quality over the duration of the field study is listed in **Table 6.1**. The feed pretreatment system provided RO feed water of turbidity $\lesssim$ 0.1 NTU and enabled fouling-free operation of the RO over the study period. In one specific experiment, the RO

system was allowed to foul, by reducing the level of feed pretreatment in order to assess the capability of the controller; the change in membrane permeability was tracked and accordingly system operation settings self-adapted to maintain energy optimal operation. Other experiments included evaluation of system controller performance (i.e., with respect to maintaining permeate productivity and energy optimal operation) subject to step changes in permeate production set-point and short-term temporal variability of RO feed water salinity.

Table 6.1. Feed water quality at Port Hueneme US Naval Base

Variable	**Range**
TDS (Total Dissolved Solids)	33,440-36,800 ppm
TSS (Total Suspended Solids)	0.1-5.2 ppm
Turbidity	1.7-14 NTU
Temperature	11.2-19.7 °C
pH	7.5-8.2

6.4 Results & Discussion

The controller performance under both steady-state and non-steady-state conditions initially focused on establishing the capability for energy optimal operation under a permeate flow rate set-point of 31.4 L/min with constraints of minimum feed flow rate (Q_f) of 66 L/min, maximum recovery (Y) of 38.6% and maximum feed pressure (P_f) of 6.9 MPa. The controller was able to maintain the RO permeate flow-rate set-point with a deviation of ± 0.6% and the target maximum RO water recovery with a deviation of ± 0.3%. Based on the recorded pump electrical power utilization, system pressures, flow rates, and stream salinities, the pump efficiency was determined to be 91.5% ± 1% and salt rejection was calculated to be 99.6% ± 0.01%. Optimal

energy operation was achieved as illustrated in **Figure 6.6** that depicts the SEC curves as described by **Eq. 6.2**. System operation was along the SEC curve for the permeate flow rate set-point, at the maximum possible recovery (and thus lowest energy consumption; see **Section 6.2.2**) given the above constraints. Lower energy consumption is possible by running the system at the minimum possible feed flow rate; however, this would result in a permeate production flow rate that is 22% below the desired set-point.

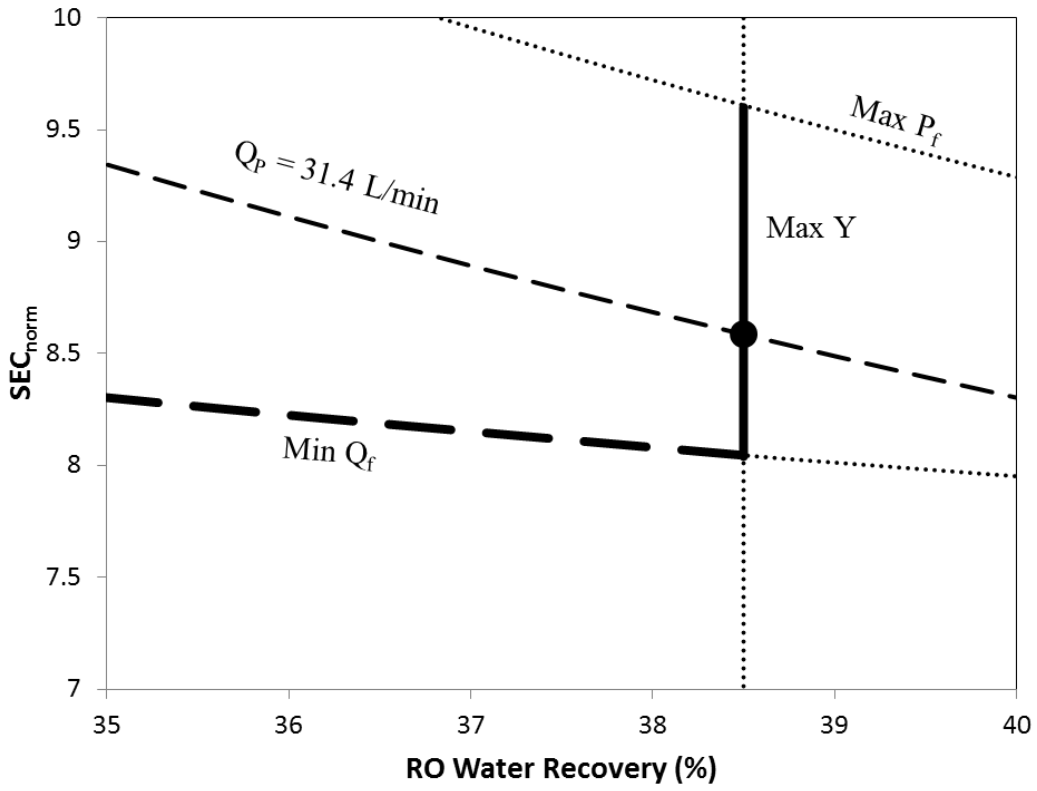

Figure 6.6. Normalized SEC with respect to RO recovery under constraints of Min(Q_f) = 60 L/min, Max(P_f) = 6.9 MPa, and Max(Y) = 38.6% for the target permeate flow rate set-point (Q_p = 31.4 L/min). The solid circle denotes the plant operating point as established by the controller which matches the expected theoretical prediction. **Eq. 6.2** was used to plot the constrained Q_P (Q_P = 31.4 L/min and max P_f) and constrained Q_f (min Q_f) curves. How **Eq. 6.2** was used to create a constrained Q_f curve was explained in **Section 6.2.1**.

The controller time-response to a permeate flow rate set-point change was subsequently evaluated in an experiment in which the system was first operated at a permeate flow rate set-

point of 26.5 L/min. Once steady state was reached, the permeate flow rate set-point was then reduced by 14% to 22.7 L/min with the response as shown in **Figure 6.7.** For the above operation system constraints were set as Min(Q_f) = 72.7 L/min, Max(P_f) = 6.9 MPa, and Max(Y)= 30%. The low recovery constraint was chosen to be below the system maximum physical recovery constraint (38.6%) in order to test a wider range of controller operability (i.e. above and below the set-point). As evident in **Figure 6.7a** and **Figure 6.7b**, upon a step change in the target permeate production, the controller drove the system to its new steady state within a short period (~30 s) and maintained the maximum allowable recovery (i.e., for the set recovery constraint). The controller performance as shown in **Figure 6.7a** and **Figure 6.7b** was achieved through the supervisory RO controller that established the new pressure and feed flow rate set points as 5.07 MPa and 78 L/min, respectively, relative to their previous corresponding values of 5.43 MPa and 90.8 L/min. Subsequently, the lower level RO controller drove the system toward steady state with relatively minor oscillations (**Figure 6.7c** and **Figure 6.7d**); this was largely because the lower-level controller utilizes a slightly under-damped closed-loop response for both the pump VFD and concentrate valve (**Section 6.2.4**). The operating conditions established by the RO controller can be visualized on the SEC plots for the constrained permeate flow rates (before and after the set-point change) as shown in **Figure 6.8**. It is clear that the RO system operation, for both permeate flow rate constraints, results in the lowest attainable SEC (corresponding to the highest achievable constrained recovery) as predicted per **Eq. 6.2**.

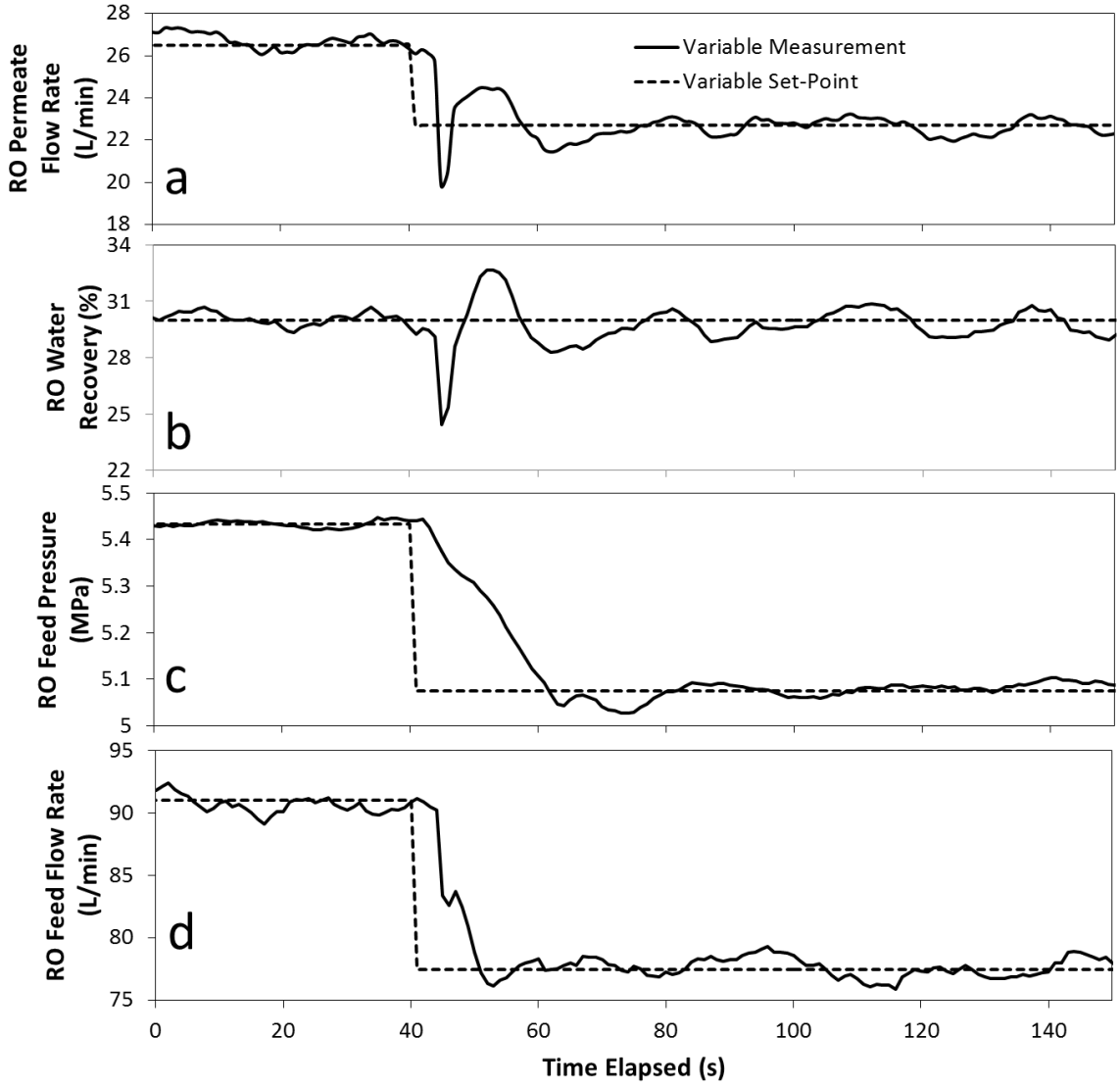

Figure 6.7. Profiles of (a) RO permeate flow rate, (b) RO water recovery, (c) RO feed flow rate, and (d) RO feed pressure with respect to time, for a permeate flow rate set-point transition from 26.5 L/min to 22.7 L/min. Constraints were set at Min (Q_p) = 72.7 L/min, Max(P_f) = 6.9 MPa, and Max(Y)=30%. The feed pressure set-point was changed from 5.43 MPa to 5.07 MPa. The feed flow rate set-point was changed from 90.8 L/min to 77 L/min.

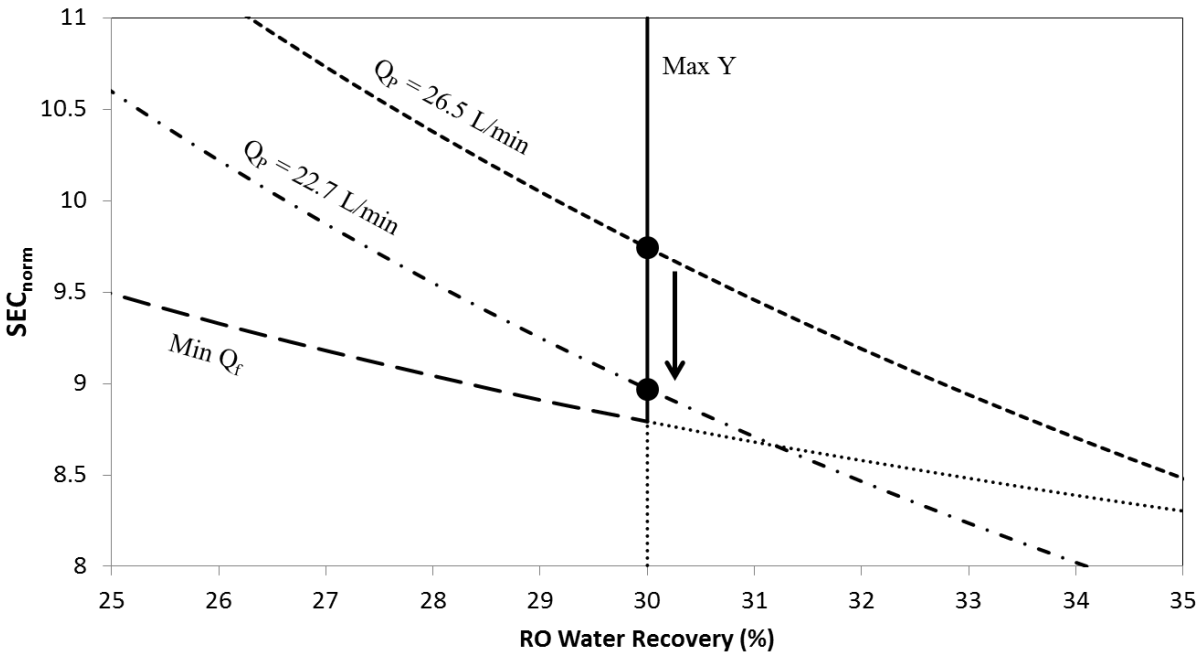

Figure 6.8. Normalized SEC with respect to RO recovery under constraints of Min(Q_f) = 72.7 L/min, Max(P_f) = 6.9 MPa, and Max(Y) = 30%. The short dashed line is the constrained permeate flow rate curve for the initial flow rate set-point of 26.5 L/min. The dash-dotted line is the constrained permeate flow rate curve for the final flow rate set-point of 22.7 L/min. The solid circles denote the operating point of the experiment and the arrow indicates the set-point change. **Eq. 6.2** was used to plot the constrained Q_P (The two constant Q_P curves and max P_f) and constrained Q_f (min Q_f) curves. How **Eq. 6.2** was used to create a constrained Q_f curve was explained in **Section 6.2.1**.

In order to evaluate the impact of the minimum feed flow rate constraint on the controller's performance, the RO permeate flow rate set-point was reduced by 35%, from 26.5 L/min to 17 L/min. The SEC curves (**Figure 6.9**) for the above constrained permeate production (Q_p = 17 L/min) and for operation at the minimum feed flow rate (Min(Q_f)) intersect at Y = 23.4%. Clearly, one would have to operate at the highest possible recovery to achieve the lowest SEC for the above constraints, which for the previous example (**Figure 6.8**) was constrained to a maximum of 30%. However, in transitioning from the higher to lower permeate flow rate set-points, the SEC curve for Min(Q_f) cannot be crossed. In fact, in order to achieve the target permeate productivity the RO system would have to operate at the recovery where the SEC curves for Q_p=17 L/min and Min(Q_f) = 72.7 L/min intersect. Accordingly, the low level RO controller

adjusted the RO recovery to Y= 23.4% (for the Q_p set-point of 17 L/min) as instructed by the supervisory controller (**Figure 6.10**) with steady-state operation for the new set point achieved within ~ 30 s.

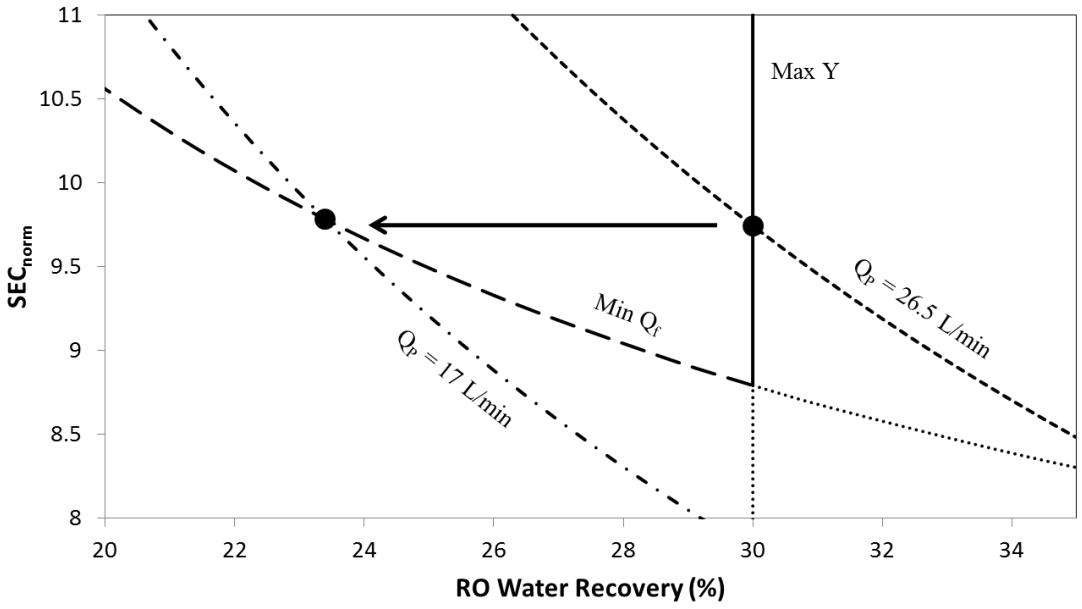

Figure 6.9. Normalized SEC with respect to RO recovery under constraints of Min(Q_f) = 72.7 L/min, Max(P_f) = 6.9 MPa, and Max(Y) = 30%. The short dashed line is the constrained permeate flow rate curve for the initial flow rate set-point of 26.5 L/min. The dash-dotted line is the constrained permeate flow rate curve for the final flow rate set-point of 17 L/min. The solid circles denote the operating point of the experiment and the arrow indicates the set-point change. **Eq. 6.2** was used to plot the constrained Q_P (The two constant Q_P curves and max P_f) and constrained Q_f (min Q_f) curves. How **Eq. 6.2** was used to create a constrained Q_f curve was explained in **Section 6.2.1**.

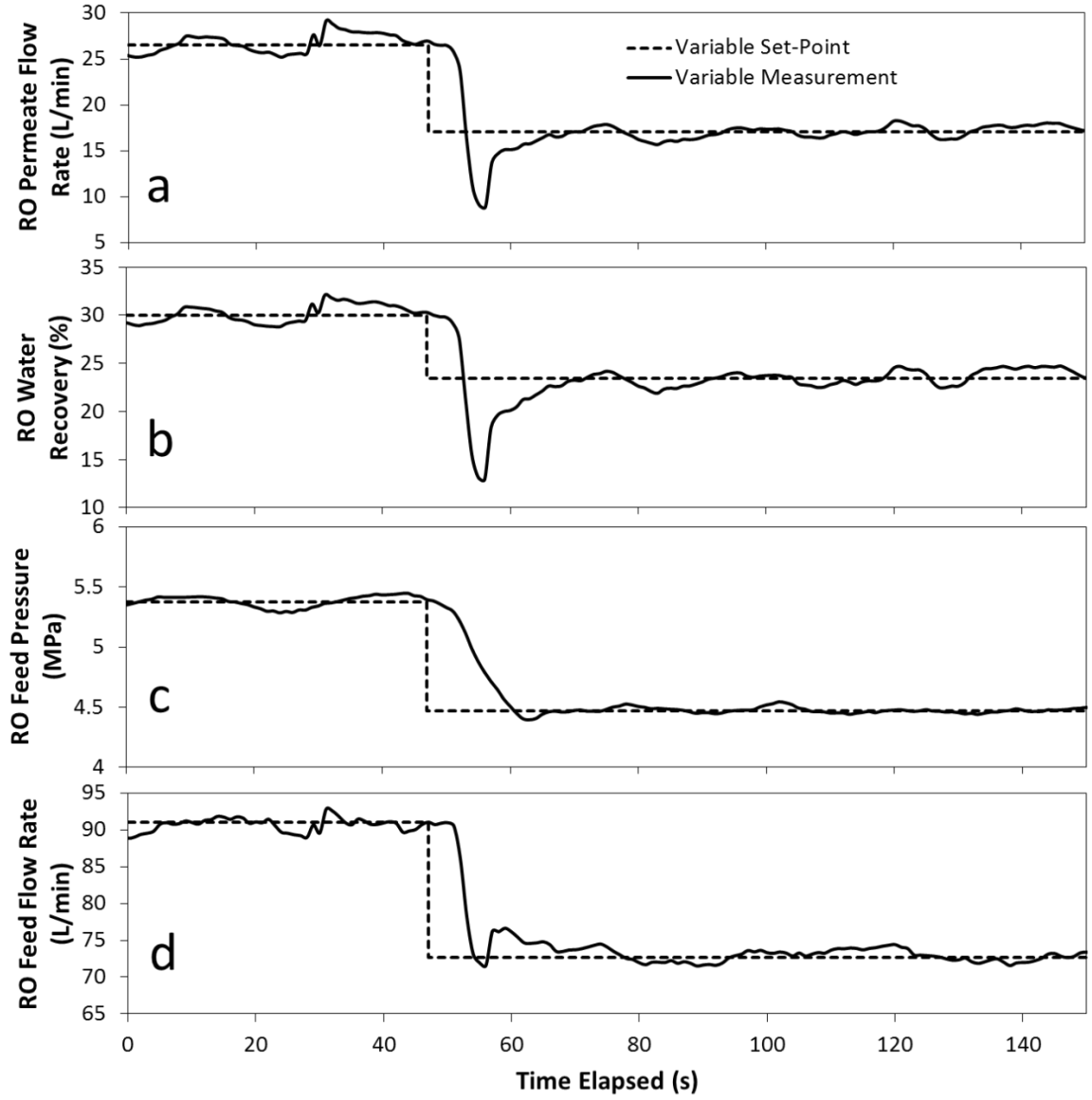

Figure 6.10. Profiles of (a) RO permeate flow rate, (b) RO water recovery, (c) RO feed flow rate, and (d) RO feed pressure with respect to time, for a permeate flow rate set-point transition from 26.5 L/min to 17 L/min. RO system constraints were set at Min(Q_f) =72.7 L/min, Max (P_f) = 6.9 MPa, and Max(Y) = 30%. Upon change in the permeate production set point, the supervisory RO controller reduced the set-point recovery from 30% to 23.4% and changed the feed flow rate and pressure set-points from 90.8 L/min to 72.7 L/min and from 5.38 MPa to 4.47 MPa, respectively.

In order to explore the controller's performance subject to temporal changes in feed salinity, a disturbance in the RO feed salinity was introduced using high salinity pulse input (**Figure 6.11**). This was achieved by mixing RO concentrate with the raw seawater feed to achieve a salinity

pulse of ~100 s during which the RO feed salinity peaked up to 17% above the raw seawater feed). Under the above operational mode, increased RO feed salinity will result in reduced permeate productivity and decreased RO water recovery due to the rise in the feed-side osmotic pressure. Comparison of RO system performance, with and without the controller, for a set of three consecutive feed salinity pulses is shown in **Figure 6.11** with the SEC given in **Figure 6.12**.

Without control action, the RO system was set to operate at feed pressure and feed flow rates of 5.5 MPa and 72.7 L/min, respectively, providing permeate production of 26.9 L/min for desalting raw seawater (~33,000 mg/L TDS). Operation under control action was for the same permeate production set-point. Although in principle both the feed flow rate and pressure can be controlled for optimal operation (**Section 6.2.4**), feed pressure has the most significant impact on permeate flux. Therefore, in this test the low level RO controller was simplified to maintain a constant feed flow rate. However, the optimal pressure set-point was adjusted continuously (**Figure 6.11c**), in response to changing feed water salinity (**Figure 6.11b**), as instructed by the supervisory RO controller, in order to minimize the SEC. It is apparent that without control action, permeate productivity decreased (up to 26% at the feed pulse peak salinity, **Figure 6.11a**) and SEC increased (up to 10% at the feed pulse peak salinity, **Figure 6.12**) with rising feed salinity. For example, over the duration of each of the three feed salinity pulses shown in **Figure 6.11b**, permeate productivity loss was up to about 12%. In contrast, RO operation under dynamic SEC control action permeate flow rate was nearer the set point and SEC was lower (**Figure 6.12**) even when confronted with rising feed salinity. As shown in the SEC contours for plant operation during a high feed salinity pulse (**Figure 6.12**), with and without control action (dotted and dashed lines, respectively), the SEC rises with increase feed salinity as the recovery decreases but decreases as feed salinity decreases. However, in plant operation with the RO

controller the feed pressure is continuously adjusted in response to the salinity pulse in order to set the recovery for operation at the lowest possible SEC.

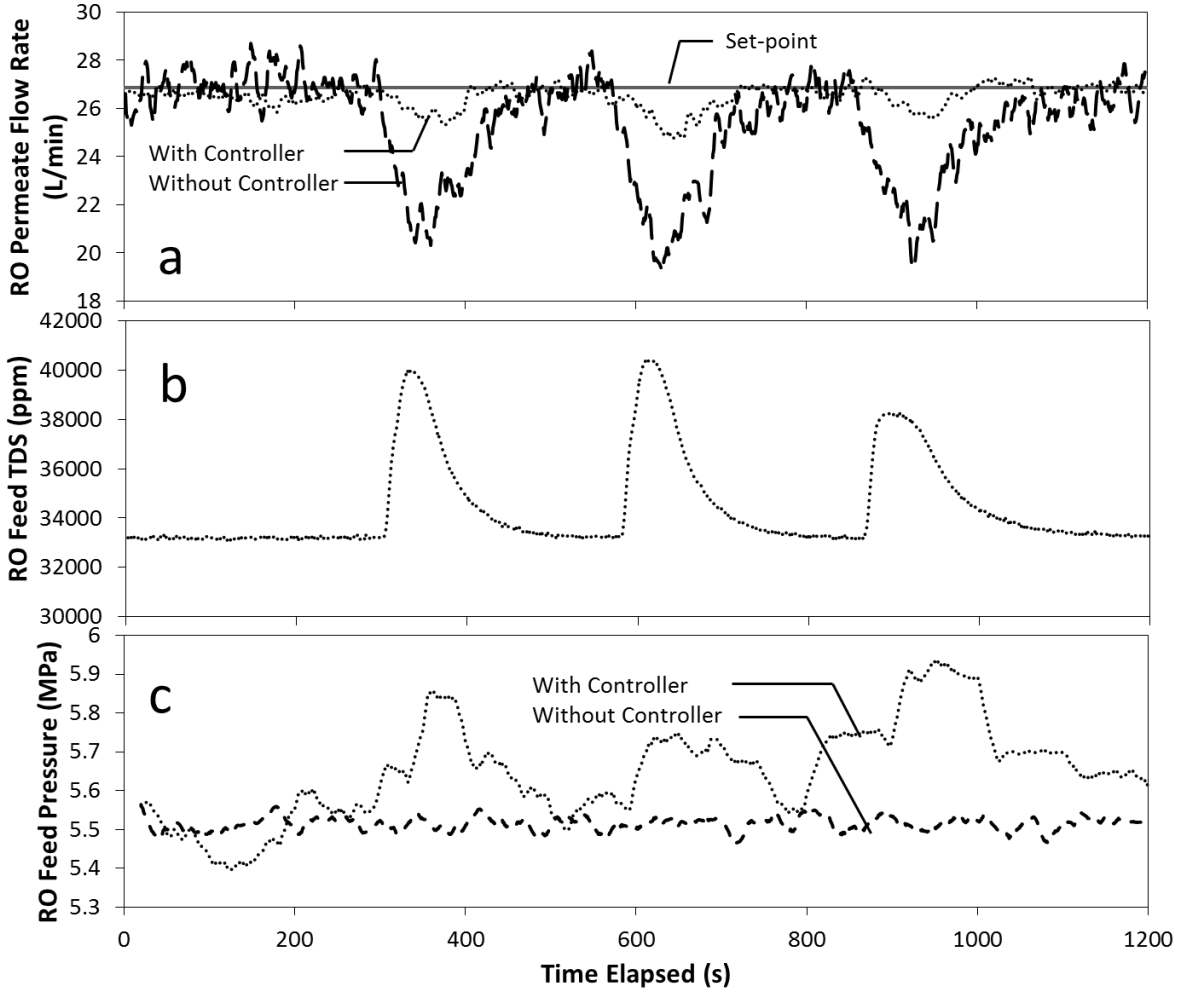

Figure 6.11. Profiles of the (a) RO permeate flow rate, (b) RO feed salinity, and (c) RO feed pressure RO feed salinity with respect to time. The solid line in (c) is the permeate flow-rate set-point, which is 26.9 L/min. RO system constraints were set at Min(Q_f) =72.7 L/min, Max (P_f) = 6.9 MPa, and Max(Y)= 30%. Plot (b) was produced using an average of both experiments since they were nearly identical.

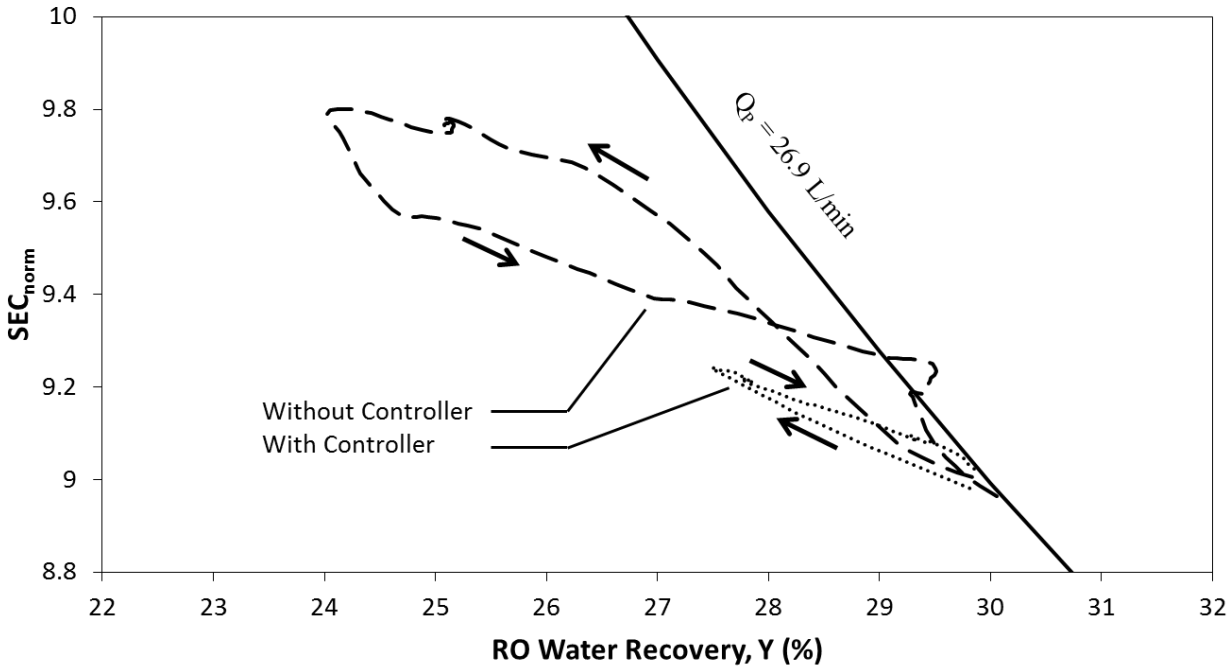

Figure 6.12. Normalized SEC with respect to RO recovery with the permeate flow rate set-point over the duration of the first pulse. The solid line is the SEC curve for constant Q_p operation of 26.9 L/min. Dotted lines denote the experiment done with the controller, the dashed lines denote the experiment done without the controller, and the arrows indicate the dependence of SEC_{norm} and Y on time. Note how operation without a controller leads to lower permeate flow rate as well as higher SEC. **Eq. 6.2** was used to plot the constrained Q_P curve.

Degradation of membrane permeability due to fouling can occur in field operations of RO desalting. As membrane permeability decreases in between cleaning periods, it is desirable to maintain the desired permeate productivity while operating at a recovery that is optimal with respect to the SEC (**Section 6.2.2**). Therefore, in the present control scheme membrane permeability is calculated (**Section 6.2.3**) and updated continuously by the supervisory RO which is necessary for determination of the feed pressure set point. Accordingly, as membrane permeability declines, the RO controller adjusts the feed pressure as well as feed flow rate necessary to achieve the maximum set recovery. A demonstration of the controller's performance under RO membrane fouling conditions was carried out over a 10-day continuous RO operation with reduced feed pretreatment. As a consequence, the RO membrane fouled with

membrane permeability decline of up to 5.8% over the test period (**Figure 6.13a**). At the same time, the RO controller continuously adjusted the feed pressure upward (via control of the concentrate valve) to compensate for the decrease in permeability, while permeate production (**Figure 6.13c**) and recovery (**Figure 6.13d**) remained essentially constant at the desired level.

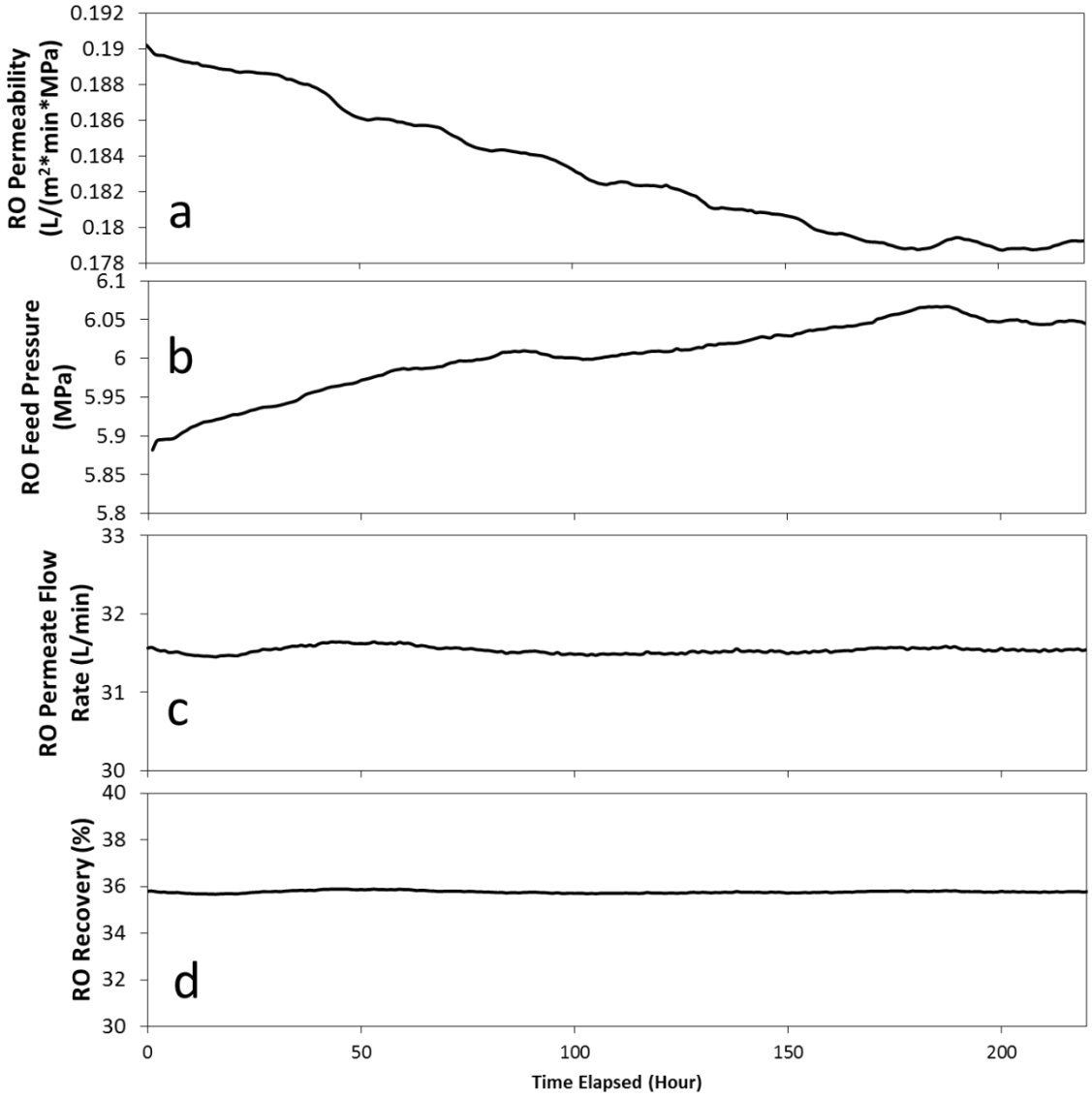

Figure 6.13. Profiles of RO process variables (a) membrane permeability, (b) feed pressure, (c) water recovery, and (d) permeate flux with respect to time. System constraints were set at Min (Q_f)=72.7 L/min, Max(Y)= 36% and Max(P_f)=6.9 MPa, with a permeate production target of 31.4 L/min. The system set the feed flow rate at 87.2 L/min.

6.5 Summary

A model-based control system was implemented for energy optimal operation of spiral-wound RO membrane desalination and for maintaining system operational set points with respect to feed pressure and flow rates (feed and permeate streams). The control scheme utilized a basic RO operational model with real-time calculations for continuous updates of membrane permeability and feed pressure set point. Operational control set points were determined by a supervisory level controller and then communicated to the lower-level controllers which then adjusted the RO feed pressure and flow rates via control of the high pressure VFD pump and RO concentrate valve. Field tests for seawater desalination have demonstrated controller ability to self-adapt system operation, so as to maintain energy optimal operation subject to constrains imposed by system physical components (e.g., minimum and maximum feasible or allowable flow rates and pressures) and the thermodynamic restriction for cross flow RO operation. It was also demonstrated that the control system succeeded in maintaining both permeate production and energy-optimal operation under conditions of temporal changes in feed water salinity. Although the present scheme was demonstrated for RO operation without an ERD, the developed control principles for energy optimal operation should be adaptable to RO system operation with ERD.

Chapter 7 Energy-Optimal Control of Two-Stage RO Desalination

7.1 Overview

This chapter presents a novel two-level model-based control system for the energy-optimal operation of a two-stage RO membrane desalination system. The control approach is based on the specific energy consumption (SEC) framework for a two-stage RO desalination system accounting for pump efficiencies, various physical system constraints and temporal variability of feed salinity. This SEC framework was then implemented as a higher-level (supervisory) control system for real-time optimization of the RO SEC. The supervisory controller combined real-time plant data obtained from plant sensors and the SEC model of two-stage RO to solve for energy-optimal values of the overall water recovery (Y) and the first-stage water recovery (Y_1) for a given water productivity target, feed salinity, and membrane permeability. The derived operating state was then applied to control the RO plant through a lower-level control system, consisting of three separate feedback loops regulating the RO feed flow rate, the first-stage RO pressure, and the second-stage RO pressure through the actuation of the first-stage RO feed pump, the second-stage RO feed pump, and the RO concentrate valve, respectively. The two-level control system was implemented and demonstrated for high-recovery brackish water desalination in a brackish water desalination plant capable of permeate productivity up to 40,000 gallons/day (**Section 3.2**). Field testing demonstrated robust simultaneous control of dynamically coupled control variables and effective energy-optimal operation, subject to feed salinity fluctuations.

7.2 Energy Optimization of Two-Stage RO

7.2.1 Two-Stage RO

In order to formulate a real-time energy-optimal control system for two-stage RO, an optimization algorithm which can determine the energy-optimal water recovery and the permeate production split between the two stages must be formulated. A two-stage RO configuration is defined as an RO system which contains two membrane trains that is separated by an intermediate booster pump, which serves to pressurize the first-stage concentrate stream and feeds it into the second membrane stage. The total permeate flow rate (Q_P) is permeate water collected from both membrane stages, and the overall water recovery (Y) is defined as the total permeate flow rate (i.e., combined from the two membrane stages) divided by the overall feed flow rate (i.e., which is the same as the feed flow rate to the first membrane stage). The first-stage water recovery (Y_1) and the second-stage water recovery (Y_2) are their respective permeate flow rates divided by their respective feed flow rates. A general schematic of the two-stage RO system is depicted in **Figure 7.1**, the variables used to represent the flow rate, pressure, and salinity of the different streams are shown in **Table 7.1**, and the equations for water recoveries are shown in **Eq. 7.1**.

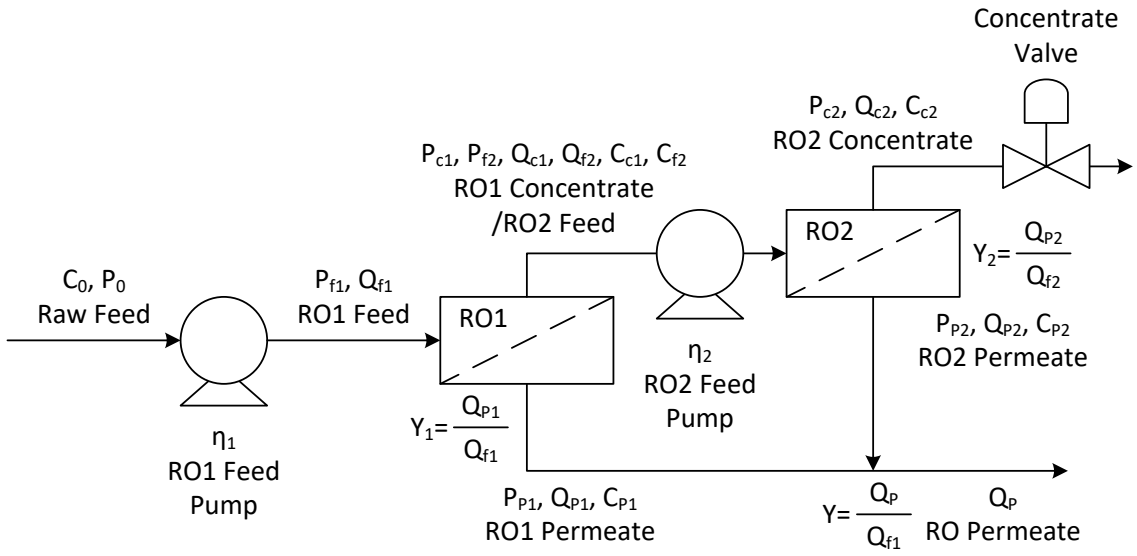

Figure 7.1. Schematic of a two-stage RO system, where P is pressure, Q is flow rate, C is salt concentration, *Y* is water recovery, and η is pump efficiency. Lettered subscripts indicate stream, with f for feed, c for concentrate, and p for permeate. Numbered subscripts denote whether stream is in stage 1 or stage 2.

Table 7.1. Nomenclature of flow rate, pressure, and salinity variables of different streams in a two-stage RO process.

	Flow Rate (Q)	Pressure (P)	Salinity (C)
Raw Feed	Q_f	P_0	C_f
RO First-Stage Feed	$Q_{f1} = Q_f$	P_{f1}	$C_1 = C_f$
RO First-Stage Concentrate	Q_{f2}	P_{f2}	C_{f2}
RO Second-Stage Feed	$Q_{C1} = Q_{f2}$	P_{C1}	$C_{C1} = C_{f2}$
RO Second-Stage Concentrate	Q_{C2}	P_{C2}	C_{C2}
RO First-Stage Permeate	Q_{P1}	P_{P1}	C_{P1}
RO Second-Stage Permeate	Q_{P2}	P_{P2}	C_{P2}

$$Y = \frac{Q_P}{Q_f} \ , \ \ Y_1 = \frac{Q_{P1}}{Q_f} \ , \ \ Y_2 = \frac{Q_{P2}}{Q_{f2}} = \frac{Q_P - Q_{P1}}{Q_f(1 - Y_1)} = \frac{Y - Y_1}{1 - Y_1} \qquad \textbf{7.1}$$

Even if the raw feed flow rate and the total RO permeate flow rate were kept constant (constant *Y*), the permeate production split between the two stages can vary. For a constant overall total RO permeate production, increasing the permeate production in the first-stage results in an increase in Y_1 and a decrease in Y_2. For a given *Y* and Y_1, Y_2 can be expressed with a simple mass balance calculation where $Y_2 = (Y - Y_1) / (1 - Y_1)$ (**Eq. 7.1**). Therefore, fixing *Y* and Y_1 will set the operating state for the entire two-stage RO system (i.e., since Y_1 by itself is sufficient for quantifying the recovery split between the two stages).

7.2.2 SEC Optimization of Two-Stage RO

The SEC of a two-stage RO as a function of *Y* and Y_1 can be then derived in order to explore how SEC is affected by the overall water recovery and the permeate production split between the two stages. The normalized SEC of an RO process with an ERD is the total work done by pumps (i.e., to pressurize RO feed water), subtracted by the energy recovered by the ERD, and divided by the product water flow rate. The expanded plant work is the product of the applied feed pressure and feed flow rate. For a two-stage RO, the SEC equation is obtained by taking the sum of the work done by the two pumps and dividing it by the total permeate flow rate. Work for each component of a two-stage RO with an ERD (i.e., the first-stage pump, the second-stage pump, and the ERD) are all expressed in **Eq. 7.2**. The SEC of a two-stage RO with an ERD, with the flow rates with being replaced by the recovery terms (**Eq. 7.1**), is shown in **Eq. 7.3**.

$$W_{Total} = W_1 + W_2 - W_{ERD}$$

$$W_1 = \frac{\Delta P_1 \cdot Q_f}{\eta_1} \qquad \textbf{7.2}$$

$$W_2 = \frac{\Delta P_2 \cdot Q_f \cdot (1 - Y_1)}{\eta_2}$$

$$W_{ERD} = (\Delta P_1 + \Delta P_2) \cdot (1 - Y) \cdot Q_f \cdot \eta_{ERD}$$

$$SEC(2ROs) = \frac{W_{Total}}{Q_P} = \frac{\Delta P_1}{Y \cdot \eta_1} + \frac{\Delta P_2 \cdot (1 - Y_1)}{Y \cdot \eta_2} - \frac{(\Delta P_1 + \Delta P_2) \cdot (1 - Y) \cdot \eta_{ERD}}{Y} \qquad \textbf{7.3}$$

where W_1 is the work done by the first-stage feed pump, W_2 is the work done by the second-stage feed pump, W_{ERD} is the work recovered by the ERD, η_1 is the first-stage feed pump efficiency, η_2 is the second-stage feed pump efficiency, η_{ERD} is ERD efficiency, Q_P is the total permeate flow rate, ΔP_1 is the pressure applied by the first-stage pump relative to the source water feed pressure (i.e., $\Delta P_1 = P_{f1} - P_0$), and ΔP_2 is the pressure applied by the second-stage pump relative to the first-concentrate pressure (i.e., $\Delta P_2 = P_{f2} - P_{C1}$). The first term of the right-hand side is the energy consumption of the first-stage feed pump, the second term represents the energy consumption of the second-stage feed pump, and the third term is the energy recovered through the ERD. In a previous study, Zhu et al. [58] concluded when the RO feed pressure is equivalent to the osmotic pressure difference at the RO membrane exit region (i.e., when permeate productivity is ensured along the entire RO membrane module), then the RO system is operating at the global SEC minimum achievable for RO systems. The global SEC minimum achievable for RO systems is defined as the thermodynamic limit of cross-flow RO desalting, and is referred to as the thermodynamic restriction in this work. For a two-stage RO system, the feed pressure required to operate the RO desalination system at the thermodynamic restriction (i.e., which is

equivalent to the value of the osmotic pressure difference at the end of both stages) can be expressed as follows:

$$\Delta P_1 = \pi_{1,exit} = \frac{\pi_0 R_1}{(1-Y_1)}, \quad \Delta P_1 + \Delta P_2 = \pi_{2,exit} = \frac{\pi_0 R_T}{(1-Y)} \tag{7.4}$$

$$R_1 = 1 - \frac{C_{p1}}{C_f} \quad , \quad R_T = 1 - \frac{C_p}{C_f}$$

where π_0 is the feed osmotic pressure, R_1 is the observed first-stage membrane salt rejection, and R_T is the observed overall salt rejection for the combined two stages. It is noted that the observed membrane rejection is not an intrinsic property of the membrane and may vary due to operating conditions. The normalized SEC (i.e., with respect to feed osmotic pressure) for a two-stage RO process at the thermodynamic restriction can be then derived given the reasonable assumption that the pressure drop within the RO module is negligible (i.e., the contribution of frictional losses are <1% of the total required pressure [58]) leading to the following expression:

$$SEC_{tr,norm}(2ROs) = \frac{SEC}{\pi_0} = \frac{R_1}{\eta_1 Y(1-Y_1)} + \frac{1}{\eta_2 Y}\left[\frac{R_T(1-Y_1)}{(1-Y)} - R_1\right] - \frac{R_T \cdot \eta_{ERD}}{Y} \tag{7.5}$$

In which the first term is the energy consumption of the first-stage feed pump, the second term is the energy consumption of the second-stage feed pump, and the third term is the energy recovered through the ERD. **Eq. 7.5** indicates that the SEC depends on Y, Y_1, η_1, and η_2. Therefore, it is essential to analyze how SEC and the energy-optimal Y shift as a function of these variables. First, the effects of pump efficiencies on the SEC can be analyzed by solving for the partial derivatives $\partial[SEC_{tr,norm}(2ROs)] / \partial \eta_1$ and $\partial[SEC_{tr,norm}(2ROs)] / \partial \eta_2$.

$$\frac{\partial\left[SEC_{tr,norm}(2ROs)\right]}{\partial \eta_1} = \frac{-1}{\eta_1^2 Y(1-Y_1)} \quad , \quad \frac{\partial\left[SEC_{tr,norm}(2ROs)\right]}{\partial \eta_2} = \frac{-(Y-Y_1)}{\eta_2^2 Y(1-Y)} \tag{7.6}$$

It is noted both derivatives are negative throughout the range of all possible values of $Y > Y_1$, Y = (0,1], Y_1 = (0,Y], η_1 = (0,1], and η_2 = (0,1]. Therefore, it can be concluded that increasing pump

efficiencies decreases the SEC and that the optimal pump efficiency will be to operate at the highest possible efficiencies. The optimal Y_1 at a given Y can be obtained by solving for the equation $\partial[SEC_{tr,norm}(2ROs)]/\partial Y_1 = 0$ and is given by [58]:

$$Y_{1,optimal} = 1 - \sqrt{\frac{R_1 \cdot \eta_2}{R_T \cdot \eta_1}(1 - Y)} \qquad \textbf{7.7}$$

Since $Y_{1,optimal}$ for a given Y is a function of η_1 and η_2, it can be expected that changes in the pump efficiencies will result in a change in $Y_{1,optimal}$. However, for cases where the pump efficiencies and rejections are equivalent between the two stages (i.e., $\eta_2 = \eta_1$, $R_T = R_1$), it can be shown through a mass balance calculation that the $Y_{2,optimal}$ is equal to $Y_{1,optimal}$ and $Y_{1,optimal}$ is not a function of pump efficiencies [58]:

$$Y_{2,optimal} = \frac{Y - Y_{1,optimal}}{1 - Y_{1,optimal}} = \frac{Y - 1 + \sqrt{1 - Y}}{\sqrt{1 - Y}} = 1 - \sqrt{1 - Y} = Y_{1,optimal} \qquad \textbf{7.8}$$

However, for the case where the second-stage pump is less efficient relative to the first-stage pump (i.e., the ratio of η_2 / η_1 decreases), then **Eq. 7.7** will result in a larger value of $Y_{1,optimal}$ compared to a case where the second-stage pump is more efficient (i.e., the ratio of η_2 / η_1 increases). As a consequence if the first-stage pump is more efficient, then it is more energy-optimal to increase the permeate production in the first-stage by increasing Y_1. This general trend of the optimal Y_1 increasing as the first-stage pump becomes more efficient relative to the second-stage pump can be seen in **Figure 7.2a**. The overall trend of SEC as a function of Y_1 for a given Y is illustrated in **Figure 7.21** and **Figure 7.22**.

The value of Y at which the minimum SEC occurs (i.e., energy-optimal Y) can be then calculated by inserting the optimal Y_1 calculated through **Eq. 7.7** into **Eq. 7.5**, and by solving for $\partial[SEC_{tr,norm}(2ROs)]/\partial Y = 0$.

$$\frac{\partial\left[SEC_{tr,norm}(2ROs)\right]}{\partial Y}$$

$$= \frac{R_1^2\eta_2}{2R_T\eta_1^2 Y(1-Y_1)^3} - \frac{R_1}{\eta_1 Y^2(1-Y_1)}$$
$$+ \frac{1}{\eta_2 Y}\left[\frac{R_T(1-Y_1)}{(1-Y)^2} - \frac{R_1\cdot\eta_2}{2\eta_1(1-Y)(1-Y_1)}\right] \quad \textbf{7.9}$$
$$- \frac{1}{\eta_2 Y^2}\left[\frac{R_T(1-Y_1)}{(1-Y)} - R_1\right] + \frac{R_T\cdot\eta_{ERD}}{Y^2}$$

It is noted that for the sake of simplicity, Y_1 in **Eq. 7.9** is used as a substitution for the term in the right-hand side of **Eq. 7.7**. Instead of expressing **Eq. 7.9** as an explicit function for Y, **Eq. 7.9** is left as an implicit function and is solved numerically for Y. The resulting $Y_{optimal}$ as a function of η_2 and η_1 is illustrated in **Figure 7.2b**. It is noted if the first-stage pump becomes more efficient relative to the second-stage pump (e.g., η_1 increases or η_2 decreases), the optimal Y value decreases. The overall trend of SEC as a function of Y is illustrated in **Figure 7.23** and **Figure 7.24**. Even when a two-stage RO system is operating at the thermodynamic restriction, there is still a potential to further reducing energy consumption by optimizing for Y and Y_1.

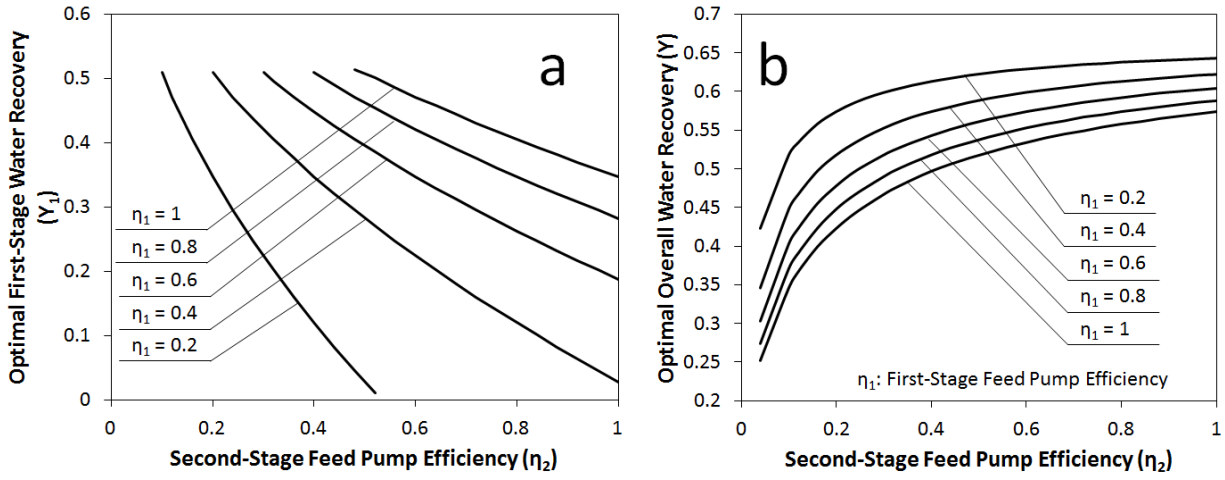

Figure 7.2. Profiles of the optimal operating single-stage water recovery (Y_1) and the overall water recovery (Y) as a function of the first-stage pump efficiency (η_1) and the second-stage pump efficiency (η_2). The optimal Y_1 is calculated through **Eq. 7.7**, while the optimal Y is calculated through **Eq. 7.9**.

For cases where the first and second stage pump efficiencies differ it is of interest to determine whether it is more energy-optimal to have the more efficient pump in the first or second stage. The difference between the SEC of a two-stage RO system with the more efficient pump in the first stage and the SEC of a system with the more efficient pump in the second stage can be quantified by the following approach: First, two pump efficiencies, η_{Eff} and η_{NotEff}, where η_{Eff} is the more efficient pump ($\eta_{Eff} > \eta_{NotEff}$) are defined; Then, η_{Eff} and η_{NotEff} are substituted in for η_1 and η_2, respectively, in **Eq. 7.5**, then subtracted by **Eq. 7.5** where η_{Eff} and η_{NotEff} are substituted in for η_2 and η_1, respectively (i.e., the opposite of the previous case). This can be expressed with the following inequality:

$$0 < \frac{R_1}{\eta_{Eff} Y(1-Y_1)} + \frac{1}{\eta_{NotEff} Y}\left[\frac{R_T(1-Y_1)}{(1-Y)} - R_1\right] - \frac{R_1}{\eta_{NotEff} Y(1-Y_1)} - \frac{1}{\eta_{Eff} Y}\left[\frac{R_T(1-Y_1)}{(1-Y)} - R_1\right] \quad \textbf{7.10}$$

If the above inequality holds true, then this is evidence that it will always be more energy-optimal to install the more efficient pump in the first stage. **Eq. 7.10** can be rearranged into the following form:

$$0 > \left(\frac{1}{\eta_{Eff}} - \frac{1}{\eta_{NotEff}}\right)\left(\frac{R_1}{Y(1-Y_1)} - \frac{1}{Y}\left[\frac{R_T(1-Y_1)}{(1-Y)} - R_1\right]\right) \quad , \quad \eta_{Eff} > \eta_{NotEff} \qquad \textbf{7.11}$$

Since the inequality as specified by **Eq. 7.11** will always hold true, it can be concluded that installing the more efficient pump in the first stage will always result in a more energy efficient RO operation relative to the alternative of installing the more efficient pump in the second stage.

7.2.3 Comparison of SEC between Single-Stage versus Two-Stage RO

The SEC equations for single-stage operation and two-stage operation can be compared to assess the impact of pump efficiencies on the relative SEC for these two RO plant configurations.

The equation for operation of a single-stage RO at the thermodynamic limit is represented by the first (i.e., energy consumption of the first-stage pump) and the third term (i.e., energy recovered by the ERD) of **Eq. 7.3** which describes the SEC for a single stage. Following the analysis approach used in **Section 7.2.2** where the system is operating at the thermodynamic restriction and the feed pressure is equivalent to the osmotic pressure at the membrane exit (i.e., thermodynamic restriction), the SEC of a first-stage RO system can be expressed as follows [58]:

$$SEC_{tr,norm}(1RO) = \frac{R_T}{\eta_1 Y(1-Y)} - \frac{R_T \cdot \eta_{ERD}}{Y} \qquad \textbf{7.12}$$

Given **Eq. 7.12**, two-stage operation will be more optimal than one-stage operation if the condition $SEC_{tr,norm}(2ROs) < SEC_{tr,norm}(1RO)$ is met. This inequality is expressed below:

$$\frac{R_1}{\eta_1 Y(1-Y_1)} + \frac{1}{\eta_2 Y}\left[\frac{R_T(1-Y_1)}{(1-Y)} - R_1\right] - \frac{R_T \cdot \eta_{ERD}}{Y} < \frac{R_T}{\eta_1 Y(1-Y)} - \frac{R_T \cdot \eta_{ERD}}{Y} \qquad \textbf{7.13}$$

For the special case of where the R_T is assumed to be equal to R_1. **Eq. 7.13** can be then simplified to:

$$Y_1 > 1 - \frac{\eta_2}{\eta_1} \qquad \textbf{7.14}$$

where $\eta_1 = (0,1]$, $\eta_2 = (0,1]$, and $Y_1 = (0,Y]$. Since Y_1 is strictly a value between 0 and 1, it can be concluded that if $\eta_1 = \eta_2$ or $\eta_1 < \eta_2$, then the right-hand side of the equation will always be < 0 and therefore the inequality will always hold true; hence, a two-stage operation will always be more energy-efficient than a single-stage operation. However, if $\eta_1 > \eta_2$, then the second term on right-hand side of **Eq. 7.14** will be a positive value that is less than 1. The right-hand side of **Eq. 7.14** will then be a value in the range of [0,1] and it becomes possible that the right-hand side of **Eq. 7.14** can be greater than Y_1. Therefore, for two-stage RO systems with a second-stage pump that is less efficient than the first-stage pump, a single-stage mode (if possible) if Y_1 is less than the right-hand side of **Eq. 7.14**.

7.2.4 Operation at a Constrained Permeate Flow Rate

In **Section 7.2.2** it was shown that the recovery, *Y*, at which the global minimum SEC occurs is in the range of ~25 – 65% (i.e., depending on pump efficiencies, **Figure 7.2b**). However, in brackish water desalination it is typically desirable to achieve high recovery in the range of 70-90% due to the significant costs associated with brine management [117-119]. Achieving high recovery requires the utilization of multiple RO stages [99, 100]. Therefore, there may be cases where RO operation at a higher water recovery will force plant operation away from the global SEC minimum. RO system are typically designed to operate at a desired level of permeate productivity and thus operation away from the thermodynamic restriction is at a constrained permeate flow rate. The feed pressures required to achieve a desired permeate flow rate can be estimated from the classical RO flux equation [62]:

$$Q_p = A_m L_p (\Delta P_m - \overline{\Delta\pi}) \qquad \textbf{7.15}$$

where Q_P is the permeate flow rate, A_m is the active membrane area, L_p is the membrane permeability, ΔP_m is the average transmembrane pressure along the membrane module, and $\overline{\Delta\pi}$ is the average osmotic pressure difference between the concentrate and permeate streams along the membrane module. Assuming a linear pressure profile along the retentate channel of the RO elements [95], the average transmembrane pressure can be expressed as:

$$\Delta P_m = \frac{P_f + P_c}{2} - P_p \qquad \textbf{7.16}$$

where P_P is the permeate-side pressure, P_f is the feed pressure, and P_c is the concentrate pressure at the module exit. The average feed osmotic pressure can be approximated as the log-mean average along the membrane [70], and the average feed-side osmotic pressure difference can be expressed as follows [116, 120]:

$$\overline{\Delta\pi} = \pi_0 \frac{ln\left(\frac{1}{1-Y}\right)}{Y} \cdot \overline{CP} - \pi_0 \cdot (1-R) \qquad \textbf{7.17}$$

in which π_0 is the feed osmotic pressure, $\overline{CP}$ is the average concentration polarization modulus (**Section 7.4.1**, **Eq. 7.25)** in each RO membrane element (i.e., $\overline{CP} = C_m/C_b$, where C_b and C_m are the average salt concentrations in the bulk and at the membrane surface, respectively, and R is the observed salt rejection (**Eq. 7.4**). **Eqs. 7.16 – 7.18** can be then inserted into **Eq. 7.15** and rearranged into the following equation [110]:

$$Q_p = A_m L_p \left[\frac{P_f + P_c}{2} - P_p - \frac{\pi_0}{Y} ln\left(\frac{1}{1-Y}\right) \cdot \overline{CP} + \pi_0 \cdot \frac{C_p}{C_f}\right]$$

$$P_f = 2\left[\frac{Q_{p,Desired}}{A_m \cdot L_p} + P_p + \frac{\pi_0}{Y} ln\left(\frac{1}{1-Y}\right) \cdot \overline{CP} - \pi_0 \cdot \frac{C_p}{C_f}\right] - P_c \qquad \textbf{7.18}$$

By replacing variables with those that correspond to each RO stage and by replacing variables Y_2, Q_{P1} and Q_{P2} with the expressions $Y_2 = (Y - Y_1) / (1 - Y_1)$, $Q_{P1} = Q_{P,Desired} \cdot Y_1 / Y$, and $Q_{P2} = Q_{P,Desired} \cdot (Y - Y_1) / Y$ (**Eq. 7.1**), **Eq. 7.18** can be used to derive two similar equations for the feed pressures of both stages in a two-stage RO system:

$$P_{f1} = 2\left[\frac{Q_{P,Desired} \cdot Y_1}{Y \cdot A_{m1} \cdot L_{p1}} + P_{p1} + \frac{\pi_0}{Y_1} ln\left(\frac{1}{1-Y_1}\right) \cdot \overline{CP_1} - \pi_0 \cdot \frac{C_{p1}}{C_{f1}}\right] - P_{c1} \qquad \textbf{7.19}$$

$$P_{f2} = 2\left[\frac{Q_{P,Desired} \cdot (Y - Y_1)}{Y \cdot A_{m2} \cdot L_{p2}} + P_{p2} + \frac{\pi_0}{Y - Y_1} ln\left(\frac{1-Y_1}{1-Y}\right) \cdot \overline{CP_2} - \frac{\pi_0}{1-Y_1} \cdot \frac{C_{p2}}{C_{f2}}\right] - P_{c2} \qquad \textbf{7.20}$$

where variables with the subscript 1 and 2 correspond to values for the first stage and second stage, respectively (**Table 7.1**).

A special case is considered where a 2-stage RO system where the frictional pressure losses are negligible (i.e., $P_f = P_C$), the membranes are high rejection such that R=1 and where concentration polarization is negligible (i.e., $\overline{CP}$ = 1), and where both membrane stages have the

same number of membrane elements ($A_{m1} = A_{m2} = A_m$) where all membranes are of the same permeability ($L_{P1} = L_{P2} = L_P$). It is noted that this special case is not used for the control system described in this work and variables such as the rejection and membrane area are taken into account by the presented control system. By defining a normalized permeate flow rate as $Q_{P,norm} = Q_P / (\pi_0 \cdot A_m \cdot L_p)$, **Eqs. 7.19** and **7.20** can be simplified to the following forms:

$$P_{f1} = \pi_0 \left[\frac{Q_{p,norm} \cdot Y_1}{Y} + \frac{1}{Y_1} ln \left(\frac{1}{1 - Y_1} \right) \right] \quad \textbf{7.21}$$

$$P_{f2} = \pi_0 \left[\frac{Q_{p,norm} \cdot (Y - Y_1)}{Y} + \frac{1}{Y - Y_1} ln \left(\frac{1 - Y_1}{1 - Y} \right) \right] \quad \textbf{7.22}$$

Eqs. 7.21 and **7.22** can be then substituted into **Eq. 7.3** assuming $\Delta P_1 = P_{f1}$ (i.e., assume inlet pressure into the first-state feed pump is zero) and $\Delta P_1 = P_{f2} - P_{f1}$ (i.e., no pressure drop between the first-stage exit and second-stage pump inlet):

$$SEC_{norm} = \frac{1}{Y \cdot \eta_1} \left[\frac{Q_{p,norm} \cdot Y_1}{Y} + \frac{1}{Y_1} ln \left(\frac{1}{1 - Y_1} \right) \right] + \frac{(1 - Y_1)}{Y \cdot \eta_2} \left[\frac{Q_{p,norm} \cdot (Y - Y_1)}{Y} + \frac{1}{Y - Y_1} ln \left(\frac{1 - Y_1}{1 - Y} \right) \right] \quad \textbf{7.23}$$

Eq. 7.23 expresses the SEC of a two-stage RO system as a function of the desired Q_P, Y, and Y_1. For a given value of Q_P, the Y and Y_1 which will result in the minimum SEC can be solved by using standard constrained multivariable nonlinear optimization. The constraint where the SEC calculated by **Eq. 7.23** must be greater than the SEC at the thermodynamic restriction calculated by **Eq. 7.5** is used. Examples with a given pump efficiency of $\eta_1 = 0.45$ and $\eta_2 = 0.4$ is shown in **Figure 7.3**, where **Eq. 7.23** for two different values of normalized permeate flow rate are plotted. In the above example, the values of Y and Y_1 were calculated using the Solver function in Microsoft Excel, and the SECs calculated using these values are illustrated as solid circles in **Figure 7.3**. This approach of solving for the SEC of an RO system at a constrained permeate

flow rate operation and then numerically solving for its minimum through a constrained nonlinear optimization algorithm can be then utilized for an energy-optimal control system described in the next section.

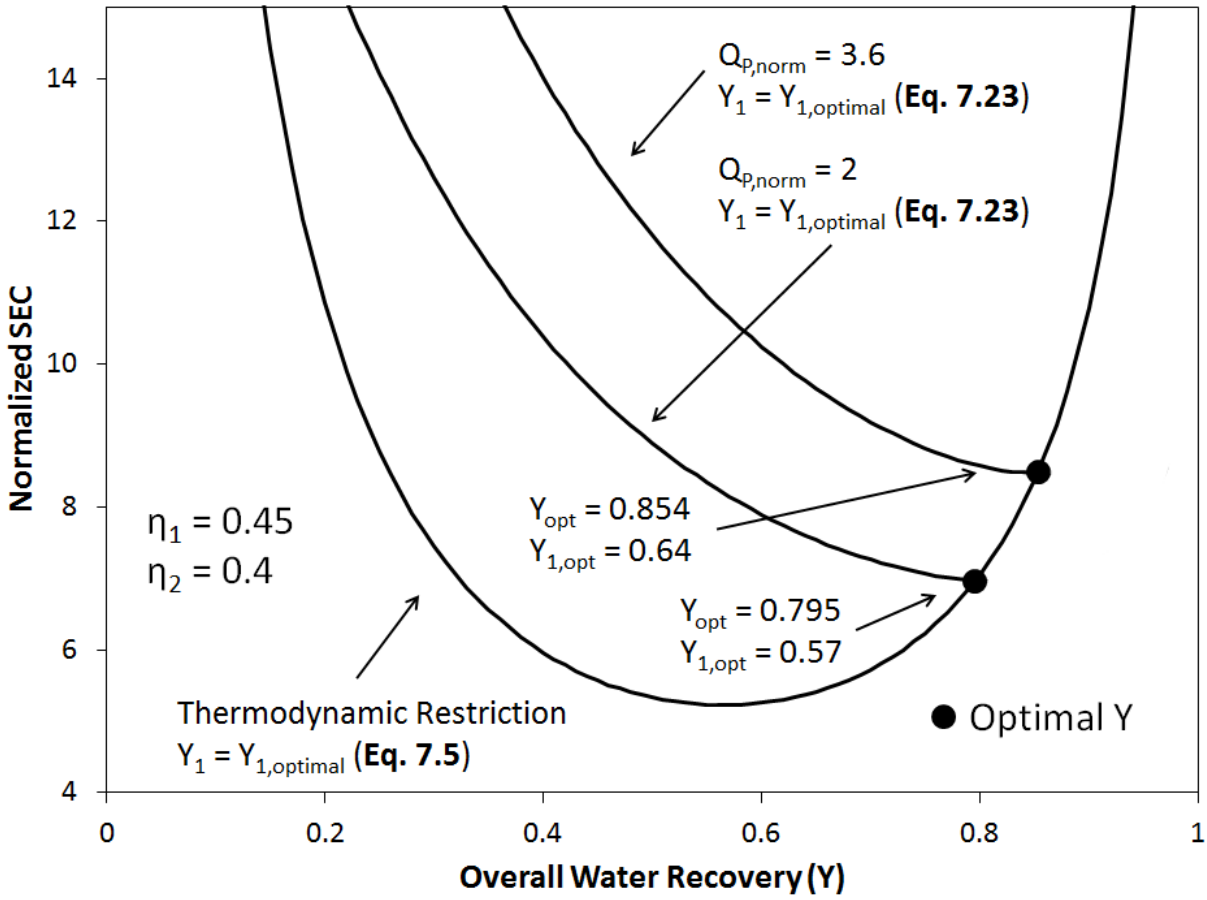

Figure 7.3. Plot of SEC vs *Y* at a constrained permeate flow rate for this study's pilot plant at a constant η_1 and η_2. Optimal *Y*s are highlighted, and for an ideal system, the energy-optimal operating point for operation at a constrained permeate flow rate occurs on the thermodynamic restriction. **Eq. 7.5** is used to plot the thermodynamic restriction, while **Eq. 7.23** is used to plot the constrained permeate flow rate curves.

7.3 Energy-Optimal Control of Two-Stage RO

7.3.1 Supervisory RO Control System

In **Section 7.2.4**, a method of solving for the energy-optimal Y and Y_1 of a two-stage RO system operating at a constrained permeate flow rate was described. However, for the purposes of a control system, a method to convert these operational values (e.g., Y and Y_1) into values useful for a physical system (e.g., pump rotation speed, valve position) is required. Therefore, a two-level control architecture described and successfully implemented in a previous work [110] which contain a supervisory-level controller (i.e., which calculates the energy-optimal operating point) and a lower-level controller (i.e., which applies calculated operating such as feed flow rate and pressure set-points to system) is adopted for this study. The general work-flow diagram of the control system is shown in **Figure 7.4**. The supervisory controller collects available sensor data and calculates the value of both first-stage and second-stage membrane permeabilities through a rearrangement of **Eqs. 7.19** and **7.20**. It is noted that **Eqs. 7.19** and **7.20** can be used directly for the purpose of calculating membrane permeabilities and pressure given that the pressures, flow rates, and conductivities are all monitored on the RO plant. While the above equations are reasonable approximations, it is noted that any suitable models for the stage 1 and stage 2 feed pressures (which also consider membrane permeability and area) can be utilized in the controller architecture, without a loss of generality. Once the membrane permeabilities are calculated with the latest sensor data, these values are then used in **Eqs. 7.19** and **7.20** to estimate the first and second-stage feed pressures required for a given desired permeate flow rate as a function of Y and Y_1. The calculated pressure set-points are then utilized in **Eq. 7.3** to estimate the SEC as a function of Y and Y_1. The Y and Y_1 which result in the minimum SEC can be then solved for numerically through **Eq. 7.3**. The constrained optimization problem that yields the

energy-optimal two-stage SEC values for Y and Y_1 based on **Eqs. 7.3**, **7.19**, and **7.20** can be stated as follows:

$$\min_{Y,Y_1} SEC_{2stage} = \frac{\Delta P_1}{Y \cdot \eta_1} + \frac{\Delta P_2 \cdot (1 - Y_1)}{Y \cdot \eta_2}$$

$$s.t.$$

$$\begin{aligned}
&a.\ Q_P = Q_{P,Set-Point} && j.\ Y_{min} \le Y \le Y_{max}\\
&b.\ \Delta P_1 = P_{f1} - P_0 && k.\ Y_{1,min} \le Y_1 \le Y_{1,max}\\
&c.\ \Delta P_2 = P_{f2} - P_{c1} && l.\ Q_{f1,min} \le Q_{f1} \le Q_{f1,max}\\
&d.\ P_{f1} = f(Q_P, Y, Y_1)\ (\boldsymbol{Eq.7.19}) && m.\ Q_{f2,min} \le Q_{f2} \le Q_{f2,max}\\
&e.\ P_{f2} = f(Q_P, Y, Y_1)\ (\boldsymbol{Eq.7.20}) && n.\ P_{f1,min} \le P_{f1} \le P_{f1,max}\\
&f.\ Q_{f1} = \frac{Q_P}{Y} && o.\ P_{f2,min} \le P_{f2} \le P_{f2,max}\\
&g.\ Q_{f2} = Q_f \cdot (1 - Y_1) && p.\ Y_1 \le Y\\
&h.\ \eta_1 = f(\Delta P_1, Q_{f1})\ (\boldsymbol{Eq.7.26})\\
&i.\ \eta_2 = f(\Delta P_2, Q_{f2})\ (\boldsymbol{Eq.7.27})
\end{aligned}$$

7.24

The inequality constraints in the right column (i.e., constraints j – p) are to guarantee that the RO is operated within its operating range. The ranges for recovery values are imposed by the functional limitations on pressure, permeate flux and crossflow velocity for the RO elements. Constraints on feed flow rates are also set by the capacity of the feed pumps. Also, pressure constraints are set by the feed pumps as well as the RO membrane pressure vessels.

The efficiencies of certain pumps (e.g., centrifugal pumps), which can vary significantly with flow rate and output pressure [121] can impact the energy-optimal operating states of RO systems [99, 100]. Therefore, implementation of a real-time energy optimization scheme must account for variable pump efficiencies, η_1 and η_2 as a function of flow rate and pressure. How variable pump efficiency is calculated is described in **Section 7.4.2** (i.e., **Eqs. 7.26** and **7.27**).

The constrained nonlinear optimization problem described in **Eq. 7.24** can be solved using the sequential quadratic programming method [122]. Once $Y_{optimal}$ and $Y_{1,optimal}$ are calculated, the

flow rates and the feed pressures for both stages are calculated using **Eqs. 7.19** and **7.20**, and these values are provided as set points to the lower-level controllers. The system is then driven to a new operational state by the lower-level controllers, during which the supervisory controller remains inactive while it waits for the system to converge to the new set-point. The entire process of set-point calculation and set-point application is defined as one iteration of the supervisory controller. At the start of the next iteration, the updated sensor values (e.g., pressures, flow rates, conductivities) and the membrane permeabilities are used for the next round of supervisory control calculations. Based on preliminary step change experiments of the lower-level controller (**Section 7.5.1**), an iteration timer of 300 seconds was chosen as it was sufficient for the controllers to drive the system to a new operational steady-state.

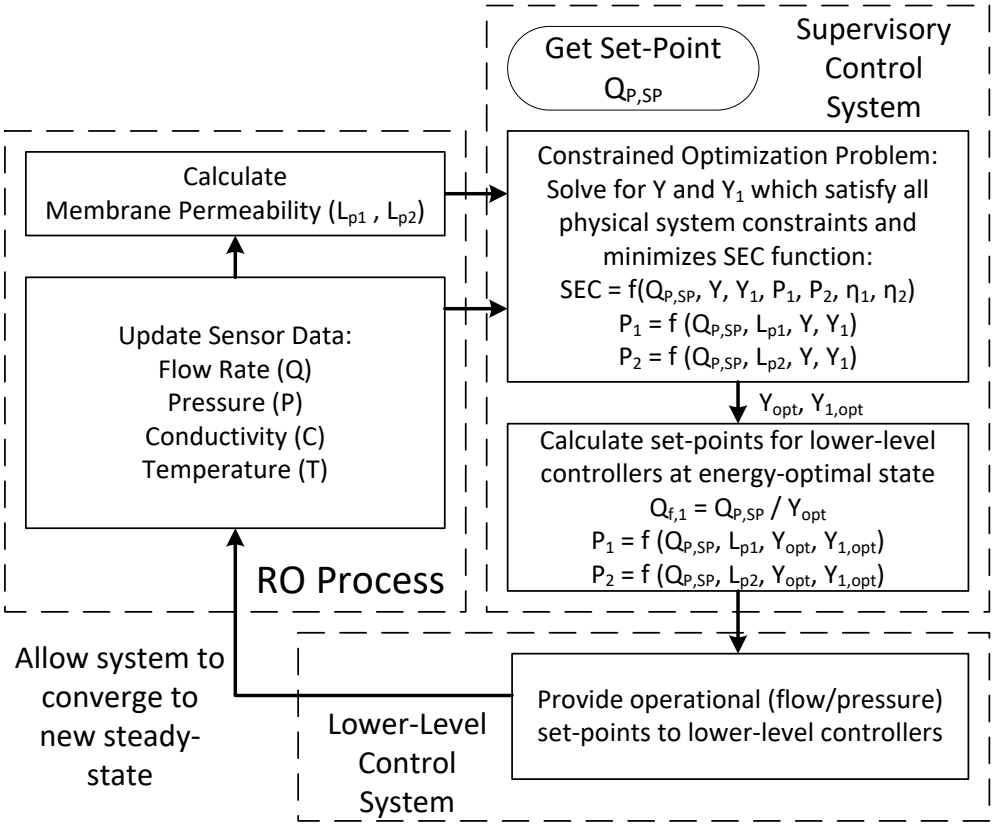

Figure 7.4. A logic flow diagram of the energy-optimal controller. The supervisory controller estimates the energy-optimal Y and Y_1 and the lower-level controller applies the calculated set-points onto the system. An iteration is defined as the execution of one full loop depicted here.

7.3.2 Lower-Level RO Controller

Once the energy-optimal Y and Y_1 have been determined, the supervisory controller passes set-points for the feed flow rate (Q_f), the first-stage feed pressure (P_{f1}), and the second-stage feed pressure (P_{f2}) to the lower-level RO controller to establish the RO system operation based on the above set pints. It is noted that control of a two-stage RO system is more complicated than for a single-stage RO [110] which requires control of only two variables (i.e., feed flow rate and feed pressure). Two-stage RO require simultaneous control three control variables (e.g., feed flow rate, first-stage feed pressure, and second-stage feed pressure) which are dynamically coupled. In order to accomplish the above, for the present two-stage RO multivariable control with the use of single-loop feedback control [123] was selected due to its simplicity (**Section 7.5.1**).

In order to ensure a fast response while avoiding overshoots while using a single-loop feedback control with multiple control loops, it is noted that pairings of a process output variable and a manipulated input variable should be determined by choosing pairs with the strongest couplings [123]. In the present work, the three relevant actuators used to manipulate the input variables were the first-stage feed pump, the second-stage feed pump, and the concentrate valve (i.e., these 3 actuators are illustrated in **Figure 7.1**). Preliminary step change experiments have shown that the best pairing is to have the first-stage feed pump regulate the feed flow rate, the second-stage feed pump to regulate the first-stage feed pressure, and the concentrate valve to regulate the second-stage feed pressure (**Figure 7.5**). For the single stage RO, the control architecture [110] includes two control loops such that in one, the feed pump regulates the feed flow rate, while in the other, a concentrate valve is used to regulate the pressure. In a two-stage RO system, a third control loop is involved in which the second-stage pump acts as the "concentrate valve" for the first RO stage and regulates the first-stage feed pressure. The

comparison between the control architectures for a single-stage RO (**Figure 7.5a**) and two-stage RO (**Figure 7.5b**) is shown in **Figure 7.5**.

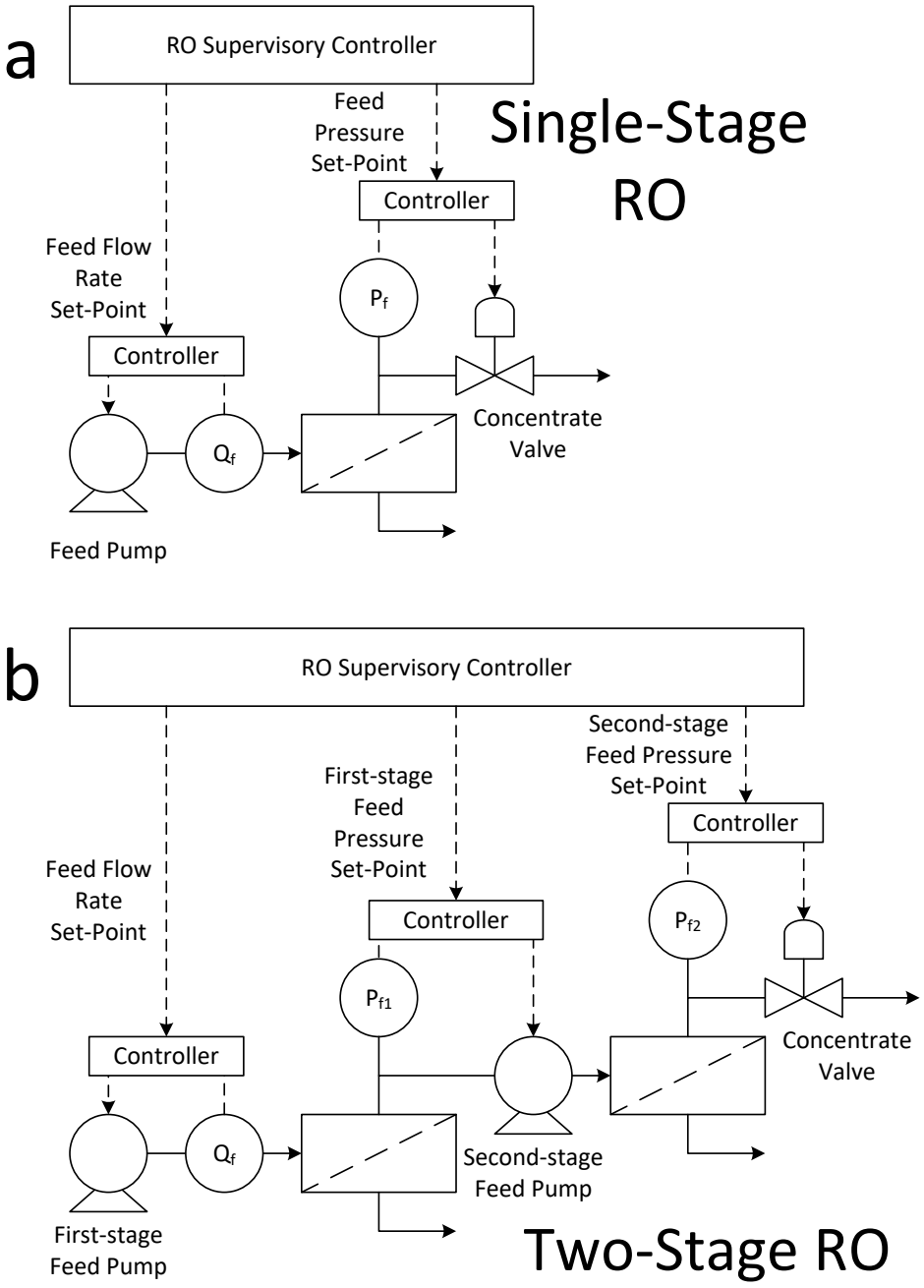

Figure 7.5. Illustration of the control architecture and the three feedback control loops for (a) a single-stage RO system [110] and (b) a two-stage RO system. The intermediate booster pump, or the second-stage pump, acts as a "concentrate valve" for the first stage and controls the first-stage feed pressure.

The three single loops can be tuned by first tuning the controller of the most important loop, tuning the other controllers in sequence, then reducing the gain and/or increasing the integral time of the controllers in the least important loops in order to ensure stability and avoid oscillations [123]. In the present architecture, the control loop which regulates the feed flow rate through the first-stage feed pump was chosen as the most important loop; the first-stage feed pump is the most important actuator since it drives fluid flow through the entire system and significantly impacts all process variables. The second most important control loop was selected to be the loop which regulates the first-stage pressure through the second-stage feed pump since the second-stage pump also has an impact on the feed pressures of both stages. The supervisory controller and the three lower-level control loops are shown in **Figure 7.6**.

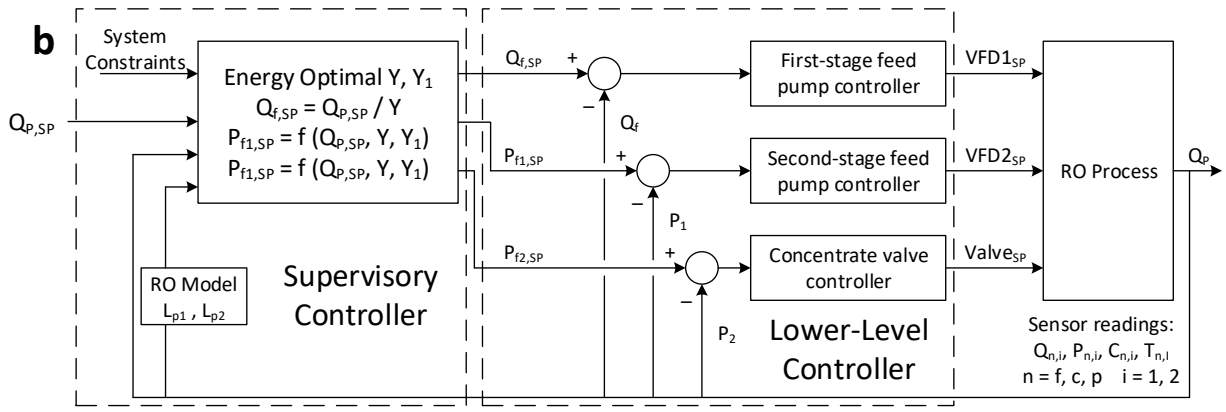

Figure 7.6. Process control diagram of the RO system control architecture with the supervisory controller and the three lower-level control loops. The supervisory controller which calculates the flow rate and pressure set-points for the lower-level controller is depicted on the left. The three feedback control loops and their inputs and outputs which form the lower-level controllers are depicted in the middle. The first control loop involves the first-stage feed pump regulating the feed flow rate, the second control loop involves the second-stage feed pump regulating the first-stage feed pressure, and the third control loop involves the concentrate valve regulating the second-stage feed pressure.

7.4 Experimental

7.4.1 Concentration Polarization

Field studies were carried out using the SIMS-BWD (**Section 3.2**). The concentration polarization of the RO elements used on the pilot plant (i.e., TM710D Toray in the first stage, TM810V Toray in the second stage) was calculated through manufacturer provided equations and definitions [124] shown below:

$$\overline{CP} = \frac{Q_P}{A_m K_f} \quad , \quad K_f = \frac{Sh \cdot D}{d_h} \quad , \quad Sh = 0.38 \cdot Re^{0.54} \cdot Sc^{0.33}$$
$$Re = \frac{v \cdot dh}{\mu} \quad , \quad Sc = \frac{\mu}{D} \quad , \quad v = \frac{Q_f + Q_C}{2A_c} \qquad \textbf{7.25}$$

where $\overline{CP}$ is the average concentration polarization, Q_P is the permeate flow rate, A_m is the active membrane area, K_f is the mass transfer coefficient, *Sh* is the Sherwood number, *D* is the solute diffusivity, d_h is the hydraulic diameter, *Re* is the Reynolds number, *Sc* is the Schmidt number, *v* is the crossflow velocity, μ is the kinematic viscosity of water, Q_f is the feed flow rate, Q_c is the concentrate flow rate, and A_c is the cross sectional area. For the first-stage membranes elements (TM710D) A_m = 113.2 m^2, dh = 0.001 m, and A_c = 0.00345 m^2 while for the second-stage membrane elements (TM810V) A_m = 47.5 m^2, dh = 0.00109 m, and A_c = 0.0032 m^2. Constants used for water are D = $1.23 \cdot 10^{-5}$ and $\mu = 10^{-6}$.

7.4.2 Pump Efficiencies

As described [99, 100], it is important to incorporate variable pump efficiencies when attempting to optimize for the SEC for the operation for a given RO desalination system. However, before the RO system described in this study can be used to demonstrate the effectiveness of the proposed energy-optimal control, its pump efficiencies must be defined. The

pilot plant used in this study (**Section 3.2**) is equipped with two high-pressured centrifugal pumps with efficiencies which vary with pressure and flow rate. These two RO feed pumps were equipped with sensors which output pump power consumption. This sensor value was used to calculate pump efficiency, and several preliminary studies were carried out to investigate pump efficiency as a function of flow rate and pump head. Efficiency data as a function of flow rate and pressure was compiled and a 3-D surface was fit using a Gauss method for the first-stage pump efficiencies and a parabola method for the second-stage pump efficiencies (i.e., surface fitting was done on OriginPro software). Surface fitting methods were chosen based on the highest R^2 values obtained (i.e., R^2 = 0.98 for the first-stage pump, R^2 = 0.96 for the second-stage pump) as given below for the first and second-stage pumps.

$$\eta_1 = z_0 + A \cdot exp\left[-0.5 \cdot \left(\frac{Q_f - x_c}{W_1}\right)^2 - 0.5 \cdot \left(\frac{\Delta P_1 - y_c}{W_2}\right)^2\right] \quad \textbf{7.26}$$

$$\eta_2 = z_1 + a \cdot Q_{f2} + b \cdot \Delta P_2 + c \cdot {Q_{f2}}^2 + d \cdot {\Delta P_2}^2 \quad \textbf{7.27}$$

Table 7.2. Constants for calculating pump efficiencies via **Eqs. 7.26** and **7.27**.

Pump 1		Pump 2	
z_0 =	0.35973	z_0 =	0.24349
A =	0.16491	a =	0.00174
x_c =	29.51651	b =	3.43E-04
w_1 =	12.48741	c =	2.91E-04
y_c =	435.75828	d =	-4.16E-07
w_2 =	378.3261		

The example given in **Section 7.2.4** of a theoretical 2-stage RO system operating at a constrained permeate flow rate is re-plotted by substituting **Eqs. 7.26** and **7.27** into **Eq. 7.23** and the result is shown **Figure 7.7**. The importance of incorporating variable pump efficiencies in order to more accurately estimate the energy-optimal *Y* and Y_1 can be seen in **Figure 7.7**.

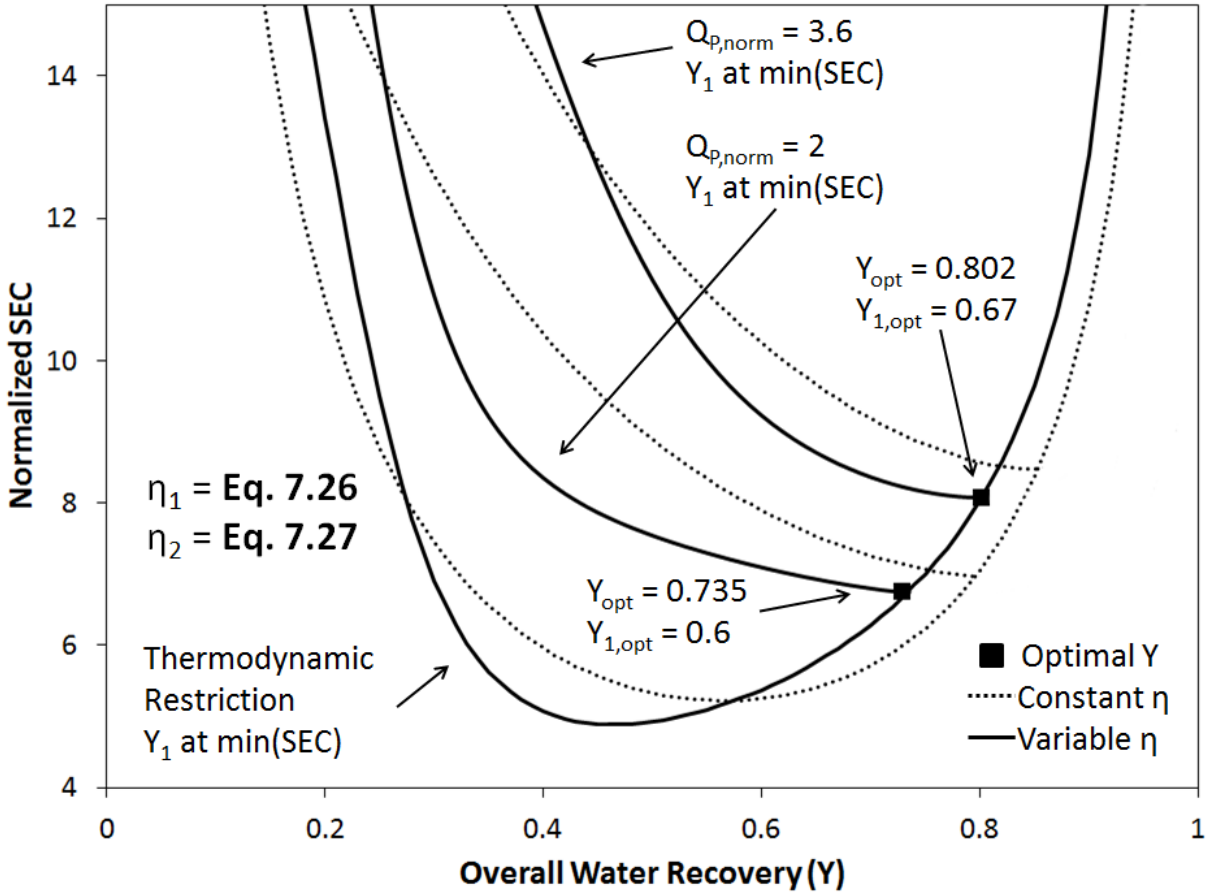

Figure 7.7. Plot of SEC vs *Y* at a constrained permeate flow rate for this study's pilot plant with variable η_1 and η_2 calculated through **Eq. 7.26** and **Eq. 7.27**. Solid line denote SEC calculated with variable pump efficiencies, while the dotted line are the same as the constant efficiency curves show in Fig. 3. Optimal *Y*s are highlighted, and it is important to note taking into account varying pump efficiencies shifts optimal *Y* and Y_1 to different values.

7.4.3 Lower-Level RO Controller Tuning

The supervisory RO controller described in **Section 7.3.1** provides the lower-level RO controllers (**Figure 7.6**) with the necessary feed flow rate and pressure set-points. The three lower-level controllers are all PI controllers. The expressions for each of the PI controllers are listed below:

$$VFD_{1,SP} = K_{p,1}\left(Q_{f,SP} - Q_f(t)\right) + \frac{K_{p,1}}{\tau_{i,1}}\int_0^t \left(Q_{f,SP} - Q_f(\tau)\right)d\tau \quad \textbf{7.28}$$

$$VFD_{2,SP} = K_{p,2}\left(P_{f1,SP} - P_{f1}(t)\right) + \frac{K_{p,2}}{\tau_{i,2}}\int_0^t \left(P_{f1,SP} - P_{f1}(\tau)\right)d\tau \quad \textbf{7.29}$$

$$Valve_{SP} = K_{p,3}\left(P_{f2,SP} - P_{f2}(t)\right) + \frac{K_{p,3}}{\tau_{i,3}}\int_0^t \left(P_{f2,SP} - P_{f2}(\tau)\right)d\tau \quad \textbf{7.30}$$

where $VFD_{1,SP}$ is the first-stage feed pump's VFD setting in % (0-100%), $VFD_{2,SP}$ is the second-stage feed pump's VFD setting in % (0-100%), and $Valve_{SP}$ is the concentrate valve opening in % (0-100%). Tuning each control loop was accomplished through preliminary experiments using the approach described in **Section 7.3.2** in order to decouple the three control loops. The PI constants were chosen so as to minimize oscillations and are listed in **Table 7.3**. While it is noted that a multivariable control design could be used to provide multivariable control accounting for multi-loop interactions, any improvements in the achievable closed-loop performance would be minimal since the single-loops are being tuned with significantly different time constants. At the same time, the use of a multivariable control approach would increase the computational power required as well as decrease the modularity of the overall control architecture. Results will be shown in **Section 7.5.1** to demonstrate the control system's ability to regulate the controlled outputs to the set-points values established by the supervisory controller

Table 7.3. Proportional and integral constants for the lower-level PI controllers.

Proportional Constants	Integral Constants
$K_{P,1} = 2\,\frac{\text{VFD1\%}}{\text{GPM}}$	$\tau_{i,1} = 40$ s
$K_{P,2} = -0.25\,\frac{\text{VFD2\%}}{\text{PSI}}$	$\tau_{i,2} = 100$ s
$K_{P,3} = -0.003\,\frac{\text{Valve\%}}{\text{PSI}}$	$\tau_{i,3} = 100$ s

7.5 Results and Discussion

The pilot RO desalination system was deployed for brackish water desalination of agricultural drainage water near Los Banos, CA. Raw feed water salinity and turbidity varied in the range of 10,000 - 17,000 mg/L TDS and 2~10 NTU, respectively. The feed pre-treatment (300 micron filter and UF) consistently provided RO feed water of turbidity < 0.1 NTU, which was sufficiently below the recommended maximum limit for RO desalting. Field tests included: (a) demonstration of the lower-level controller tuning, (b) optimization of Y_1 under the conditions of a constant Y, (c) optimization of both Y_1 and Y, (d) controller performance under conditions of changing feed salinity, and (e) demonstration of a transition from two-stage to single-stage operation.

7.5.1 Lower-Level RO Controller Performance

The lower-level controller's time response to set-point changes to all three controllers was initially for system operation at a feed flow rate of 75.7 L/min, first-stage feed pressure of 1.84 MPa, and a second-stage pressure of 2.66 MPa. At ~70s in **Figure 7.8**, the set-points for each PI controller were changed to 90.8 L/min, 2.17 MPa, and 3.16 MPa, respectively. As shown in **Figure 7.8**, all three controllers eventually converged to their new set-points without major oscillations. Approximately ~150s was required to reach the new feed flow rate set-point (**Figure 7.8a**), ~280s to reach the new stage 1 feed pressure set-point (**Figure 7.8b**), and ~430s to reach the new stage 2 feed pressure set-point (**Figure 7.8c**). Minor overshooting is seen in **Figure 7.8b** (~ 0.11 MPa) and **Figure 7.8c** (~ 0.15 MPa). It is noted that these are not due to controller tuning, but because the fastest control loop (**Figure 7.8a**) also impacts the control variables in **Figure 7.8b** and **Figure 7.8c**. When the controller in **Figure 7.8a** detects a positive error (i.e., measured flow rate is lower than the flow rate set-point), it will respond by increasing the first-stage

pump's RPM. Increasing the first-stage pump RPM has the effect of increasing both the first-stage pressure (**Figure 7.8b**) and the second-stage pressure (**Figure 7.8c**); therefore, even though the controllers for the first-stage pressure and second-stage pressured are tuned at a slower time-scale, slight overshoots such as the ones seen in **Figure 7.8b** and **Figure 7.8c** may occur simply due to the first-stage pump controller. It is noted that variability of water salinity are reported to typically occur over the time-scales of days and months [96-98]. Therefore, the time required by the lower-level controller to converge to new set-points should not pose a problem for RO operation.

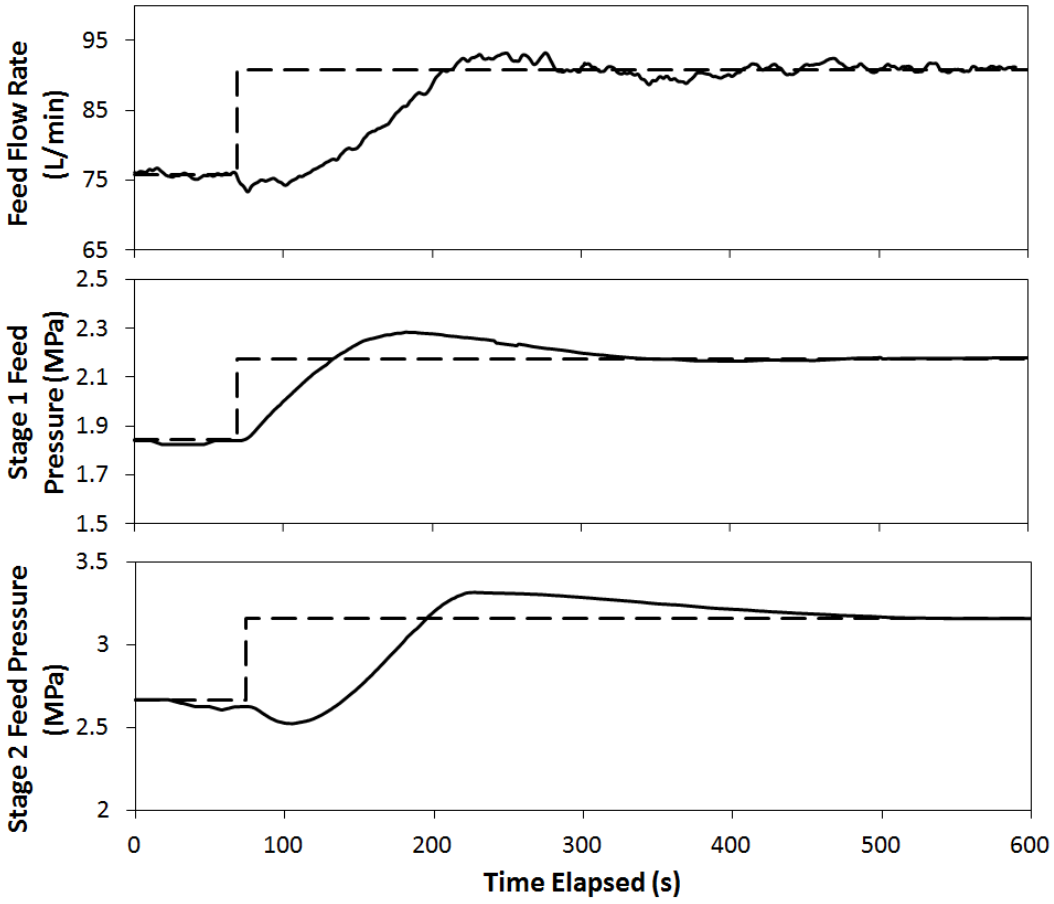

Figure 7.8. Profiles of (a) RO feed flow rate, (b) RO stage 1 feed pressure, and (c) RO stage 2 feed pressure with respect to time. (a) is controlled by the first-stage feed pump, (b) is controlled by the second-stage feed pump, and (c) is controlled by the concentrate valve. The set-points for all three controllers are changed simultaneously at 70s from (a) 75.7 L/min to 90.8 L/min, (b) 1.84 MPa to 2.17 MPa, and (c) 2.66 MPa to 3.16 MPa.

7.5.2 Optimization of Y_1 under condition of constant Y

In order to demonstrate the energy-optimal control system, two tests were conducted where the controller was activated following an initial operation with the conventional method of the RO plant operating at an equivalent flux for both stages [70]. The first test was conducted with a constant overall water recovery, *Y*, in order to demonstrate the importance of optimizing the permeate production load distribution (i.e., optimizing Y_1). The second test, described in **Section 7.5.3**, was conducted with both variable *Y* and Y_1 in order to demonstrate the simultaneous optimization of the overall permeate water recovery and permeate production load distribution (i.e., optimizing *Y* and Y_1).

The first test was carried out at a fixed overall recovery *Y*. Initially, the system was operated at 74% recovery and a permeate water productivity set-point of 60.6 L/min at a measured feed salinity of ~11591 mg/L. For plant operation whereby the flux was set equal in both stages, the system is expected to operate at an RO permeate flux of 22.6 L/m^{2}h. When both stages were operated at this flux, the stage 1 recovery was Y_1 of 52%. This corresponded to set-points of 81.8 L/min for the first stage feed flow rate, 1.88 MPa for the first-stage feed pressure, and 2.79 MPa for the second-stage feed pressure. The energy-optimal controller was then activated and the supervisory controller determined the energy-optimal Y_1 using **Eqs. 7.24**, **7.26**, and **7.27** (i.e., **Eq. 7.24** is the constrained nonlinear optimization problem, while **Eqs. 7.26** and **7.27** were used to calculate pump efficiencies). The supervisory controller determined that minimum SEC would occur at Y_1 = 60%, which is the constraint of $Y_{1,max}$ or the largest Y_1 value possible for the RO membrane modules used in this study (**Section 3.2**). The predicted SEC as a function of Y_1 is plotted in **Figure 7.9** using **Eqs. 7.3, 7.19, 7.20, 7.26,** and **7.27** (i.e., the overall SEC was

calculated from **Eq. 7.3**, pressures calculated by **Eqs. 7.19** and **7.20**, and pump efficiencies calculated by **Eqs. 7.26** and **7.27**).

This shift to the max Y_1 is due to a combination of factors: the first-stage pump is more efficient than the second-stage pump during the initial operating conditions (i.e., η_1 = 0.47 and η_2 = 0.34 at Y_1 = 52%) but the first-stage pump becomes even more efficient relative to the second pump when Y_1 increases (i.e., η_1 = 0.48 and η_2 = 0.3 at Y_1 = 60%). In **Section 7.2.2,** it was concluded that as the second-stage pump efficiency decreases, the optimal Y_1 increases. Indeed, as increasing Y_1 increases the required pressure output for the first-stage pump which increases η_1 (**Eq. 7.26**), while decreasing both the flow rate and the pressure output of the second-stage pump both of which leads to decreased η_2 (**Eq. 7.27**). Hence, as Y_1 increases, η_2 is expected to decrease, and as a consequence this will further increase the optimal Y_1 until the maximum possible Y_1 (i.e., the constraint of $Y_{1,max}$) is achieved. The change in Y_1 and the corresponding reduction in SEC are shown in **Figure 7.9** noting that SEC reduction of approximately 4.2% was achieved relative to the initial operating condition.

During the transition from Y_1 = 52% to 60%, in the previous experiment, the supervisory controller calculated the flow rates and pressures required to attain the optimal Y_1 of 60% and provided the determined operational parameters set-points to the lower-level controllers. The first iteration the supervisory controller calculated a first-stage feed pressure of 2.14 MPa, and a second-stage feed pressure of 2.46 MPa. After 300 seconds, the supervisory controller re-calculated the required pressures, and provided set-points of 2.11 MPa and 2.50 MPa for the first and second stages, respectively, to the lower-level controllers. The transition with respect to flow rates and pressures can be seen in **Figure 7.10** and **Figure 7.11.** The control system was able to increase Y_1 by increasing the first-stage pressure (**Figure 7.11a**) while still maintaining the

permeate productivity set-point (**Figure 7.10a**) and the overall water recovery (by maintaining the feed flow rate, shown in **Figure 7.10d**).

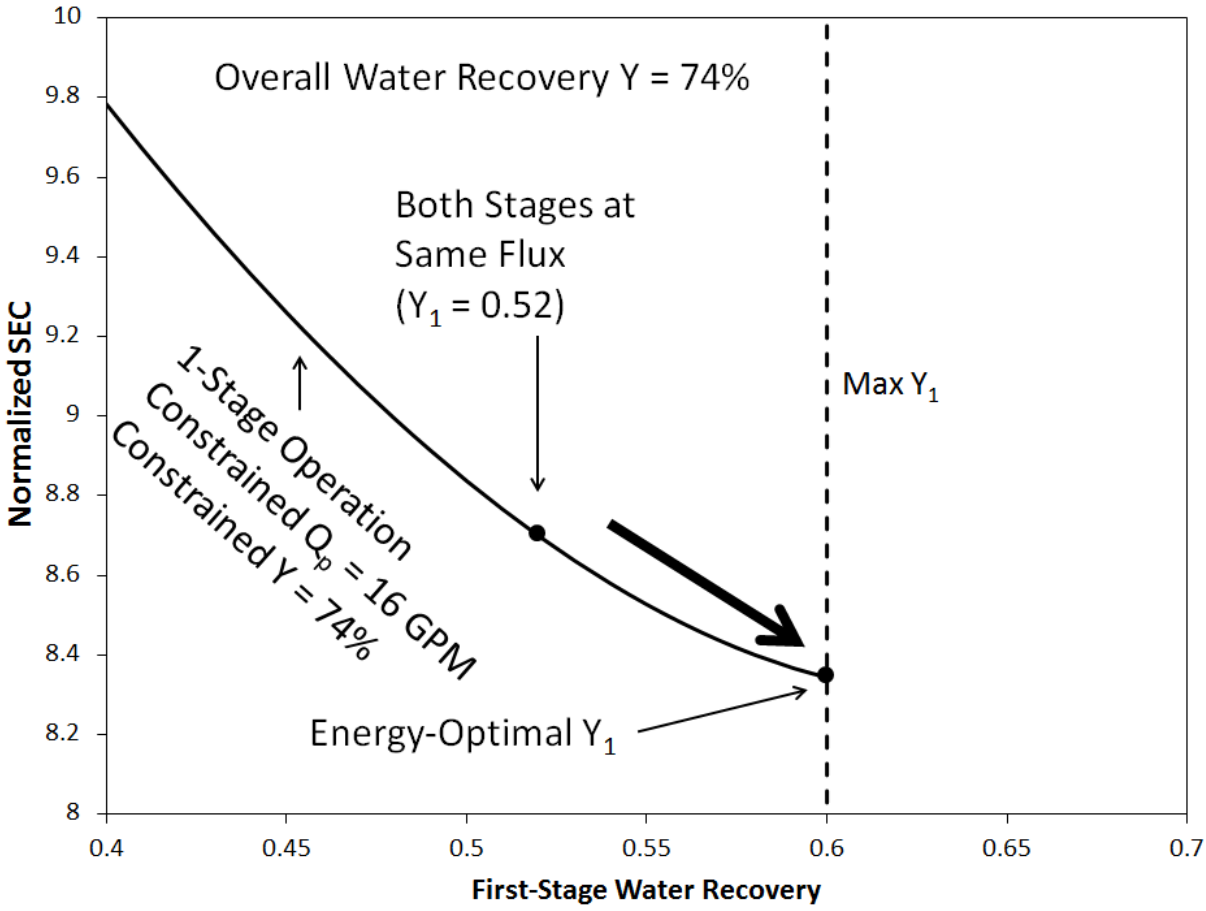

Figure 7.9. Normalized SEC with respect to RO recovery under the constraints of constant Y = 74% and max Y_1 = 60% for a permeate flow rate set-point of Q_p = 60.6 L/min. Solid circles denote the plant operating points established by the controller, both of which match expected theoretical predictions, which were calculated using **Eq. 7.3**.

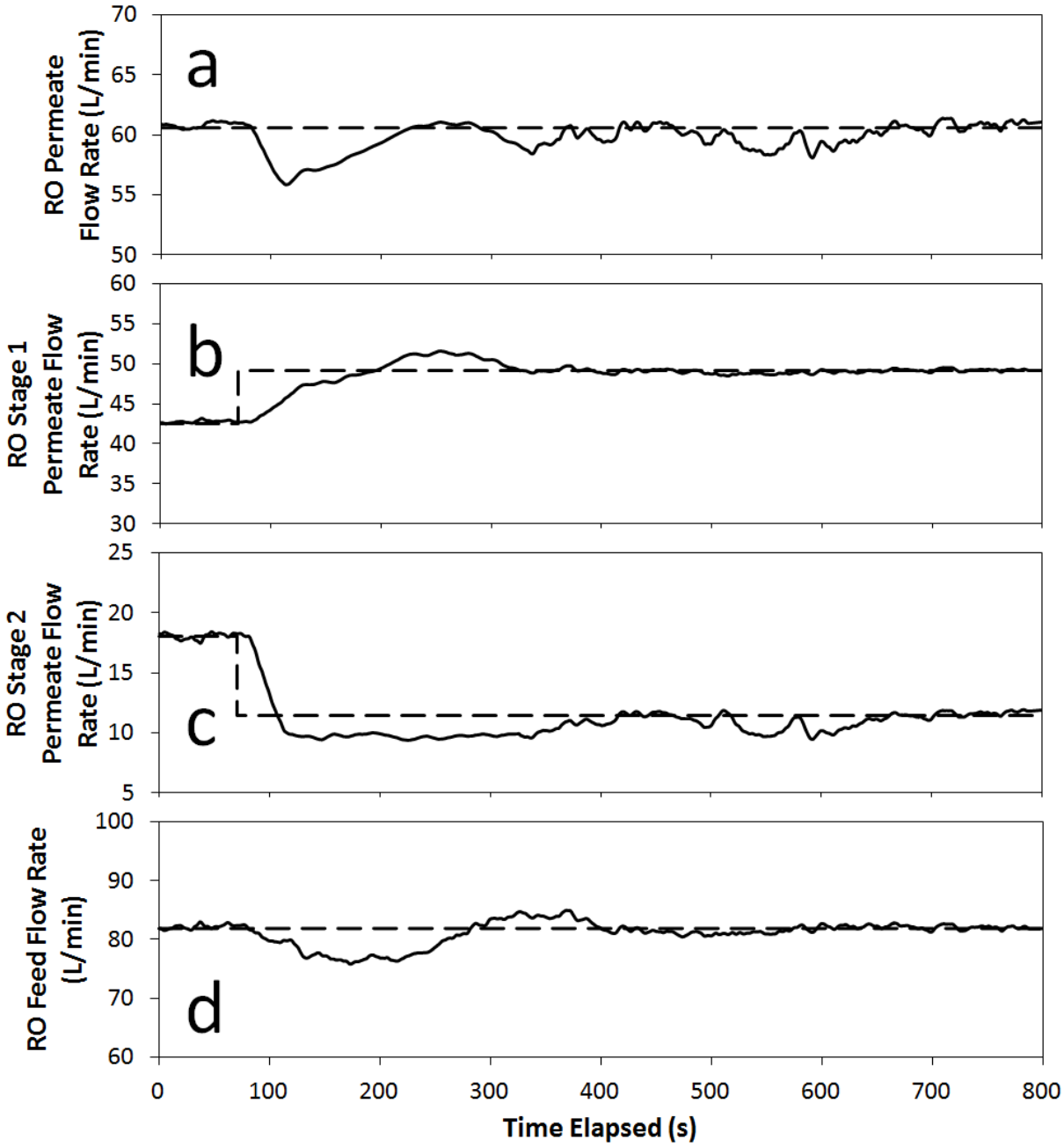

Figure 7.10. Profiles of (a) RO permeate flow rate, (b) RO first-stage permeate flow rate, (c) RO second-stage permeate flow rate, and (d) RO feed flow rate with respect to time. The recovery set-point was changed from Y_1 = 0.52 to Y_1 = 0.6. The permeate flow-rate, feed flow rate, and overall water recovery set-points were all kept constant at Q_p = 60.6 L/min, Q_{f1} = 81.8 L/min, and Y = 0.74, respectively.

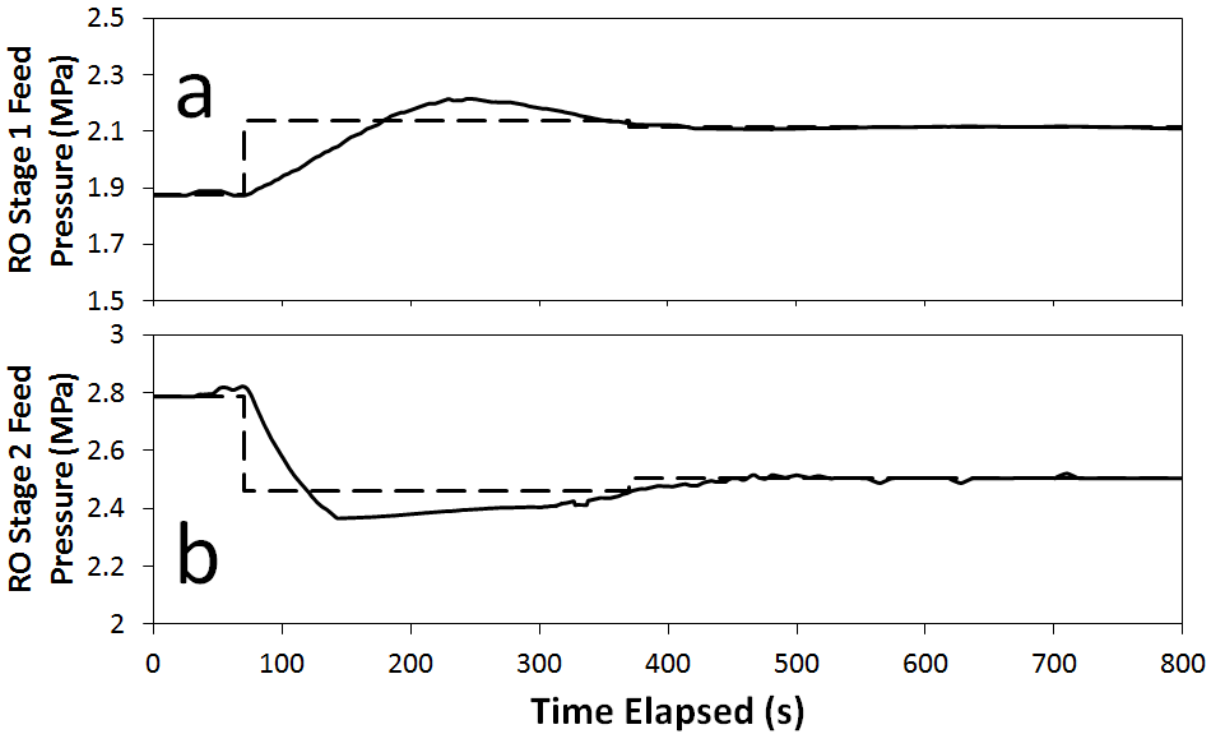

Figure 7.11. Profiles of (a) RO first-stage feed pressure and (b) RO second-stage feed pressure with respect to time. The RO stage 1 feed pressure set-point changed from 1.88 MPa to 2.11 MPa, while the RO stage 2 feed pressure set-point changed from 2.79 MPa to 2.50 MPa.

7.5.3 Optimization of Y_1 and Y

Following the test described in **Section 5.2** which demonstrated SEC reduction through optimization of only Y_1, the next test was carried out to demonstrate controller's ability to reduce the SEC through simultaneous optimization of both Y and Y_1. The system was initially operated at a permeate production set-point of 45.4 L/min for a feed water salinity of 17326 mg/L. As in the previous tests, the plant was set to initially operate at equal permeate flux for both stages of 17.0 L/m^{2}h which corresponded to Y = 74%, Y_1 = 52%, at feed flow rate of 61.4 L/min, and first- and second stage feed pressures of 2.07 MPa and 3.50 MPa, respectively. Similar to the previous test, the controller was activated and calculated Y and Y_1 values which resulted in a minimum SEC established with considerations of the constrained optimization problem as described in **Eq.**

7.24. For the set permeate productivity of 45.4 L/min, the supervisory controller calculated the optimal operating state to be at Y_1 = 42%, and Y = 58%. Similar to **Section 5.2**, due to the dependence of pump efficiencies on flow rates and pressure, the calculated operating state was determined to be the highest Y_1 possible; however, this value was constrained by the maximum allowable first-stage pressure (max P_{f1} = 2.17 MPa). The above constraint was due to the maximum allowable second stage feed pump's inlet pressure (i.e., the manufacturer specified maximum pressure is 2.41 MPa, but a value of 2.17 MPa was chosen to ensure equipment safety). The SEC at the constraint of maximum allowable first-stage pressure was calculated through using **Eqs. 7.3, 7.19, 7.20, 7.26,** and **7.27** and shown in **Figure 7.12** in order to illustrate the reduction in energy consumption achieved by the energy-optimal controller. The change in Y, Y_1, the corresponding reduction in SEC, and the new operating point on the SEC curve for operation at the constraint of maximum first-stage pressure are shown in **Figure 7.12.** The SEC reduction achieved through the shift from equal-flux operation (Y = 74%, Y_1 = 52%) to an energy-optimal operation (Y = 58%, Y_1 = 42%) for the above optimal operation was approximately 7.1% was achieved. During the transition from equal-flux operation to an energy-optimal operation, the set-points provided to the lower-level controllers for the feed flow rate, first-stage feed pressure, and the second-stage feed pressured were changed from 61.4 L/min to 78.3 L/min, 2.07 MPa to 2.17 MPa, and 3.50 MPa to 2.82 MPa, respectively. The transition to the optimal operating conditions, with respect to flow rates and pressures, is shown seen in **Figure 7.13** and **Figure 7.14**. Overall, the results of the tests described in **Sections 7.5.2** and **7.5.3** demonstrate the importance of optimizing for both Y and Y_1 in order to achieve energy-efficient two-stage operation.

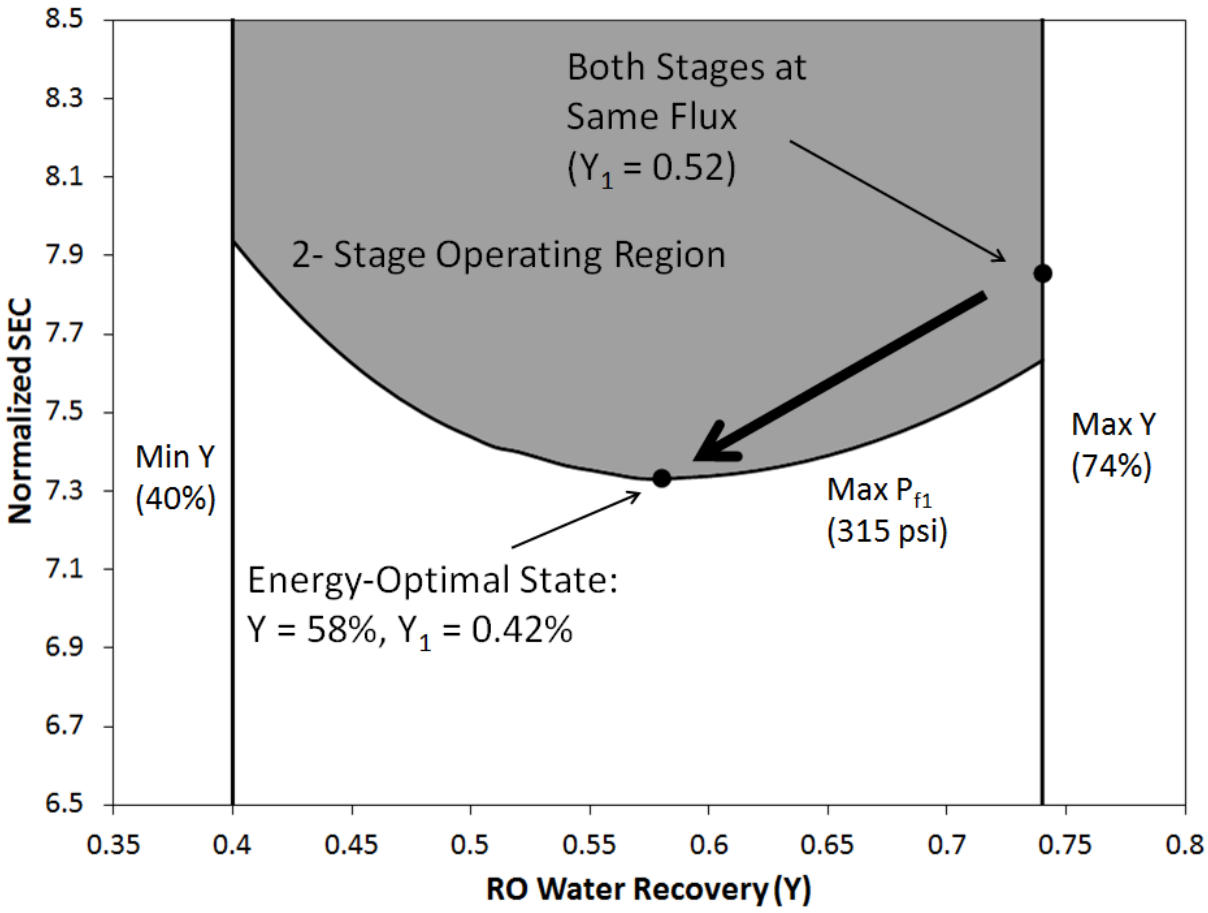

Figure 7.12. Normalized SEC with respect to RO water recovery (*Y*), with the constraints of minimum *Y* (40%), maximum *Y* (74%), and maximum P_{f1} (2.17 MPa). Solid circles denote the plant operating points established by the controller, the arrow shows the transition between the initial state and the calculated energy-optimal state. How the max P_{f1} curve was calculated and plotted is explained in **Figure 7.25**.

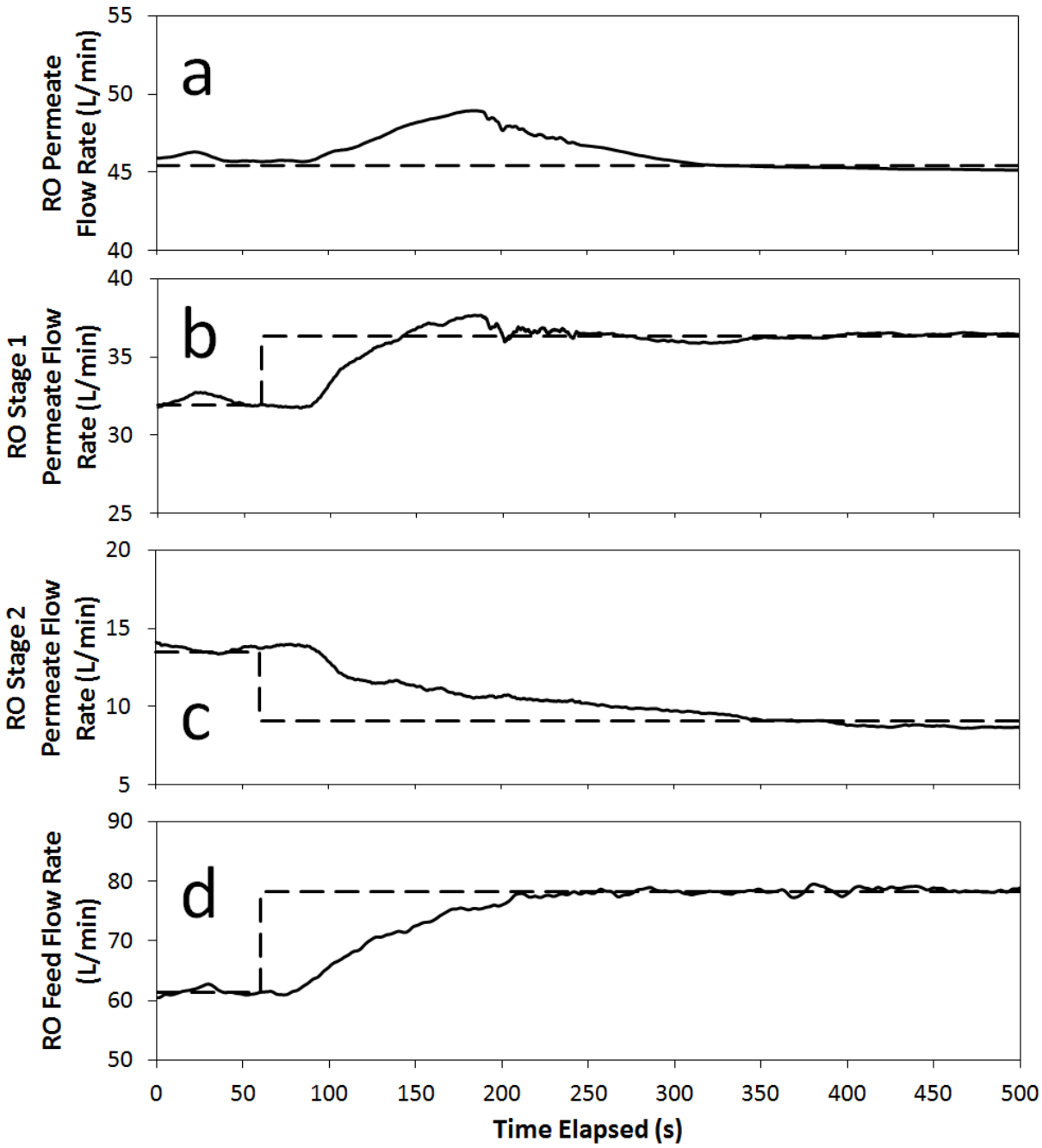

Figure 7.13. Profiles of (a) RO permeate flow rate, (b) RO first-stage permeate flow rate, (c) RO second-stage permeate flow rate, and (d) RO feed flow rate with respect to time. The overall water recovery set-point was changed from Y = 74% to Y = 58%, and the first-stage water recovery set-point was changed from Y_1 = 0.52 to Y_1 = 0.42. The feed flow rate controller set-point was changed from 61.4 L/min to 78.3 L/min.

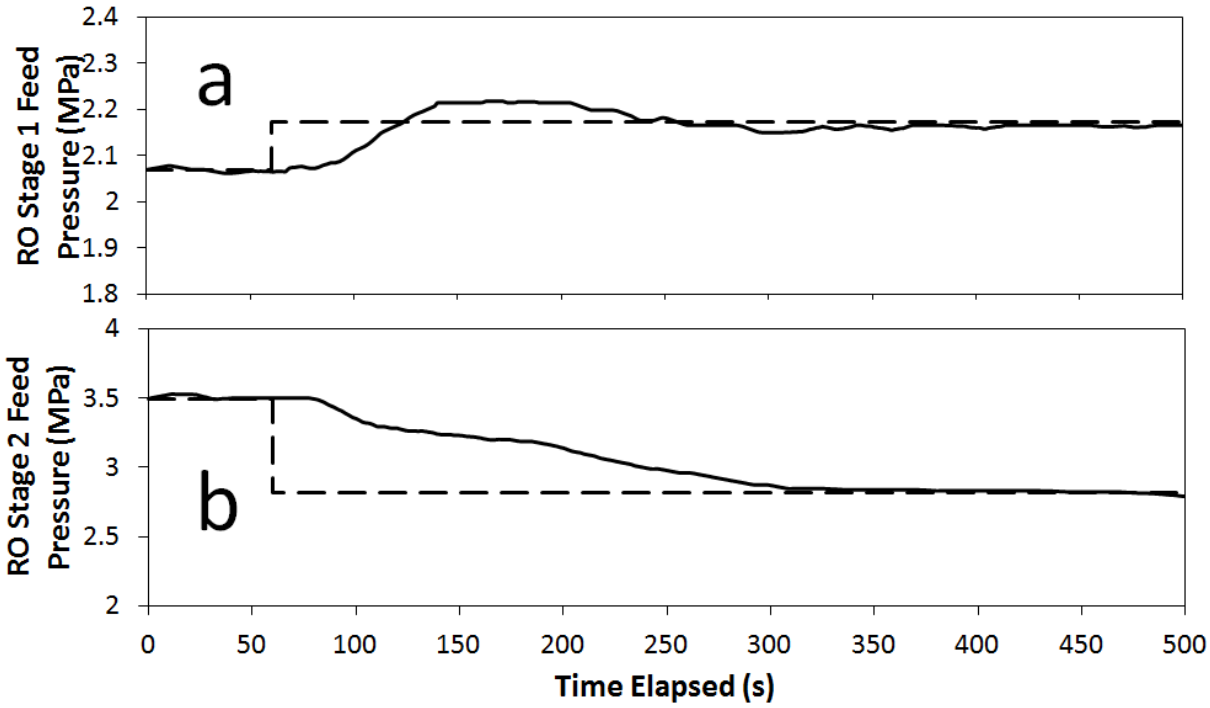

Figure 7.14. Profiles of (a) RO first-stage feed pressure and (b) RO second-stage feed pressure with respect to time. The feed pressure controller set-points were changed from (a) 2.07 MPa to 2.17 MPa and (b) 3.50 MPa to 2.82 MPa.

7.5.4 Operation during Changing Feed Salinity

In order to evaluate the controller's performance subject to temporal changes in feed salinity, a disturbance in the form of an increase in feed water salinity was introduced. This was achieved by diverting the RO concentrate to a feed tank where it was mixed with the raw seawater feed to achieve a higher feed salinity. The flow rate of recycled RO concentrate was decreased from 6.94 L/min to 0 over a period of 270 s in order to produce a raw feed stream with a salinity which decreased from 24,190 mg/L mg/L TDS to 17,833 mg/L TDS over the above period (**Figure 7.16a**). The RO plant was first operated under energy-optimal RO control at the initial constant feed salinity of 24,190 mg/L. The desalination plant initially operated at a permeate production set-point of 45.4 L/min, overall and first stage water recoveries of Y = 69% and Y_1 =

27.3%, respectively (**Figure 7.15**). The overall water recovery and first-stage recovery at which the system was initially operated was determined by the supervisory controller to be the optimal operating conditions for the given feed salinity of 24,190 mg/L (**Figure 7.15**). It is noted that the first-stage water recovery is constrained by the maximum P_{f1} limit of 2.17 MPa. The energy-optimal controller was kept on, and at t = 160s the feed salinity began its gradual decrease.

At the approximate time of t = 300s (140s after commencing with the feed salinity decrease), the supervisory controller performed an iteration and determined a new energy-optimal operating state for the feed salinity measured at that moment (i.e., t = 300 s). At approximately t = 600s (440s after commencing with the prescribed feed salinity decrease and after feed salinity reached new steady-state value of approximately 17,833 mg/L at around t = 400s), the supervisory controller again determined the energy-optimal operating state for the final feed salinity value of 17,833 mg/L TDS. For both iterations, the supervisory controller established that operation at the maximum first-stage pressure (2.17 MPa) was the energy-optimal operating set point (i.e., same as the conclusion reached in **Section 7.5.3**); thus, the first-stage pressure set-point did not change for either controller iterations. The only change in pressure was to decrease the second-stage pressure (**Figure 7.17c**), 3.63 MPa to 3.19 MPa, then to 2.90 MPa. The final calculated operating point for operation with feed salinity of 17,833 mg/L TDS was at Y = 58 %, and Y_1 = 41.5 %. The transition between the two states can be seen in **Figure 7.16** and **Figure 7.17**.

The transition with respect to the SEC can be seen in **Figure 7.15**. It is noted that two unique SEC curves exist for the max P_{f1} constraint at different feed salinities (**Figure 7.15**). This is due to factors discussed in **Section 7.5.2** and **7.5.3** (i.e., first-stage pump is more efficient than the second-stage pump, and becomes even more efficient as Y_1 increases), where it is energy-optimal to operate the system at the highest Y_1 possible. If the feed salinity decreases when the system operates at a constant max P_{f1}, then the flux in the first stage increases and Y_1 increases as a

result. This decreases the load on the less efficient second-stage pump and causes the SEC curve for the max P_{f1} constraint to be at a decreased SEC value.

A comparison of the controller's SEC reduction relative to an operation for desalination plant operation with a more traditional control methodology of maintaining constant permeate flux for both stages (i.e., constant Y, Y_1) is shown in **Figure 7.15**. The SEC for the latter traditional two-stage operation was calculated for the present plant using **Eq. 7.3**. In this example, permeate water productivity is maintained but the first stage pressure is decreased in order to maintain a constant flux in the first stage. For a system without an energy-optimal controller driving the system to operate at the constraint of max P_{f1}, the RO system would no longer operate at the energy-optimal operating point. Achieving the new set-point through a traditional control method will result in operation for which the SEC is about 10% higher compared to operation with the energy-optimal controller. The above tests and analysis demonstrated the ability of energy-optimal control to adjust system operation when feed salinity changes so as to minimize the SEC.

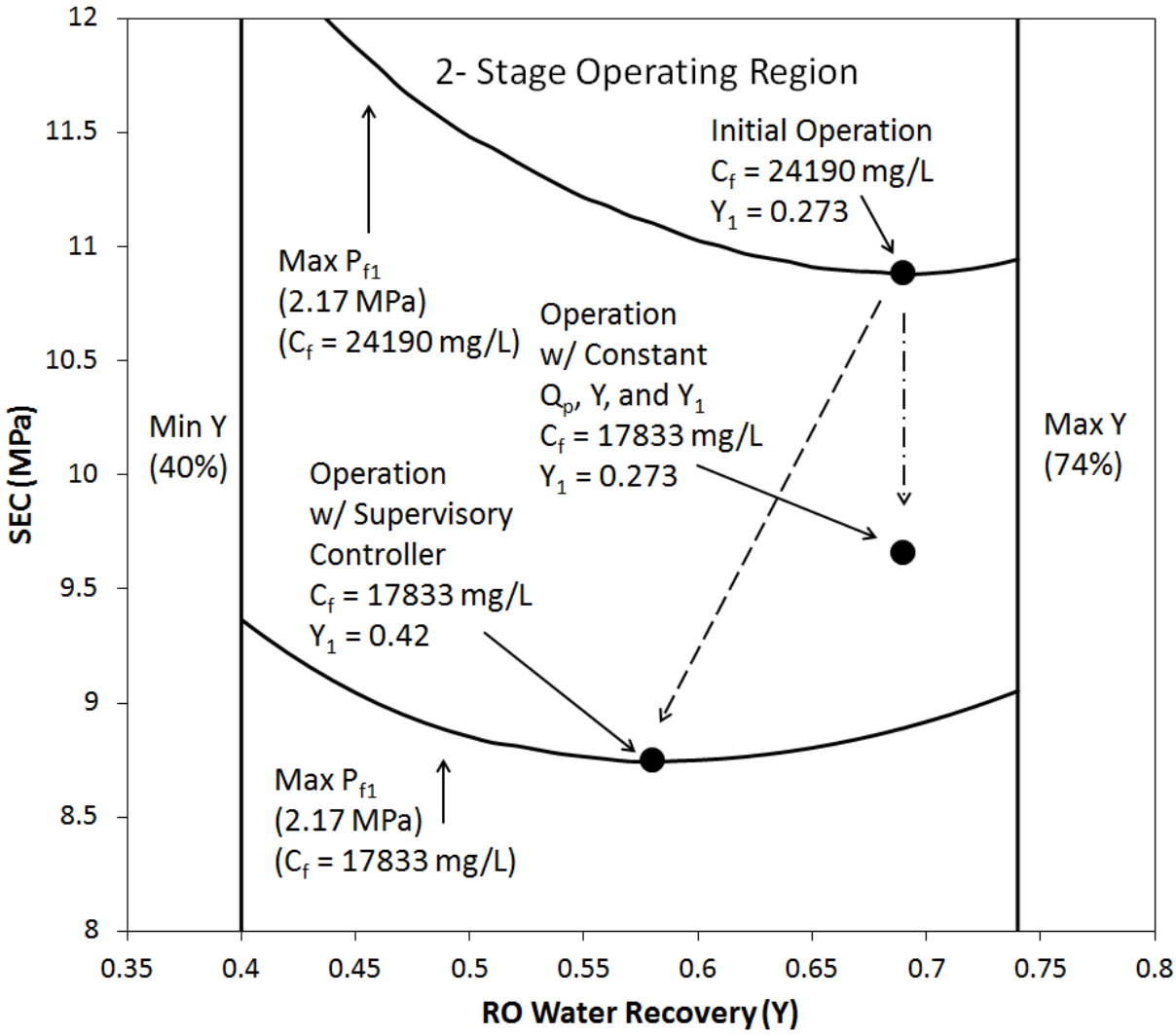

Figure 7.15. Normalized SEC with respect to RO water recovery (*Y*), with the constraints of minimum *Y* (40%), maximum *Y* (74%), and maximum P_{f1} (2.17 MPa). Solid circles denote the plant operating points established by the controller. The arrows shows the transition between the initial and final operating states during a change in feed salinity under conditions of energy-optimal control (dashed line) and with constant flux control (dash-dotted line). The final operating point of the constant flux control was calculated via **Eq. 7.3**. How the max P_{f1} curve was calculated and plotted is explained in **Figure 7.25**.

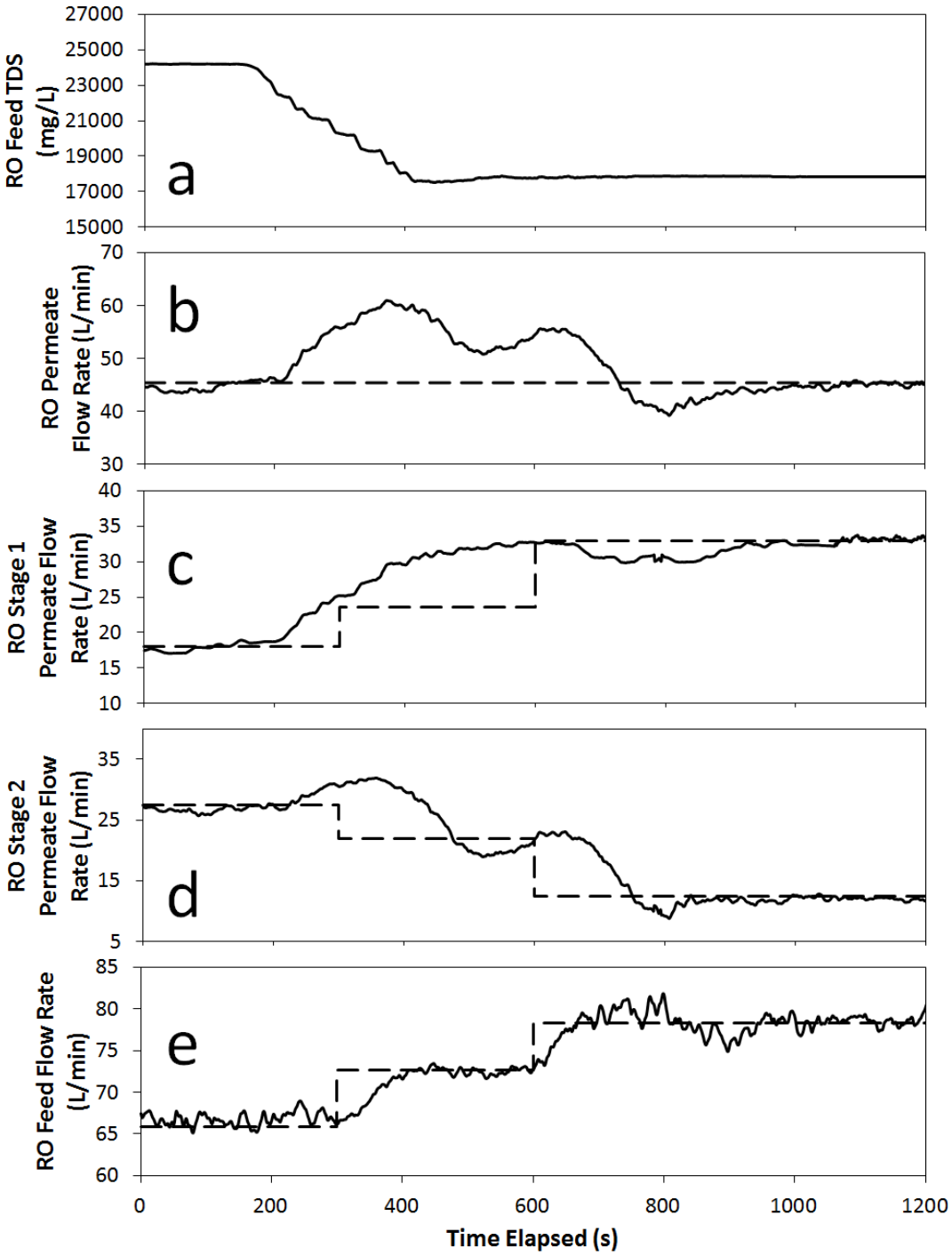

Figure 7.16. Profiles of (a) raw feed water salinity, (b) RO permeate flow rate, (c) RO first-stage permeate flow rate, (d) RO second-stage permeate flow rate, and (e) RO feed flow rate with respect to time. The controller was iterated at 300s and again at 600s. Originally, the feed flow rate controller set-point was at 65.8 L/min 78.3 L/min. At 300s, the controller went through an iteration while the feed salinity was changing, calculating a new set-point for feed flow rate of 72.6 L/min. At 600s, the controller used the new high feed salinity and calculated a feed flow rate set-point of 78.3 L/min.

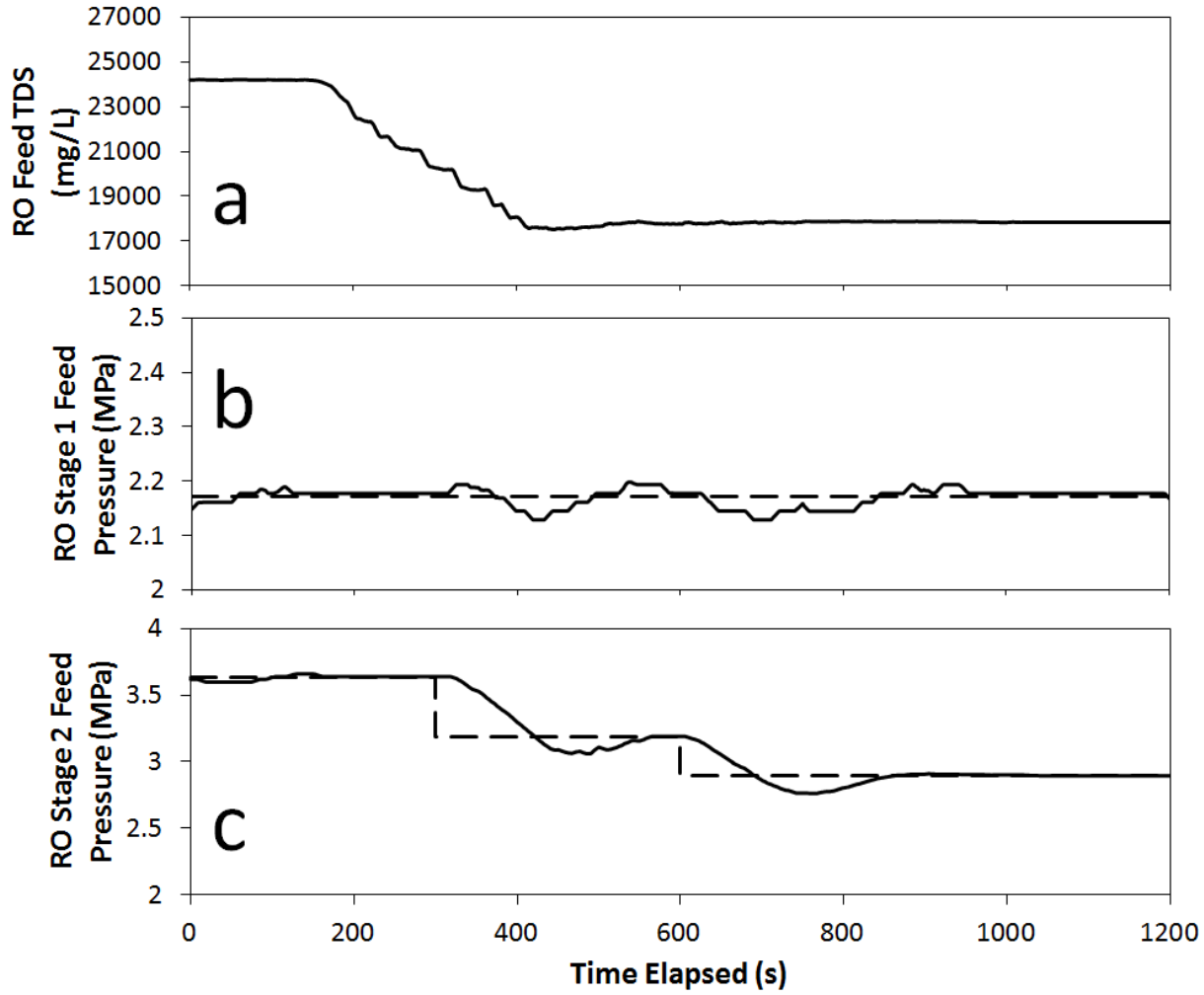

Figure 7.17. Profiles of (a) raw feed water salinity, (b) RO first-stage feed pressure, and (c) RO second-stage feed pressure with respect to time. The controller was iterated at 300s and again at 600s. Originally, the lower-level controllers' feed pressure set-points were at 2.17 MPa, and 3.63 MPa for the first-stage feed pressure and the second-stage feed pressure, respectively. After the first controller iteration at 300s, the second-stage feed pressure set-point changed to 3.34 MPa. The first-stage feed pressure set-point remained constant at 2.17 MPa since that is the maximum first-stage pressure constraint. After the second controller iteration at 600s, the second-stage feed pressure set-point was set to 2.90 MPa.

7.5.5 Transition from Two-Stage to Single-Stage Operation

In **Section 7.2.3**, it was concluded that when in a two-stage RO system the first-stage pump is more efficient than the second-stage pump, then a single-stage operation will be more energy-

efficient (**Section 7.2.3**) when Y_1 is lower than the right-hand side of **Eq. 7.14** (i.e., $1 - \frac{\eta_2}{\eta_1}$). As discussed in **Section 7.5.4**, for RO systems with a constraint on the first-stage inlet feed pressure, a change in the feed salinity when the pilot plant is already operating at the max P_{f1} constraint will also lead to a change in Y_1. It was shown in **Section 7.5.4** that when comparing operation at the max P_{f1} constraint for high feed salinity (24,190 mg/L) and low feed salinity (17833 mg/L), operation during high salinity conditions resulted in a lower Y_1 (i.e., Y_1 was 27.3 % for high salinity feed as compared to 42% low salinity feed). Therefore, for operation at a high feed salinity, there may be cases where a single-stage operation may be more energy-efficient than a two-stage operation. In order to investigate whether at high feed salinities single-stage or two-stage is more energy-optimal, the RO plant operation was assessed for two different feed salinities: at 17,196 mg/L and 24,676 mg/L. For operation at 17,196 mg/L and a permeate production set-point of 45.4 L/min, the SEC as a function of Y for two-stage operation (**Eq. 7.3**) as well as the theoretical SEC curve for single-stage operation (**Eq. 7.3**, but only using the first term on the right hand side for single-stage RO) are plotted in **Figure 7.18**. The energy-optimal operation for two-stage RO appears on the max P_{f1} SEC curve, at Y_1 = 42% (**Eq. 7.24**). This operating point is of an SEC that is lower than the optimal SEC value for single-stage operation (**Figure 7.18**).

The theoretical SEC curves for two-stage and single-stage RO operation for a feed salinity of 24,676 mg/L and a permeate production set-point of 45.4 L/min are plotted (i.e., both calculated through **Eq. 7.3**) in **Figure 7.19**. When the feed salinity increased to 24,676 mg/L, the SEC for a two-stage operation increases due to the max P_{f1} constraint since the first stage is operating at a lower Y_1 of 27.3% (**Section 7.5.4**). As discussed previously, operating at a lower Y_1 means that the second-stage feed flow rate is increased and the less efficient second-stage feed pump must do more work in order to product the same overall permeate flow rate (**Section 7.5.2**), resulting

in an increase in the overall SEC (**Figure 7.19**). When operating in a two-stage RO configuration, the max P_{f1} constraint is dictated by the max pressure of the feed input to the second-stage pump (2.17 MPa) which limits the permeate production of the first stage. However, when the RO system operates in a single-stage configuration, the max P_{f1} constraint is no longer dictated by the input of the second-stage pump and instead set by the pressure limits of the first-stage RO pressure vessels, which is significantly higher (4.14 MPa). Due to the above, single-stage operation with the first stage operating at a high pressure (3.43 MPa, **Eq. 7.19**) is predicted to be more energy-efficient (**Figure 7.19**) than two-stage RO configuration where the first-stage is operated at a lower pressure (2.17 MPa, **Eq. 7.19**) relative to the second stage (3.65 MPa, **Eq. 7.20**).

In order to confirm the predicted result of first-stage RO being more energy-efficient than two-stage RO at high feed salinity for this specific pilot plant, the RO system was transitioned from a two-stage configuration to a single-stage configuration under conditions of high feed salinity (24,676 mg/L). The plant was initially operated in a two-stage configuration operated with the energy-optimal controller on at water recoveries of Y = 69% and Y_1 = 27.3%). The system was then shut-down and re-started in a single-stage configuration. The transition between two-stage operation and single-stage operation is shown in **Figure 7.20**. The measured normalized SEC of the two stages was 6.72 for single-stage RO and 8.31 for two-stage RO (difference of 23 %, **Figure 7.19**). This experiment confirmed that two-stage RO operated at a low value of Y_1 can be less energy-efficient than single-stage RO.

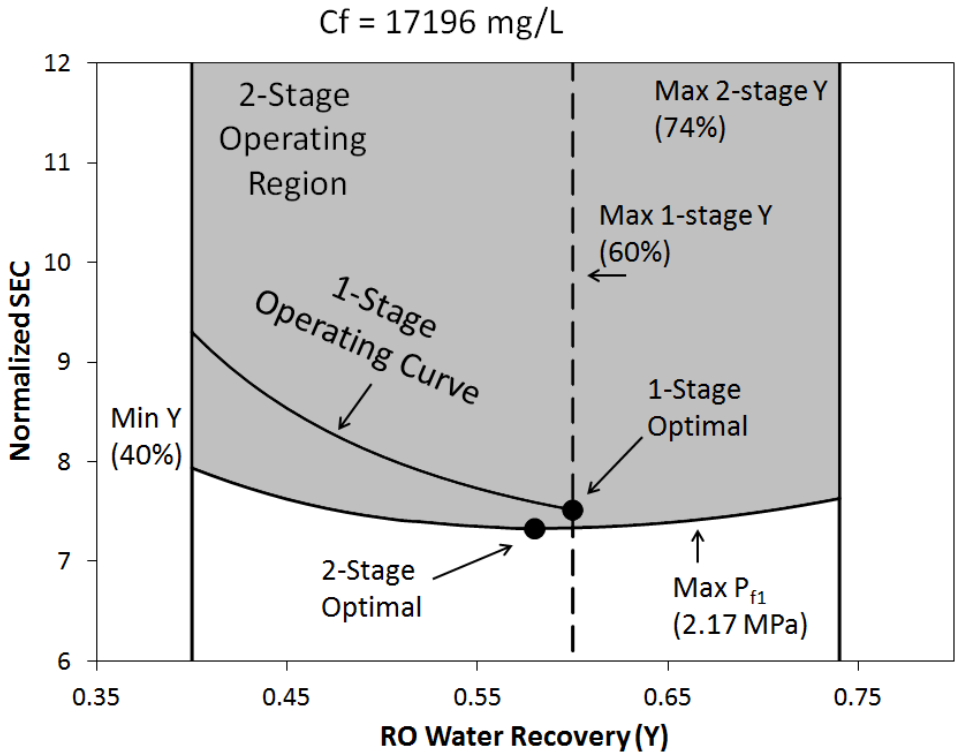

Figure 7.18. Normalized SEC for single-stage RO and two-stage RO with respect to RO water recovery (*Y*), with the constraints of minimum *Y* (40%), maximum *Y* (74%), and maximum P_{f1} (2.17 MPa) at a feed salinity of 17,196 mg/L. Solid circles denote the energy-optimal operating states for single-stage and two-stage RO operation. The grey area represents the two-stage operation region. The first-stage SEC curve is calculated through the first term in **Eq. 7.3**. How the max P_{f1} curve was calculated and plotted is explained in **Figure 7.25**.

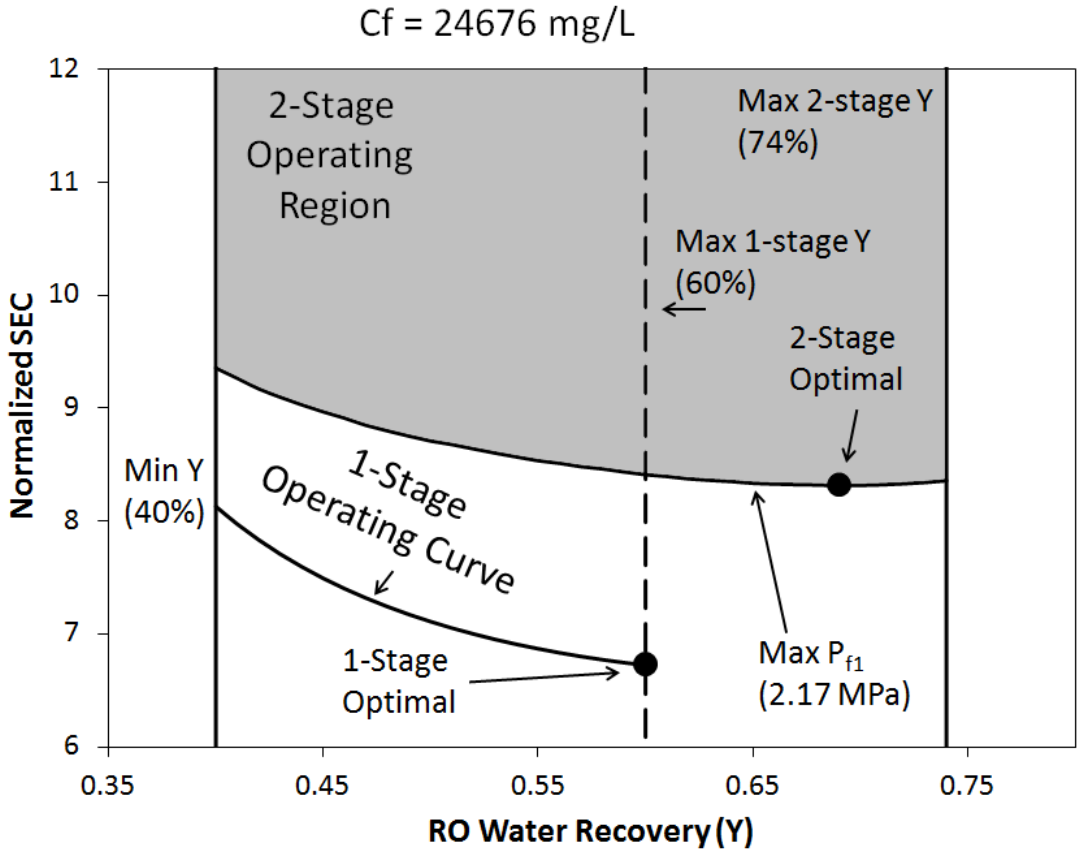

Figure 7.19. Normalized SEC for single-stage RO and two-stage RO with respect to RO water recovery (*Y*), with the constraints of minimum *Y* (40%), maximum *Y* (74%), and maximum P_{f1} (2.17 MPa) at a feed salinity of 24,676 mg/L. Solid circles denote the energy-optimal operating states for single-stage and two-stage RO operation. The grey area represents the two-stage operation region. The first-stage SEC curve is calculated through the first term in **Eq. 7.3**. How the max P_{f1} curve was calculated and plotted is explained in **Figure 7.25**.

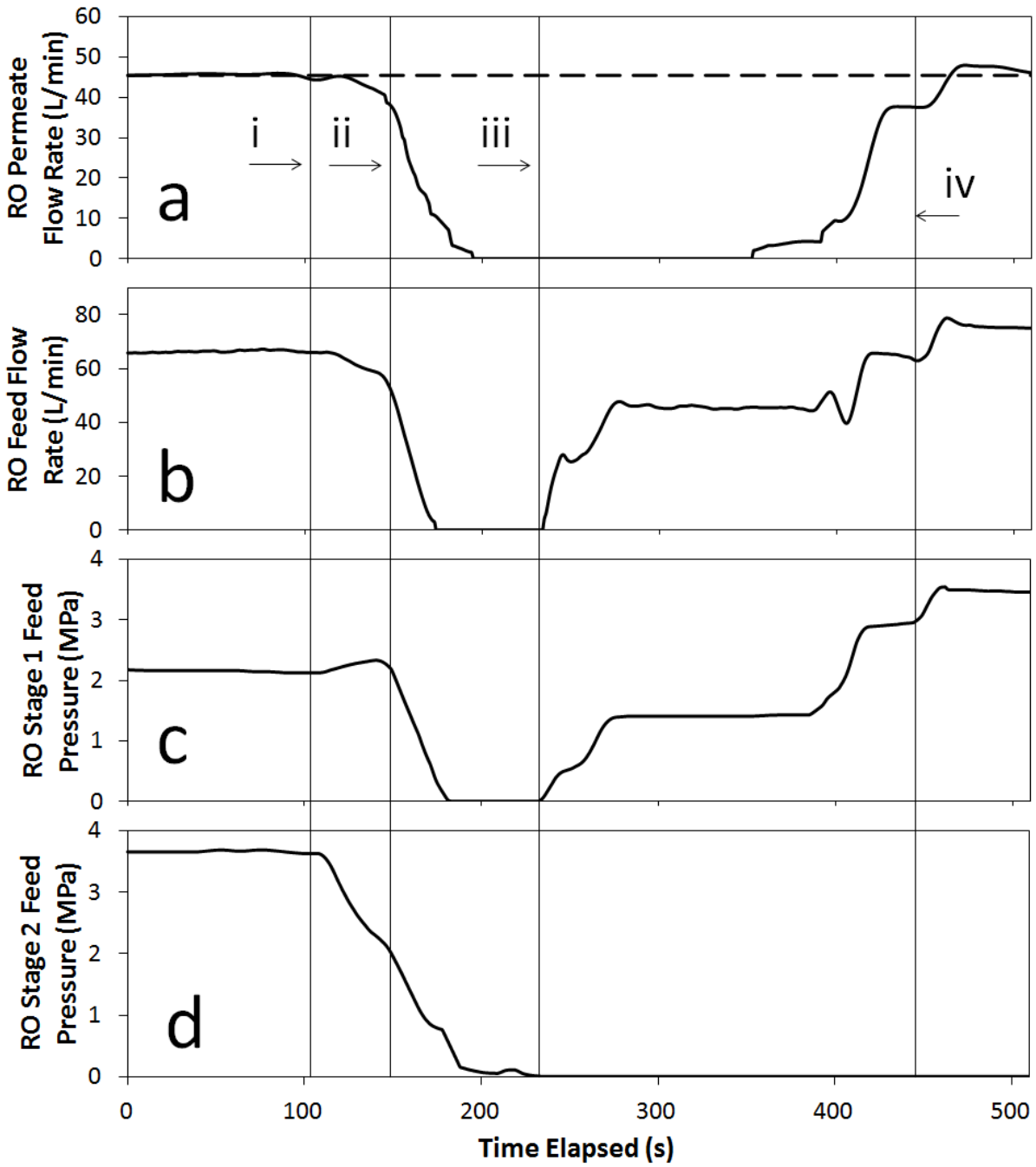

Figure 7.20. Profiles of (a) RO permeate flow rate, (b) RO feed flow rate, (c) RO first-stage feed pressure, and (d) RO second-stage feed pressure with respect to time during a transition from two-stage operation to single-stage operation. Roman numerals denote events which correspond to (i) shut-down of the second-stage pump, (ii) shut-down of the first-stage pump, (iii) activation of the first-stage pump, and (iv) activation of the supervisory controller.

7.6 Summary

A novel model-based control system for energy-optimal operation of a two-stage RO membrane desalination system was developed. Specific energy consumption (SEC) was used as a framework to develop a model for energy consumption for a two-stage RO system. This model was then combined with real-time sensor and plant data to solve for energy-optimal values for the overall (Y) and first stage permeate recovery (Y_1) for a given water productivity (i.e., total permeate flow rate) target, feed salinity, and membrane permeability. The determined operating state was then applied to the RO plant through its lower-level control system, which consists of three separate feedback loops controlling the RO feed flow rate, the first-stage RO pressure, and the second-stage RO pressure through actuation of the first-stage RO feed pump, the second-stage RO feed pump, and the RO concentrate valve, respectively. The control system was demonstrated of the operation of a high-recovery brackish water desalination plant, capable of permeate productivity up to 40,000 gallons/day. Field testing demonstrated robust simultaneous control of dynamically coupled control variables and effective energy-optimal operation, subject to feed salinity fluctuations.

7.7 Supplementary Materials

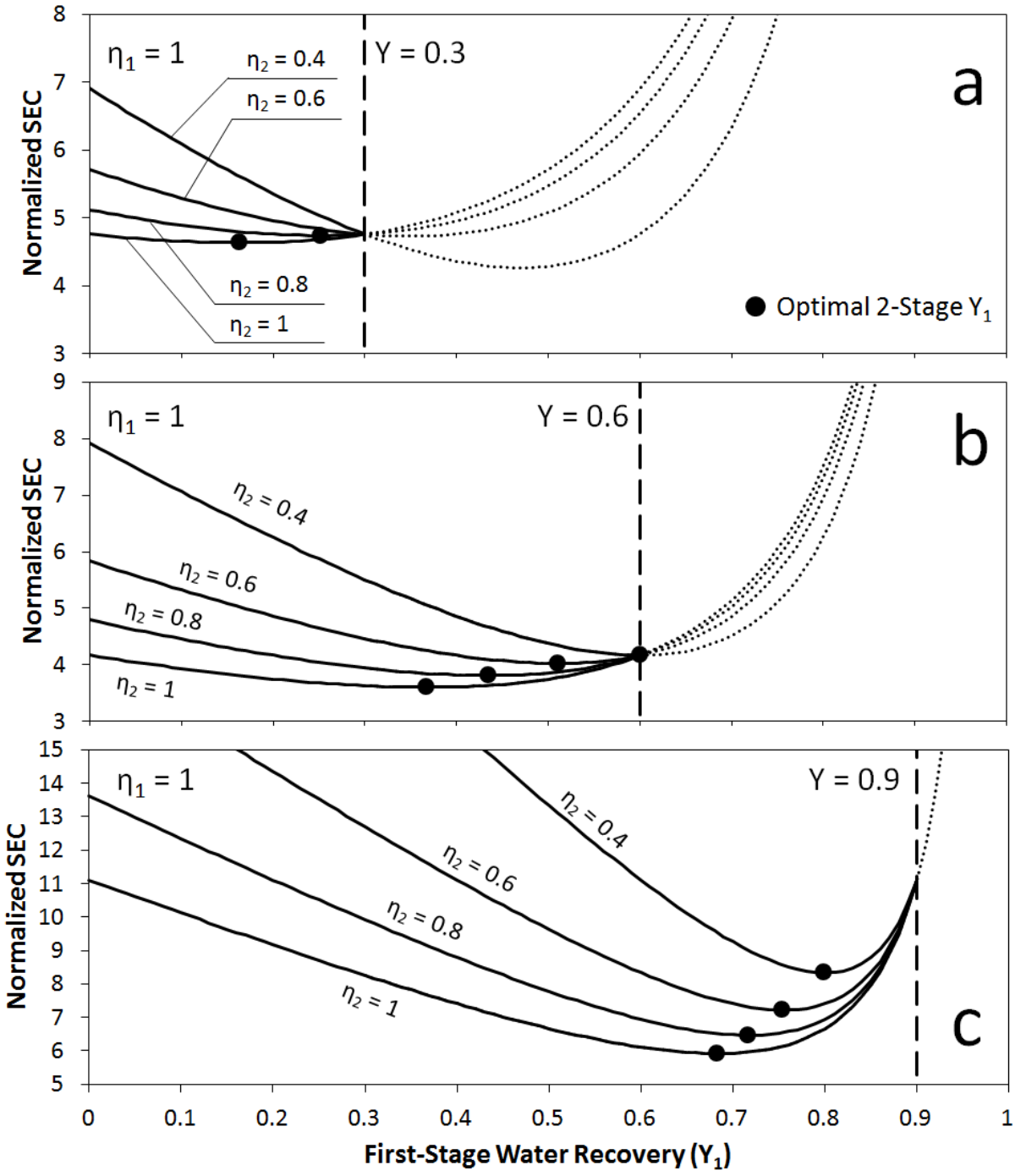

Figure 7.21. Plot of SEC vs first-stage water recovery (Y_1) at a fixed overall water recovery (Y) of (a) 30%, (b) 60%, and (c) 90%, constant $\eta_1 = 1$ and varying η_2. As η_2 decreases, SEC increases, and the optimal Y_1 increases. SEC curves were calculated through **Eq. 7.7**.

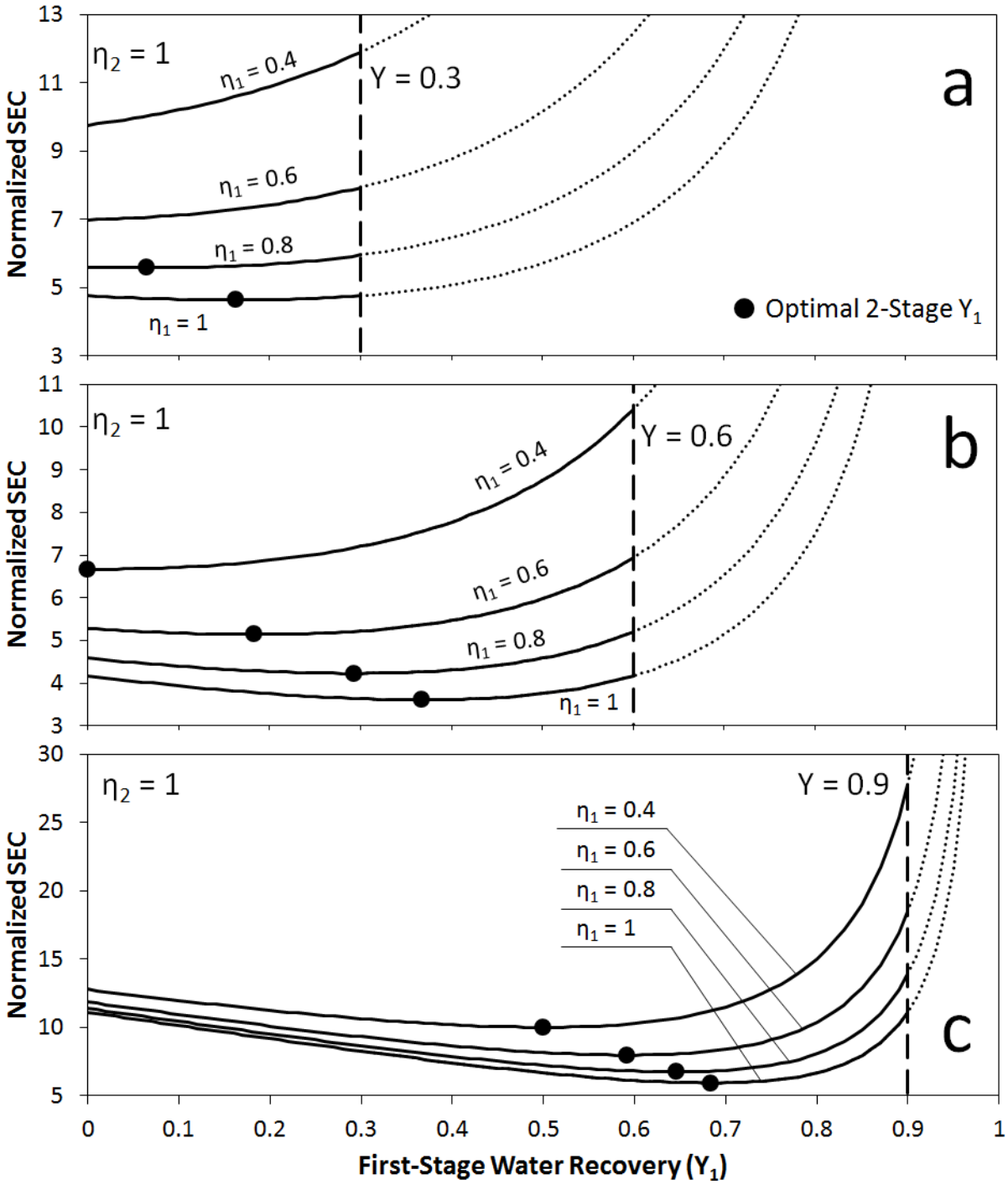

Figure 7.22. Plot of SEC vs first-stage water recovery (Y_1) at a fixed overall water recovery (Y) of (a) 30%, (b) 60%, and (c) 90%, constant $\eta_2 = 1$ and varying η_1. As η_2 decreases, SEC increases, and the optimal Y_1 increases. SEC curves were calculated through **Eq. 7.7**.

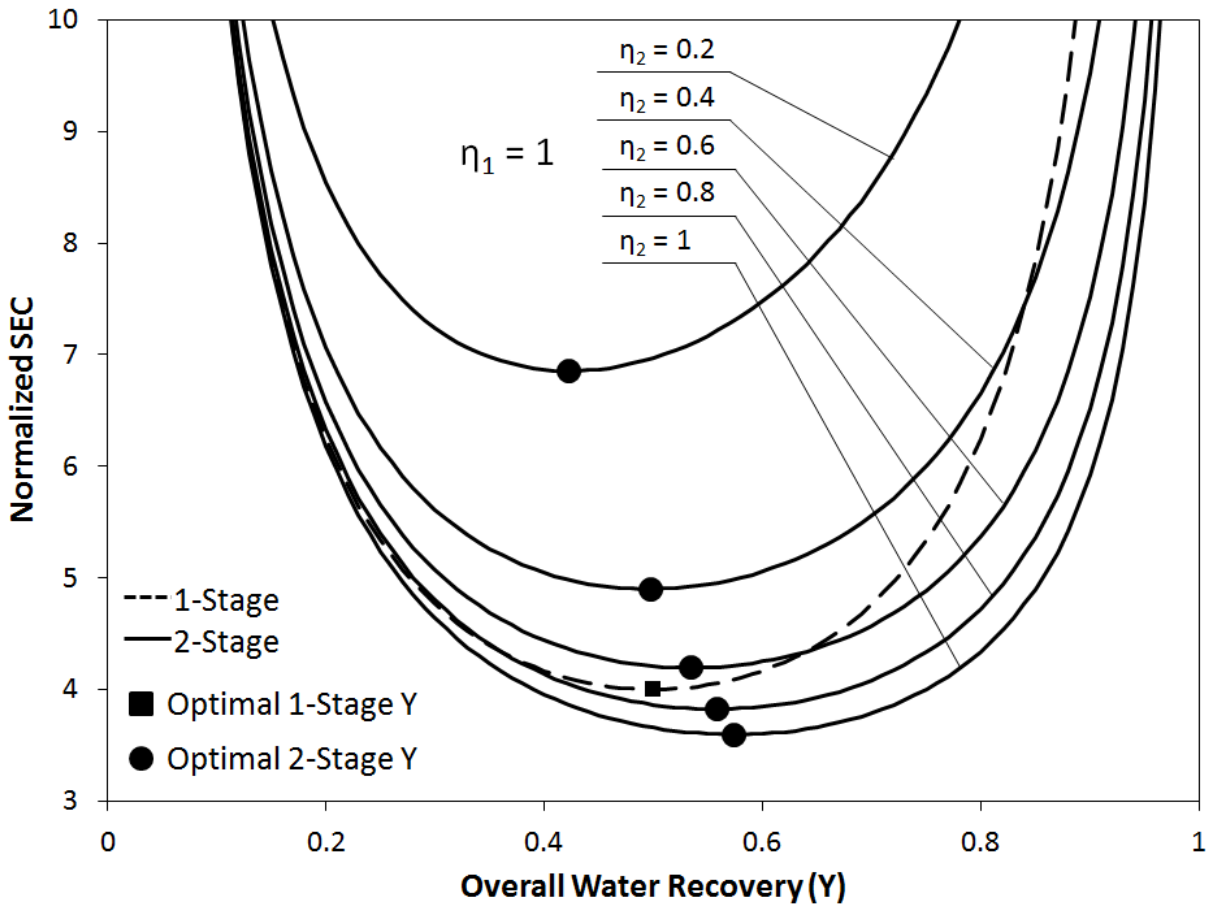

Figure 7.23. Plot of SEC vs Y for two-stage and single-stage operation for constant $\eta_1 = 1$ and varying η_2. Energy-optimal Y, or the value of Y which results in the lowest SEC, are marked with circles for two-stage and a square for single-stage. As η_2 decreases, SEC increases, and the optimal Y decreases. Solid lines denote 2-stage and dashed line is 1-stage operation at $\eta = 1$. SEC curves were calculated through **Eq. 7.5**.

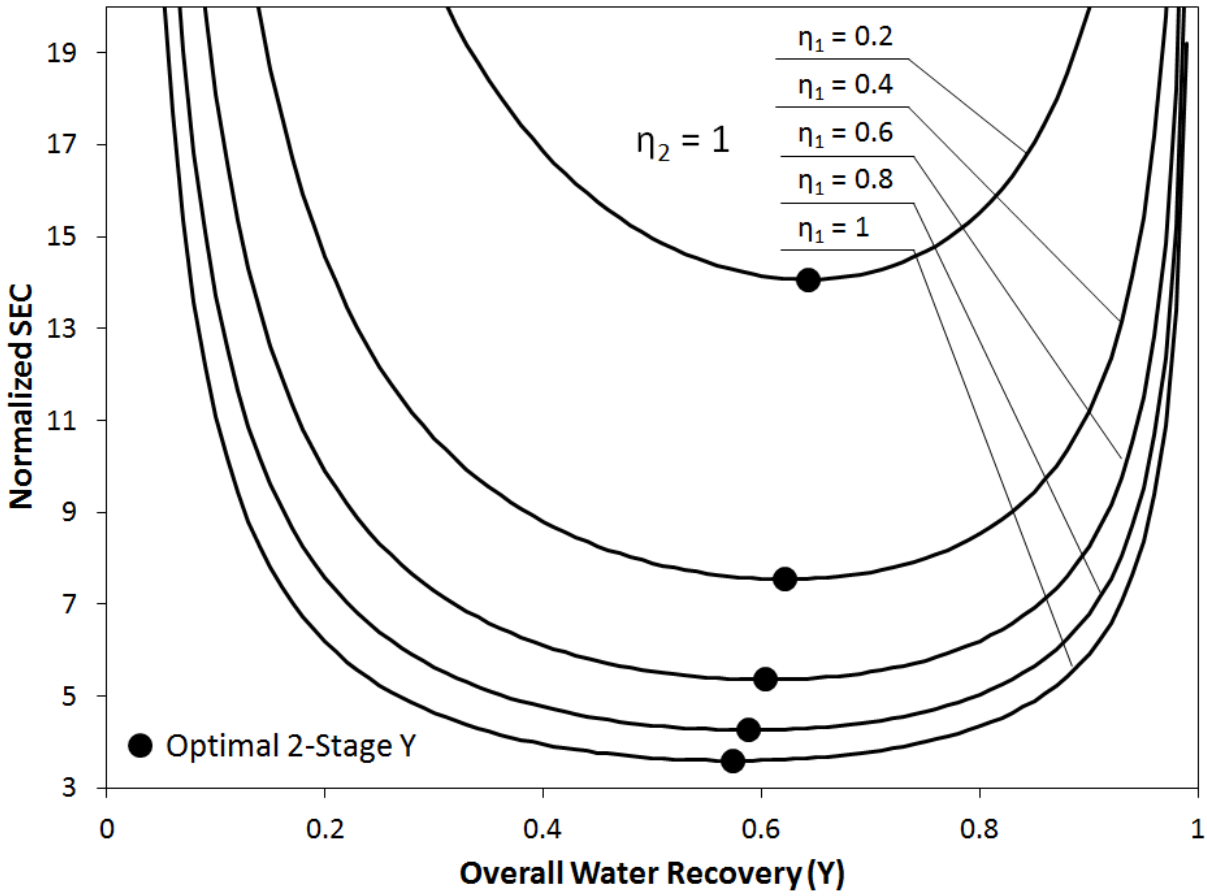

Figure 7.24. Plot of SEC vs Y for two-stage operation for constant $\eta_2 = 1$ and varying η_1. Energy-optimal Y, or the value of Y which results in the lowest SEC, are marked with circles. As η_1 decreases, SEC increases, and the optimal Y increases. SEC curves were calculated through **Eq. 7.5**.

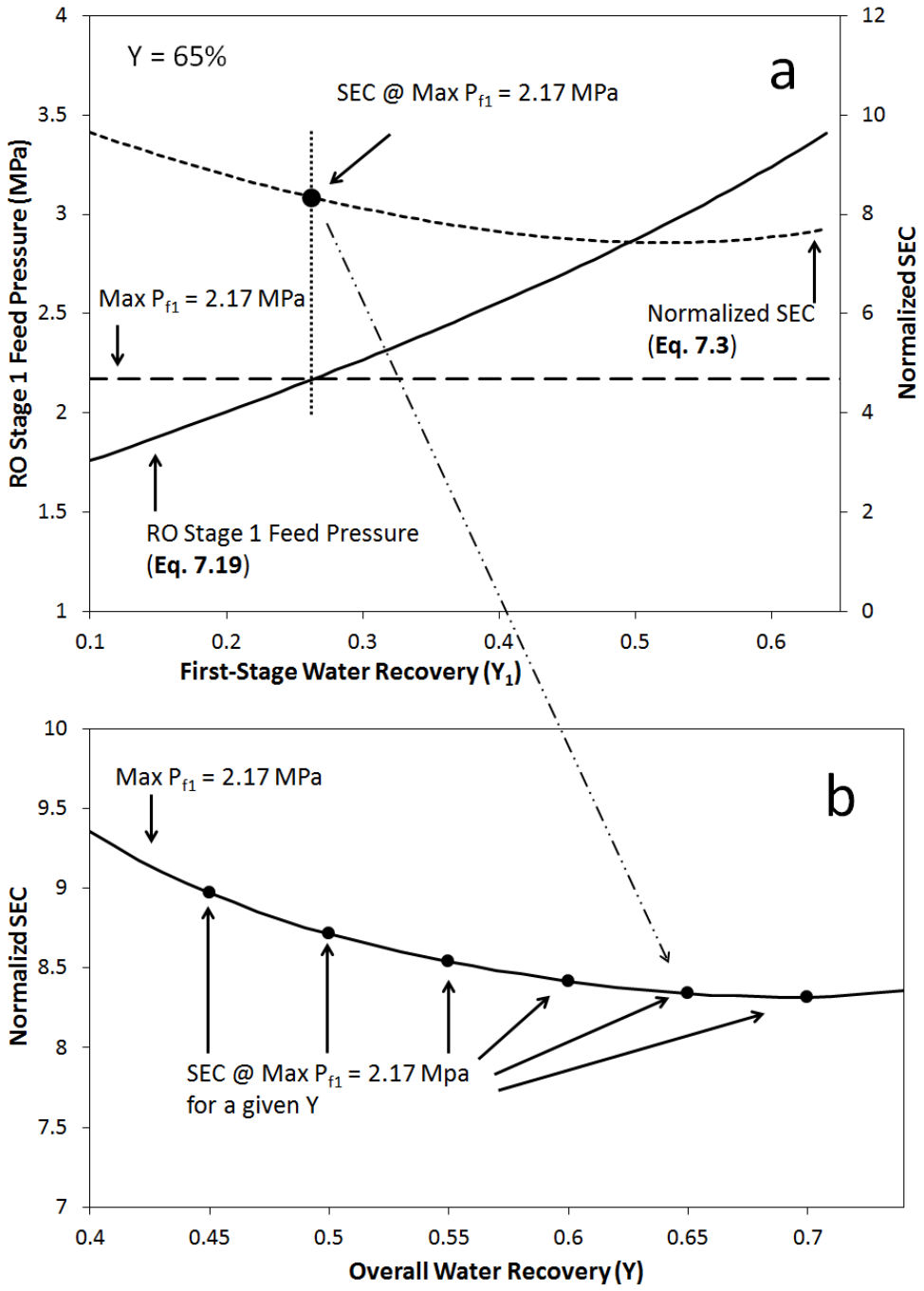

Figure 7.25. An illustration of how the max P_{f1} SEC curve is plotted. For a given value of desired Q_p (45.4 L/min), feed salinity (**24,676 mg/L**), and Y, the predicted first-stage feed pressure P_{f1} can be calculated as a function of Y_1 with **Eq. 7.19**. The value of Y_1 which corresponds to the max P_{f1} constraint can be obtained, and is shown in (a) as the intersection between the solid and dashed lines. The SEC at this value of Y_1 can be the calculated through **Eq. 7.3** and this value will be the SEC at the max P_{f1} constraint for a given Y. This process can be repeated for all values of Y to obtain the SEC at the max P_{f1} constraint as a function of Y, and the resulting curve is plotted in (b).

Chapter 8 Conclusions

The objective of this dissertation was to reduce the operational cost of RO desalination through the implementation of advanced, self-adaptive process control strategies. The development and implementation of self-adaptive control algorithms for both RO feed pre-treatment and RO desalination on pilot-plants successfully achieved reduction in RO desalination operational cost. Several novel approaches to improve pre-treatment of RO desalination systems and reduce RO energy consumption were presented.

With respect to improving RO feed pre-treatment, in **Chapter 4** the direct integration of UF-RO where RO concentrate was used for UF backwash was developed and demonstrated. The control system enabled this direct integration by successfully regulating the pressure and flow rate at the UF-RO interface. This direct integration significantly reduced the footprint of RO systems and enabled the implementation of a variable frequency UF backwash strategy which lengthened the operational duration before chemical cleaning was required. In **Chapter 5**, UF backwash was further enhanced with a self-adaptive coagulant dose controller. The RD-factor was developed as a metric to quantify in real-time the impact coagulant dose has on the effectiveness of UF backwash and was used to determine the optimal coagulant dose for pre-treatment. The coagulant controller was successful at adjusting the coagulant dose by reducing UF fouling during periods of worsening feed water quality while reducing coagulant chemical consumption during periods of improving feed water quality.

For the RO desalination unit, an energy-optimal control system was implemented using fundamental models of specific energy consumption (SEC) of RO systems in **Chapter 6**. A novel two-layered control system was proposed and implemented on pilot plant. Field studies successfully demonstrated the control system's ability determine the energy-optimal operation condition and to reduce energy consumption by maintain energy-optimal operation despite

variable feed salinity conditions. In **Chapter 7**, this method was expanded and implemented on a two-stage RO system. The energy-optimal controller was successful at calculating the energy-optimal permeate production split between the two stages and was able to operate a two-stage RO system at its energy-optimal operating point.

In summary, this dissertation details the development of novel control methods for the operation of both UF pre-treatment and RO desalination. The implementation of the various control methodologies on pilot plants and their effectiveness at reducing operational cost of RO desalination was evaluated and documented. The control systems developed in this dissertation was successful at reducing the operational costs of RO desalination through the improvement of RO feed pre-treatment and the reduction of RO energy consumption.

Appendix A. SIMS-BW Software

This section, provides a summary of the general software architecture used in the SIMS-BW plant. The SIMS-BW software was written in LabVIEW. The SIMS-BW software is hosted in two main locations: The real-time controller (RTC) which is hosted on the National Instruments Compact Real-time Input Output (NI cRIO) (i.e., located in the electrical box) and the PC connected to it which hosts the graphical user interfaces (GUI). The PC and the cRIO are connected and the cRIO are connected to all the electrical components on the system inside the electrical box. The general diagram of the electrical connections are shown in **Figure A.1**.

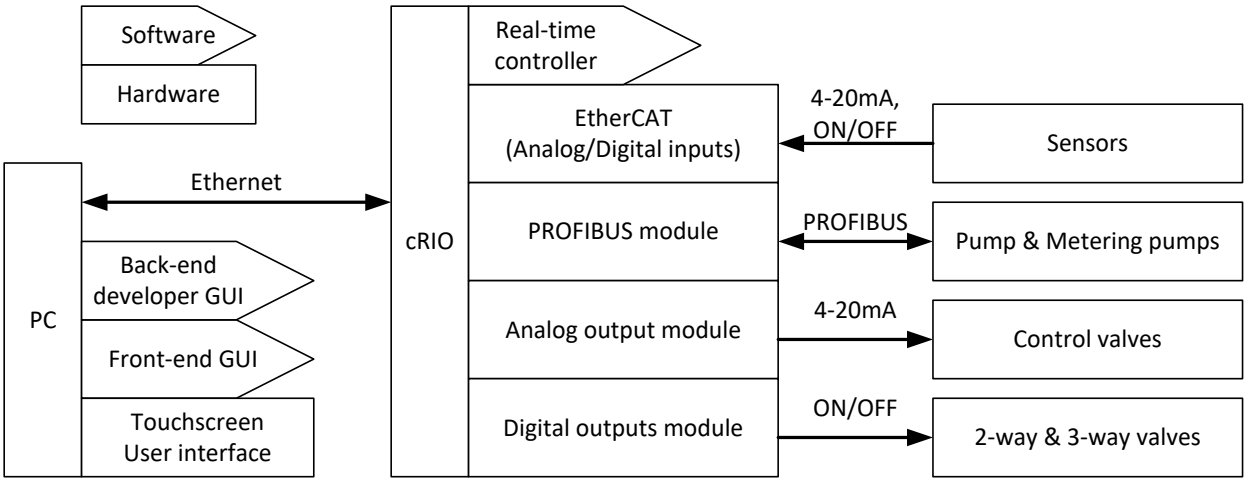

Figure A.1. A general diagram of the SIMS-BW software architecture and electrical connections

The PC hosts two versions of the GUI. Their outward appearance is similar, but the front-end GUI runs as an .exe application file (under Windows). The back-end GUI runs as a LabVIEW code to enable the administrator to code changes as necessary.

The cRIO hosts the RTC which controls every aspect of the SIMS-BW. The cRIO is also connected to several modules which allows it to interface with various sensors and actuators on the system. The analog output modules (NI 9265) allows the cRIO to send out 4-20 mA signals the adjustable control valves on the system. The digital output modules (NI 9476) are connected

to and used to control all on/off actuators, such as 2-way or 3-way valves. The EtherCAT is an expansion module which is used to make more connections available to the cRIO. In the SIMS-BW, the EtherCAT is used interface with various analog (4-20 mA signal) and digital sensors (on/off). The EtherCAT is equipped with NI 9426 modules for digital inputs (e.g., valve limit switches, whose values are on/off) and NI 9208 modules for analog inputs (e.g., sensors which output a 4-20 mA signal). The cRIO is also equipped with the PROFIBUS module to allow it to communicate to the GUNDFOS pumps and metering pumps using the PROFIBUS communication protocol. The specifics of the PROFIBUS protocol are discussed in **Appendix D**.

Appendix B. SIMS-BW GUI and RTS Block Diagram Layout

This section describes the organization of the SIMS-BW GUI and RTS's LabVIEW codes. A LabVIEW code has two parts: the front panel and the block diagram. The front panel contains all the inputs and outputs into the LabVIEW function, while the block diagram consists of all the code which processes the data. In general, when discussing the LabVIEW code, the reference is to the block diagram unless it is explicitly stated otherwise.

The block diagrams of the GUI and RTS are divided into several While loops, each with a unique function. The layout of the While loops in the GUI and RTS block diagrams are illustrated in **Figure B.1**:

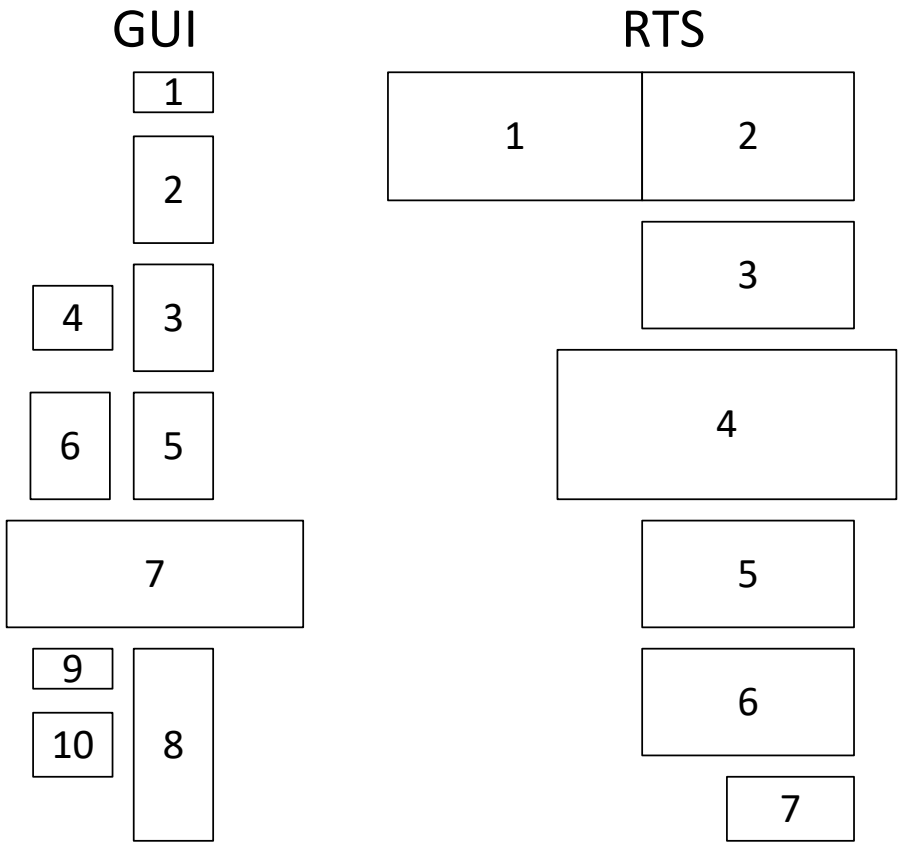

Figure B.1. A depiction of the LabVIEW block diagram layout of the graphical user interface (GUI) and real-time controller (RTS).

A list of the While loops in the GUI and a brief description of their functions:

1. Manual control syncing across all GUIs. This syncs the “Manual Control” button on the GUI with all the other GUIs If this button is ON in one GUI, it will get turned ON in all other active GUIs
2. Digital output syncing. This syncs various digital output buttons on the GUIs (e.g., button to turn 2-way valve open/close) such that if a button is turned ON in one GUI, it will get turned ON in all other active GUIs.
3. Analog output syncing. This syncs the various analog outputs (e.g., input to change the valve opening using a value between 0-100) across all active GUIs.
4. Analog output PI syncing. This syncs the analog output displayed on the GUI to the value set by a PI controller hosted on the RTS.
5. PROFIBUS syncing. This syncs all inputs related to the PROFIBUS (e.g., pump value, pump control method, pump ON/OFF) across all GUIs.
6. PROFIBUS PI syncing. When a pump is being controlled by a PI controller on the RTC, this syncs the output displayed on the GUI with the output of the PI controller.
7. Inputs sorting. Sorts both analog and digital inputs (e.g., sensors, limit switches) into appropriate variables which can be then displayed on the GUI or recorded by a data logger.
8. Operation controls syncing. Inputs of operational parameters (i.e., UF filtration duration, RO configuration) are synced across all active GUIs. This While loop also handles the initialization of the GUI based on values given from the RTC such that the stopping/starting the GUI will not interfere with RTC operations.
9. Unpress start/shut-down buttons 5 seconds after they have been pressed.

10. RO supervisory controller interface. The RO supervisory controller requires inputs for the permeate flow rate, recovery, and feed flow rate. This While loop ensures that if one value is changed the other two also change to reflect this change (e.g., if recovery was reduced and the feed flow rate is kept constant, the permeate flow rate is automatically reduced).

For the RTC, below is a list of the While loops and a brief description of their functions:

1. Initialization. Various string arrays used to sort sensors values into variables are initialized. If a sensor connection is ever changed, this is where the connections should be updated. This While loop also contains the calibrations for all the sensors.
2. FPGA interface. The RTC interfaces with the FPGA and reads all the input signals as well as organize and send out all the output signals. This is the core loop of the RTC, and every signal going in and out of the cRIO is processed here.
3. Analog output PIs. This loops contains the 3 PI controllers for the 3 control valves controlled through the analog output module (NI 9265)
4. Automated sequences. This loop contains the structure used for all of the SIMS-BW's automated sequences. An automated sequence is defined as a series of pre-set commands to valves and pumps designed to transition the system from one configuration to another (e.g., from UF filtration to UF backwash mode). The structure is described in more detail in **Appendix C**.
5. Statechart. The statechart is used to keep track of the order in which the automated sequences are executed (e.g., making sure the system start-up is executed before UF backwash can trigger). The statechart is described in more detail in **Appendix C**.
6. RO supervisory control & error handling. This loop contains the RO supervisory controller and the error handling functions. The RO supervisory calculates pressure and

flow rate set-points required to achieve the desired permeate flow rate and recovery set by the operator. The error handling takes care of various errors during operation (e.g., pump is not providing pressure even when commanded to be on) and shuts down the system when it detects such errors.

7. Soft sensors. Contains the UF and RO soft sensors, which take pressure, flow, conductivity, and temperature sensor readings and calculates the values of parameters such as UF resistance and RO permeability.

Appendix C. Automated Sequence and Statechart

The automated sequence structure mentioned in **Appendix B** is a core component of the SIMS-BW's automated operations. It contains a series of automated sequences, which are defined as a series of pre-set commands to valves and pumps designed to transition the system from one configuration to another. This section describes the structure functions.

The While loop containing the automated structure sequence is shown in **Figure C.1**. Below is a brief description of each numbered object:

1. Automated sequence number. This indicates which automated sequence is currently being displayed in the block diagram. The full list of all the sequences is located to the right of the structure in (6).
2. Automated sequence step. This indicates the step within an automated sequence that is currently being displayed in the block diagram. There are in general two types of steps: the step itself, and the guard, which always follows a step. In the screenshot, the step displayed in the block diagram indicated by (2) is a step, not a guard.
3. Timer. This is a counter which increments upward by 1 every 0.1 seconds and is used to time the step duration. Since the ticks are once every 0.1 seconds, 10 ticks is equivalent to 1 second.
4. Step transition. This indicates the program that will execute after the current step is executed. If the current step is a normal step, then the transition will always be to its corresponding guard. The steps should be organized in the order they are executed in the drop down menu in (2).
5. Overview of steps. This is a comment with a summary of all the steps in the sequence.

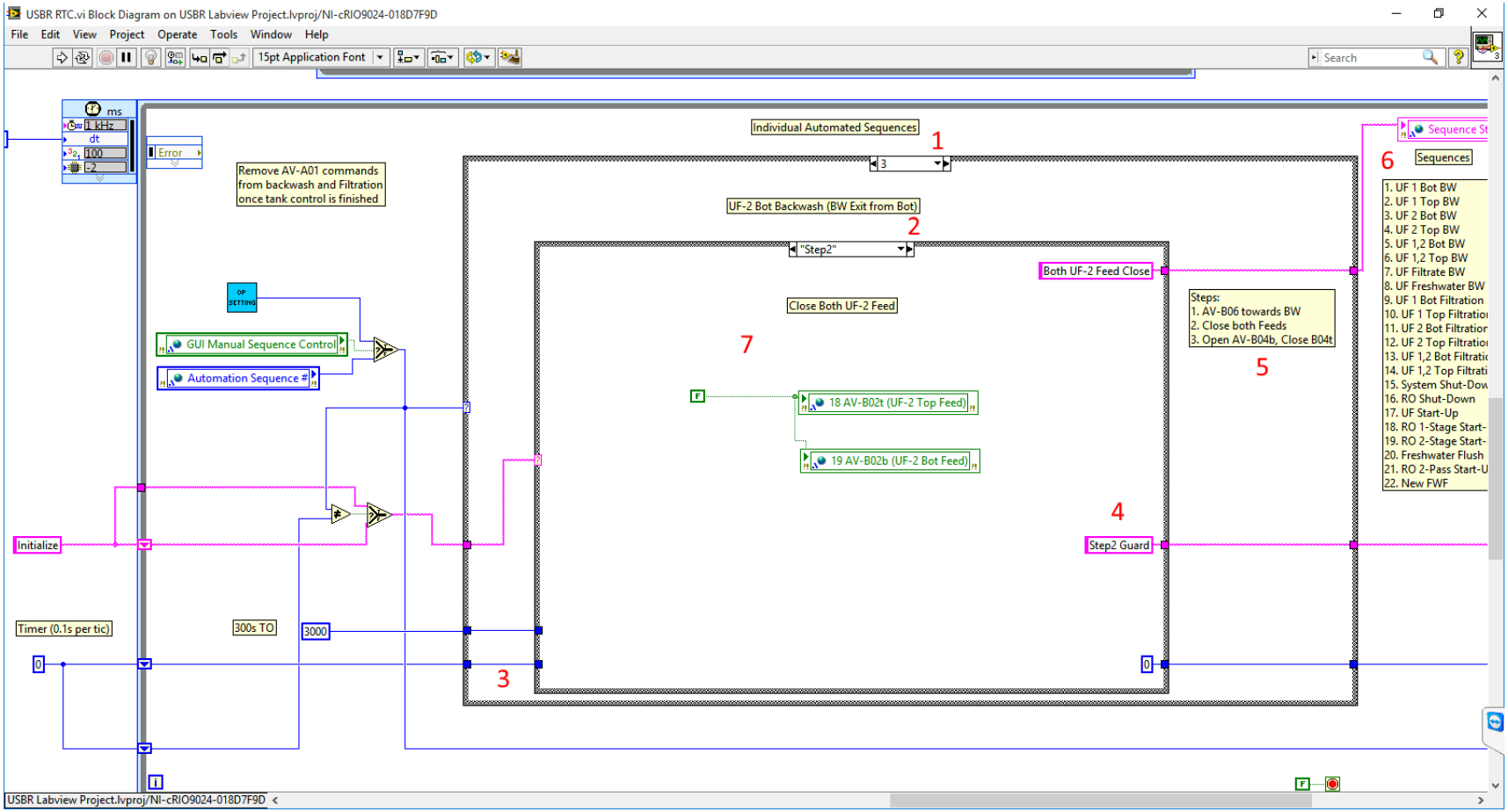
USBR RTC.vi Block Diagram on USBR Labview Project.lvproj/NI-cRIO9024-018D7F9D
File Edit View Project Operate Tools Window Help
15pt Application Font
Search
ms
1 kHz
dt
100
-2
Error
Remove AV-A01 commands from backwash and Filtration once tank control is finished
Individual Automated Sequences
1
3
UF-2 Bot Backwash (BW Exit from Bot)
2
"Step2"
Close Both UF-2 Feed
7
Both UF-2 Feed Close
Steps:
1. AV-B06 towards BW
2. Close both Feeds
3. Open AV-B04b, Close B04t
5
6
Sequences
1. UF 1 Bot BW
2. UF 1 Top BW
3. UF 2 Bot BW
4. UF 2 Top BW
5. UF 1,2 Bot BW
6. UF 1,2 Top BW
7. UF Filtrate BW
8. UF Freshwater BW
9. UF 1 Bot Filtration
10. UF 1 Top Filtratio
11. UF 2 Bot Filtratior
12. UF 2 Top Filtratio
13. UF 1,2 Bot Filtrati
14. UF 1,2 Top Filtrati
15. System Shut-Dow
16. RO Shut-Down
17. UF Start-Up
18. RO 1-Stage Start-
19. RO 2-Stage Start-
20. Freshwater Flush
21. RO 2-Pass Start-U
22. New FWF
OP SETTING
GUI Manual Sequence Control
Automation Sequence #
18 AV-B02t (UF-2 Top Feed)
19 AV-B02b (UF-2 Bot Feed)
Initialize
Step2 Guard
4
Timer (0.1s per tic)
300s TO
3000
3
USBR Labview Project.lvproj/NI-cRIO9024-018D7F9D

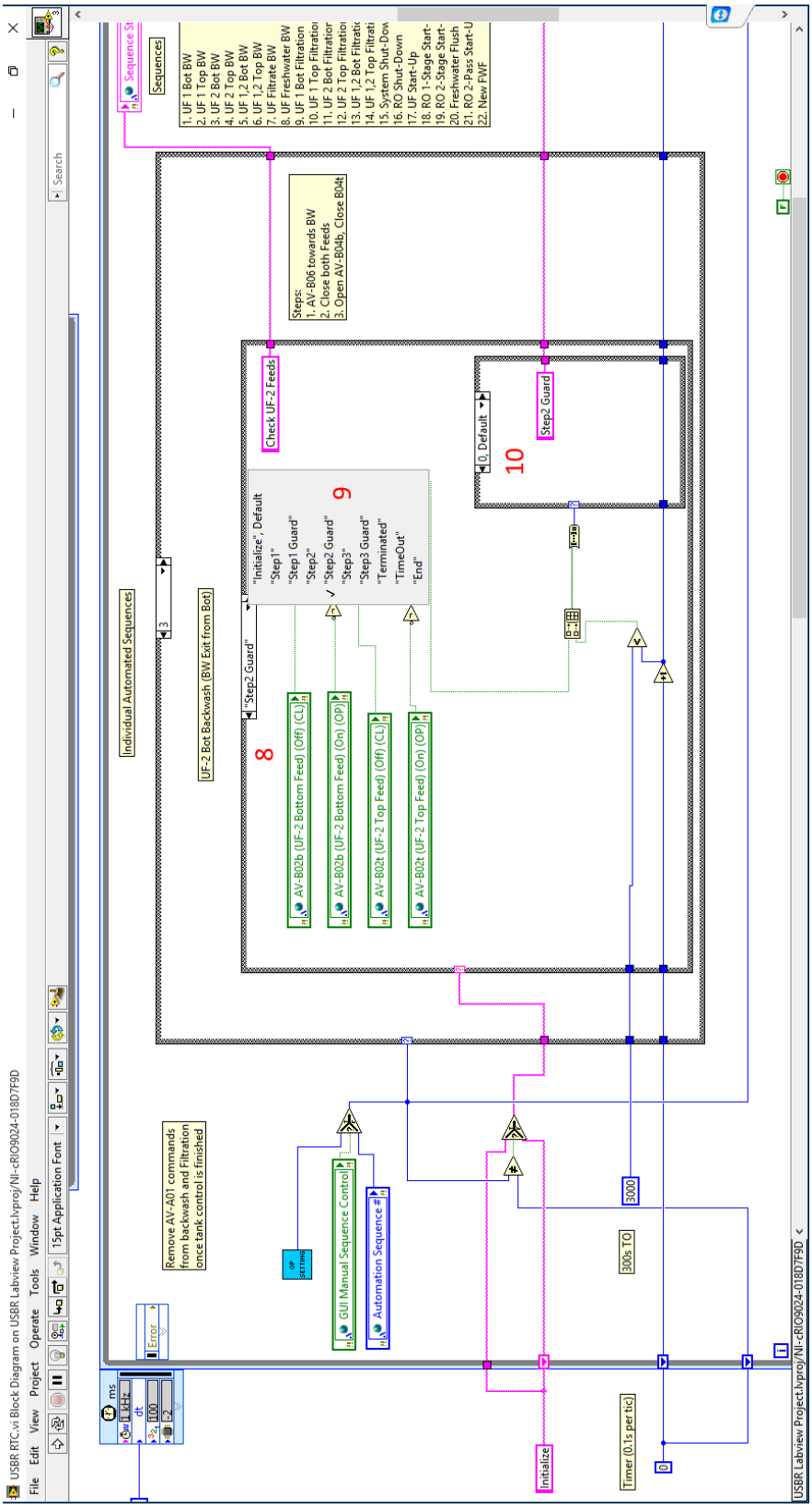

Figure C.1. Screenshots of the LabVIEW block diagram of the automated sequence structure.

6. List of all sequences. This is a list of all the sequences which have been programmed, and the corresponding number required to run them.
7. Step body. The body of a step includes all the commands to be executed in this step. In this example, an AV-B02t and AV-B02b are set to FALSE.
8. Guard body. The body of a guard is designed to detect whether the commands have been executed and whether to proceed to the next step or not. Typically, the guard checks valves' limit switches or a pump speed to ensure that the commands sent in the previous step were executed. Only when all the guard requirements are satisfied, will the program move onto the next step.
9. Drop-down menu of all steps in a sequence. The steps should be organized by the order of their execution. Note that there are steps to initialize, terminated, time out, and end. These steps are required for the automated sequences to function within the program itself and should never be edited.
10. Guard transition. Very similar to (4), this indicates what the next step the program should execute. However, unlike a normal step, the guard transition has three possible results: to remain in guard, to proceed to the next step, or time out. The program will decide to remain in guard to continue monitoring the system if all the requirements have not been satisfied. When all the requirements are satisfied, then the program will proceed to the next step. If the requirements are not satisfied within the set time out period, then the system will time out and display an error message.

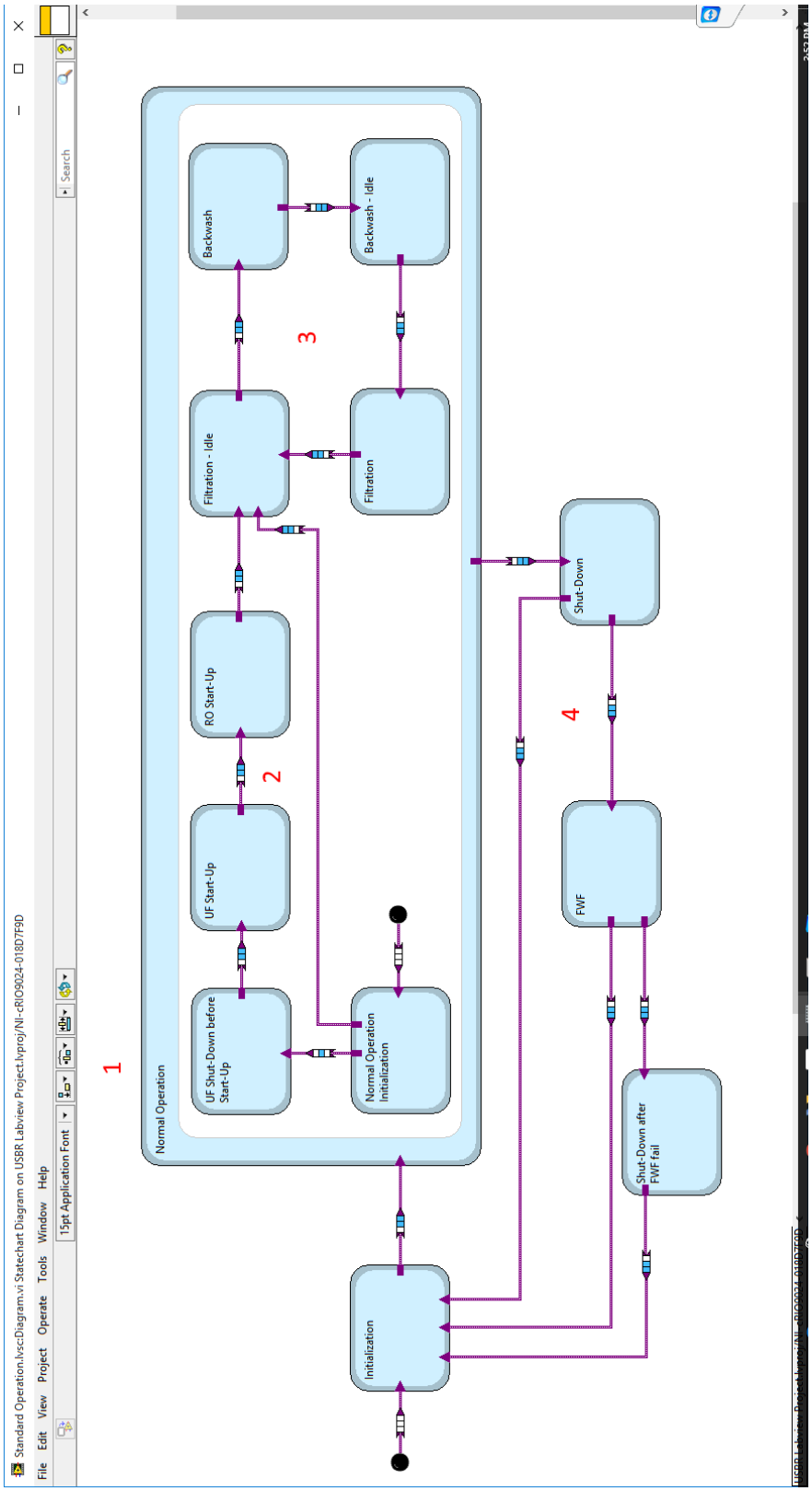

Figure C.2. A screenshot of the statechart module

The statechart serves to provide a clear visual structure for the automated sequences to be executed in the correct order. The blocks shown in **Figure C.2** are called "states," and most states include a command to execute one automated sequence. After a state is finished executing an automated sequence, it then follows the arrow connecting two states to determine which state (and the corresponding automatic sequence) to execute next. Below is a brief description of each numbered object depicted on **Figure C.2**:

1. Normal Operation. Normal operation is defined as when the system is producing fresh water while under the control of the statechart. It involves a system start-up sequence where the UF and RO are started up and then switched between UF filtration/UF backwash modes.
2. Start-up sequence. There are 3 automated sequences involved in the start-up sequence: a system shut-down sequence to ensure a correct starting configuration for the subsequent start-ups, a UF start-up sequence, and an RO start-up sequence. When the start-up is complete, the system enters a configuration where the UF is in a filtration configuration and the RO is in a configuration that was set by the operator.
3. UF Filtration and UF backwash. Once the start-up is completed, the UF is in its filtration configuration and a filtration cycle begins. A filtration cycle is defined as the combination of a UF filtration period and a UF backwash period. While in 3, the statechart will switch to UF backwash when it is triggered, then switch back to UF filtration once the pre-set duration for UF backwash is finished. The SIMS-BW will continue to execute filtration cycles until a shut-down is initiated by the user or by an error.
4. System shut-down. When the user or an error initiates a shut-down, the statechart exits from normal operation and executes the shut-down automated sequence. Following shut-

down, the system will execute a freshwater flush sequence. The operator can set the system to not execute the freshwater flush.

Appendix D. PROFIBUS

PROFIBUS is an industrial communication protocol and is used in the SIMS-BW to communicate with the 5 GRUNDFOS pumps and 7 GRUNDFOS chemical metering pumps. The many intricacies of the PROFIBUS are not discussed in this section, since much of it is irrelevant with respect to the SIMS-BW. Instead, this section provides an overview of the interfacing of the real-time controller with PROFIBUS.

The block diagram of the function which interfaces the RTC with the PROFIBUS protocol is shown in **Figure D.1**. Below is a brief description of each numbered object depicted on **Figure D.1**:

1. PROFIBUS Master. This function is provided by LabVIEW and is used to interface a LabVIEW program with PROFIBUS.
2. Structure of a PROFIBUS signal. This is not a part of the block diagram, but a simple illustration of the appearance of a PROFIBUS signal. It is an array of bytes, with the first byte indicating the address. When this signal is sent out, only equipment with the corresponding address will read the signal. Each byte contains information regarding a unique parameter (e.g., pump speed, pump electrical consumption).
3. Address. Each pump has a unique address assigned to it, and all the code related to a specific pump can be found by selecting the number which corresponds to that pump's address in the drop-down menu.
4. PROFIBUS output. This function sorts out all the outputs for one pump and sorts them into a signal which can be read by PROFIBUS. The signal structure is illustrated in (2).

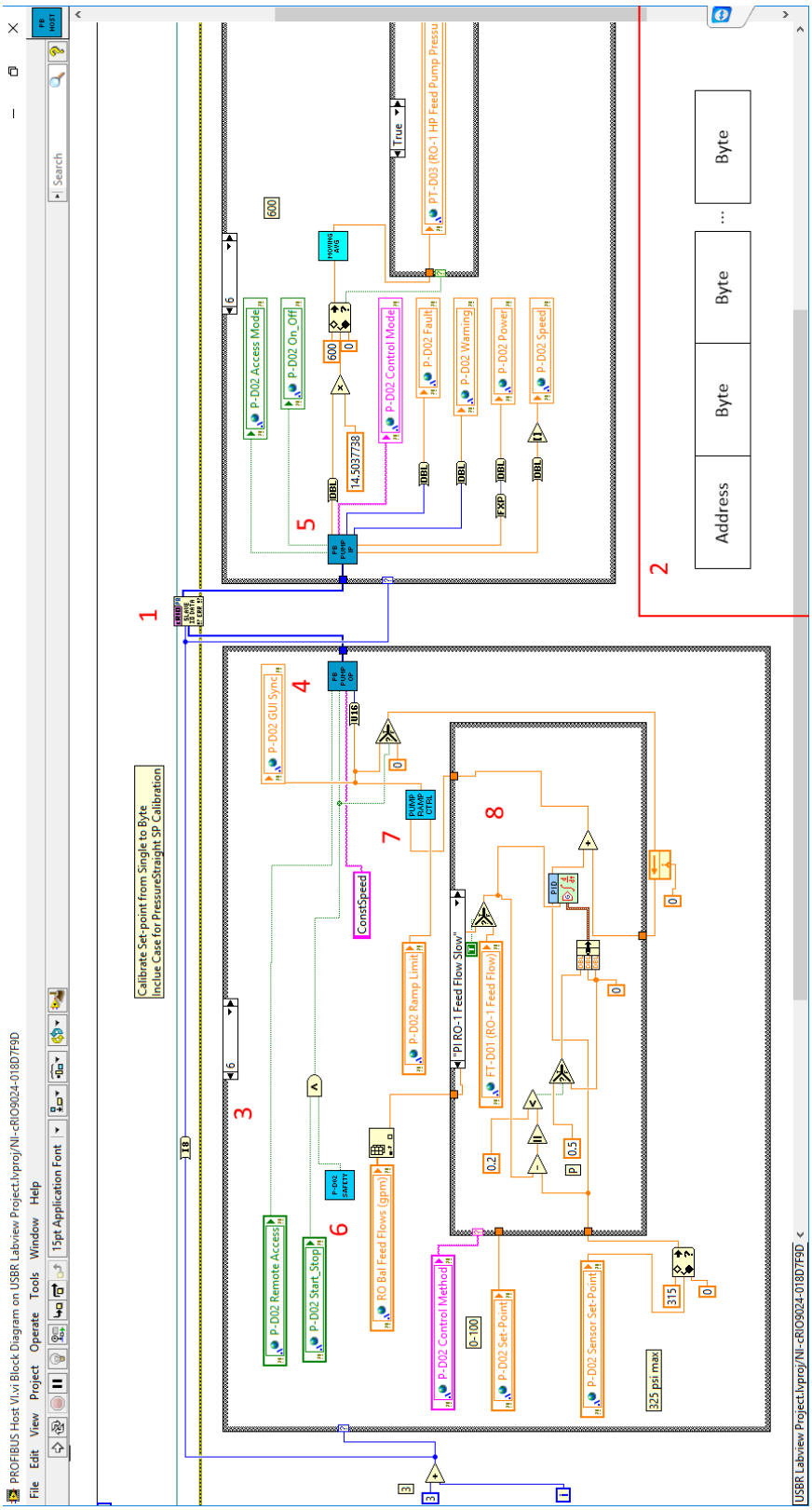

Figure D1. A screenshot of the LabVIEW block diagram of the PROFIBUS function

5. PROFIBUS input. This function reads the signal sent back from PROFIBUS to the RTC and converts it into variables that the RTC can use.
6. Safety. This function includes several safety requirements unique to each pump. The pump will only turn on if all safety requirements are met.
7. Pump ramp control. This is implemented to reduce pressure swings caused by the high-pressured pumps changing settings. When the pump speed is changed from one setting to another, the pump speed does not immediately change to the new setting; instead, the speed gradually approaches the new setting based on the ramp speed limit set.
8. PROFIBUS PI control is where all the PROFIBUS pumps' corresponding PI controllers are included.

Appendix E. SIMS-BW GUI

In this section, the graphical user interface (GUI) used in the SIMS-BW and all its components will be explained.

System Status

The SIMS-BW GUI is organized into several different tabs. The majority of these tabs (1-7) are dedicated to displaying the system status. Different tabs show different of the system, and the section corresponding to the tabs are labeled in the tabs themselves. On the screen, a P&ID of the system with all its sensors and actuators is presented. Each system component is labeled (A). If it is a sensor, it will have a read out (B). If it is an actuator, it will have a button (C) which the user can use to turn the actuator on/off. A grey button (C) indicates that the actuator is being commanded to be in the OFF, or FALSE, position. If the button is green, this is an indication that the actuator is being commanded to be in the ON, or TRUE, position. The actuator's actual position is indicated by the colored circles on the actuator symbol. Green indicates that a line is open for water to flow, while red means the passage is blocked. It is possible that the command and the actual positions do not match (e.g., when the actuator has a fault and doesn't move, the indicators will not change despite a command).

Tab 10 contains a time trace plot of select sensors used for controller tuning experiments. Currently, it displays the first-stage feed pressure and second-stage feed pressure as a function of time. Tabs 8, 9, and 11 are used for controlling the system and where the commands are input into the system.

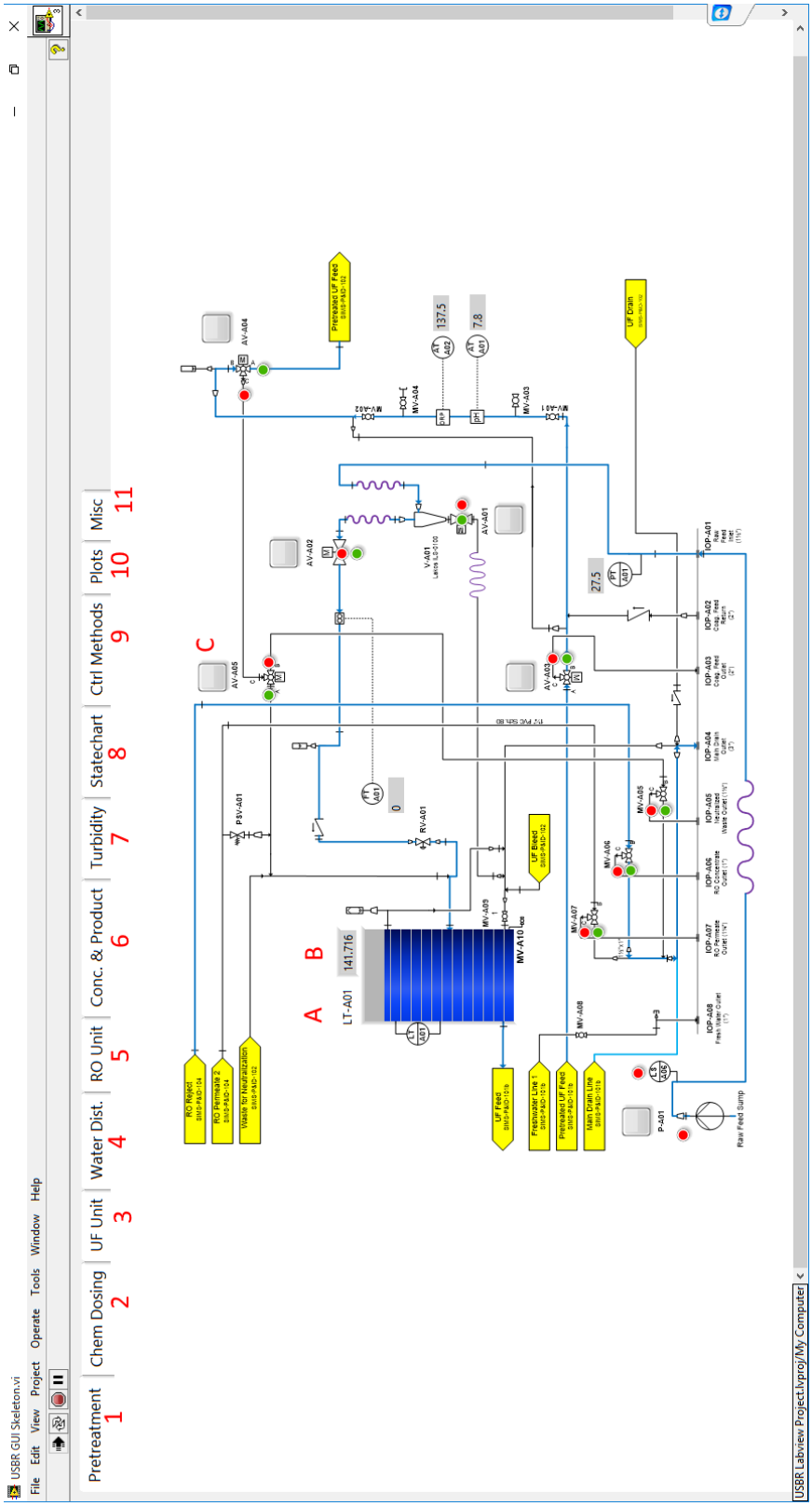

Figure E1. A screenshot of the front panel of the SIMS-BW GUI

Misc Tab

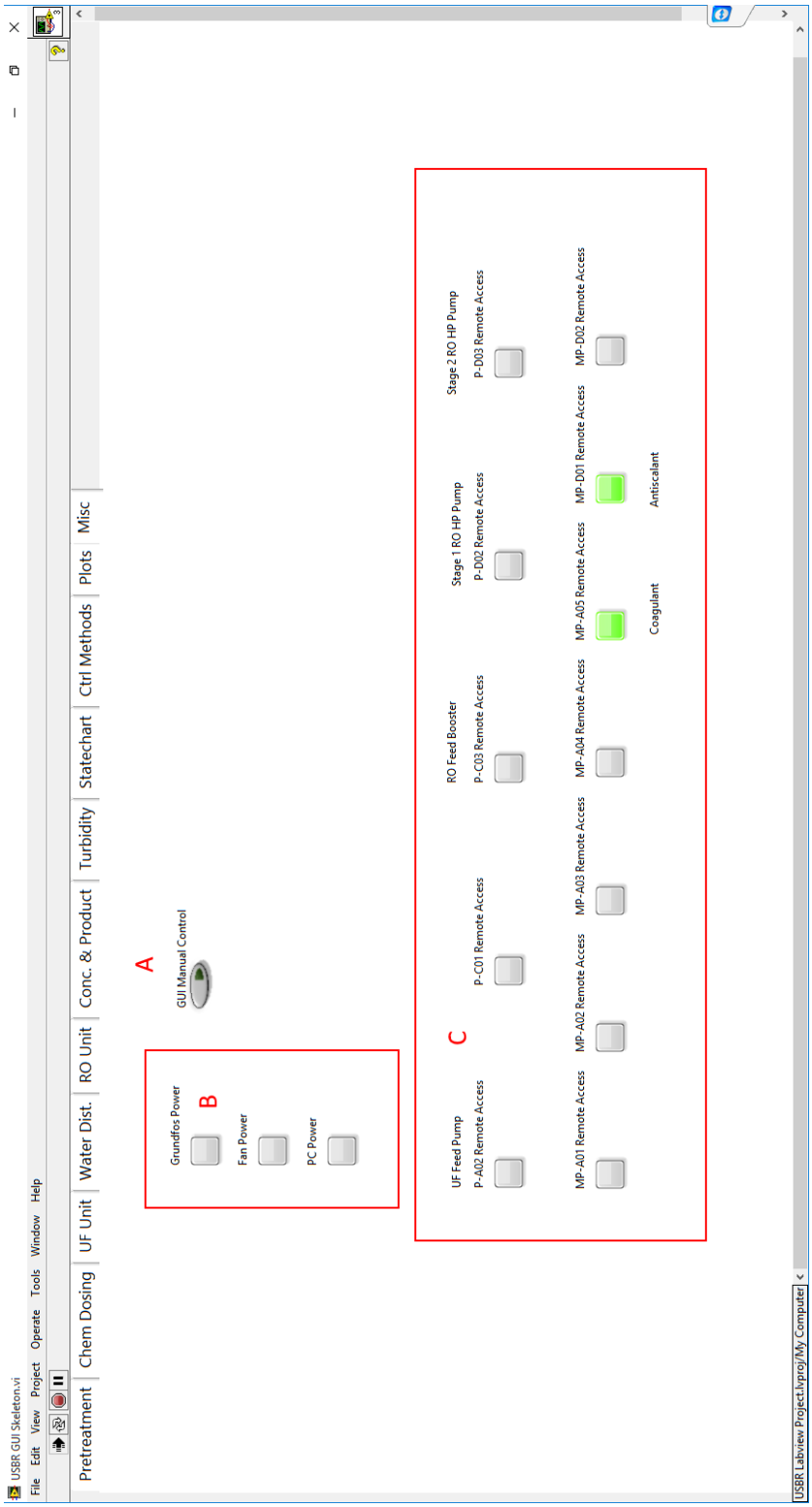

Figure E.2. A screenshot of the Misc Tab on the SIMS-BW GUI

Tab 11 in **Figure E.1** is labeled as “Misc.” A screenshot of the tab is shown in **Figure E.2**. In this tab, the “GUI Manual Control” button (A) switches the system between Automatic/Manual modes. In Automatic mode, all commands to system actuators are from the real-time controller. The user does not have access to actuator controls. If a user attempts to change an actuator setting while the system is in Automatic mode, the GUI will ignore and override the user’s command. The user will only be able to give commands to the system if the system is set to Manual mode, by pressing the “GUI Manual Control” button in A. If this button is green, then the GUI is in Manual mode.

There are several buttons in (B). Grundfos Power controls the power supply to the high-pressured pumps. For system operations, this button must be ON, or green. Fan power controls the power to the ventilation fans installed on the side of the RO plant container. This button is not necessary for the operation of the system. PC Power controls the power to the computer inside the electrical box which connects to the RTC. However, since in the current configuration the real-time controller is only accessible via the PC, this button is disabled.

The buttons in (C) are for enabling “remote control” of all the PROFIBUS (**Appendix D**) high-pressured pumps and metering pumps. This enables the PROFIBUS pumps to receive commands from the real-time controller, instead of locally from the interface on the pumps themselves. These buttons should always be ON, or green, during normal operation.

Statechart Tab

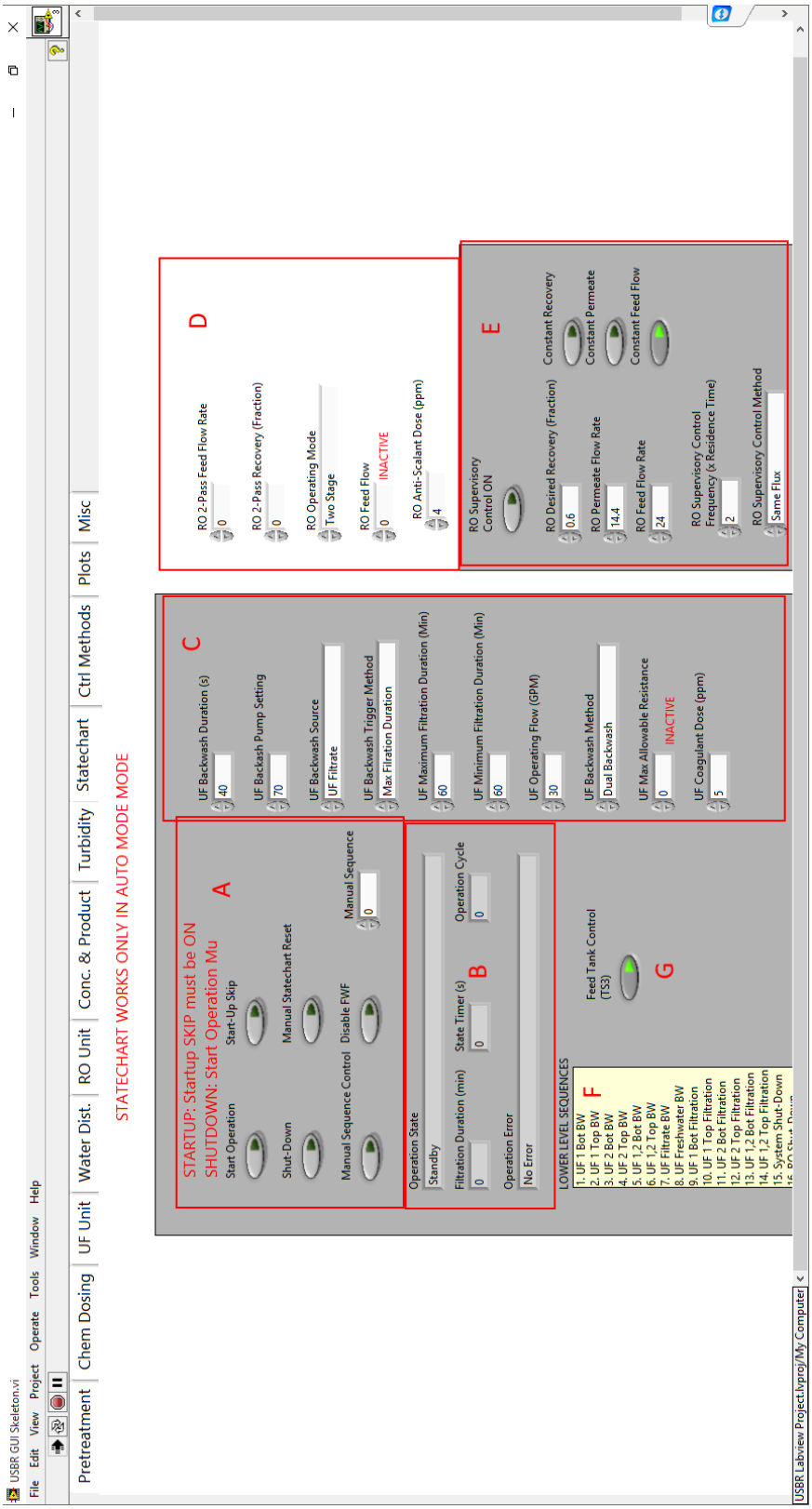

Figure E.3. A screenshot of the Statechart Tab on the SIMS-BW GUI

The Statechart tab is primarily used to control system operations. In section A, there are several buttons which controls basic system operation. Pressing the button Start Operation will command the system to enter Normal Operation (**Appendix C**). The system will undergo a UF start-up sequence, followed by the RO start-up sequence, and then will repeat UF filtration cycles until the system is shut down. Typically, a user will only need to press this button to run the system under pre-set conditions.

The Start-Up Skip button is used to enable the system to enter Normal Operation and start a UF filtration cycle without undergoing the automated start-up sequences. If the Start Operation button is pressed while the Start-Up Skip button is also pressed (green), then the system will skip the UF/RO start-ups and immediately enter UF filtration mode. Note that, if the system does not execute the start-up sequences, the system may not physically be in a UF filtration configuration, despite the fact that the software recognizes it to be in Normal Operation. The Start-Up Skip button should be used if the user starts the system up manually, but wants to turn on the automated UF filtration/UF backwash cycling, which is handled by Normal Operation.

The Shut-Down button will force the entire system to shut-down, regardless of its state, then immediately executes a Fresh Water Flush sequence. The shut-down sequence turns off all the pumps and all valves to their FALSE positions. If the Disable FWF button is pressed, then the system will undergo a shut-down sequence but will not execute a Fresh Water Flush sequence after the shut-down is completed.

The Manual Statechart Reset will force the control software to exit Normal Operation. This button has no impact on the physical configuration of the system itself, but resets the statechart to its initialization state (**Appendix C**).

Section B contains several displays of the system state.

1. Operation State. Indicates the current state of the SIMS-BW.

2. Filtration duration. Indicates the length of the current UF filtration period.
3. State timer. Indicates the time period that the current automated sequence has been running.
4. Operation cycle. Indicates the UF filtration cycle that the system is on, and increases by 1 at the conclusion of each UF backwash operation.
5. Operation Error. If the system is shut down due to an error, the operation error will display the specific error which caused the shutdown.

Section C contains UF operation settings.

1. UF backwash duration. This sets the duration of a UF backwash
2. UF backwash pump setting. This sets the UF backwash pump setting (0-100) during a backwash. Higher settings lead to higher backwash flow rates.
3. UF backwash source. This designates the tank from which the UF backwash draws water (i.e., either the UF filtrate tank or the RO permeate tank).
4. UF backwash trigger method. This determines how the UF backwash is triggered. The only option available currently is to trigger UF backwash after a fixed UF filtration duration.
5. UF maximum filtration duration. This determines the maximum UF filtration duration before UF backwash is triggered. Currently, this setting is used to control the UF filtration duration since UF backwash is triggered based on time.
6. UF minimum filtration duration. If the UF backwash is triggered based on a threshold other than a time limit (e.g., UF filtration resistance thresholds) then this sets a minimum filtration duration during which the UF backwash cannot be triggered unless the UF filtration duration exceeds the number set here.

7. UF operating flow. This sets the desired operating feed flow rate of the UF. Since the UF operates at 100% recovery, this also sets the UF filtrate flow rate.
8. UF backwash method. The user can choose between a single-direction backwash and a dual-backwash. In a single-direction backwash, only one direction of the UF module is backwashed, whereas in a dual-backwash, both directions are backwashed simultaneously. It is noted that preliminary studies have shown that single-direction backwash is generally more effective and single-direction backwash is generally recommended.
9. UF max allowable resistance. This setting currently does not function properly since the functionality is not coded. It is meant for UF backwash trigger based on a maximum allowable increase of the UF filtration resistance.
10. UF coagulant dose. This sets the coagulant dose into the UF feed.

Section D contains RO operation settings.

1. RO 2-pass feed flow rate. This setting is for the feed flow rate into the second RO pass when the RO is operating in a two-pass configuration.
2. RO 2-pass recovery. This setting is to control the recovery in the second pass when the RO system is operating in a two-pass configuration.
3. RO operating mode. This setting determines the configuration in which the RO system operates (e.g., single-stage, two-stage, two-pass).
4. RO feed flow. This setting is inactive.
5. RO anti-scalant dose. This sets the anti-scalant dose into the RO feed.

Section E contains the controls for the RO supervisory controller.

1. RO supervisory control ON. This button turns on the RO supervisory controller. Currently, this button is set automatically to be on when the user starts the system.

2. RO desired recovery. This is where the user inputs a desired RO recovery.
3. RO permeate flow rate. This is where the user inputs a desired RO permeate flow rate.
4. RO feed flow rate. This is where the user inputs a desired RO feed flow rate.
5. Constant ____ button. When this button is pressed, the user will not be able to change the setting which corresponds to the button. When a user changes another setting, the third setting will automatically change based on the constant setting and the new user input (e.g., if feed flow rate is held constant, changing the desired recovery will change the desired permeate flow rate automatically)
6. RO supervisory control frequency. This dictates how frequent the RO supervisory controller calculates a new set of set-points and applies them to the RO system.
7. RO supervisory control method. This dictates how the first and second stage recoveries are split (e.g., same flux, energy-optimal).

Control Methods Tab

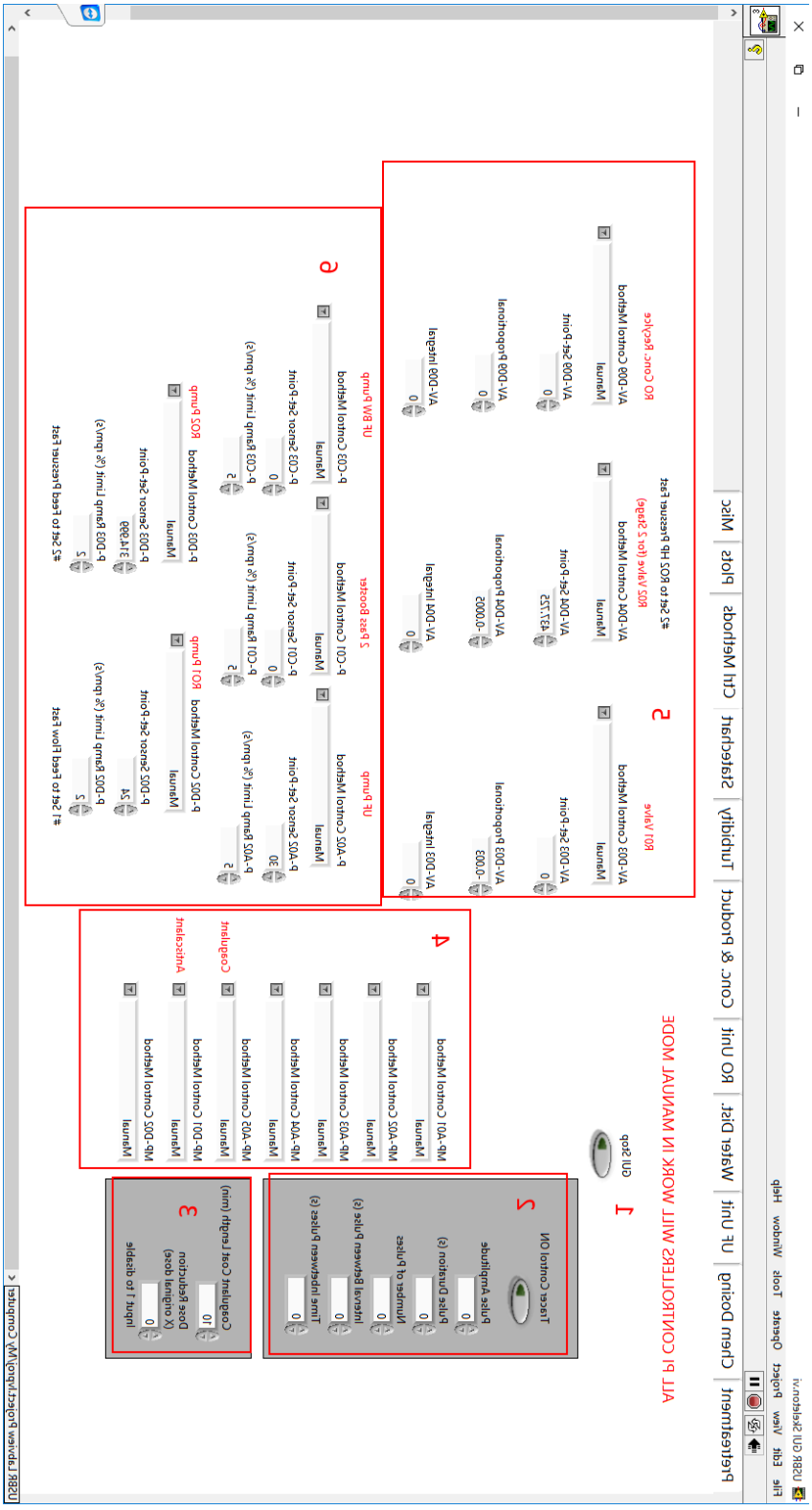

Figure E4. A screenshot of the Control Methods Tab on the SIMS-BW GUI

The Control Methods tab contains settings for the controllers associated with pumps, metering pumps, and valves.

1. GUI Stop. This button stops the GUI program.
2. Tracer control ON. This controls the pulse injection of a tracer into the RO feed.
3. Coagulant coat control. The coagulant coat is a method in which coagulant is dosed at a certain dose initially during UF filtration, but after a certain period of time it is reduced.
4. Metering pump control. This is used to control the metering pumps. Manual means that the setting is sent to the metering pumps as mL/h values. When set to a stream (e.g., feed flow) then the metering pump is controlled to achieve a certain concentration in the specified stream.
5. Control valve PI controllers. This contains the settings for PI controllers of the control valves.
6. Pump PI controllers. This contains the settings for controlling the high-pressured GRUNDFOS pumps.

References

[1] L.F. Greenlee, D.F. Lawler, B.D. Freeman, B. Marrot, P. Moulin, Reverse osmosis desalination: Water sources, technology, and today's challenges, Water Research, 43 (2009) 2317-2348.

[2] S. Gray, R. Semiat, M. Duke, A. Rahardianto, Y. Cohen, 4.04 - Seawater Use and Desalination Technology, in: W. Editor-in-Chief: Peter (Ed.) Treatise on Water Science, Elsevier, Oxford, 2011, pp. 73-109.

[3] B.C. McCool, A. Rahardianto, J. Faria, K. Kovac, D. Lara, Y. Cohen, Feasibility of reverse osmosis desalination of brackish agricultural drainage water in the San Joaquin Valley, Desalination, 261 (2010) 240-250.

[4] G. Raluy, L. Serra, J. Uche, Life cycle assessment of MSF, MED and RO desalination technologies, Energy, 31 (2006) 2361-2372.

[5] H.C. Flemming, G. Schaule, T. Griebe, J. Schmitt, A. Tamachkiarowa, Biofouling—the Achilles heel of membrane processes, Desalination, 113 (1997) 215-225.

[6] L.O. Villacorte, S.A.A. Tabatabai, D.M. Anderson, G.L. Amy, J.C. Schippers, M.D. Kennedy, Seawater reverse osmosis desalination and (harmful) algal blooms, Desalination, 360 (2015) 61-80.

[7] J.S. Baker, L.Y. Dudley, Biofouling in membrane systems — A review, Desalination, 118 (1998) 81-89.

[8] L. Henthorne, B. Boysen, State-of-the-art of reverse osmosis desalination pretreatment, Desalination, 356 (2015) 129-139.

[9] K.T. Chua, M.N.A. Hawlader, A. Malek, Pretreatment of seawater: Results of pilot trials in Singapore, Desalination, 159 (2003) 225-243.

[10] M. Wilf, M.K. Schierach, Improved performance and cost reduction of RO seawater systems using UF pretreatment, Desalination, 135 (2001) 61-68.

[11] P.H. Wolf, S. Siverns, S. Monti, UF membranes for RO desalination pretreatment, Desalination, 182 (2005) 293-300.

[12] K. Burashid, A.R. Hussain, Seawater RO plant operation and maintenance experience: addur desalination plant operation assessment, Desalination, 165 (2004) 11-22.

[13] M. Kazemimoghadam, T. Mohammadi, Chemical cleaning of ultrafiltration membranes in the milk industry, Desalination, 204 (2007) 213-218.

[14] D.F. Halpern, J. McArdle, B. Antrim, UF pretreatment for SWRO: pilot studies, Desalination, 182 (2005) 323-332.

[15] P. Blanpain-Avet, J.F. Migdal, T. Bénézech, Chemical cleaning of a tubular ceramic microfiltration membrane fouled with a whey protein concentrate suspension—Characterization of hydraulic and chemical cleanliness, J Membrane Sci, 337 (2009) 153-174.

[16] S. Delgado Diaz, L. Vera Peña, E. González Cabrera, M. Martínez Soto, L.M. Vera Cabezas, L.R. Bravo Sánchez, Effect of previous coagulation in direct ultrafiltration of primary settled municipal wastewater, Desalination, 304 (2012) 41-48.

[17] H.-C. Kim, In-line coagulation with quaternary amine polymer prior to microfiltration of humic-rich water, Journal of Colloid and Interface Science, 459 (2015) 151-159.

[18] T. Nguyen, F. Roddick, L. Fan, Biofouling of Water Treatment Membranes: A Review of the Underlying Causes, Monitoring Techniques and Control Measures, Membranes, 2 (2012) 804.

[19] K. Kimura, Y. Hane, Y. Watanabe, Effect of pre-coagulation on mitigating irreversible fouling during ultrafiltration of a surface water, Water Science and Technology, 51 (2005) 93-100.

[20] X. Zheng, S. Plume, M. Ernst, J.-P. Croué, M. Jekel, In-line coagulation prior to UF of treated domestic wastewater – foulants removal, fouling control and phosphorus removal, J Membrane Sci, 403–404 (2012) 129-139.

[21] B.-B. Lee, K.-H. Choo, D. Chang, S.-J. Choi, Optimizing the coagulant dose to control membrane fouling in combined coagulation/ultrafiltration systems for textile wastewater reclamation, Chemical Engineering Journal, 155 (2009) 101-107.

[22] M. Yao, J. Nan, T. Chen, D. Zhan, Q. Li, Z. Wang, H. Li, Influence of flocs breakage process on membrane fouling in coagulation/ultrafiltration process—Effect of additional coagulant of poly-aluminum chloride and polyacrylamide, J Membrane Sci, 491 (2015) 63-72.

[23] L. Quinn, Reverse osmosis systems in military or emergency operations, Desalination, 113 (1997) 297-301.

[24] J. Chen, G. Li, Marine reverse osmosis desalination plant — a case study, Desalination, 174 (2005) 299-303.

[25] R. Ordóñez, D. Hermosilla, I.S. Pío, Á. Blanco, Evaluation of MF and UF as pretreatments prior to RO applied to reclaim municipal wastewater for freshwater substitution in a paper mill: A practical experience, Chemical Engineering Journal, 166 (2011) 88-98.

[26] A.P. Echavarría, V. Falguera, C. Torras, C. Berdún, J. Pagán, A. Ibarz, Ultrafiltration and reverse osmosis for clarification and concentration of fruit juices at pilot plant scale, LWT - Food Science and Technology, 46 (2012) 189-195.

[27] C.W. Aeijelts Averink, W. Buijs, Recycling of water with canal water supplement at Artis Zoo, Amsterdam, by means of ultrafiltration and reverse osmosis, Desalination, 132 (2000) 167-171.

[28] S.A.A. Tabatabai, S.I. Gaulinger, M.D. Kennedy, G.L. Amy, J.C. Schippers, Optimization of inline coagulation in integrated membrane systems: A study of FeCl3, Desalin Water Treat, 10 (2009) 121-127.

[29] H. Ratnaweera, J. Fettig, State of the Art of Online Monitoring and Control of the Coagulation Process, Water, 7 (2015) 6574.

[30] M. Aboabboud, S. Elmasallati, Potable water production from seawater by the reverse osmosis technique in Libya, Desalination, 203 (2007) 119-133.

[31] P.J. Smith, S. Vigneswaran, H.H. Ngo, R. Ben-Aim, H. Nguyen, Design of a generic control system for optimising back flush durations in a submerged membrane hybrid reactor, J Membrane Sci, 255 (2005) 99-106.

[32] P.J. Smith, S. Vigneswaran, H.H. Ngo, R. Ben-Aim, H. Nguyen, A new approach to backwash initiation in membrane systems, J Membrane Sci, 278 (2006) 381-389.

[33] M.L. Richlen, S.L. Morton, E.A. Jamali, A. Rajan, D.M. Anderson, The catastrophic 2008–2009 red tide in the Arabian gulf region, with observations on the identification and phylogeny of the fish-killing dinoflagellate Cochlodinium polykrikoides, Harmful Algae, 9 (2010) 163-172.

[34] T. Manth, M. Gabor, E. Oklejas, Minimizing RO energy consumption under variable conditions of operation, Desalination, 157 (2003) 9-21.

[35] M. Busch, W.E. Mickols, Reducing energy consumption in seawater desalination, Desalination, 165 (2004) 299-312.

[36] M. Wilf, C. Bartels, Optimization of seawater RO systems design, Desalination, 173 (2005) 1-12.

[37] R. Prakash, A. Arian, S. Paul, R.M. William, III, B. Sabine, D. Caroline, P. Kevin, S. Prateeti, W. Nicholas, C. Joe, Volume 1: Survey of Available Information in Support of the

Energy-Water Bandwidth Study of Desalination Systems, in, Lawrence Berkeley National Laboratory, 2016.

[38] K. Fethi, Optimization of energy consumption in the 3300 m^3/d RO Kerkennah plant, Desalination, 157 (2003) 145-149.

[39] J.E. Nemeth, Innovative system designs to optimize performance of ultra-low pressure reverse osmosis membranes, Desalination, 118 (1998) 63-71.

[40] M. Wilf, Design consequences of recent improvements in membrane performance, Desalination, 113 (1997) 157-163.

[41] J. Beca, Pharmaceutical discharge: Zero discharge for pharma plant, Filtr Separat, 44 (2007) 40-41.

[42] R. Singh, S.V. Cabibbo, Hydraulic turbine energy recovery - R.O. System, Desalination, 32 (1980) 281-296.

[43] D.J. Woodcock, I. Morgan White, The application of pelton type impulse turbines for energy recovery on sea water reverse osmosis systems, Desalination, 39 (1981) 447-458.

[44] E. Oklejas Jr, W.F. Pergande, Integration of advanced high-pressure pumps and energy recovery equipment yields reduced capital and operating costs of seawater RO systems, Desalination, 127 (2000) 181-188.

[45] R. Rautenbach, W. Dahm, Design and optimization of spiral-wound and hollow fiber RO-modules, Desalination, 65 (1987) 259-275.

[46] S. Avlonitis, W.T. Hanbury, M. Benboudinar, Spiral wound modules performance - an analytical solution .1., Desalination, 81 (1991) 191-208.

[47] M.B. Boudinar, W.T. Hanbury, S. Avlonitis, Numerical simulation and optimisation of spiral-wound modules, Desalination, 86 (1992) 273-290.

[48] S. Avlonitis, W.T. Hanbury, M. Benboudinar, Spiral wound modules performance - an analytical solution .2., Desalination, 89 (1993) 227-246.

[49] W.G.J. van der Meer, J.C. van Dijk, Theoretical optimization of spiral-wound and capillary nanofiltration modules, Desalination, 113 (1997) 129-146.

[50] V. Geraldes, N.E. Pereira, M.N. de Pinho, Simulation and optimization of medium-sized seawater reverse osmosis processes with spiral-wound modules, Ind Eng Chem Res, 44 (2005) 1897-1905.

[51] A. Villafafila, I.M. Mujtaba, Fresh water by reverse osmosis based desalination: simulation and optimisation, Desalination, 155 (2003) 1-13.

[52] S.A. Avlonitis, M. Pappas, K. Moutesidis, A unified model for the detailed investigation of membrane modules and RO plants performance, Desalination, 203 (2007) 218-228.

[53] A.M.K. El-ghonemy, Waste energy recovery in seawater reverse osmosis desalination plants. Part 1: Review, Renew. Sust. Energ. Rev., 18 (2013) 6-22.

[54] C.R. Bartels, K. Andes, Consideration of energy savings in SWRO, Desalin Water Treat, 51 (2013) 717-725.

[55] Y. Kim, M.G. Kang, S. Lee, S.G. Jeon, J.S. Choi, Reduction of energy consumption in seawater reverse osmosis desalination pilot plant by using energy recovery devices, Desalin Water Treat, 51 (2013) 766-771.

[56] A.H. Zhu, P.D. Christofides, Y. Cohen, Minimization of energy consumption for a two-pass membrane desalination: Effect of energy recovery, membrane rejection and retentate recycling, J Membrane Sci, 339 (2009) 126-137.

[57] A.H. Zhu, A. Rahardianto, P.D. Christofides, Y. Cohen, Reverse osmosis desalination with high permeability membranes - Cost optimization and research needs, Desalin Water Treat, 15 (2010) 256-266.

[58] A.Z. Zhu, P.D. Christofides, Y. Cohen, Effect of thermodynamic restriction on energy cost optimization of RO membrane water desalination, Ind Eng Chem Res, 48 (2009) 6010-6021.

[59] A.H. Zhu, P.D. Christofides, Y. Cohen, Energy consumption optimization of reverse osmosis membrane water desalination subject to feed salinity fluctuation, Ind Eng Chem Res, 48 (2009) 9581-9589.

[60] A.R. Bartman, A.H. Zhu, P.D. Christofides, Y. Cohen, Minimizing energy consumption in reverse osmosis membrane desalination using optimization-based control, J Process Contr, 20 (2010) 1261-1269.

[61] C. Fritzmann, J. Löwenberg, T. Wintgens, T. Melin, State-of-the-art of reverse osmosis desalination, Desalination, 216 (2007) 1-76.

[62] M. Mulder, Basic Principles of Membrane Technology, Kluwer Academic Publishers, Boston, 1997.

[63] E.L. Cussler, Diffusion, Cambridge University Press, 1997.

[64] Nalco, Spiral Wound Membrane Elements, in, 2015.

[65] A. Brehant, V. Bonnelye, M. Perez, Comparison of MF/UF pretreatment with conventional filtration prior to RO membranes for surface seawater desalination, Desalination, 144 (2002) 353-360.

[66] A. Teuler, K. Glucina, J.M. Laîné, Assessment of UF pretreatment prior RO membranes for seawater desalination, Desalination, 125 (1999) 89-96.

[67] O. Lorain, B. Hersant, F. Persin, A. Grasmick, N. Brunard, J.M. Espenan, Ultrafiltration membrane pre-treatment benefits for reverse osmosis process in seawater desalting. Quantification in terms of capital investment cost and operating cost reduction, Desalination, 203 (2007) 277-285.

[68] D.A. Seiberling, Appendix B - Tank Cleaning, in: S. Hall (Ed.) Branan's Rules of Thumb for Chemical Engineers (Fifth Edition), Butterworth-Heinemann, Oxford, 2012, pp. 429-432.

[69] R. Rautenbach, T. Linn, D.M.K. Al-Gobaisi, Present and future pretreatment concepts — strategies for reliable and low-maintenance reverse osmosis seawater desalination, Desalination, 110 (1997) 97-106.

[70] Dow, FilmTec's Technical Manual, in. "http://dowac.custhelp.com/app/answers/detail/a_id/3428."

[71] A. Basile, A. Cassano, N.K. Rastogi, Advances in Membrane Technologies for Water Treatment: Materials, Processes and Applications, Elsevier Science, 2015.

[72] A.J. Abrahamse, C. Lipreau, S. Li, S.G.J. Heijman, Removal of divalent cations reduces fouling of ultrafiltration membranes, J Membrane Sci, 323 (2008) 153-158.

[73] S. Li, S.G.J. Heijman, J.Q.J.C. Verberk, A.R.D. Verliefde, A.J.B. Kemperman, J.C. van Dijk, G. Amy, Impact of backwash water composition on ultrafiltration fouling control, J Membrane Sci, 344 (2009) 17-25.

[74] C. Ma, L. Wang, S. Li, S.G.J. Heijman, L.C. Rietveld, X.B. Su, Practical experience of backwashing with RO permeate for UF fouling control treating surface water at low temperatures, Separation and Purification Technology, 119 (2013) 136-142.

[75] Y. Cohen, P.D. Christofides, A. Rahardianto, A.R. Bartman, A. Zhu, H. Gu, L.X. Gao, Apparatus, system and method for integrated filtration and reverse osmosis desalination, in: US Patent Application Publication No. US20140048462 A1, US Patent App. 13/822,622, 2011.

[76] G. Gilabert-Oriol, M. Hassan, J. Dewisme, V. Garcia-Molina, M. Busch, Backwashing pressurized ultrafiltration using reverse osmosis brine in seawater desalination and its potential costs savings, Desalination and Water Treatment, (2014) 1-13.

[77] L. Katebian, S.C. Jiang, Marine bacterial biofilm formation and its responses to periodic hyperosmotic stress on a flat sheet membrane for seawater desalination pretreatment, Journal of Membrane Science, 425–426 (2013) 182-189.

[78] K.Y.-j. Choi, B.A. Dempsey, In-line coagulation with low-pressure membrane filtration, Water Research, 38 (2004) 4271-4281.

[79] C.J. Gabelich, T.I. Yun, B.M. Coffey, I.H.M. Suffet, Effects of aluminum sulfate and ferric chloride coagulant residuals on polyamide membrane performance, Desalination, 150 (2002) 15-30.

[80] P. Jackson, E. Tomlinson, Automatic coagulation control—evaluation of strategies and techniques, Water Supply, 4 (1986) 55.

[81] Y. Sangu, H. Yokoi, H. Tadokoro, T. Tachi, Development of automatic coagulant dosage control technology for rapid change of raw water quality parameters, Water Science and Technology: Water Supply, 12 (2012) 918-925.

[82] Y. Sangu, H. Yokoi, H. Tadokoro, T. Tachi, Verification of automatic coagulant dosage control technology based on aluminum concentration at a water purification plant, Water Science and Technology: Water Supply, 15 (2015) 26-33.

[83] B. Blankert, B.H.L. Betlem, B. Roffel, Development of a control system for in-line coagulation in an ultrafiltration process, J Membrane Sci, 301 (2007) 39-45.

[84] I. Alatiqi, H. Ettouney, H. El-Dessouky, Process control in water desalination industry: an overview, Desalination, 126 (1999) 15-32.

[85] I.M. Alatiqi, A.H. Ghabris, S. Ebrahim, System-Identification and Control of Reverse-Osmosis Desalination, Desalination, 75 (1989) 119-140.

[86] A.R. Bartman, P.D. Christofides, Y. Cohen, Nonlinear Model-Based Control of an Experimental Reverse-Osmosis Water Desalination System, Ind Eng Chem Res, 48 (2009) 6126-6136.

[87] C.W. McFall, A. Bartman, P.D. Christofides, Y. Cohen, Control and monitoring of a high recovery reverse osmosis desalination process, Ind Eng Chem Res, 47 (2008) 6698-6710.

[88] A. Abbas, Model predictive control of a reverse osmosis desalination unit, Desalination, 194 (2006) 268-280.

[89] A.R. Bartman, C.W. McFall, P.D. Christofides, Y. Cohen, Model-predictive control of feed flow reversal in a reverse osmosis desalination process, J Process Contr, 19 (2009) 433-442.

[90] A. Gambier, E. Badreddin, Application of hybrid modeling and control techniques to desalination plants, Desalination, 152 (2003) 175-184.

[91] M. Krstic, Performance improvement and limitations in extremum seeking control, Syst Control Lett, 39 (2000) 313-326.

[92] S. Kremen, M. Wilf, P. Lange, Operating results and economics of single stage and two stage large size sea water RO systems, Desalination, 82 (1991) 3-13.

[93] M. Taniguchi, M. Kurihara, S. Kimura, Behavior of a reverse osmosis plant adopting a brine conversion two-stage process and its computer simulation, J Membrane Sci, 183 (2001) 249-257.

[94] E. Cardona, A. Piacentino, F. Marchese, Energy saving in two-stage reverse osmosis systems coupled with ultrafiltration processes, Desalination, 184 (2005) 125-137.

[95] Y.-Y. Lu, Y.-D. Hu, X.-L. Zhang, L.-Y. Wu, Q.-Z. Liu, Optimum design of reverse osmosis system under different feed concentration and product specification, J Membrane Sci, 287 (2007) 219-229.

[96] J. Sprintall, J.T. Potemra, S.L. Hautala, N.A. Bray, W.W. Pandoe, Temperature and salinity variability in the exit passages of the Indonesian Throughflow, Deep Sea Research Part II: Topical Studies in Oceanography, 50 (2003) 2183-2204.

[97] N.G. Pace, F.B. Jensen, Impact of Littoral Environmental Variability on Acoustic Predictions and Sonar Performance, Springer Netherlands, 2012.

[98] S.L. Morey, D.S. Dukhovskoy, Analysis Methods for Characterizing Salinity Variability from Multivariate Time Series Applied to the Apalachicola Bay Estuary, Journal of Atmospheric and Oceanic Technology, 29 (2012) 613-628.

[99] M. Li, Optimal plant operation of brackish water reverse osmosis (BWRO) desalination, Desalination, 293 (2012) 61-68.

[100] M. Li, B. Noh, Validation of model-based optimization of brackish water reverse osmosis (BWRO) plant operation, Desalination, 304 (2012) 20-24.

[101] L. Gao, A. Rahardianto, H. Gu, P.D. Christofides, Y. Cohen, Energy-Optimal Control of RO Desalination, Ind Eng Chem Res, 53 (2014) 7409-7420.

[102] C.R. Bartels, R. Franks, W. Bates, Design Advantages for SWRO Using Advanced Membrane Technology, IDA Journal of Desalination and Water Reuse, 2 (2010) 21-25.

[103] R.-W. Lee, J. Glater, Y. Cohen, C. Martin, K. Kovac, M.N. Milobar, D.W. Bartel, Low-pressure RO membrane desalination of agricultural drainage water, Desalination, 155 (2003) 109-120.

[104] L.X. Gao, A. Rahardianto, H. Gu, P.D. Christofides, Y. Cohen, Novel design and operational control of integrated ultrafiltration — Reverse osmosis system with RO concentrate backwash, Desalination, 382 (2016) 43-52.

[105] H. Huang, K. Schwab, J.G. Jacangelo, Pretreatment for Low Pressure Membranes in Water Treatment: A Review, Environmental Science & Technology, 43 (2009) 3011-3019.

[106] I. GmbH, Dizzer XL Ultrafiltration Modules, in, 2012. "http://www.inge.ag/assets/Technical_Specification_dizzerXL_MB2(2012-11)E-inge.pdf"

[107] É. Clapeyron, Mémoire sur la puissance motrice de la chaleur, Jacques Gabay, 1834.

[108] P. Chapple, Principles of Hydraulic Systems Design, Second Edition, Momentum Press, 2014.

[109] S. Mamèic, M. Bogdevièius, Simulation of dynamic processes in hydraulic accumulators, Transport, 25 (2010) 215-221.

[110] L. Gao, A. Rahardianto, H. Gu, P.D. Christofides, Y. Cohen, Energy-Optimal Control of RO Desalination, Industrial & Engineering Chemistry Research, (2013).

[111] S. Whitaker, Flow in porous media I: A theoretical derivation of Darcy's law, Transp Porous Med, 1 (1986) 3-25.

[112] J. Kim, F.A. DiGiano, Fouling models for low-pressure membrane systems, Separation and Purification Technology, 68 (2009) 293-304.

[113] G. Crozes, C. Anselme, J. Mallevialle, Effect of adsorption of organic matter on fouling of ultrafiltration membranes, J Membrane Sci, 84 (1993) 61-77.

[114] Y.S. Polyakov, A.L. Zydney, Ultrafiltration membrane performance: Effects of pore blockage/constriction, J Membrane Sci, 434 (2013) 106-120.

[115] A.C. Chang, D.B. Silva, Salinity and Drainage in San Joaquin Valley, California: Science, Technology, and Policy, Springer London, Limited, 2013.

[116] D.W.P. Solutions, Design Equations and Parameters in Filmtec Reverse Osmosis Membranes Technical Manual, in.

[117] C.A.D. Technology, W.S.T. Board, D.E.L. Studies, N.R. Council, Desalination:: A National Perspective, National Academies Press, 2008.

[118] R. Bond, S. Veerapaneni, Zero liquid discharge for inland desalination, AWWA Research Foundation, 2007.

[119] M.C. Mickley, Membrane Concentrate Disposal: Practices and Regulation, Final Report, US Department of the Interior, Bureau of Reclamation, Technical Service Center, Water Treatment Engineering and Research Group, 2001.

[120] A. International, Standard Practice for Standardizing Reverse Osmosis Performance Data, in, ASTM International, 2010.

[121] I.J. Karassik, Pump Handbook, McGraw-Hill, 2001.

[122] P.T. Boggs, J.W. Tolle, Sequential Quadratic Programming, Acta Numerica, 4 (1995) 1-51.

[123] D.E. Seborg, T.F. Edgar, D.A. Mellichamp, Process dynamics and control, Wiley, 2004.

[124] Toray, High Rejection BWRO, Enhanced Chemical Tolerance TM700D, in, 2014. "http://www.toraywater.com/products/ro/pdf/TM700D.pdf"